SMART COMPOSITES: EVALUATION OF EMBEDDED SENSORS IN COMPOSITE MATERIALS

by

Nathan Reed Palmer

A thesis submitted in partial fulfillment
of the requirements for the degree

of

Masters of Science

in

Mechanical Engineering

MONTANA STATE UNIVERSITY
Bozeman, Montana

August 2009

APPROVAL

of a thesis submitted by

Nathan Reed Palmer

This thesis has been read by each member of the thesis committee and has been found to be satisfactory regarding content, English usage, format, citation, bibliographic style, and consistency, and is ready for submission to the Division of Graduate Education.

Dr. Douglas S. Cairns

Approved for the Department Mechanical & Industrial Engineering

Dr. Christopher H.M. Jenkins

Approved for the Division of Graduate Education

Dr. Carl A. Fox

STATEMENT OF PERMISSION TO USE

Nathan Reed Palmer

August 2009

ACKNOWLEDGEMENTS

I would like to acknowledge and thank all who participated in the work which has culminated in this report. First, my thanks to Sandia National Laboratories and Dr. Cairns for your expertise and trust throughout this project. My thanks to Jonathan Ehresman for his help during development, manufacturing and testing of the samples which comprises the whole of this work. Thanks to Dr. Mandell, and his composite group, Daniel Samborsky, Tio Agastra, Aaron Sears, for allows access to your space, equipment, and experience. And finally to all the friends and family who have given their moral support.

TABLE OF CONTENTS

TABLE OF CONTENTS - CONTINUED

LIST OF TABLES

LIST OF TABLES - CONTINUED

LIST OF TABLES - CONTINUED

LIST OF FIGURES

LIST OF FIGURES - CONTINUED

Figure Page

LIST OF FIGURES - CONTINUED

LIST OF FIGURES - CONTINUED

LIST OF FIGURES - CONTINUED

LIST OF FIGURES - CONTINUED

Figure Page

LIST OF FIGURES - CONTINUED

GLOSSARY

Active control; method of controlling the loading and energy capture of wind turbines. Accomplished by adjustment of the blade pitch.

Active Control Surfaces; surfaces along the blades surface which can be altered during operation to increase energy capture and reduce loading.

Aerodynamic wind turbine; Design method which harvests energy through momentum transfer and aerodynamic effect over the blade surface.

Airfoil cross section; the cross-sectional geometry of an aerodynamic blade which produces lift as the air flows over the blade.

Bedplate; the support structure for the drive train and rotor hub.

Betz factor; a theoretical maximum amount of energy which can be harvested from a free field stream of air.

Chord length; the length between the two farthest points on the leading edge and trailing edge of an aerofoil shape.

Chordwise; referring to the plane coincident with that of the chord length.

Cladding; outer layer of glass of a fiber optic which contains the light within the core.

Core; the inner cylinder of glass of a fiber optic which light is transferred through.

CTE; coefficient of thermal expansion.

Drag based wind turbine; Design method which harvests energy through only momentum transfer between the stream of air and the turbine blades.

Far Field strain; material strain not effected by inclusions and geometrical discontinuities.

Fiber Bragg Grating; Periodic changing in the index of refraction along the length of the core, which produces periodic reflections of light launched into the core.

Field Emission Scanning Electron Microscopy (FESEM); imaging technique which collects the secondary electrons given off by a material when an electron gun is shot at the surface of the material.

Finite Element Method (FEM); method employed by engineering software to represent material response mathematically. This is accomplished by dividing an object into small volumes with distinct point (nodes) which can be followed mathematically as loading displaces the nodes from the original configuration.

Flapwise; referring to the plane perpendicular to that of the chord length

Foot print; the area taken up in the XY plane of the sensor.

Minimum bend radius; the smallest radius which a fiber optic can be bent without introducing flaws within the fiber.

Nacelle; the housing of a wind turbine in which the drive train is protected.

Passive control; A method of controlling the load and energy capture of wind turbines. Accomplished by designing the blades to an optimal angle of attack, with no adjustment of the blade during operation.

Pitch control; method of controlling the angle of attack of the turbine blade during operation.

Power coefficient; the amount of power harvested from a free field stream of air compared to the amount of power present in the same stream of air.

Repeatability; the ability to obtain the same response given the same set of conditions or procedures.

Tip speed ratio; the relationship between the tangential velocity of the blade tip to the wind velocity.

Vacuum Assisted Resin Transfer Molding (VARTM); method of fiber reinforced composite material construction. Fiber reinforcement is saturated with resin which is injected into the reinforcement compacted by the application of a vacuum.

Wind turbine radius; the radius of the circle swept out by the turbine blades during operation.

Yaw control; method of controlling the direction the wind turbine is facing. This controls the rotation of the nacelle and rotor hub about the tower.

.

ABSTRACT

As an emerging form of renewable energy, horizontal wind turbines have experienced advancements in improving efficiency and reliability. These advances have pushed the limits of current technology used in wind turbines. Smart blades have been proposed as a method of addressing these limitations.

Sensor integration within blade construction is the first step in development of smart blades. Thus, several low cost sensors were chosen, 1 axis strain gages, polyvinylidene fluoride films (PVDF), and single mode fiber optics either coated in acrylate or polyimide. To ensure successful bonding between sensor and composite two surface treatment techniques were developed. The first, dipping of the sensor into a bath of 20% by weight solution of nitric acid and the second was submersion of the sensor in the nitric acid for ten seconds prior to removal. These treatments were compared against sensors not surface treated prior to embedding. These sensors were embedded within samples created of fiberglass and epoxy or vinyl ester resin. Two different material tests were conducted. Tensile testing allowed for evaluation of sensor sensitivity, sensor failure point, material tensile modulus, and material tensile strength. Mode I fracture toughness evaluation, indicated the level of successful bonding which occurred during resin curing. Field Emission Scanning Electron Microscopy (FESEM) was conducted to further confirm the level of bonding between resin and sensor, post fracture.

Results for embedded strain gages showed an adverse effect for vinyl ester samples. Epoxy samples fared better, thus concluding manufacturing success for epoxy samples, submersion being preferred, and alternative methods needed for vinyl ester samples. PVDF films had good qualitative FESEM images combined with increasing trends. It was concluded that integration for both resin groups with sensors submerged in nitric acid was successful. Fiber optics coated in acrylate also showed good bonding under FESEM imaging as well as testing. It was thus concluded that submersion was the preferred treatment. Lastly, fiber optics coated in polyimide embedded in vinyl ester composites showed significant drawbacks and it was concluded that alternative methods need exploration. Those embedded in epoxy were successfully integrated and submersion in nitric acid showed the most potential.

INTRODUCTION

Energy is a fundamental entity of nature that is transferred between parts of a system, in the production of physical change within the system and usually regarded as the capacity for doing work [1]. This is the definition of the driving force behind the majority of physical, chemical, electrical, and biological phenomena. The need for energy is one of the reasons man-kind has developed farming techniques to increase food production throughout the ages. The chemical energy in petroleum provides the energy that drives the internal combustion engine which has allowed humans to travel farther, faster than in any other time in history. Stored mechanical energy is the reason pneumatic nail guns are used in the construction of personal homes. Reducing the flow of thermal energy is how houses stay warm in the winter, and cool in the summer. Electrical energy is responsible for the modern age's current explosion in technology. With advances in technology comes an increased in need for energy, as illustrated in Figure 1.

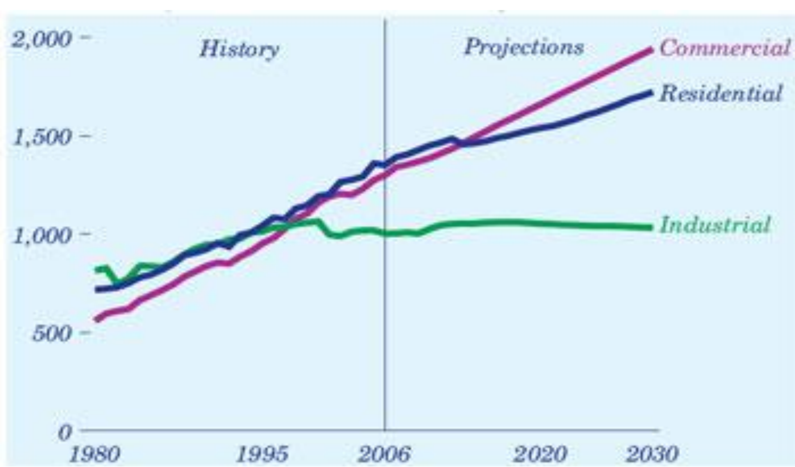

Figure 1. Annual electricity sales by sector 1980-2030 (billion kilowatt-hours) [2]

The escalating need for energy has led to advancements in harnessing energy from alternative sources. The production of wind farms to gather energy from wind is a part of this movement. Using wind turbines as a method of collecting energy has been implemented for centuries. However, before the 1970's this technology had only a small niche as a mechanical means of producing power, on a small scale, often in pumping water, grinding grain, and in a few cases charging banks of batteries. Because of the limited uses for these wind turbines, they have been practically unchanged from the first designs developed as far back as 1200 AD [3]. The last half of the 20th century, however, saw an impressive evolution in the wind turbine design. Simple drag and lift based blade designs gave way to high lift rotors, with pitch control. Additionally, the large wind turbines of the 1970's and before (50kWs) are now dwarfed by 1.5 to 3.6 MW goliaths, being developed, for increased power production today [3]. The increase in size is precipitated, by the fact, that more power can be produced with larger diameter wind turbines. An example of this is a 3.6 MW turbine which has a rotor diameter of 100m compared to .1MW wind turbines constructed at Altamont Pass, California, in the 1980s, which has a rotor diameter of 18m [4] [5].

Increasing the size has amplified the persisting issues with wind turbines. The primary issue is the failure of gearboxes connecting the turbine blade\rotor assembly with the generator, in the nacelle of the horizontal axis turbines; dominate in today's industrial wind farm applications [6]. The deficiency of gearboxes is systemic throughout gearbox manufacturers and turbine manufacturers. Failure does not occur due to lack of sound design or construction, which is generally the suspect. Failure has been found to occur primarily in the gearbox bearings, which were developed using the best design practices available [6]. Increasing the size of the wind turbine blades has also pushed material limits, thus forcing engineering advances in composite structures, to satisfy the "square-cube law". The "square-cube law" refers to the fact that power production of a wind turbine is proportional to the square, of the rotor diameter; while the mass of the turbine increases by the cube, of the rotor diameter, [3] [4]. The increasing body forces add additional stress to components, already stressed by increasing wind loads associated with the rise in surface area of the blades. All these load combinations, which change frequently, causes damage to the blades. This leads to failure of the blade and potentially destruction of the whole system [4].

Addressing these issues and developing appropriate solutions has the potential to increase the reliability of wind turbines, as well as their versatility. Current wind farms have been constructed in regions with sustained high wind velocities, illustrated in Figure 2, for the United States [7]. Location of wind farms is a first step towards incorporating wind energy into the repertoire of energy collection techniques. However, these areas do not coincide with the areas in need of energy. For now the issue of location vs. area of need is currently resolved with the construction of costly transmission lines. Construction of wind farms closer to the locations in need of energy would reduce or even eliminate the cost of transmission lines [8]. The above avenue can only be realized with the development of wind turbines, with increased efficiency. Increased efficiency would allow for more energy production at lower wind resource regions, closer to sites with high energy consumption. Both issues of increased reliability and efficiency can potentially be resolved in several different ways but there is one constant throughout; more information.

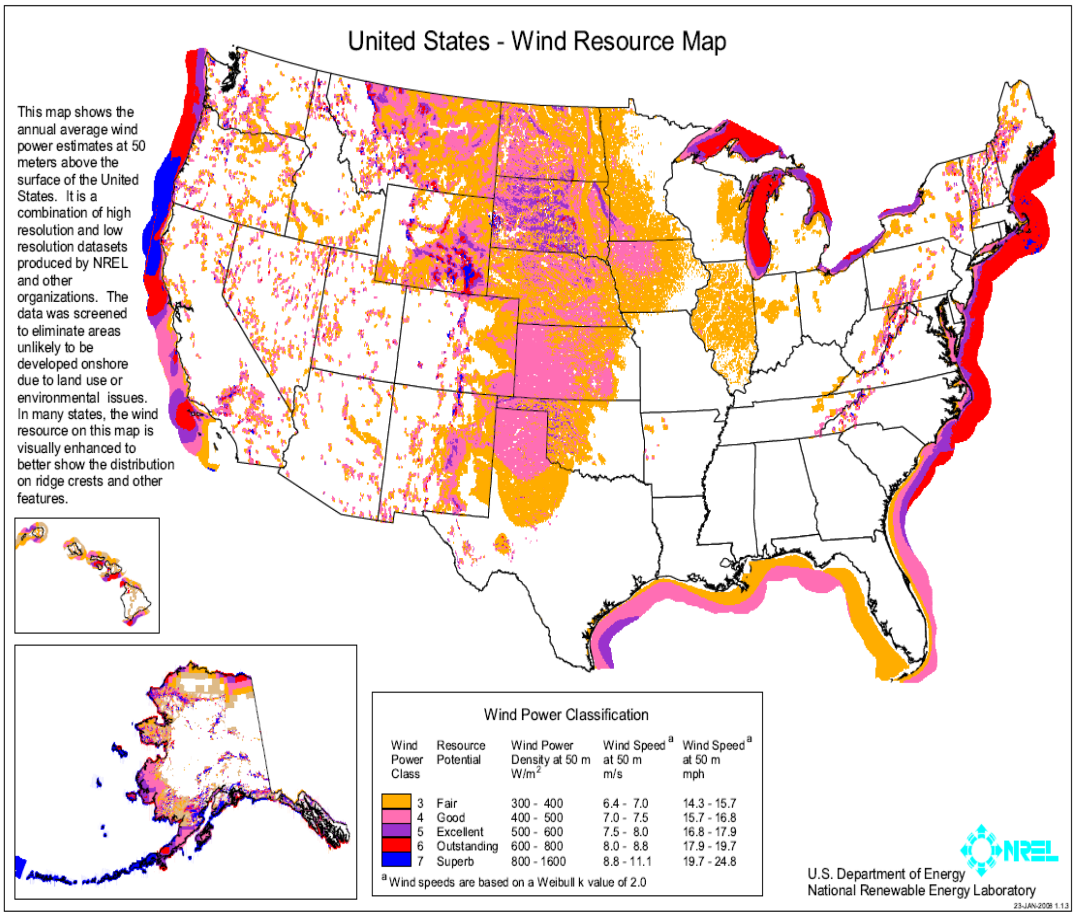

Figure 2. A map of the regions in the United States with desirable wind velocity levels [7]

Current wind turbine design incorporates data collection sensors at the base and in the nacelle of the turbine, but nothing in the blades themselves, as can be seen in Figure 3 below. This is an odd choice for data collection points as the blades themselves are the means through which energy is captured. By incorporating sensors into these large portions of wind turbine construction a more full description of load and health conditions could be developed. The detail collected could further refine the wind load regime used in design of gearbox bearings, and composite blade construction. Additional implications of including sensors into the wind turbine blades would be blade health monitoring, and potentially active control surface manipulation. Incorporating sensors would be an easy way of monitoring the structural health of the wind turbine blades, thus preventing catastrophic failures; which lead to down time for repair or the complete destruction of the turbine.

Figure 3. Location of current sensors monitoring turbine health and efficiency [8]

Sensors could be used to adjust the pitch and yaw of the wind turbine, to increase the efficiency of the turbine. Further, active control surfaces such as those used to control airplanes, could be included and controlled by an algorithm which derives its conclusions from the data collected. The active control approach would increase the efficiency of the machine allowing for construction in areas with lower wind rating, closer to the area with high energy demand.

Sensor integration into wind turbine blades would have two paths. Retrofit of existing blades in the field, and the incorporation of sensors into new blade construction. Due to the cost of current industrial wind turbines, retrofitting blades to increase the efficiency and longevity of the system is a sound investment. For wind turbines that have already failed or are in need of repair, new blades with sensors integrated into their design would be appropriate.

While retrofitting current industrial wind turbine blades is not a trivial task, there is a wealth of knowledge already assembled with regards to external adhesion of sensors to critical structures. The integration of sensors into the blades composite material is not as extensively understood. Issues of material degradation, sensor compatibility, longevity, sensor composite interface bonding, and signal retrieval, can be found in fabricating composite materials with sensors embedded.

Thus, the first objective of this study was the co-development and evaluation of manufacturing techniques which were designed to successfully integrate four chosen sensors within two fiberglass reinforced composites. These manufacturing techniques were tailored to composite architectures similar to that used in the wind industry. Upon complete analysis of the results gathered from testing, recommendations were made as whether or not to continue such manufacturing techniques or explore other alternatives. The last objective of this study was to develop a hierarchical evaluation procedure based on the work performed, which could be used to evaluate future combinations of sensors and composite structures.

These objectives were achieved through a combination of qualitative evaluation through tensile, and mode I fracture testing, and quantitative assessment through visual instrumentation. Sensor and material responses were monitored and analyzed prior to, during and after tensile loading. Further material sensor interaction was explored through mode I fracture testing. Lastly, imaging of post fractured sensor surfaces and coupon cross thicknesses provided an avenue through which to evaluate the bonding between the composites matrix resin and the sensor surface coatings.

BACKGROUND

An understanding of the components which comprise the technologies combined in the hopes of improving turbine performance is necessary. First, without an understanding of the physics and engineering design behind current wind turbines operate, development of representative test configurations would be difficult. Current wind turbines blades are constructed with composite materials. Thus, background knowledge of this group of materials would prove to be beneficial in the development and evaluation of the success of sensor integration. Lastly, prior knowledge of sensor design, operation, and conditioning allows for proper sensor selection based on the physical conditions experienced by the blades of a wind turbine.

Wind Turbines

Current industrial wind turbines are built using a multitude of different design criteria. These criteria differ from location to location, but in general the overall design concepts have been narrowed down to a few, which have been proven to work. Design aspects covered here do not constitute the complete design picture needed for implementation of industrial wind turbines. Only the design concepts which were most intimately related to the implementation of sensors into the blade construction are addressed.

Neglecting the long history associated with wind energy there are basically two types of wind turbines. Vertical axis wind turbines commonly called Darrieus-rotor type. The other type which is the common style of wind collection used in industrial application to date it the horizontal axis wind turbine [9]. Horizontal axis wind turbines have developed as the dominant form because of several aspects; the first is the ability to control the power output of the turbine via blade pitch control. Second, the blade shape can be aerodynamically tailored to achieve the highest possible efficiency, and such designs have a significant technical developmental advantage over its counterparts [9]. Current industrial wind turbines are primarily constructed in the form shown, in Figure 4. These turbines have three blades, variable gearbox, pitch and yaw control, and a generator housed in the nacelle of the structure [9].

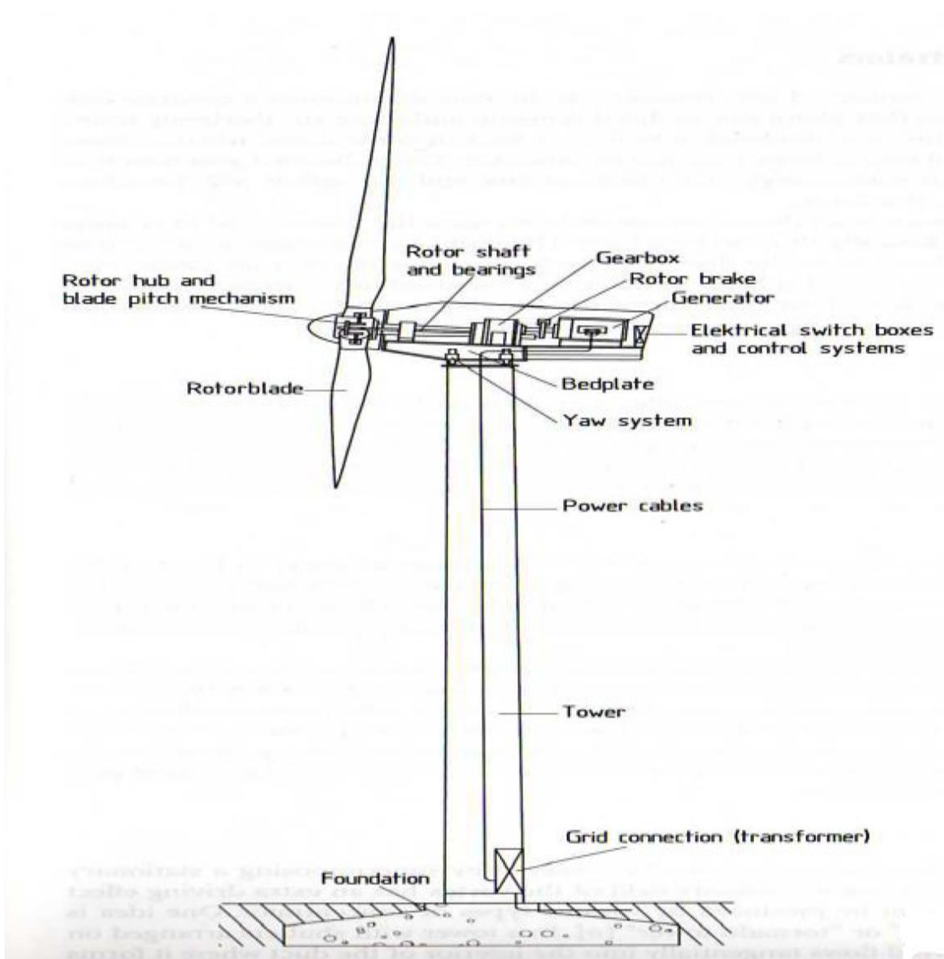

Figure 4. General Configuration of Current Industrial Wind Turbines [9]

Kinetic energy harvested by horizontal wind turbines is converted in to electrical power made available for societal consumption by Eqn. 1 below. Equation 1, developed by Albert Betz, characterizes the amount of power generated by any arbitrary energy converter in a free stream field of moving fluid [9]. Therefore, by evaluating its theoretical maximum an upper limit of efficiency can be determined. Quantifying this upper limit is thus useful in determining how efficient a turbine with integrated sensors and control surfaces can become.

$$\boldsymbol{P} = \tfrac{1}{4}\boldsymbol{\rho A}(\boldsymbol{v_1}^2 - \boldsymbol{v_2}^2)(\boldsymbol{v_1} + \boldsymbol{v_2}) \qquad (\boldsymbol{W}) \qquad \text{Equation 1}$$

P = power (W)
ρ = density (kg/m^3)
A = cross-sectional area (m^2)
v_1 = velocity before converter [before the turbine] (m/s)
v_2 = velocity after converter [after the turbine] (m/s)

The ratio between the power collected and the power present in the wind without the converter is defined as the "power coefficient" c_p.

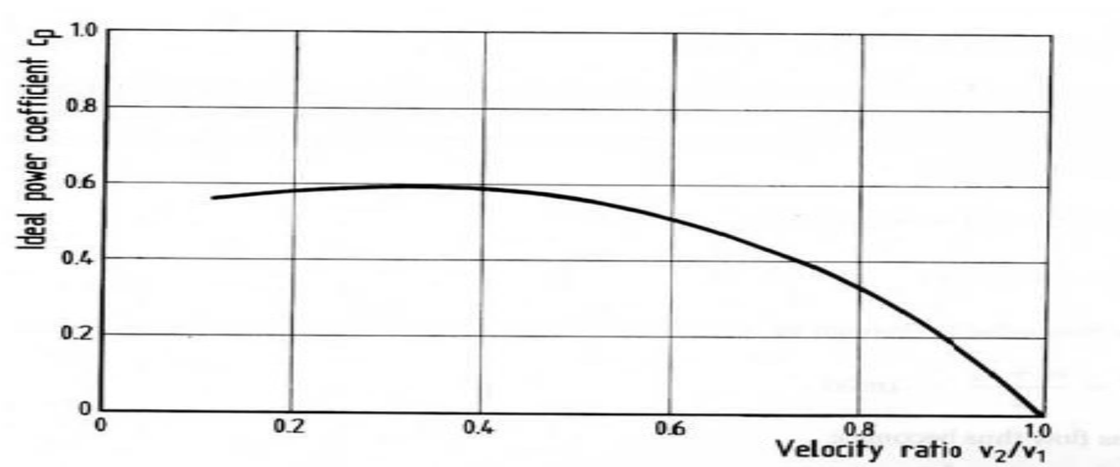

Figure 5. Curve of Convertible Wind Power over Contained Power as related to wind velocity downstream of the turbine over upstream wind velocity [9]

The coefficient is dependent on the ratio of downstream to upstream wind velocity, as seen in Figure 5. The maximum value is known as the "Betz factor" which has a nominal value of .593. The Betz factor represents the theoretical maximum amount of power which can be extracted from any free-stream airflow. However, this limit does not take into consideration the design of the energy converter. It is in the design of the converter where the phenomena of drag and lift affect the actual value of the power coefficient. Pure drag type wind converters can only harvest about 20% of the wind energy. The lack of efficiency in drag-wind converters is the reason current industrial wind turbines implement aerodynamic lift blade designs, into their construction. A more detailed description of Betz's work can be found in, *Wind Turbines,* by Erich Hau [9].

The designs of current industrial wind turbines employ this aerodynamic design for increased power conversion and results in loading which is unique to this design. Both drag based designs and lift based designs have load components, in the direction of air flow, and in the plane of the turbine blades. These loads are due to momentum transfer between the air and the blades. However, aerodynamic blades have additional load components due to the lift generated from the change in air velocity around the blades. The load profiles can be seen in Figure 6 [9]. These loads are highly dependent on the angle of attack of the leading edge of the blade into the incoming air flow, thus are dependent on the pitch of the blade. Successful integration of sensors as well as active control surfaces within wind turbine blades will need to anticipate these loading conditions.

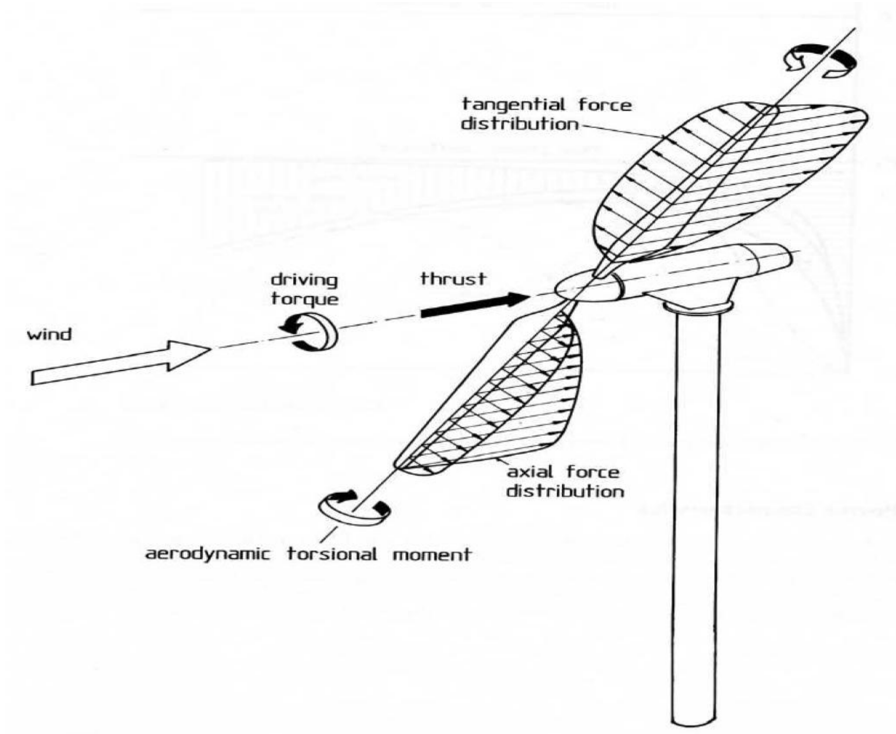

Figure 6. Characteristic load distribution on wind turbine blades [9]

Anticipation of these loads and the effect they have on the structure will lead to appropriate location choices, for both sensors and control surfaces.

Because of the dependence on pitch two different dominate methods of power control have been developed, active pitch control or passive or stall control. Passive control refers to wind turbines that are designed with a fixed angle of attack into the wind. Active pitch control systems can mechanically adjust the angle of attack of the wind turbine blades, which provides for the optimal performance of the wind turbine over an operational range of wind velocities. Inclusion of sensors into such a design is more difficult given the wider range of loading conditions. However, sensor integration would be beneficial for this design because of the ability of the sensor to inform the pitch control system of less than optimal positioning. The disadvantage of active pitch control is the additional weight and load complexity. However, unlike passive pitch control the blades of an active control method can be feathered out of the wind during extreme conditions. Feathering further reduces the loads on the blades which would have to be endured in a passive control system. The adjustability of active control translates into an increased power coefficient which can be seen in Figure 7 [9]. Clearly, sensor integration would aid in increasing the efficiency of the turbine.

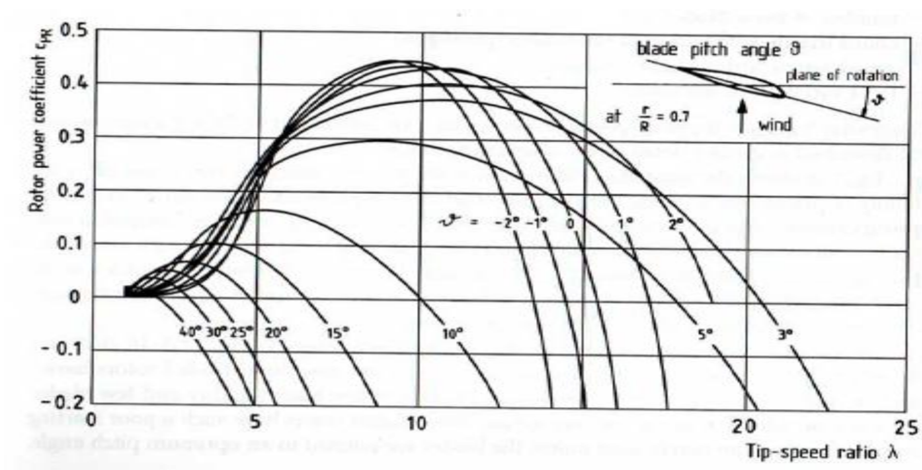

Figure 7. Array of Power Coefficient Curves as related to the ratio of angular blade tip speed over wind velocity through the turbine. [9]

To date active control systems have taken the lead in large scale models due to the disadvantages of passive control. Economically, it becomes harder to justify the increase in material needed to maintain the structural integrity of passive control designs. The aerodynamic designs begin to become unpredictable at the megawatt level and in operation the load fluctuation becomes intolerable. Therefore, large industrial wind turbines are generally constructed with active control systems [9]. The unpredictability of the aerodynamic design is un-doubtably being addressed and refined, but sensor integration could accelerate the process, achieving turbine design maturity sooner.

Most industrial wind turbine blades employ an aerodynamic design to increase the power coefficient. Design of an aerodynamic blade is not a trivial task. Still there are some basic rules to aid in the design process. First is the optimal aerodynamic shape of the blade itself. Without delving into the mathematics, Figure 8 shows the optimum rotor blade shape based on the blades tip speed ratio and the number of blades used. The optimal chord length follows a hyperbolic trend with respect to the wind turbine radius. Chord length references to the length between the leading edge and trailing edge of the blade. This shape produces some difficulties in manufacturing. First, such contours are difficult to reliably manufacture, and second, as Figure 8 would indicate, at high tip speed ratios the blade shape is too thin to successfully construct with adequate stiffness [9].

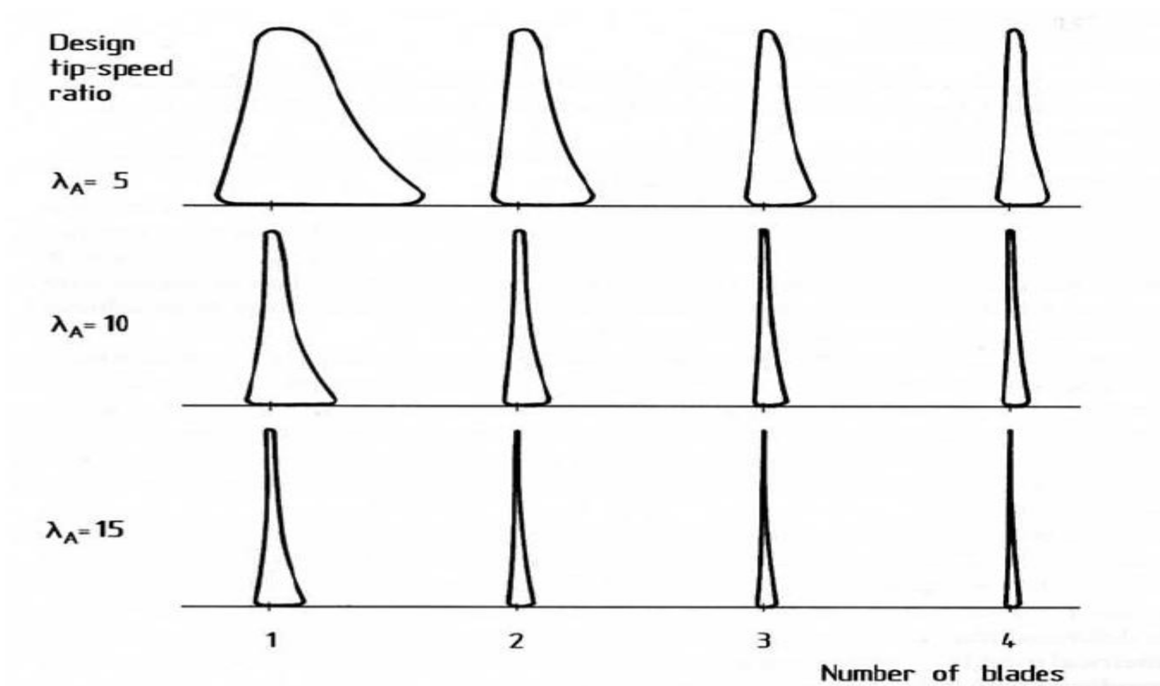

Figure 8. Array of Aerodynamically optimal blade contours [9]

It has been found that a trapezoidal shape is a good approximation of the optimal blade shape. There are only minimal differences between this design which is very feasible and the optimum. While a blade with its entire length conforming closely to this optimum shape has its advantages the most critical portion of the blade for power generation is the outer half [9]. Understanding the aerodynamic design behind current blades construction, allows for better placement of sensors and active control surfaces. Clearly, if the out half to the blade is the most critical, locating active control surfaces near the root is not cost affective. Contrary, placement of sensors at the tip to monitor material strain is not as beneficial because the tip does little to counteract the applied load.

In addition to this optimum blade shape the airfoil shape of the blades cross section is used to increase efficiency. The airfoil cross sections of wind turbine blades were developed from those used in the aviation industry. This approach is justified because of the similarities between the wind and aviation industry. The requirements placed on wind turbine blades are not identical to those for aircraft and therefore need special considerations. With this goal in mind the LS and SERI series airfoil shapes have been developed [9]. These designs minimize losses associated with surface roughness which is a significant problem for airfoil shapes. These design improvements for wind turbines can be seen in Figure 9, where the LS-1 blade design is considerably more resilient, with regard to surface roughness, the airfoil designs developed for aviation [9]. Blade cross section is important to sensor and control surface integration.

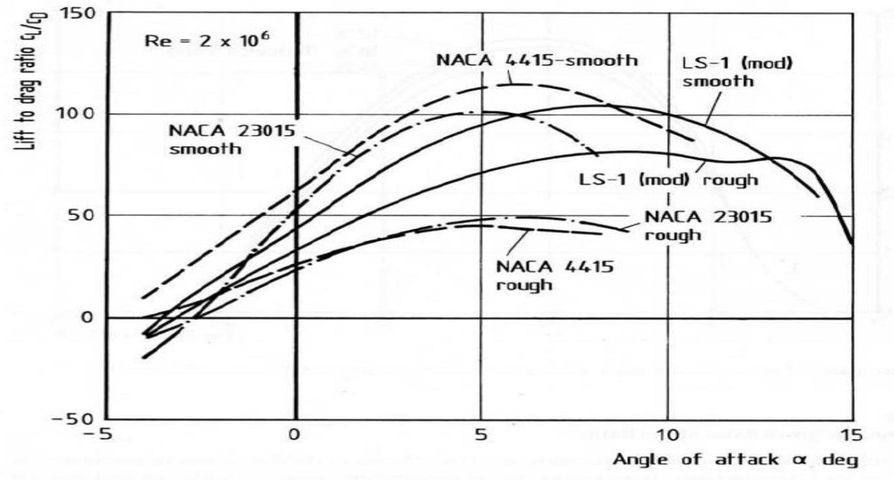

Figure 9. Effects of Surface roughness on lift to drag [9]

Because of the pressure difference developed by the aerofoil shape, any pressure sensor used to operate the turbine must be calibrated to the pressure difference at the sensors location.

The amount of wind energy that can be converted into electrical energy, and the design of the components to achieve this, all play a major role in the loads and stresses experienced by the assembled wind turbine. During operation there are numerous sources of loads, but all can be grouped into three distinct categories. Steady state loads which do not change in value greatly with the rotation of the rotor. Cyclic loads, which alternate depending on the orientation of the rotor. Lastly, stochastic loads are truly random. All loads associated with these three categories, which can be seen below in Figure 10, can occur independently and simultaneously depending on the situation [9]. To design for these loads and stresses, wind turbines are divided into classes, depending on what wind conditions they were designed for. Classes are generally based on average wind velocity, the maximum wind speed expected for a given duration, and the level of turbulence expected. Additionally, wind turbines are designed based on what are normal wind conditions and extreme wind conditions, the data from which has generally been collected from meteorological studies in the area of interest. Extreme wind conditions for obvious reasons, exclude natural disasters. Besides these load conditions wind turbines must also be developed to survive other influences, such as lightning strikes, ice accretion, solar radiation, and changes in air density.

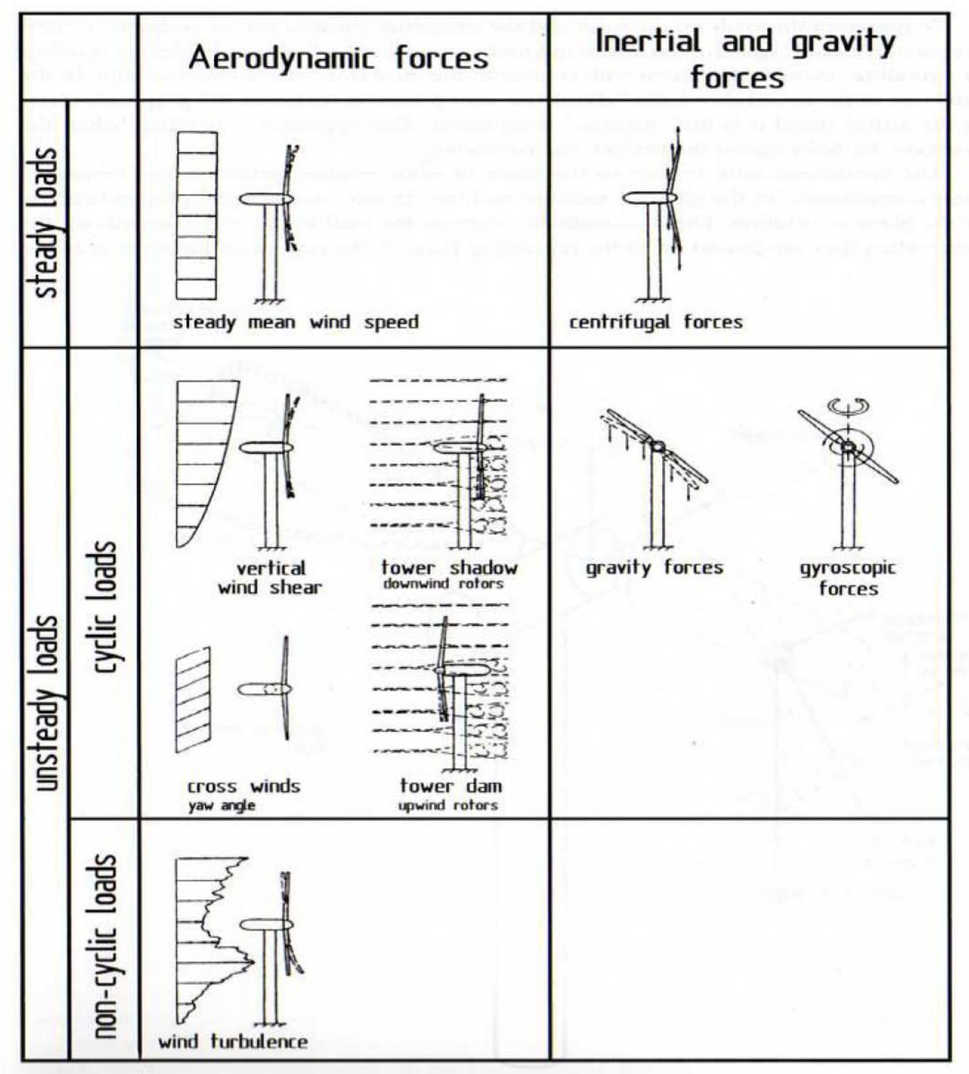

Figure 10. General Categories of loading components on wind turbines [9]

All these load conditions must consequently take into consideration the operating state of the wind turbine, for example start up, and shut down. By including these states of operation, the wind conditions can further be divided, into load cases over each state. Lastly, wind turbines are designed to withstand additional loads associated with failure of a subsystem, which could add stresses to the subsequent systems which are not covered by the load cases [9]. Addition of sensors and active control surfaces would add additional information to refine the load categories used in design, and increase design efficiency by allowing the blade structure to adapt to its environment.

Industrial wind turbine components are designed on an ultimate or limit load design basis, and on a fatigue design basis. In fact, many of the main components of a turbine are fatigue design driven, such as the blades which capture the wind energy, the gearbox bearing which stabilize the rotor axles, even the tower and nacelle in some designs. As seen in Figure 10 the number of load conditions which are cyclic or stochastic greatly outweigh those few steady state conditions. The two main sources of failure in industrial wind turbine are blades and gearboxes. Both of which are primarily designed on a fatigue basis [9]. Integration of sensors within the blades would allow for accurate monitoring of significant fatigue loading events. Active control surfaces in combination with integrated sensors would increase the longevity of a blade and subsequent components by reducing the magnitude and duration of the event.

The blades are the vehicle through which the wind's energy is captured and are subject to the full array of load cycles. The two primary sources of cyclic loading on wind turbine blades are wind velocity variations, which cause changes in load in the flapwise, and chordwise directions of the wind turbine blade, and gravitational loads associated with the weight of the blades themselves as the rotor rotates about its axis. Figure 11 below is an example of these two fatigue load components at work on the WKA-60 [9]. The chordwise bending moment is nearly constant throughout the load cycles with the flapwise bending moment decreasing as things progress. The reason for the decrease is that while the aerodynamic loads on the flapwise direction alternate with wind velocity, pitch, and yaw, the chordwise bending moments will always fluctuate with the same intensity as the wind turbine rotates. Leading to the notion that while fluctuations in wind velocity can produce ultimate loads with enough magnitude to damage the structure, the level of damage developed through fatigue of the blade in the chordwise direction may very well produce failure of the structure before such an extreme event could ever occur [9].

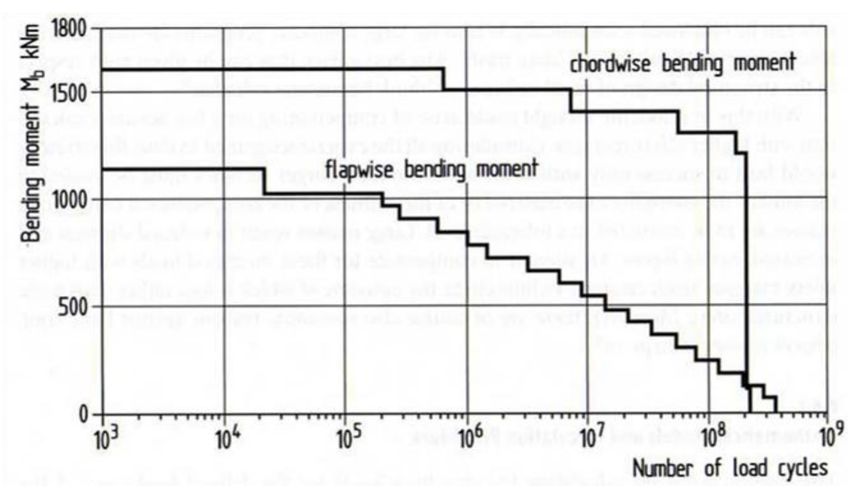

Figure 11. Stress magnitude of the two major directions on a blade as related to load cycles [9]

The results shown in Figure 11 were collected for an instrumented WKA-60. These results are indicative of most blades loading but without instrumentation this information is lost, hence the need for integrated sensors within turbine blades.

By understanding the load conditions likely to be experienced by the rotor blades the design of the blade structure was developed. These designs stem from those developed in the field of aeronautics. Current wind turbine blade cross sections are comprised of the outer aerofoil geometry with a bonded spar box and spar webs used to stiffen the blade in the longitudinal direction as can be seen in Figure 12 [9]. Smart composites, with integrated sensors, could reduce the safety factors on blade components by fully understanding the load conditions expected by the component in the field.

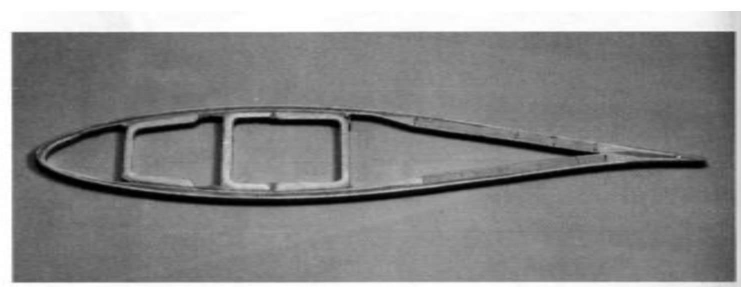

Figure 12. Typical Cross Section of Composite Wind Turbine blade [9]

These designs are currently constructed of fiber reinforced composites, because this material can not only be tailored to the load conditions but is a strong and stiff material compared to its weight. However, composite materials possess their own unique challenges with regard to connection with other components, which are constructed of metallic materials. Two current techniques used to achieve connection between components is the cross bolt connection, shown in Figure 13, and the bonded-in sleeve, shown in Figure 14.

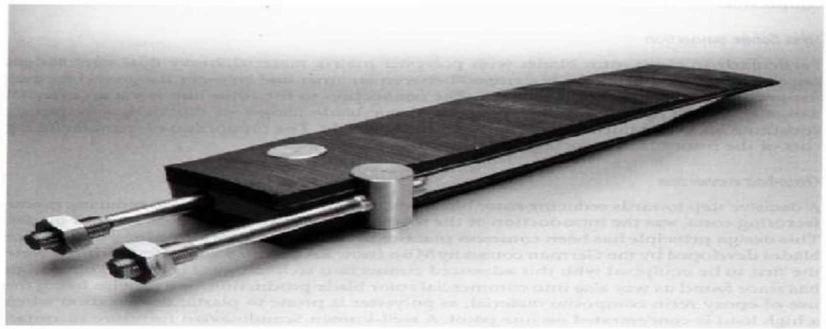

Figure 13. Cut away of cross bolt connection method used on turbine blades [9]

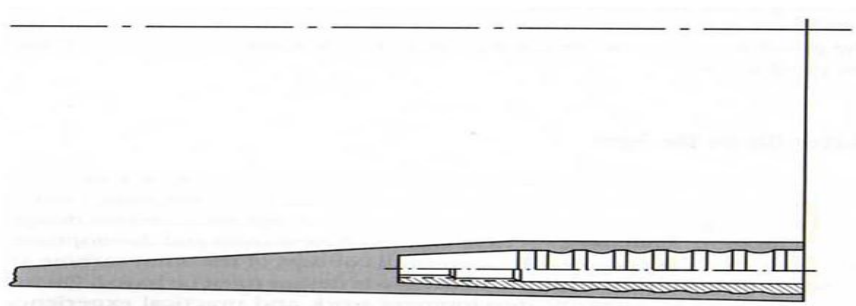

Figure 14. Connection sleeves bonded in blade root pioneered by Vestas [9]

These designs marry the ability to reliably fasten the blades to the rotor hub while not adding undue weight to an already massive structure [9]. Regions of blade construction such as these are however more susceptible to composite failure which if monitored by sensors could be detected prior to catastrophic failure.

Current industrial wind turbines employ active pitch controls to address these load conditions. The ability to control the magnitude of these loads can increase structural survivability [9]. Active control surfaces such as flaps and false walls combined with structural health monitoring systems could aid in controlling these loads.

While the load conditions seen by the blades of a wind turbine are primarily determined by the aerodynamics of wind flow over the blades, this is not the case for the turbines mechanical drive train. The conversion of the kinetic energy to mechanical energy is the sole purpose of the blades and is governed by aerodynamics. The drive train of the wind turbine is designed to convert that mechanical energy into electrical energy. These components are conventional for power plant technology, but it is the unique use which poses problems for an otherwise mature form of technology [6].

Drive train refers to the rotor hub, low speed axle, gear box, high speed axle, brake, and generator; other components are included but these are the primary components needed for successful mechanical electrical conversion. There are several different possibilities of arrangement of these components, but there are only two that are current standard system designs. The first of which is the series connection from the hub to the gearbox, via the low speed axle, and then to the generator through the high speed axle, which has the brake mounted to it. The other is the direct rotor driven generator design were the rotor hub is directly connected to the generator. The latter design has the advantage of reliability and servicing. Both designs can be seen in Figures 15 and 16 below, but the series design is the dominate design in industry [9]. Of the primary components used in the construction of the turbine one stands, in current history, as the component most susceptible to premature failure despite no fundamental deficiency in design approach.

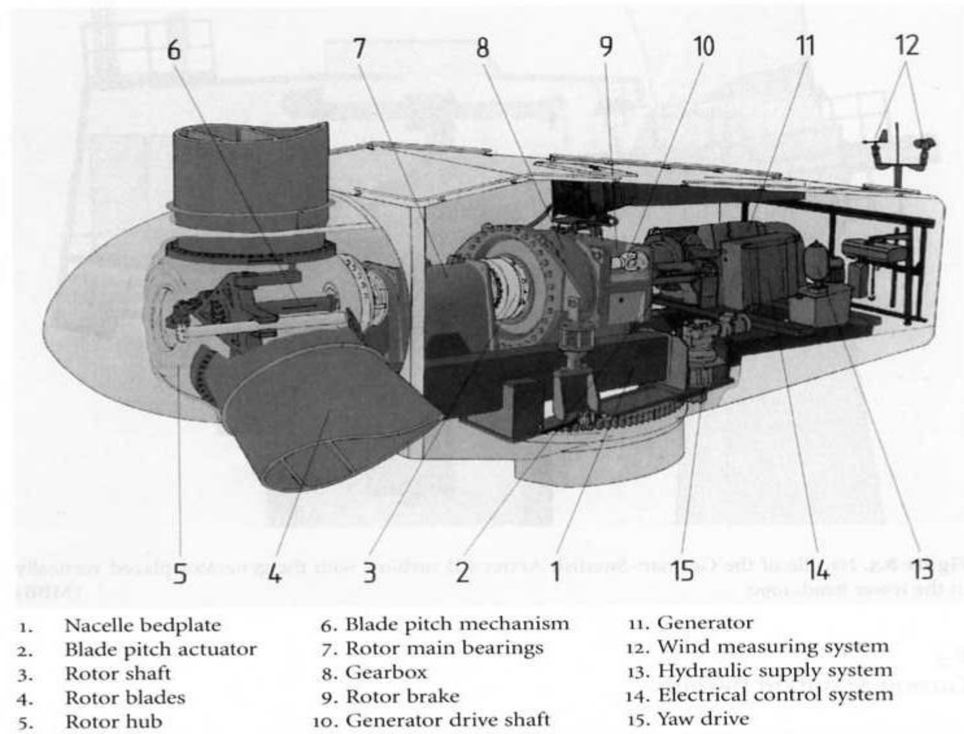

Figure 15. Traditional Series Configuration of Wind Turbine Drive train [9]

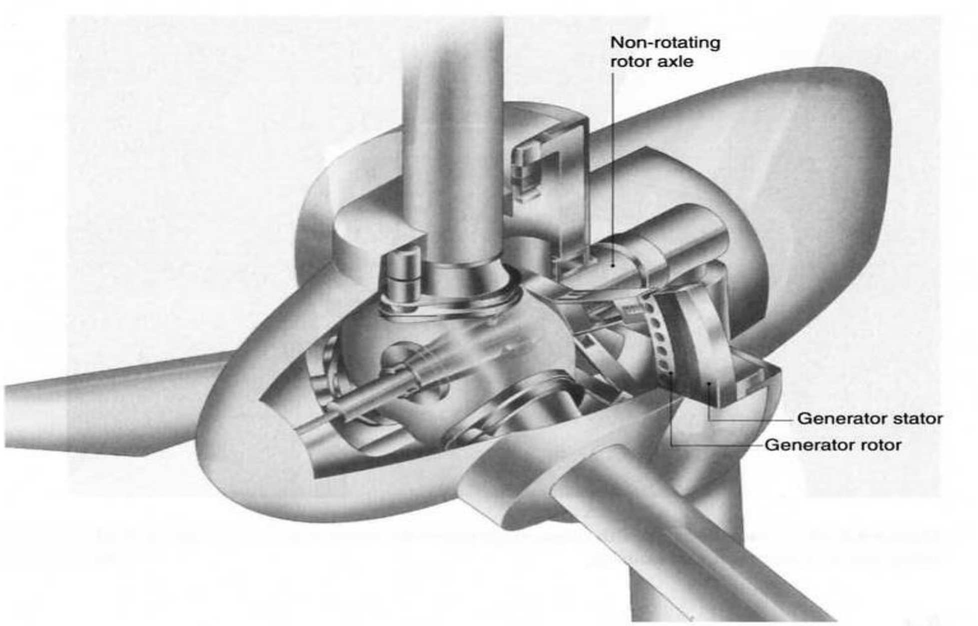

Figure 16. Configuration of Direct Rotor-Generator Drive train [9]

That component is the gearbox used in the series connection design. Originally, these problems were most likely due to inaccurate assessment of the loads on the gearbox however this does not appear to be the source of the problem [9].

The integration of the gearbox into the wind turbine has primarily fallen into one design. Generally, it involves one roller bearing, on the low speed axle close to the rotor hub and two Trunnion mounts, which attach the gearbox to the bedplate of the nacelle, as seen in Figure 17 below. These Trunnion mounts, generally, are connected to the bedplate via elastomeric materials to reduce noise emissions [6][9].

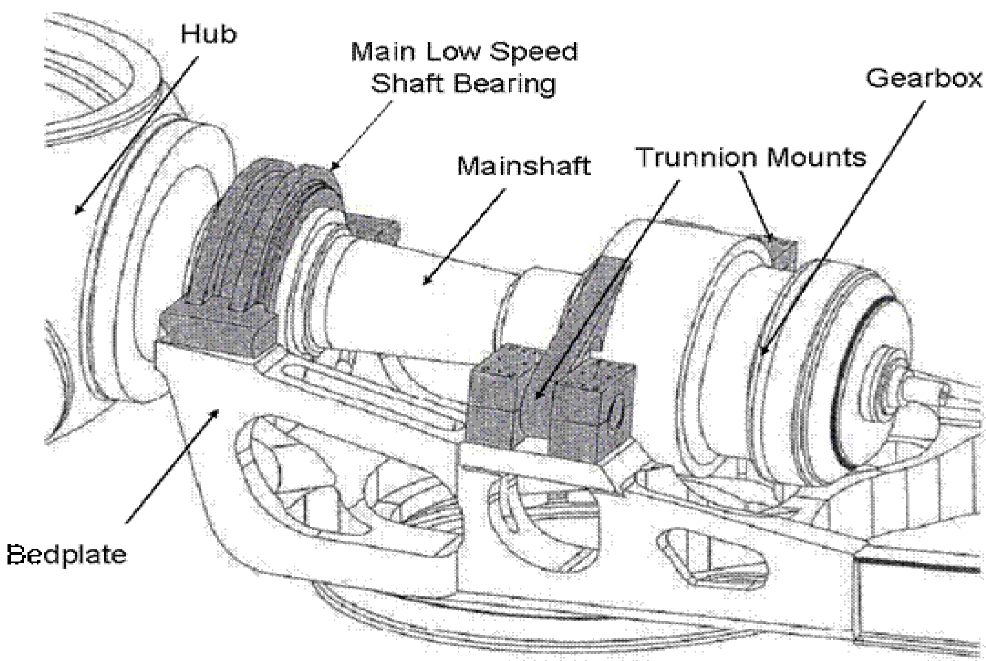

Figure 17. Traditional Three Point Slow Speed Axle and Gearbox Mounting [6]

The Trunnion configuration is preferable over other designs, such as two separate bearing supporting the low speed axle, because of the reduced size and weight placed on the tower. However, the three point mounting does place additional loads on the gearbox, which could be avoided in a two bearing design [6].

Due to the great difference in rotational speed of the low speed axle and the high speed axle, turbine gearboxes are, primarily, a modified planetary gear configuration [6]. The reason for this is the increase gear ratio per stage of the planetary gear configuration as well as the significant reduction in gearbox size and weight over the parallel shaft system. The gearbox is modified from traditional planetary gearbox design because it marries the parallel gearbox approach with the planetary gearbox.

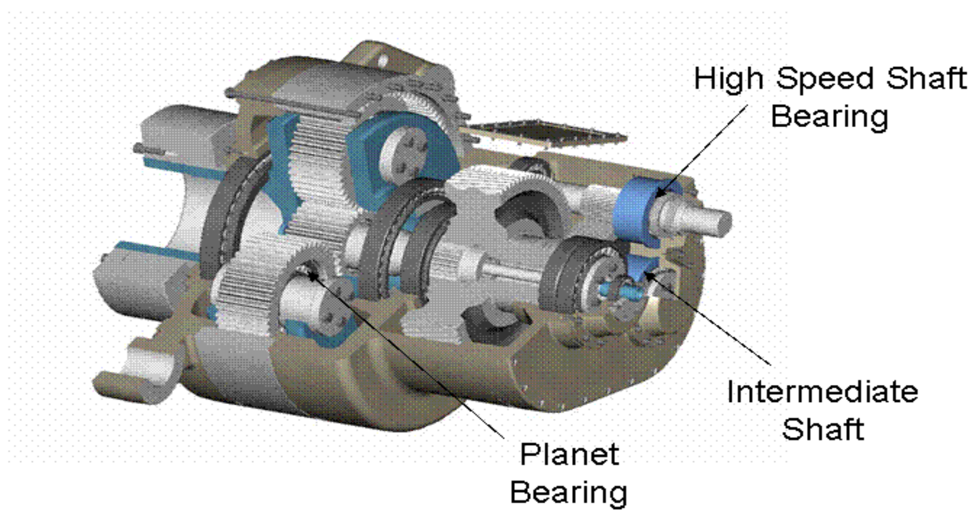

Figure 18. General Modified Gearbox Configuration used in Wind Turbines [6]

The justification for this approach is that by including the parallel gear design the low speed and high speed axles are no longer coaxial. This allows for easy supply of power through the low speed axle to the pitch control components in the hub. The modified planetary configuration of the gearbox has three bearing locations which are susceptible to failure, the planetary gear bearing, intermediate shaft-locating bearing and the high speed shaft-locating bearing [6]. Figure 18, was a clear view of the three bearing locations which have shown consistent failures despite sound bearing design considerations. While these failures are not completely understood further field testing is underway to try and evaluate these sources. By integrating load monitoring systems in turbine blades a direct correlation between loads seen by the blades and their effect on the gearbox can be developed. By correlating the loading between components active control surfaced could be employed to reduce the amount of premature gearbox failures.

Lastly, integration of sensors and active control surfaces would decrease the stochastic electrical output of the generator. Pitch control is currently used to smooth the power generation over time but fluctuations are still present [9]. The effect of this approach can be seen, in Figure 19 below.

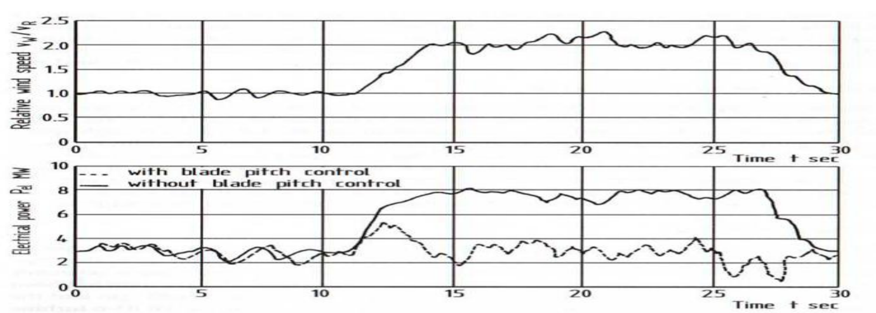

Figure 19. Generator power smoothing using blade pitch control [9]

Besides gearboxes and blades, one of the more frequent failures is that of the electrical converter components used to manipulate the electrical power prior to introduction within the power grid [10]. Smoothing the power generated by developing smart blades capable of constantly tailoring themselves would greatly reduce the failure of these components, and further increasing efficiency and operation time.

These issues only briefly touch on what is a very dynamic and complex system, which has been in use for centuries. By systematically addressing these issues wind turbines can become a more efficient and economically attractive form of energy capture, than is currently possible. A further detailed discussion of the design basis used in current wind turbine construction can be found in Appendix A; Technical Background of Wind Turbines.

Active Control Surfaces

"Active control surfaces" refers to portion of a blade that can be activated to alter the flow of the fluid over the cross-section. This is how current aircraft maneuver during flight [4]. Considering the similarities between turbine blades and aircraft wings, it is feasible that an emerging technology, such as wind turbines, would employ active control surfaces a system to improve reliability.

Exploration into the logistics of including these control surfaces within wind turbine blades has already been initiated. Scott Johnson, C.P van Dam of the University of California (Davis) and Dale Berg of Sandia National Labs developed a case study of potential active control surfaces that could prove to be beneficial for wind turbines [11]. Delving into prototype design, construction, and testing, James Blockey of Montana State University in conjunction with Jonathan Ehersman , constructed several prototypes of a deployable Gurney flap and false wall [4] [12]. An active control surface, developed for wind turbines by Flexsys Wind Energy, employs an adaptive trailing edge that could be actuated by structural monitoring sensors [13].

Each form of active control surface possesses its own challenges to successful construction of the blade. James Blockey and Jonathan Ehersman removed a sizeable section of the trailing edge to integrate the Gurney flap prototype [4] [12]. Removal of the section in operation would have a significant effect on the structural stability of the blade. Stress concentration around the cut out would be likely initiation points for delamination, as well as mounting brackets used to fasten the Gurney flap to the blade. False walls and adaptive trailing edged mounted to spars in the blade would also produce locations susceptible to premature failure. All of which through detailed research and design could be overcome with the help of integrated sensors.

Research and design would not be focused only around the region of control surface. Integration of the active control surface would also introduce new loading scenarios. Full deployment of the Gurney flap during operation of the turbine would result in torque on the blade which would need to be counteracted by the pitch controls. Also, change in the mass distribution would alter the natural frequencies, and required starting torque of the rotor leading to further redesign of the system. By developing a means through which to monitor such events a fuller picture can be developed at a rate not currently seen in industry. Hence the necessity of exploration into integrated structural health monitoring systems.

Composite Design

Industrial wind turbines employ composite materials in blade construction. The capability to tailor the material's architecture and the materials favorable strength to weight characteristics are the reason for its use. These advantages are not without cost.

The extra degrees of freedom inherent in the use of fiber reinforcements, is often a double edged sword, increasing the complexity of design considerations and material response. The increased complexity would also extent to the inclusion of sensors and active control surface mounts. Knowledge of composite design, and response, aids in addressing this complexity.

Fiber reinforce composite materials derive their stiffness and strength through the combination of two separate materials. As the name suggests fibers of a stiffer material are used to reinforce a second more compliant material. As it relates to the wind industry, composite materials are generally constructed by combining glass fibers or carbon fibers with some thermoset plastic such as epoxy, vinyl-ester, or polyester. Fundamentally the greater the amount of fiber reinforcement within a given volume the stiffer and stronger the composite is in the direction of the fiber. So a composite structure constructed with a higher “fiber volume fraction” will exhibit a response more characteristic of the fibrous material than that of the binding or matrix material. The complexity of the material stems from the fact that such a construction is inherently heterogeneous [14][15]. Characterization of even one layer of fabric saturated with resin, know as a ply, is nontrivial. Compliance of this built up material can be semi-accurately derived, with the knowledge of several parameters, of both the fiber and the matrix. These parameters along with the ratio of fiber to either the overall volume or weight of the combined constituents, completes the information needed to characterize the ply. Development of a global constitutive response of the combined plies is developed through coordinate transformation and assumptions developed in the characterization of plate stiffness; which are valid for composites materials due to their similarity in nature [14].

The strength of fiber reinforced materials does not share the same simplicity as stiffness. Accurate strength values can be obscured by the complex relationship between modes of failure, which can independently or collaboratively work to compromise the performance of the structure. Forms of failure can initiate because of fiber rupture, matrix cracking, fiber/matrix de-bonding, and delaminating [16]. The intimate relationship between fibers and the matrix generally inhibit conclusive initial failure mode identification and therefore has been found to be impractical [15]. However, delamination; separation of the individual plies in the material layup, is among the most severe form of composite failure. Delamination can cause significant reductions in global material compliance, leading to unfavorable load response and catastrophic failure [16].

Delamination poses a critical concern in construction of turbine blades. Delamination in such a large structure, which is extremely heterogeneous due to the thick fabrics employed in construction, leading to a reduced compliancy response could spell disaster. Delamination stems from stress concentrations, in the material, which emerge from geometrical discontinuities, such as, ply drops and edge effects [16]. Ply drops have shown to be a considerable issue, with regards, to delamination. Thick fabrics (greater than 1.0mm for fiberglass, and 0.6mm for carbon fiber), used in industry, produce large geometrical discontinuities, which have been shown to cause delamination at ply drops and ply joints. These delaminations were not exclusively developed by large load conditions; in fact the material failures initiated, in otherwise good quality test coupons, at strain levels in the range of 0.2 to 0.4% [17].

While fiber reinforced composite materials are favorable, especially for wind turbine blade construction, there is a level of care needed that is not shared with its metallic material counterparts. Due to the heterogeneity of the material, detailed evaluation of strength and stiffness is paramount to a successful design. Any variable, be it a ply drop, unfavorable composite architecture, or inclusion of sensors, could introduce premature failure.

Sensors

Integration of sensors within wind turbine blades requires background knowledge of sensors. The development of sensors derives from the need to successfully monitor and evaluate parameters of interest which are otherwise unknown. These parameters are known as measurands [18]. Depending on the measurand, an array of sensing elements can be used to detect changes in the measurand. These sensing elements have some characteristics which are favorable for the job; be it a change in density, change in electrical resistance, or in physical appearance. Accurate evaluation of the changes in measurands, via sensors, can be used to characterize the measurand response to confirm a theory or to develop new theories which advance technology.

Sensors have been developed for a myriad of purposes; material strain, position, load, acceleration, flow rate, temperature, etc. Within these measurands different groupings of sensors have been developed depending on the conditions. For example, position can be monitored by several traditional types of sensors; linear variable differential transformers (LVDTs), potentiometers, and digital image correlation using cameras and computer software. All of these sensors can easily be used to accurately measure strain of a material, given the correct configuration. An alternate, strain could be monitored directly via a resistive strain gage. While a strain gage could be successfully bonded to a test specimen and data collected, this may not be the correct approach, if the material is compliant compared to that of the strain gage.

Correctly determining which sensor is best suited is complex. Things to consider when evaluating which sensor will be best suited:

- Exactly what is the variable of interest? Stress may be the desired variable, but knowing how to accurately monitor the measurand is not as simple.
- Knowing the principles behind the operation of the sensor is vital. Without this knowledge, problems in signal or response retrieval could never be solved. Additionally, knowledge of the sensor operation ensures that the sensor is used within the correct range of conditions.
- Understanding how the sensor will interact with the measurand is important. If the sensor disturbs the response of the measurand, accurate data will not be collected.
- Knowing the conditions the sensor will be exposed to will prevent potential inaccuracies. For example, LVDTs measure position by modifying the spatial distribution of an alternating magnetic field [18].

Employing such a sensor in an area prone to high magnetic fields could prove to be problematic.

- How the signal from the sensor will be retrieved is a necessary requirement for accurate data. If the equipment used, to record the sensors response, is ill equip to monitor the sensors the data can be compromised.
- Signal conditioning is different for every sensor and understanding the complexity behind this can save valuable time.

Navigating the quagmire of considerations takes experience and time but careful consideration can pay off immensely.

Signal Conditioning

Any sensor embedded in a wind turbine must be conditioned to accuracy monitor the given measurand of interest. There are considerable advantages to electrical signal measurements. These advantages are the reason most modern engineering measurements use sensors with electrical outputs [18]. Signals from these sensors must be conditioned to ensure accurate data. Conditioning is an important step in the process, if adequate care is not given to signal conditioning, major errors can be introduced during this step of the process.

Signal conditioners are as numerous as the sensors they condition. The difficulty is in correctly conditioning the signal. Sensor signals commonly appear as changes in resistance, capacity, voltage, and frequency, current or electrical charge [18]. These signals can be sensitive to external stimuli, or are not in the proper form for the signal processer to retrieve. Signal conditioning serves many functions in addressing this issue, to name a few.

- Amplification
- Filtering
- Linearization
- Conversion of resistance to voltage
- Signal combination with reference.

One of the most prevalent disruptions to signal retrieval is noise. Noise is a byproduct of the second law of thermodynamics. The issue is that noise manifests in many ways, therefore, it must be addressed on a situation to situation basis. For example, elimination of noise, in the system, is impractical; differentiating the signal from the noise is the preferred method. To accomplish the differentiation, prior knowledge of the type of noise is beneficial. If the noise is at a low frequency, a high pass filter can be developed, to restrict the signal processer from viewing the noise in the system. No matter the circumstances noise will always be an issue [19]

SENSORS

The primary goal of this study was to explore and evaluate the integration of sensors into fiber reinforced composites used in the wind industry. Sensor selection preceded the investigation, but before sensor selection, conditions important to monitor in an industrial wind turbine, were evaluated using a decision matrix, shown in Table 1. Within this group of sensors there are two subcategories, sensors considered for embedment, and sensors considered for external adhesion.

Table 1. Decision Matrix of what conditions on an industrial blade were deemed important. [20]

What to sense	Why to Sense	Comments	How	Where (location)	Final
Wind Velocity	Exteme wind velocities for monitoring limitations	May already be velocity sensors on turbines, but used to identify possible failure situations.	Wind speed sensor, Anemometer	Top of tower or Nacelle	9
Temperature	Extreme variations to correspond with other data and corrections.	May already be temperature sensors on turbines, but used to identify possible failure situations.	Thermocouple, RTD, digital thermometers	Top of tower or Nacelle	6
Blade Strain	Check for extreme strain along blade length and leading/trailing edges.	Checking for delamination and strain at different positions along the blade	Metal Foil, Piezoelectrics, Fiber Optics	At various locations along blade: base, max chord length, tip, leading and trailing edges	1
Moisture/ Humidity	Moisture could effect material properties.	Moisture accumulation along blade.	Impedance moisture sensors	Atmosphere location, Top of tower or Nacelle	5
Angular Position	To correct with other acquried data for efficiency purposes.	Used in conjunction with optimizing efficiency.	In conjunction with other trim adjustment systems.	Base of blades	8
Torque	Possible torsion at base of blades.	Torque could lead to blade failure.	Infrared (IR), FM transmitter, Strain Gages	Base of the blade towards Nacelle	10
Loading	Excessive loads will lead to fatigue.	Modeling of design or life purposes.	Associated with Strain	Various locations along blade length	7
Blade Acceleration	Extreme changes in velocity could lead to failure.	To model excessive changes in force.	Piezoelectirc Accelerometers, Capacitive Accelerometers, MEMS	Internally at tip where acceleration is greatest	4
Blade Tip Deflection	To avoid tower strikes	Keep overall blade tip deflection in check.	Optical, Infared (IR), Accelerometers	Attached to base at blade length to sense blade tip position	2
Blade Imperfections	To check for impurities within blade material.	non-destructive testing, cracks, voids	Ultrasonic, Acoustics	Ideally along entire blade length	3

Blade strain was considered paramount, thus multiple forms of strain sensors were considered. Any condition in Table 1 assigned a value greater than 6 was deemed an unnecessary condition to monitor during turbine operations either because of its importance to operation or that it could be monitored indirectly by other sensors.

Sensors Investigated

Based on the conditions considered significant to turbine operation and blade health, a list of sensors was developed. All choices made were based on cost, performance, and geometry. The motivation behind the sensors chosen, as well as, comments on their limitations can be found in Table 2.

Table 2. Sensor groups considered in composites integration study. [21]

Sensors	**Impetus**	**Comments**
Metal Foil Strain Gages	Reliable, well understood strain sensor with a relatively low profile. Relatively in expensive	not well known as a reliable long term sensor in an environment were cyclical loading is present. Strain range is considerably less that that of figerglass composites
Piezoelectric Films	Great dynamic strain sensor, also capable of monitoring temperature fluctuations, without a supply source	Not a reliable static load strain sensor. Also very sespeptable to electromagnetic interference
Fiber Optic Cables	Innovative, strain sensor capable of monitoring strain in multiple location using one fiber. Capable of also monitoring temperature changes.	While not sespeptable to electromagnetic intereference, the sensor integration into manufacturing is formattable due to the brittle nature of the fibers.
Thermocouple	Simple, accurate sensor to monitor blade temperature	Due to the Seebeck effect a reference junction is needed
Ambient Humidity Sensor	Determine humidty levels which might be detremental to blade longevity	Profile would make embeddment problematic as well as potentially increasing drag if placed on the exterior of the blade
Tri-axis Accelerometer	reliable way of monitoring the forces applied to the surface of the blades	size of sensor could inhibit embeddment
Infrared emitter	Initernal flaw detection	Increased drag on blade, as well as limited viewing window.

Metal Foil Strain Gages

Metal foil strain gages (MFSG) were chosen because of their maturity, cost and geometry. Electrically resistive strain gages are a common device, used since the 1930s [22]. The linear relationship between strain and electrical resistance makes for an easily integrated sensor which can be monitored with little issue. Metal foil strain gages currently range in cost from 5 to 30 dollars depending on the number of gages desired in a given foot print [22]. Cost is small in comparison to the cost of production of one blade, which can range any were from 20,000 to 325,000 dollars depending on the size of the blade constructed [23]. The general geometry of these strain gages is typically in the range of $10mm^2$ to $200mm^2$ in area and thicknesses between .03mm and .1mm [22]. IN comparison, fiber glass reinforcements are generally 10μm to 20μm in diameter. The discrepancy in size is significant at the microscopic level, but at the macroscopic level , with material thicknesses in the range of a 1mm to .25m, the size of these sensors are not as important.

Electrically resistive strain gages were used in both configurations considered; internal integration, with composite laminates and external adhesion. The reason for external adhesion was that such integration was the originally intended form of connection with the composite host material. Internal integration of these strain sensors was considered because of the low profile, compared to other sensors. The hypothesis behind this choice was that a low profile sensor would be less of a geometrical discontinuity, and thus minimize the potential for delamination at the interface between material matrix and sensor coating.

These sensors are not without limitations, especially with regard to wind turbine blade applications. Metal foil strain gages as the name suggests are constructed from thin metal foil sheets and bonded to a plastic backing. This form of adhesion is perfect for applications where the host material is similar in response, for example low-strength steel which at yield generally has only strained .14% [18]. Fiber glass composites, however, can strain up to 3% before failure compromises the material. The difference in strain limits suggests potential accuracy problems, in high strain conditions. Additional issues of signal drift, temperature dependent resistance changes, and sensor fatigue life, also pose a problem.

Polyvinylidene Fluoride (PVDF)

Polyvinylidene Fluoride films, better known as PVDF films, are a category of piezoelectric material. PVDF films consist of long repeating monomer chains with an inherent dipole moment due to the monomers atomic structure. By solidifying and stretching the material a permanent dipole moment is imparted to the material. This net dipole moment means if strained the material will produce a similar piezoelectric response to that of traditional piezoelectric materials [24]. The piezoelectric effect can be exploited to produce strain sensors which do not require any external electrical source, making PVDF films an attractive strain sensor for wind turbine applications. PVDF films due to their polymer composition are able to handle the high strain condition present in fiber reinforced composites. Additional characteristics leading to the consideration of PVDF films as strain sensors, was the versatility to tailor the sensor geometry, and high fatigue life.

PVDF films were also considered for internal and external integration. External adhesion again was the primary form of connection for these sensors. Internal embedment was studied because the versatility to tailor the geometry.

Limitations of this category of strain sensor manifest in the realm of strain conditions. PVDF films exhibit a high level of sensitivity, but are unable to maintain the charge once developed due to the strain of the host material. This is of little concern in highly dynamic systems, which do no experience an underlying sustained load. Industrial wind turbines rarely experience this scenario; generally during operation blades experience load fluctuations about some mean load, as detailed previously. For this reason PVDF films signals are conditioned with a charge amplifier, which retards the decay of the charge generated. These charge amplifiers are easily adjusted depending on the time frame of interest. In other words, the charge amplifier can be tailored to the level of retardation desired. Adjustability is beneficial but does not eliminate the sensors time dependency. If the charge amplifier is set for too long of a time period, there is a potential for inaccuracies to develop. The potential inaccuracies are due to the extreme retardation of the charge decay. If the charge amplifier is too effective, dynamic reductions in loading could be missed, leading to an inaccurate loading regime.

Fiber Optics

Fiber optics refers to a system which effectively transmits light from one location to another. Every fiber optics system consists of at least three components, a light source, a fiber, and a receiver [25]. Depending on the application, the light source can be one of several things, a conventional light bulb, light emitting diode (LED), or a laser. The receiver is simply an electrical device capable of picking up the light from the source and converting it back into an electrical signal. The fiber consists of a thin strand of glass or plastic with a second glass or plastic layer surrounding the first, which connects the light source to the receiver. The fiber optic used, governs which type of transmitter and receiver is employed.

Fiber optics function based on the process of total internal reflection. Total internal reflection is caused by the fact that light travels at different velocities, in different media. The difference in velocity as compared to the speed of light in a vacuum is known as the refractive index. Thus, if two materials are in contact with each other and have different indexes of refraction, any light which encounters this interface between materials will be bent, and this bending is known as refraction. Total internal reflection employs this effect, characterized by Snell's Law (Eqn 2), to minimize the amount of light which travels across the interface.

$$\boldsymbol{n_1 \sin(\theta_1) = n_2 \sin(\theta_2)} \qquad \text{Equation 2}$$

n_1 = index of refraction for material 1
n_2 = index of refraction for material 2
θ_1 = angle off 90^o light is indicate on interface in material 1
θ_2 = angle off 90^o light is indicate on interface in material 2

Snell's law is characterized by the angle θ which is measured from a plane normal to the interface and the index of refraction n of the materials which compose the interface. If the light is incident on the interface, at an angle great enough, the light will be completely reflected inward on the first material. By exploiting this physical phenomena, light can be contained within a material given that the interior media, known as the core, has a greater index of refraction than that of the surrounding media, known as the cladding [25]. Now, light can enter the fiber from many different angles, and travel the length of the fiber, at different time periods. While this is a simplification, it serves to illustrate the difference between multimode fibers and single-mode fibers Multimode fibers have a larger core which can support more wavelengths of light at one time. Single mode fibers have a smaller core, thus limiting the wavelengths that can propagate through the fiber at any given instant [25]. While there are more details associated with the principles of how fiber optics function, including modal noise, graded indexes, and connection losses the fundamentals will suffice.

Fiber optics are constructed without additional layers. A diagram of general fiber optic construction can be found below Figure 20. A buffer coating is added to strengthen the fiber optic, and also to partially increase the effectiveness of the fiber. The polymer jacket protects the fiber from damage.

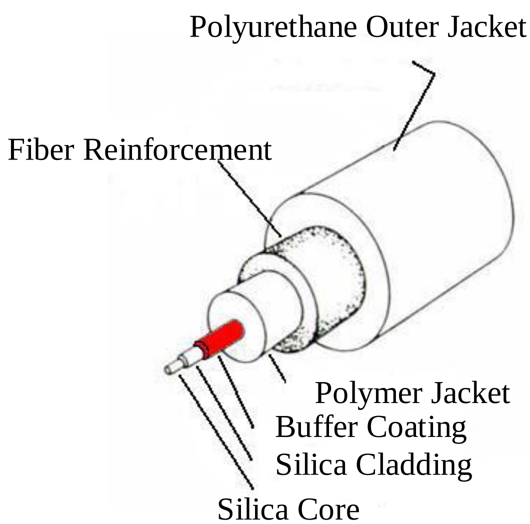

Figure 20. Generalized Construction of Fiber Optic Cables [4]

Fiber reinforcements allow the fiber optic to move within the polyurethane out jacket to prevent bending the fiber past its minimum bend radius. This construction was not designed for fibers which are implemented as structural sensors. So any fiber that is obtained in this form must be stripped of the out layers, specifically the outer jacket, fiber reinforcement, and polymer jacket, in order to be viable as a sensor.

Thus far, 60 parameters have been found which can be measured by fiber optics. Some of these parameters include temperature, strain, pressure, vibration, and rotation velocity [26]. Not all of these parameters need quantification in wind turbine blades, and thus only a few of the parameters were used. The first was as a simple flaw detector; as a crack in the structure propagates to and through a fiber, either internally or externally configured, this flaw will most likely damage the fiber in the process. The amount of light that is transferred through this crack in the fiber will be reduced thus indicating damage in the structure. Sophisticated transmitters and receivers can be employed to determine the exact location of the damage and steps can be taken to resolve the issue. Second, fiber optics can be used as temperature sensors because the refractive index is temperature dependent, and a shift in signal of an un-damaged, unstressed fiber, can be used to quantify the change in temperature. The last main form in which fiber optics can be employed in turbines requires a Fiber Bragg Grating. The details of how the grating is constructed in the fiber is not necessary here, the consequences of this grating will suffice. Fiber Bragg Grating refers to a periodic change in index of refraction within the core fiber. The periodic change in index causes the light signal to reflect some of the signal back down the fiber while allowing the remaining signal to pass. By doing this the receiver which is generally integrated with the transmitter will receive several portions of the original signal at different times, similar in concept to echolocation. Fiber Bragg Grating allows the fiber to accurately monitor the strain of a structure if securely bonded to it. By straining the structure, the strain creates a change in periodic signal return, due to the increased time of flight between changes in refractive index.

Single mode fiber optics, without Fiber Bragg Grating, were considered for both forms of integration with industrial wind turbine blades. Externally, the logistics were very similar to that of the PVDF films and MFSGs. Internally, again the low profile of the sensor made it a viable sensor for embedment. Additionally, fiber optics were considered because of the vast range of conditions, which could be monitored by this one form of sensor. Also, signals of light are not as prone to electromagnetic interference which could be a factor in turbines.

Fiber optics have several significant draw backs. First, fiber optics are not a very repeatable sensor. Connection losses, alignment issues, and the handling history make the optical signal strength unique to each fiber. These issues make it very difficult to compare signal strength between like fibers. Even with one fiber, connection losses can be considerably different if the fiber optic is disconnected and reconnected from the transmitter and receiver. Fiber optics for most purposes are constructed of glass and the brittle nature of this material makes it prone to cracks. The brittle nature of glass led to minimum bend radii recommendations for fiber optics to prevent this crack growth. The brittle behavior of glass also makes manufacturing very difficult. Unlike PVDF films and the electrically resistive sensors, handling vastly increases the risk of damage to the sensor, making it potentially un-useable. The last main drawback to fiber optics is the current cost. Wind industry does not share its aeronautic brethren's rather significant budget per structure, and therefore cannot easily afford new and innovative forms of technology, which might prove beneficial for turbine performance and longevity. The fibers are not the costly portion of this technology; it is the precise nature of the instrumentation, which is needed to successfully monitor the fiber that carries the high price tags. To simply monitor the signal strength through a fiber optic without Bragg Gratings, assuming connectors are already on the fiber, run any were from 1,000 dollars to 5,000 dollars, for the light source and receiver (power meter). Additional components such as fiber cleaver, mechanical or fusion splicers, connectors, splitters, and patch cords can bring the cost for monitoring that fiber up to 10,000 dollars or more. For fibers with Bragg Gratings the transmitter and receiver are in one unit, called an integrator, the cost, anywhere from 7,000 to 50,000 dollars [4].

Accelerometers

Accelerometers are a group of sensors, which have been developed to accurately monitor the acceleration at a location on a structure or object. There are several types of accelerometers which have been developed over the years. Piezoelectric accelerometers employ a seismic mass to impart a force on the piezoelectric material, during accelerations of the sensors housing. Within the housing is a preloading sleeve which applies an initial force to the mass and piezo-material. When the housing is accelerated, the force exerted by the mass changes, and this generates a charge in the piezo-material. Another form of accelerometer is a strain gage accelerometer, consisting of a cantilever beam, supported by the sensors housing, with a mass attached to the free end of the beam, and generally two strain gages mounted on the top and bottom surfaces of the beam near the base. Generally, the housing is filled with a fluid to dampen the oscillations of the beam. As the housing is accelerated the mass at the end of the beam will be slow to respond, and the induced strain in the beam can be monitored using the strain gages. The information can then be correlated to the acceleration experienced. The strain gage form of accelerometer has more recently been constructed on the microscopic scale using micro electrical mechanical design and manufacturing techniques. Additional alternatives to these accelerometers include servo accelerometers and vibrometers [18]. These forms will not be discussed in further detail.

Due to the size of the accelerometers and corresponding circuitry internal integration seemed impractical. The dimensions were large enough that significant composite material distortion would result if internalization was attempted. Thus, external adhesion was the only configuration considered. The logistics of which, were not entirely similar to that of the sensors previously discussed. Entire sensor and circuit encapsulation was viewed as, potentially difficult and damaging to sensor performance. It was hypothesized, that external adhesion of accelerometers could be accomplished by adhering the sensor to the interior of the blade where aerodynamic drag would not be an issue and the sensor would not likely be damaged due to debris.

Since accelerometers employ other forms of sensing; i.e. electrically resistive strain sensors, piezoelectric materials, and LVDTs, there are compounding issues with their use. These forms all require an electrical signal, which is susceptible to electrical interference. Depending on the type of accelerometer used there are response time limitations. For example, piezoelectric accelerometers exhibit a high measurement frequency, but accuracy can be affected during long steady accelerations. This makes selection of one type of accelerometer difficult for wind turbines which can see both steady state and dynamic loading.

Humidity Sensors

Moisture can degrade composite materials. Moisture also has an affects on the density of the air, which changes the loading on a wind turbine. For these reasons humidity sensors were considered. There are a number of forms of humidity devices. Hygrometric devices take advantage of the fact that certain hydroscopic materials change properties depending on the humidity. Some materials change dimensions depending on the humidity while other dielectric materials change capacitance. Additional devices include dew point devices and psychometric devices.

The humidity sensors considered were found to share similar dimensions to that of the accelerometers, making it difficult to successfully embed. Additionally, internal integration into fiber reinforced composites would yield the sensor un-operational, because there would be no avenue for the sensor to monitor the ambient humidity. For these reasons, it was determined that external integration would be the only configuration considered. External integration of a humidity sensor would require an un-obstructed means of monitoring the ambient humidity, thus it could not be adhered on the inside a sealed section of the turbine. Other than that successful adhesion of the sensor and accompanying wiring to the host structure is all that would be needed.

Issues with humidity sensors include electrical interference of the wind turbine with signal response. Additional, draw backs include accuracy of the device given that hygrometric devices used in household instruments are rarely accurate, and that the devices can also be temperature dependent.

Infrared Detectors

Infrared emitter/detector configuration was considered, because of the technique's nonintrusive means of monitoring the health of the host structure. This type of damage detection is similar to that of ultrasonic flaw detection.   The host material would be placed between the infrared emitter and corresponding detector. The amount of infrared light which would propagate through the material would result in a voltage output in the detector. In the event of damage to the structure, such as delamination, the amount of infrared light that would propagate through would be attenuated. Attenuation of the light would correlate to a change in voltage output, indicating material damage.

It is fundamentally possible to incorporate these emitters and detectors into the fiber reinforced composite construction but, it was not considered here. Internal embedment of this flaw detection system, due to the geometry of the components, was hypothesized to increase the probability of flaw development. External integration was considered as a more feasible alternative and involved bonding of the emitter and detector to opposite sides of the material in question. Complete encapsulation could be used to protect and minimize aerodynamic drag effects because the diodes were completely self-contained and only required the necessary wiring to operate effectively.

This form of flaw detection shares the same weakness, as the other electrical sensors; signal interference due to its proximity to the turbine generator. The detrimental issue to infrared flaw detection is the necessity for light to travel through the blade material. Thin fiber glass laminates are fairly transparent and can easily be monitored by this flaw detection technique; however the spar caps of industrial turbine blades reaching thicknesses of 3 to 4 inches, and infrared light propagation could be limited [27]. Also the emerging trend is the development of hybrid fiber glass/carbon fiber blades, with carbon fiber exhibiting virtually no transparent properties, making infrared useless.

Thermocouples

Thermocouples were considered before other forms of temperature dependent devices because of their cost, simplicity, and low profile. The temperature dependence of voltage between connected dissimilar metals is well documented and easily referenced from standard calibration curves, established by the National Institute of Standards and Technology (NIST) [18]. Dimensions of thermocouples governed by the diameter of dissimilar metallic wires fused, which can be less than a millimeter, makes it a prime candidate for integration with composite turbine blades.

Thermocouples were considered in new construction embedment and external adhesion. Like the strain gages included in this study the dimensions of the thermocouple made it a logical choice for the study. External incorporation was considered, because of the minimally perceived effect on the blade as a structure. Simple adhesion and even complete encapsulation of the thermocouple and accompanying wiring was thought not to affect the sensor accuracy.

Issues with thermocouples include the need for negligible current flow through the junction, connection with data acquisition systems result in additional bimetallic junctions, and often the non-linear voltage response [18]. Owe to the maturity of this group of temperature sensor all of these issues have been effectively addressed.

LITERATURE STUDY

An understanding of previous works in the field of sensor integrated composites is beneficial. Knowledge gathered by others in the field is useful to correctly place this study. This also acted as a reference for how the work presented in this study added and further the field of embedding sensors within composite materials.

Studies

Numerous sensor-integrated composite studies were found, but the vast majority of studies found were either on innovative sensors which showed great promise and were tailored to the task of sensor integration or focused on fiber optics. This reflects a perceived superiority of fiber optics over other mature forms of sensors. The perception is not unfounded, but still with the vast complexities found in the area of fiber reinforced composites, it cannot simply be taken as superior for all possible configurations. The innovative sensors show great promise, but it is suspected while not explicitly determined, that this specialization comes at a monetary cost which may not be economical for the wind industry. This hypothesis is the justification behind studying generic sensors for the application of embedding in composites.

Electrical Resistive Strain Element Integration

Despite the growing interest in the subject of smart composites there was a limited number of studies found that explored the possibilities of embedding resistive strain gages into reinforced composites. In fact only two studies could be found and only one was accessible to the author without monetary compensation. The study by Kim *et al.* (1992) explored the effects on strength of embedding thermocouples and dummy strain gages into epoxy and thermoplastic resins with graphite fabric reinforcement [28].

Dummy strain gages consisted of a Kapton film 1.27E-3 meters thick, 0.01016 meters long, and 0.00508 meters wide, with two lead wires adhered to the top surface and subsequently covered with a thin polyimide film. The dummy configuration mimicked the dimensions of a real strain gage. Thermocouples studied were Omega TT-J-36 which had a wire diameter of 0.381 mm. Composite architecture consisted of several different symmetric configurations, all of which were 16 plies thick. All samples created in the study placed the gages at the mid-plane (between the 8^{th} and 9^{th} plies). Kim *et al.* evaluated the strength of these coupons via two methods, compressive loading to failure, and three point bending to failure.

Using no less than 5 data points for each possible configuration a statistical spread of 10 percent was found. The authors of this study found that despite the configuration, there was no significant change in compressive or flexure strength of the composites. The results of which indicated that integration of either sensor into composite materials could be successfully accomplished without degradation of the material.

Despite these finding Kim *et al.* felt it necessary to caution readers in their attempts to extrapolate their results to further configurations. This warning is most likely because of the complex interaction between constituents which could easily lead to contrary results given the proper configuration.

Piezoelectric Element Integration

Studies into the incorporation of piezoelectric elements were found to be more prevalent. Multiple studies dealt specifically with the integration of polyvinylidene fluoride (PVDF) piezoelectric films. Studies employed PVDFs in a range of capacities from, strain, vibration, and shear strength. However, within the studies an interesting trend emerged. A vast majority dealt with damage detection but many studies explored, through the possibility of PVDF films as acoustic sensitive elements (AE). The acoustic technique plays into the sensors strength as a dynamic element. Damage to the composite, resulting in a sudden release of energy, generates transient elastic waves within the material. Since, these waves do not persist within the material the signal decay present in PVDF films is not a large issue. While still numerous, fewer studies explored PVDF films as embedded health monitoring elements.

Several articles were found by Caneva *et al.* which dealt specifically with the acoustic response of PVDF films embedded in composite laminates [29]. Caneva *et al.* constructed aryamid fiber reinforced epoxy laminates with two PVDF films embedded at the mid-plane of the laminate approximately 60mm apart. The coupons produced from these laminates were subjected to impact damage at specified energy levels and to flexure testing. Initial results from this study indicated that PVDF films can be successfully embedded in composite laminates with what they refer to as acceptable influence on mechanical behavior, and with great AE potential [29].

PZT was also studied by individuals as a structural health monitor. One such study was conducted by Mall and Hsu [30]. Mall and Hsu explored the response of PZT as a strain sensor in graphite reinforced epoxy matrix. The PZT was placed at the neutral axis in areas were fabric had been removed for the element. Two types of fatigue testing was performed with a majority of the efforts focused on evaluates the response of the PZT to this environment. The first fatigue test was an electromechanical fatigue test, not only was the coupons tested under mechanical cyclic loading but an ac voltage was applied in phase and out of phase with the mechanical loading. These conditions produced strain, owe to the mechanical loading and the electrical loading of a piezoelectric material. The second form of testing was solely mechanical without electrical cyclic loading present. Mall and Hsu concluded that the PZT studied functioned well when the mechanical loading and electrical loading was out of phase, even above operating ranges, but did not function well with in-phase electromechanical loading. It was also concluded that mechanical fatigue caused a majority of the actuator damage but no cracking or damage to the coupon was viewed during or after testing. The completion criteria for testing was detailed, but was only effectively concerned with actuator health. Since the criteria lead to no visible damage to the coupons, it can be concluded that under the configurations considered, successful integration of the piezoelectric element with no appreciable degradation to the composite was achieved.

While other studies explored other aspects of this field it is not necessary to delve into the details of all studies, but rather to understand the trends of this field and understand where it is headed.

Fiber Optic Integration

A host of studies have been performed over recent years on embedding fiber optics into reinforced plastics. In fact, a quick search found over 500 studies with composites and embedded fiber optics in the subject heading. As with embedded piezo-electric elements it is not necessary to review all of these studies but to simply understand what the current studies have been working towards.

The first of these studies was performed by Satori *et al* [31]. Fiber optics coated in polyimide were fabricated with Fiber Bragg Grating and embedded in composites constructed out of carbon prepreg. The laminates were constructed as so $[0,0,90,90]_s$, with the fiber optic near the interface between the 0 plies and the 90 plies. Satori *et al.* tested coupons from these laminates during curing, and during tensile loading. It was found that there was some degradation of the optical signal due to embedding but was not significant enough to prevent the use of the fiber as a strain sensor. In fact, as the temperature of the laminate was elevated after complete curing Satori *et al.* noticed a recovery of the signal response. The recovery was attributed to the residual strain associated with construction. The elevated temperature also related to a linear shift in the center wavelength of the fiber thus indicating successful measurement of the composites CTE, which Satori states is nearly equivalent to that of silica glass [31]. The embedded fiber optic showed a similar linear response to tensile strain. A shift in the central wavelength of the fiber was linearly related to an induced strain in the composite coupon up to a strain of about 1%. After which point the signal's spectrum shape deformed due to what Satori *et al.* determined was cracking of the 90^o layers. Satori *et al.* concluded that embedment of the fiber optic had not induced any noticeable structural defects and that they were able to accurately monitor strain of the coupon via the fiber optic.

Frazao, Oliveira, and Dias studies went further into the capabilities of embedded fiber optics by developing an artificial neural network (ANN) to monitor a fiber optic embedded with Bragg Grating on either side of a composite plate ply drop [32]. Due to the difference in thickness on either side of the ply drop the fiber optic is capable of distinguishing between thermal strain and mechanical strain. This distinction is accomplished because mechanical stress in the plane of the fiber reinforcement produces different levels of strain within the material due to the difference in thickness. Superimposed thermal strain is distinguishable from this mechanical strain because the thermal strain is independent of material thickness. Before implementing the ANN Frazao *et al.* characterized the fibers response to mechanical and thermal strain independently. The fiber showed a linear relationship between mechanical strain and wavelength shift, which was expected. The fibers response to thermal strain was non-linear because of the nature of the prepreg matrix used in construction of the laminate. Other than the non-linearity of the thermal response there was little difference in thermal strain found by either Bragg Grating. Implementation of the ANN showed a great ability to adapt and linearize the thermal response seen by the fiber optic, thus illustrating the versatile nature of fiber optics with Bragg Gratings.

The review of previous works is only to illustrate the work completed and currently on going, as a reference. The last of these studies discussed here was performed by Zhao, Gou, Song, and Ou. Zhao *et al* did not primarily focus on the complexity of embedding fiber optics into composite lamina but used this technology to monitor a new form of fiber reinforcement [33]. Zhao *et al.* explored the strain response of glass fiber reinforced composites which had been constructed with carbon nanopaper sheets within the laminate. To monitor the strain response, Fiber Bragg Grating (FBG) sensors were embedded within the same plane as the carbon nanopapers. The FBG sensors showed good repeatability and proved that there was successful integration of the carbon nanopapers. However, while these studies seem very promising with regards to successful integration of fiber optics into fiber reinforced composites it does not explicitly show this success.

Remarks of Literature Studies

All studies covered illustrate aspects of this field of study that show great promise. However, as stated above there appears to be a great deal of specialization which may not be suitable for wind applications. Further, by combining the fields of sensors with the field of composites there are undoubtedly going to be some unforeseen consequences to both technologies. Focusing the study on the effects of this integration on either field is a logical first step, and much can be gained from such an approach. However, there may be some un-characterized effects not seen by only focusing on one part of the combination. A holistic approach to this emerging marriage of technologies could yield further information.

LAMINATE AND TESTING DEVELOPMENT

The composite architecture and testing evaluation procedures, preceded the assessment of pervious work in the field of embedded sensors and sensor selection. Knowledge gained through the investigation of blade construction, and loading scenarios likely experienced during turbine operation, was the primary vehicle used to bound this study.

Laminate Design

The composite architecture developed for this study was not governed by those sensors chosen for external adhesion only. This was because external bonding of any of these sensors was hypothesized to have limited effect on the material's mechanical properties as was the intended design of such sensors. Given that the majority of sensors chosen for embedment were designed to evaluate strain, it was a logical choice to model the composite laminates, from which the test coupons would be cut, after a region on a wind turbine blade which would see high strain levels. Despite the increased geometric complexity associated with the blade's profile, its' support system was very similar to that of a cantilever beam. In order for a cantilever beam to be statically determinate all the applied loads must be reacted by the beam's root. This loading would cause large strains on the beam root, and due to the similarities between cantilever beams and wind turbine blades, it was decided to develop the composite test architecture after the root segment of an industrial wind turbine blade. As can be seen in Figure 21, even the construction of a 9 m blade, produces a thick composite structure which is dominated by unidirectional fibers orientated along the longitudinal direction of the blade.

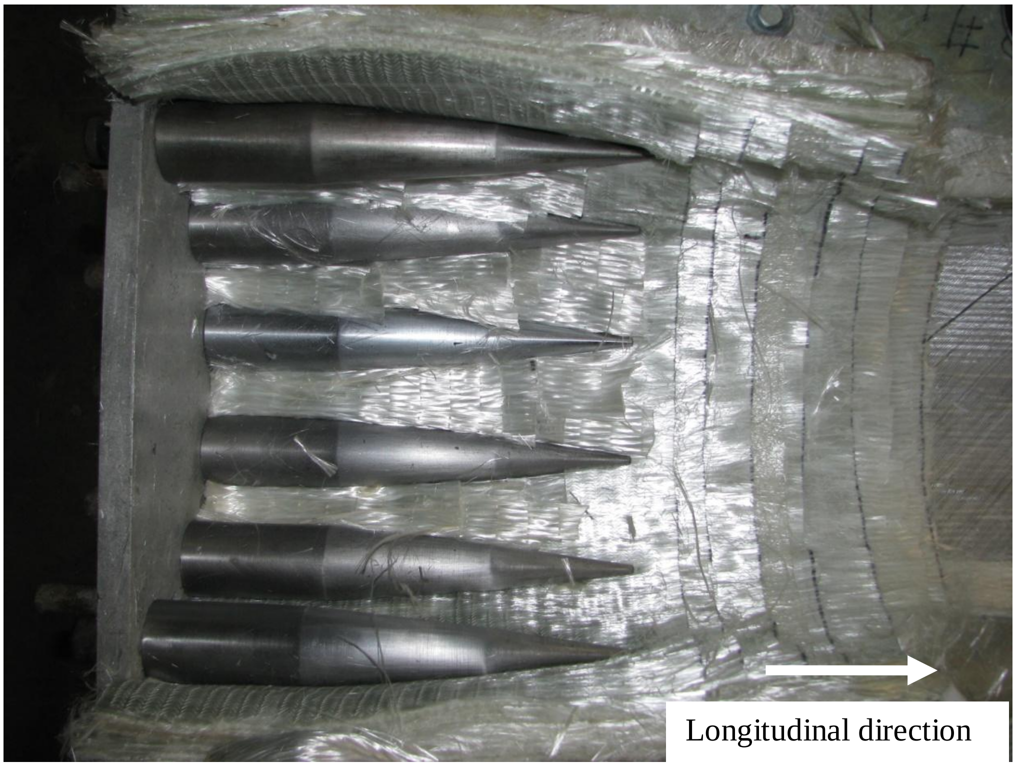

Figure 21, Composite layup of a 9m wind turbine blade by TPI. The root section is dominated by unidirectional fibers orientated along the longitudinal direction of the blade. [34]

Thus, it was decided that the composite laminates, from which the test coupons would be cut, would be constructed from a unidirectional fabric with a similar thickness to that used in the construction of industrial blades. Sensor alignment within the laminates was based on the mechanics of fiber reinforced composites. The strength of the coupons was enhanced in the direction of the fibers by the addition of the glass fabric to the matrix. Thus it was a logical choice to orient the sensors parallel to the direction in which the strength was enhanced.

Testing Development

The tests chosen to evaluate the success of embedding sensors within composite laminates were again based primarily on the loading conditions which would be experienced by the chosen section of an industrial turbine blade.

Based on the similarities in support, between cantilever beams and turbine blades, it was a fair conclusion that the root region of a blade would experience bending stress profiles. Continuing with the desire to place the strain sensors in regions known for large strains it was felt that a likely placement of such sensors would be within the outer few plies of the root region. The motivations for this potential placement were again the large strains experienced in this region, and the ease with which a sensor's wiring could be extracted. Given the intended location of the sensor within a turbine blade and the size of the root segment, it was felt that pure tensile loading of the test coupons was an adequate representation of the stress profile under which such a sensor would operate. This coupled with that simplicity of such a test, governed the decision to evaluate sensor embedding and surface treatment success by tensile testing. An image of the tensile testing performed in this study can be seen in Figure 22.

Mode I fracture evaluation was chosen as a means of quantifying the success of bonding between sensor and resin, due to surface treatment of the sensor. Of the three modes through which cracks could propagate mode I was chosen for several reasons. The first was that fact that such fracture testing was standard for composite structures as was evident by ASTM standard D5528-01[35]. Second, mode I fracture traditionally has been a more stable form of crack growth than mode II or III.

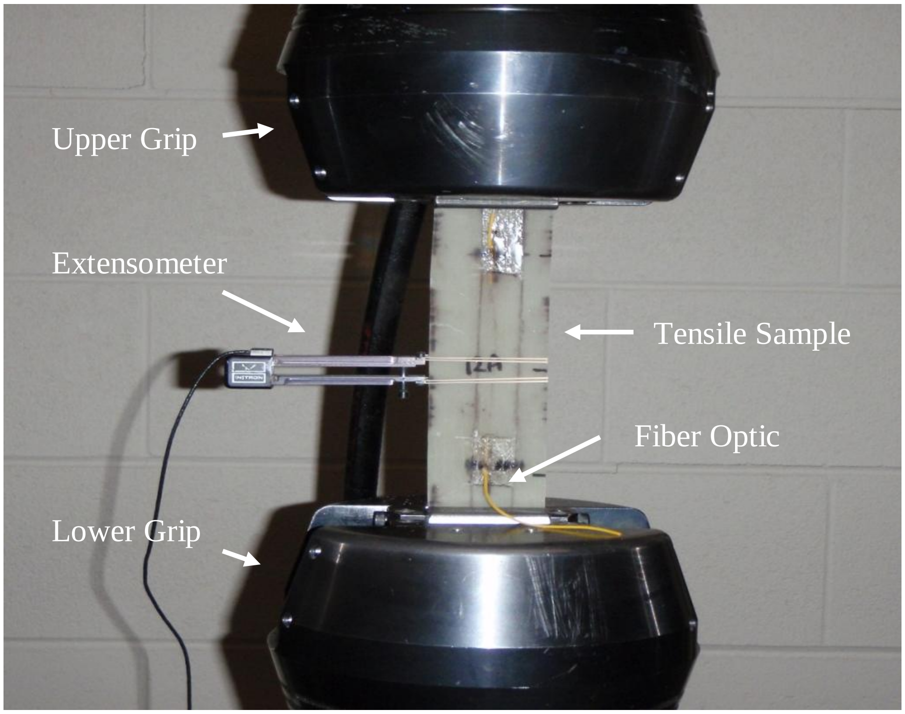

Figure 22, Tensile test configuration for evaluating embedded sensors with in fiber glass composite samples.

Third, sample testing in this manner was considered to be more reliable than other forms of fracture toughness evaluation. Lastly, it was felt that such a mode of fracture was more aggressive, given the configuration of embedded sensor, and thus would yield a conservative estimate of the bond strength between sensor and resin. An image of the mode I fracture toughness evaluation can be seen in Figure 23.

Field Emission Scanning Electron Microscopy (FESEM) was simply used as a means of quantification. FESEM imaging allowed for quantitative assessment of the bonding between sensor and matrix as well as of fracture results that were unexpected or varied widely.

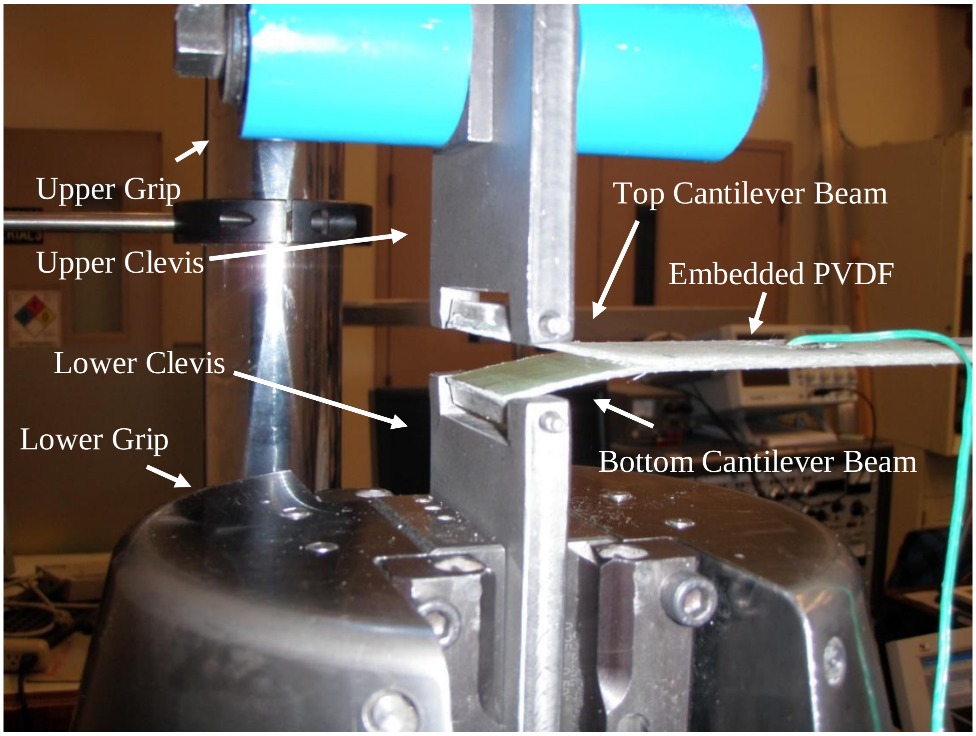

Figure 23, Mode I fracture toughness testing configuration for the Double cantilever beam test on composite materials with embedded sensors.

LAMINATES

To achieve the defined objective of this study several different parameters were needed. Tensile modulus, tensile strength, signal response, mode one fracture propagation energy release, and microscopic imaging of the sensor-matrix interface were the parameters investigated. To accomplish this task, several different test configurations were developed. Prior to development of the test configurations, selection of the resins and the fabric was necessary. In conference with senior members of the composites group, at Montana State University, it was decided that a glass fabric similarly used in wind blade construction would be adequate for this study; Saertex Unidirectional-Glass-Fabric U14EU920-00940-T1300-100000. Two resins were considered; an epoxy, which has recently become the matrix of choice due its strength, and a vinyl ester resin, because of its common use in industry. The epoxy chosen was Gurit's Prime 20V [36], which has been marketed as an epoxy resin for the wind turbine industry. A general vinyl ester was chosen, the Fibreglast 1110 series [37]. The hardener used for the Prime 20V was provided by Gurit while the hardener used in the vinyl ester resin was standard Methane Ethel Ketone Peroxide (MEKP). To evaluate all the parameters considered two coupon configurations were decided upon. The first was a tensile coupon which could be used to evaluate strength, signal response and modulus. The second test configuration used was a modified version of the G_{1c} coupons outlined in ASTM standard D5528-01 [35]. These coupons were created to evaluate fracture energy release and microscopic sensor surface imagery.

Tensile Test Construction

Tensile test coupon dimensions were based on several criteria. These criteria were limited effect of coupon edges on the sensor, test equipment capabilities, maximum possible degradation of the coupon due to sensor embedment, and present manufacturing capabilities. Based on these criteria it was decided to construct test coupons that were two plies thick, to insure that the sensor was the largest internal flaw in the coupon. Laminates were made using a hard-soft method, using Vacuum Assisted Resin Transfer Molding or VARTM. Aluminum plates of various dimensions were used as the hard side of the mold process. Injection and vacuum ports were positioned on opposite corners of the aluminum plate. Laminates were constructed off this aluminum plate in the order listed below. After which elastic double sided tape was used to seal the vacuum bag over the fabric and material used to aid in successful laminate construction.

1. Flow media (Used to enhance resin flow)
2. Peel ply (Used to peel excess resin from cured laminate)
3. Bottom glass fabric layer (Saertex glass fabric)
4. Embedded sensors (Sensors considered in study)
5. Top glass fabric layer (Saertex glass fabric)
6. Peel ply (Used to peel excess resin from cured laminate)
7. Flow media (Used to enhance resin flow)

Embedded sensor wiring retrieval was accomplished by threading the appropriate wiring through the tows of the top fabric layer. After which one inch squares were cut from the preceding peel ply and flow media around the wire egress points. The reason was to prevent damage to the wiring during laminate extraction and to develop a resin rich region around the wiring in an attempt to minimize the stress concentration that develop as a consequence of the fabric displacement. Wires were then fed through the initial vacuum bag and elastic tape was used seal the bag. A second vacuum bag was used to completely seal the laminate within the hard soft mold as can be seen in Figure 24.

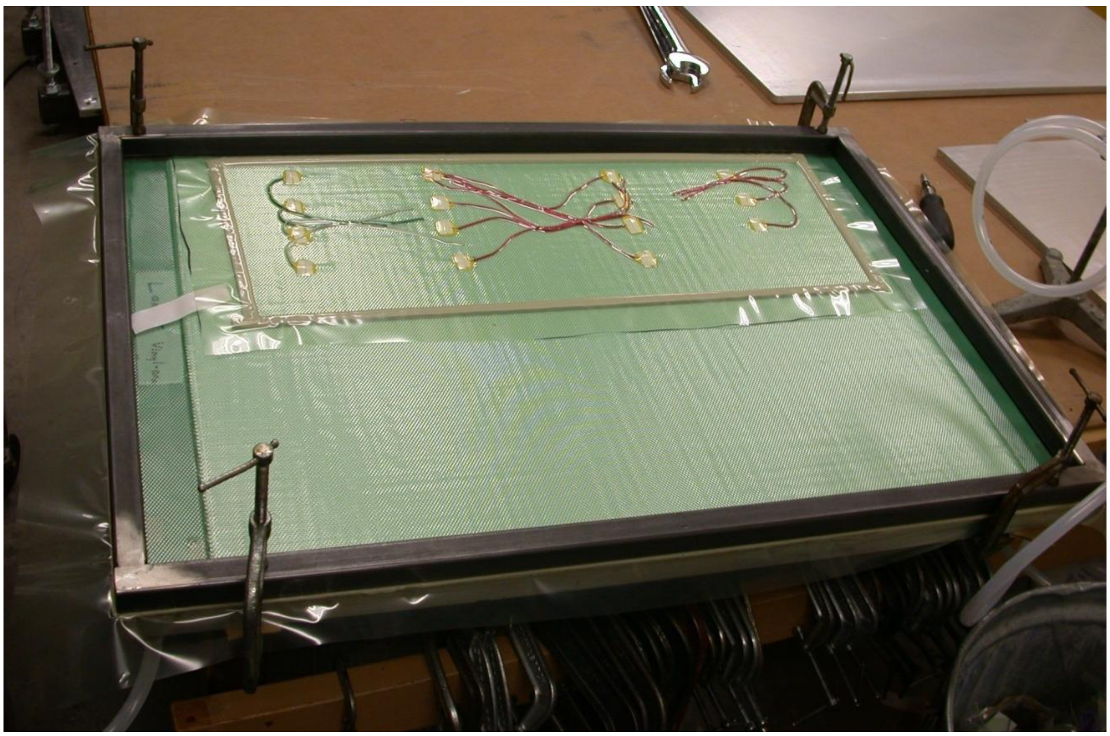

Figure 24. Complete laminate construction prior to resin injection.

A pressure difference of 25-26 psi was developed by a vacuum pump. Upon reaching this difference between outside and inside pressure, it was often allowed to sit for 30 minutes to allow the elastic tape to flow and seal any leaks. Given the size of the laminate to be constructed, 50 to 100 percent more resin that calculated was mixed prior to injection to insure proper fabric saturation. Again injection time was depended on laminate size but the largest of which (533.4mm x 838.2mm) took less than 30 minutes to completely infuse. The composite laminates were allowed to cure for 24 hours after which time the whole mold was post cured for 20 hours in a large oven at 93.3 degrees Celsius. The composite laminate was air cooled prior to laminate extraction. Laminate extraction involved removal of the vacuum bags from the top surface of the composite plate, with minimal damage to the wiring. Separation of the plate from the aluminum plate was followed by cutting of the plate's perimeter with the peel ply and flow media still attached, using a diamond cutting wheel cooled by a water jet. The peel ply and flow media was then slowly separated from either side of the composite laminate before the coupons were cut from the laminate. Coupons were labeled with a permanent marker prior to being cut from the laminate for identification purposes. Coupon dimensions were 50.8mm wide by 203.2mm long. All and coupons which stem from those laminates were recorded in the author's notebook. Detailed drawing of the coupon geometry and sensor location for each of the four sensors can be found in Appendix C.

G_{1c} Test Construction

Composite G_{1c} test coupon dimensions are well defined in ASTM D5528-01 [35]. The geometry was not altered, from that dictated by the standard, anymore than necessary given the nature of the study. G_{1c} laminates were 4 plies thick to reduce compliancy of the two beams of the coupon used in evaluation of mode 1 crack propagation energy release testing. Test dimensions are dictated to be 20 to 25 mm wide by at least 125mm long. The coupons used during testing were 38mm wide by 175mm long. The reason for this increase in size of the coupons was to avoid compounding the geometrical discontinuities associated with sensor integration and edge effects. G_{1c} values are typically taken from the initial crack which propagates for the crack initiator, in this case a thin nylon strip 60 mm wide. The initial crack approach is used because of the inherent conservative nature of the values obtained through this method. The conservative nature of this approach stems from that fact that the nylon material which does not continue throughout the coupon produces a resin rich region around the edge of this geometrical discontinuity. Compounding two discontinuities by locating the crack initiator and the sensor close to one another was not a feasible configuration. Therefore, each sensor was placed 5mm away from the nylon strip to insure minimal effect of the sensor on standard G_{1c} values. This distance likely effects the fracture toughness response of the material, but further separation of the nylon strip and the sensor would result in an increase in fiber bridging which would overshadow any effect on bonding. Construction of the laminates dedicated to Double Cantilever Beam (DCB) G_{1c} testing was very similar to that of the tensile test coupons. All composite plates were constructed using the same hard-soft mold configuration with VARTM. MFSG and PVDF sensor wires were extracted from the laminates using the same techniques used for tensile plate construction. Fiber optic ends were not removed from the composite material because it was decided that no signal would be recorded from any sensor embedded in the plates used for DCB testing. Additionally, fiber optics were placed parallel to the dominate fiber direction as well as perpendicular. The multidirectional placement of the fiber optics was chosen to explore the effect of FO orientation on G_{1c} values. All other construction techniques were identical to those used in the construction of the tensile coupons. Detailed drawing of the coupon geometry and sensor location for each of the four sensors can be found in Appendix C.

Embedded Sensor Treatment

An essential part of this study was the evaluation of bonding between the sensor and the composite matrix. Rather than evaluating the level of bonding between factory sensors and the matrix, techniques to surface treat the sensors prior to embedment were explored as a part of this study. All sensors used for embedment came with factory recommendation to clean the sensors with isopropyl alcohol before use. Exploration into the chemical reactivity of all the materials used to coat the sensors studied yielded one solution. It was found that low concentrations of nitric acid were mildly reactive with all coating [39]. Rather than explore alternative methods of surface treatment specific to each sensor, it was decided that use of just the nitric acid was a suitable surface treatment method to limit the number of variables present. The concentrations found were not uniform and thus it was decided that a 20 percent by weight solution of nitric acid would be used, as a means to surface treat the sensors, before integration. Two forms of surface treatment using the nitric acid were developed; the first was to dip the sensor into the solution and then immediately remove it and rinse it off with distilled water. The second treatment was to submerge the sensor in the nitric acid solution of 10 seconds before removal and rinsing. The reason behind the chosen treatment durations was that such durations were relatively short compared with those detailed in the chemical reactivity handbook, and posed less of on risk of sensor damage [39]. Sensors with no surface treatment were considered as controls, and all sensors were cleaned with isopropyl alcohol prior to embedment.

Wire egress of embedded sensor was explained above for MFSG's and PVDF's but successful egress of fiber optics was found to be more difficult. A method of fiber optic reinforcement was developed to increase the survivability of the fiber optic during layup, injection, curing, post curing, extraction and testing. Several alternatives were explored to accomplish this, but finally it was found that PVC wire jacketing stripped for copper wiring of similar diameter to that of the fiber optic worked best. The jacket's primary objective was to reinforce the fiber optic as it entered and exited the laminate. This form of reinforcement meant that the jacketing covered a significant portion of the fiber optic once free of the laminate and entered the laminate as to insure fiber optic survivability. Figure 25 illustrates this technique which was developed for this study.

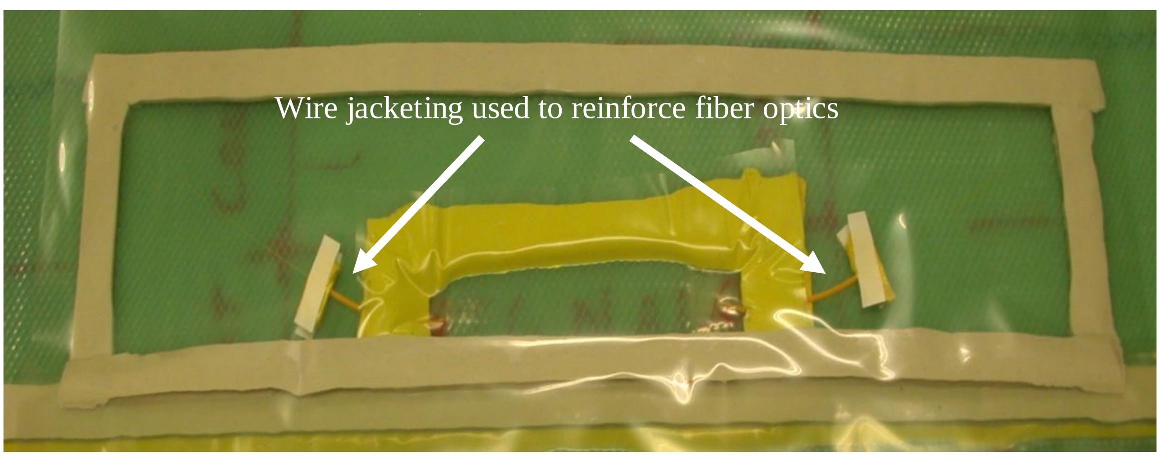

Figure 25. PVC jacketing used to reinforce fiber optics over egress from laminate.

Additional sealing of the ends of this jacketing was necessary to limit the amount of resin which would migrate into the space between vacuum bags.

TESTING & RESULTS

Several different parameters were chosen to evaluate the success of embedment and surface treatment of the sensors studied. It was first decided to start with standard testing methods and progress to more complex methods as the embedment procedures were refined. Tensile testing was chosen because of its simplistic stress profile. Tensile testing allowed for numerous measures of sensor integration success. The tensile modulus, strength, load carrying capability, and strain of the fiber reinforced composite could be monitored. A drastic reduction in any one of these material properties could signify a lack of success. Further variables of interest in the study were the responses of the sensor. Tensile testing allowed for the monitoring of two indicators of sensor survivability and reliability. The accuracy of the sensor was monitored during testing by comparing the sensors response to that of the extensometer used to measure material stiffness. The second, was monitoring of the sensor up to failure. Evaluation of sensor bonding could be inferred from the point at which the sensor response became erratic.

Further indication of successful bonding between sensor and matrix was evaluated through inter-laminar fracture testing [35]. A reduction in the fracture strength required to propagate a crack in mode 1 fracture was an indication of unsuccessful bonding. Thus, an increase in fracture strength for those sensors that were surface treated would indicate that such manufacturing techniques could minimize the effect of sensor integration. G_{1c} samples were also examined post fracture through Field Emission Scanning Electron Microscopy (FESEM) for indication of resin bonding.

The rationale and hypotheses presented for the host of variables considered were the means of evaluating the success of the manufacturing techniques developed. All the data presented here was collected using National Instruments Data Acquisitions system (USB-6229) using Labview software [40]. Images of the system and signal conditioning can be found in Appendix F; Data Acquisition System & Programs. Due the lack of data collected for externally adhered sensors no results of those configurations are presented.

Tensile Testing of Embedded Sensors

All tensile testing was performed on either of two Instron machines, the 8602 single post screw drive machine located in EPS 138, or the twin post screw drive 5882 located in EPS 008. Both machines were rated to loads above that expected at failure for the tensile coupons (8602 and, 5885 are rated to 100kN). Additionally, both machines had 50.8 mm grips capable of correctly holding the test coupons, and had electronic extensometers necessary to monitor material strain. All samples were first tested to 1% strain, after which the samples were unloaded and the response of the material and sensor were evaluated. If unsatisfactory results were obtained, the sample was tested a second time to ensure the response. Once, a satisfactory result was collected or the sensor was identified as damaged, the coupon was loaded to failure to record the sample's strength and load carrying capability. All failure modes and interesting events were recorded for evaluation later. Due to the inherent differences in fiber volume fraction between laminates, tensile modulus, tensile strength, sensor failure stress, and apparent linear strain to failure were all normalized to a defined 40 percent fiber volume fraction. The reason for this was to address the high level of dependence of these chosen material characteristics on fiber volume fraction. Forty percent fiber volume fraction was chosen because it fell within the range of fiber volume fractions calculated from the laminates created. A published relationship between fiber volume fraction and tensile modulus, which can be found as Eqn 3 [14], was used to adjust the experimental tensile modulus based on the samples' fiber volume fraction relative to the designated 40 percent.

$$E_{11} = E_f V_f + E_m(1 - V_f) \qquad \text{Equation 3}$$

E_{11} = Tensile modulus of the sample
E_f = tensile modulus of the fiber
E_m = tensile modulus of the matrix
V_f = fiber volume fraction

This equation was based on the micromechanics between the fibers and matrix for each ply. Equation 3 can be applied in this study because the laminates constructed were unidirectional with both plies orientated in the same direction. This justification is also the reason why Equation 4, which is derived in the same publication [14], can be used to adjust the tensile strength for each configuration. Tensile strength is also highly dependent on fiber volume fraction, thus Equation 4 was used to adjust the tensile strength values based on their respective fiber volume fractions.

$$F_{1t} = \sigma_{fa}[V_f + \frac{E_m}{E_f}(1 - V_f)] \qquad \text{Equation 4}$$

F_{1t} = tensile strength of the sample
σ_{fa} = tensile strength of the fiber
V_f = fiber volume fraction
E_f = tensile modulus of the fiber
E_m = tensile modulus of the matrix

Sensor failure stress and apparent linear strain at failure were adjusted based on these two equations because of the direct relationship between both values and the fiber volume fraction. Table 3, below outlines the tensile test configurations developed to evaluate the success of the two surface treatments considered in this study.

Table 3, Test matrix of all the test configurations developed to explore the success of the two surface treatments.

Tensile Test Matrix

Sensor	Surface Treatment	Minimum Number of samples	Location within in Laminate	Resins
Single Axis Strain Gage	cleaned with Isopropyl Alcohol	3	mid-plane	Prime 20 or Fibreglast 1110
Single Axis Strain Gage	Dipped in 20% by weight Nitric Acid and cleaned with Isopropyl Alcohol	3	mid-plane	Prime 20 or Fibreglast 1110
Single Axis Strain Gage	Submerged in 20% by weight Nitric Acid and cleaned with Isopropyl alcohol	3	mid-plane	Prime 20 or Fibreglast 1110
PVDF film	cleaned with Isopropyl Alcohol	3	mid-plane	Prime 20 or Fibreglast 1110
PVDF film	Dipped in 20% by weight Nitric Acid and cleaned with Isopropyl Alcohol	3	mid-plane	Prime 20 or Fibreglast 1110
PVDF film	Submerged in 20% by weight Nitric Acid and cleaned with Isopropyl alcohol	3	mid-plane	Prime 20 or Fibreglast 1110
Acrylate coated Fiber Optic	cleaned with Isopropyl Alcohol	3	mid-plane	Prime 20 or Fibreglast 1110
Acrylate coated Fiber Optic	Dipped in 20% by weight Nitric Acid and cleaned with Isopropyl Alcohol	3	mid-plane	Prime 20 or Fibreglast 1110
Acrylate coated Fiber Optic	Submerged in 20% by weight Nitric Acid and cleaned with Isopropyl alcohol	3	mid-plane	Prime 20 or Fibreglast 1110
Polyimide coated Fiber Optic	cleaned with Isopropyl Alcohol	3	mid-plane	Prime 20 or Fibreglast 1110
Polyimide coated Fiber Optic	Dipped in 20% by weight Nitric Acid and cleaned with Isopropyl Alcohol	3	mid-plane	Prime 20 or Fibreglast 1110
Polyimide coated Fiber Optic	Submerged in 20% by weight Nitric Acid and cleaned with Isopropyl alcohol	3	mid-plane	Prime 20 or Fibreglast 1110
Controls	N/A	3	N/A	Prime 20 or Fibreglast 1110

Number of vinyl ester laminates created	9
Number of epoxy laminates created	12

Metal Foil Strain Gages

A single axis metal foil strain gage produce by OMEGA (KFG-5-120-C1-11L1M2R) was chosen for integration [22]. The coating dimensions of this metal foil strain gage were 3.08 mm x 9.34 mm x 0.1 mm. All sensors were placed approximately in the middle of the coupon at the mid-surface, with the wiring threaded through the subsequent fiber glass ply.

Table 4. Sensitivity response of embedded strain gages, as a function of surface treatment, within composite laminates to 1 percent strain.

Metal Foil Strain Gage

	Vinylester	Epoxy
Treatment	V/ % strain	V/ % strain
Cleaned in Isopropyl Alcohol	2.68	2.75
Dipped in 20% by mass HNO3 & cleaned in Isopropyl Alcohol	2.64	2.39
Submerged for 10 sec. in 20% by mass HNO3 & cleaned in Isopropyl Alcohol	2.52	2.50

The ability of the embedded sensors to monitor changes in strain was important to this study. The sensitivity of the sensor to these changes was the first parameter explored. It was found that there was a slight reduction in sensitivity for both resins used, as can be seen in Table 4, but it was determined to be not a very significant reduction. The reason for this was the close grouping of values. Additionally, statistical Student T testing of the values indicated no significant increase in the mean values reported. However, there appeared to be some rebound in sensitivity for the surface treated sensors in epoxy resin, which was promising despite the t test results. Additional testing could prove this trend significant. Progressing on, sensor failure stress was analyzed. Due to the catastrophic failure of the coupons used the extensometers were not left on the coupons past one percent strain. Thus, there was no direct failure strain data to analyze. Thus, the parameter used was the stress at which the sensor was either destroyed or showed a clear issue with accuracy. The results can be seen in Table 5.

Table 5, Coupon stress at point of strain gage signal failure (Adjusted to 40% fiber volume fraction).

Metal Foil Strain Gages

	Stress at Signal Failure (MPa)	
Surface Treatment	**Vinylester**	**Epoxy**
No sensor failure	574.09	594.76
Cleaned with Isopropyl Alcohol	615.48	470.22
Dipped in 20% by weight Nitric Acid & cleaned with Isopropyl Alcohol	407.37	466.27
Submerged for 10 seconds in 20% by weight Nitric Acid & cleaned with Isopropyl Alcohol	424.93	430.52

Looking at the vinyl ester samples there is an apparent decay in stress level with increased surface treatment. The higher than no sensor failure values were investigated and determined to be products of the test scatter. As for the epoxy samples the data appears to decay as well with surface treatment, but the results are all within one standard deviation, and so the trend was considered negligible. T testing confirmed that both perceived trends were not significant. Without significant evidence supporting the need for surface treatment of strain gages prior to embedment, the material response of the composite was considered. The material's tensile modulus, in the dominant fiber direction, was the first material parameter analyzed.

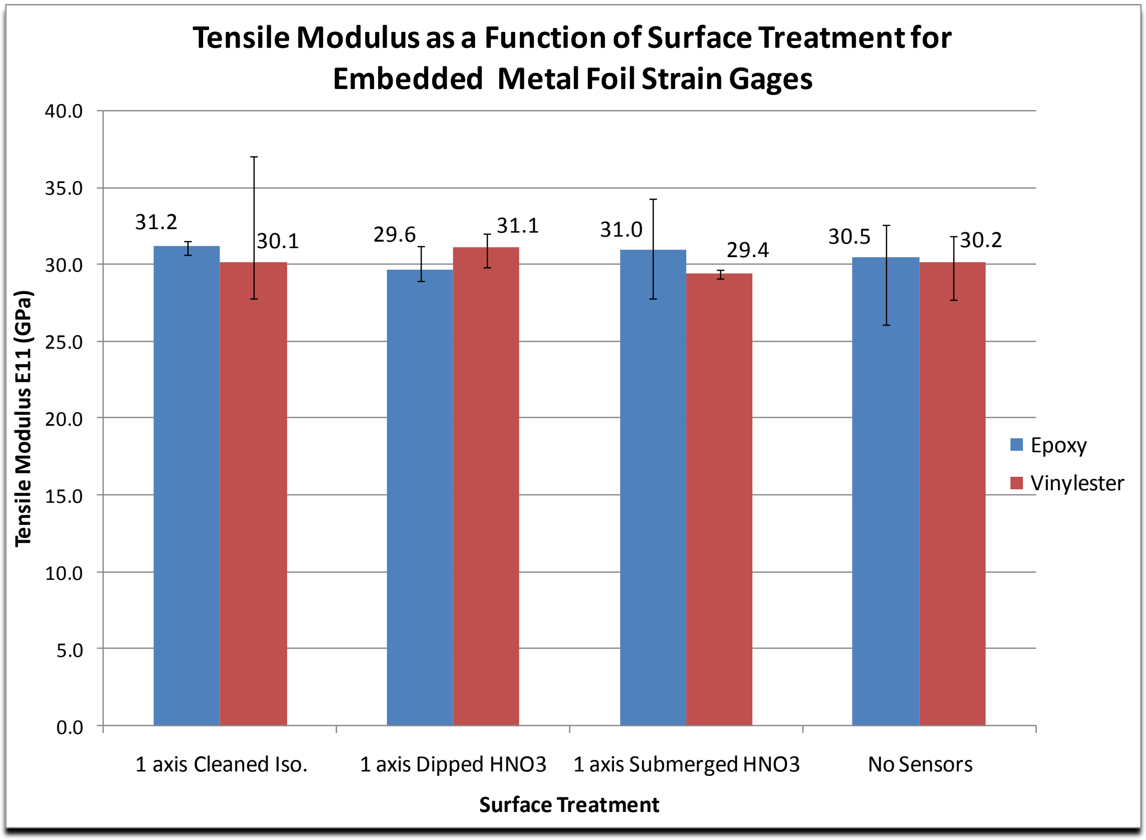

Figure 26, No noticeable effect of surface treatments on Tensile Modulus of embedded strain gages. (All values are normalized to 40% fiber volume fraction)

Cleaned, and treated sensors were compared against sample without embedded sensors, seen in Figure 26. All error bars represent maximum and minimum values for each configuration. No noticeable trends were found for either resin. Both nitric acid surface treatment options show no reduction in stiffness, as compared to these controls. Statistical t testing confirmed, that given the data collected there was no significant change in tensile modulus due to sensor integration. Thus the conclusion was draw that embedding strain gages within either composite configuration could be accomplished with no significant effect on material stiffness.

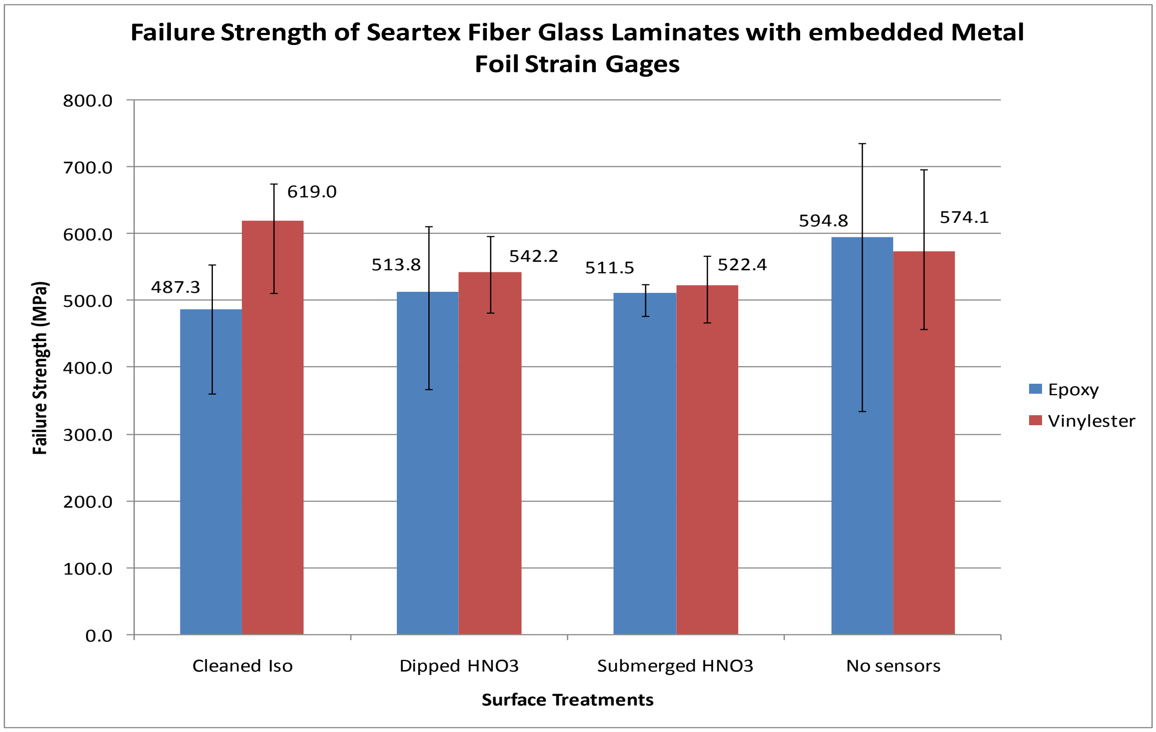

Figure 27, Strength trends for embedded strain gages as compared to control coupons. (All tests normalized to 40% fiber volume fraction)

Without any conclusive results either confirming or refuting the necessity of surface treatment, the strength of the samples was considered. Due to the local changes in stress and strain associated with the increase in cross-sectional area around the sensor, strength was based on the thickness of the sample not affected by the sensor. Figure 27, shows promise for those sensors surface treated and embedded in epoxy fiber glass materials. Surface treated strain gages show an increase in recovered material strength. The increase in strength diminishes with increased surface treatment, indicating limited effectiveness for surface treatments more extensive than those considered. Statistical t testing of the data collected however indicated that given the data collected this trend was not statistically significant. However, the data showed that surface treatment was not detrimental and with further testing could be found to be statistically significant. Conversely, there is a rather significant statistical reduction in strength due to surface treatment for coupons using vinyl ester resin. The reduction may be due to some chemical interaction between the sensor and the resin. By increasing the surface area through the treatments considered, an increase in chemical reaction occurred, leading to a reduction in strength. This is a hypothesis, since no means of evaluation of chemical reactivity between sensor and resin was performed. Again the values larger than those reported for samples without sensors were explored and found to be an artifact of data scatter.

Table 6. Average Load Carrying Capability of the test coupons with embedded strain gages

Metal Foil Strain Gage

	Load Carrying Capability (kN)	
Surface Treatment	**Vinylester**	**Epoxy**
No sensor controls	52.54	52.71
Cleaned with Isopropyl Alcohol	56.26	44.89
Dipped in 20% by weight Nitric Acid & cleaned with Isopropyl Alcohol	49.87	46.70
Submerged for 10 seconds in 20% by weight Nitric Acid & cleaned with Isopropyl Alcohol	48.45	47.16

Due to the fluctuations in local strength around the sensor, the load carrying capability of the coupons was considered. Table 6 was developed to meet this consideration, and follows the same trends as that of the strength results shown in Figure 27, this indicated that the strength results were in fact genuine. The last tensile parameter looked at for determining the effectiveness of the surface treatments considered was apparent linear strain at sample failure. The apparent linear strain was calculated given the modulus of the coupons, as well as, the stress of the samples at failure.

Table 7. Strain at failure calculated through modulus and failure strength.

Metal Foil Strain Gage

	Apparent % Strain at Failure	
Surface Treatment	**Vinylester**	**Epoxy**
No sensor controls	1.90	1.95
Cleaned with Isopropyl Alcohol	1.81	1.47
Dipped in 20% by weight Nitric Acid & cleaned with Isopropyl Alcohol	1.74	1.73
Submerged for 10 seconds in 20% by weight Nitric Acid & cleaned with Isopropyl Alcohol	1.78	1.65

Table 7 shows no noticeable effect on apparent linear strain at failure for those strain gages embedded in vinyl ester laminates. However, there is a small increase in strain for those sensors in epoxy laminates.

Based on all the parameters considered from tensile testing it was determined that the surface treatments considered in this study were not effective for strain gages embedded in vinyl ester laminates. However, it was concluded that the surface treatments were effective for those sensors embedded in epoxy laminates. These conclusions were solely made on the results of the tensile testing and are later confirmed or amended based on the results of the mode I fracture testing, and FESEM.

PVDF Films

The Polyvinylidene Fluoride (PVDF) films used in this study were produced by Measurement Specialties (LDT0-028K/L w/crimps) [41]. The sensors dimensions were 13 mm x 25 mm x .205 mm, which was the largest sensor considered for internal embedment. It was found that there was a small increase in sensitivity associated with the increase in surface treatment for both resins, seen in Table 8. There was clear increase in sensitivity for those sensors embedded in vinyl ester, and what appears to be a tapering off of the sensitivity for the epoxy samples. This indicated that no further surface treatment is necessary for PVDF films used with epoxy resins and further surface treatment may improve the sensitivity of those films embedded in vinyl ester laminates. T testing again revealed that these trends given the current limited data set was not statistically significant.

Table 8. Signal sensitivity of PVDF films to strain applied to test coupons.

PVDF films

	Vinylester	Epoxy
Treatment	**V/ % strain**	**V/ % strain**
Cleaned in Isopropyl Alcohol	2.41	3.35
Dipped in 20% by mass HNO3 & cleaned in Isopropyl Alcohol	2.43	3.86
Submerged for 10 sec. in 20% by mass HNO3 & cleaned in Isopropyl Alcohol	2.54	3.83

Table 9. Coupon Stress at point of sensor failure under tensile loading.

PVDF Films

	Stress at Signal Failure (MPa)	
Surface Treatment	**Vinylester**	**Epoxy**
No sensor failure	574.09	594.76
Cleaned with Isopropyl Alcohol	332.86	270.20
Dipped in 20% by weight Nitric Acid & cleaned with Isopropyl Alcohol	395.91	355.23
Submerged for 10 seconds in 20% by weight Nitric Acid & cleaned with Isopropyl Alcohol	404.59	422.01

However, despite this finding the trends were still considered a justification for surface treatment. The reason being additional data collection could reduce the scatter and confirm the perceived trends found for PVDF sensitivity. Continuing with the stress at sensor failure, there is an increase in the stress level present, in the samples, at the point of sensor failure for both resins, as seen in Table 9.

Both results were found to lack statistical significance, but it is suspected that this result is due to the small sample size.

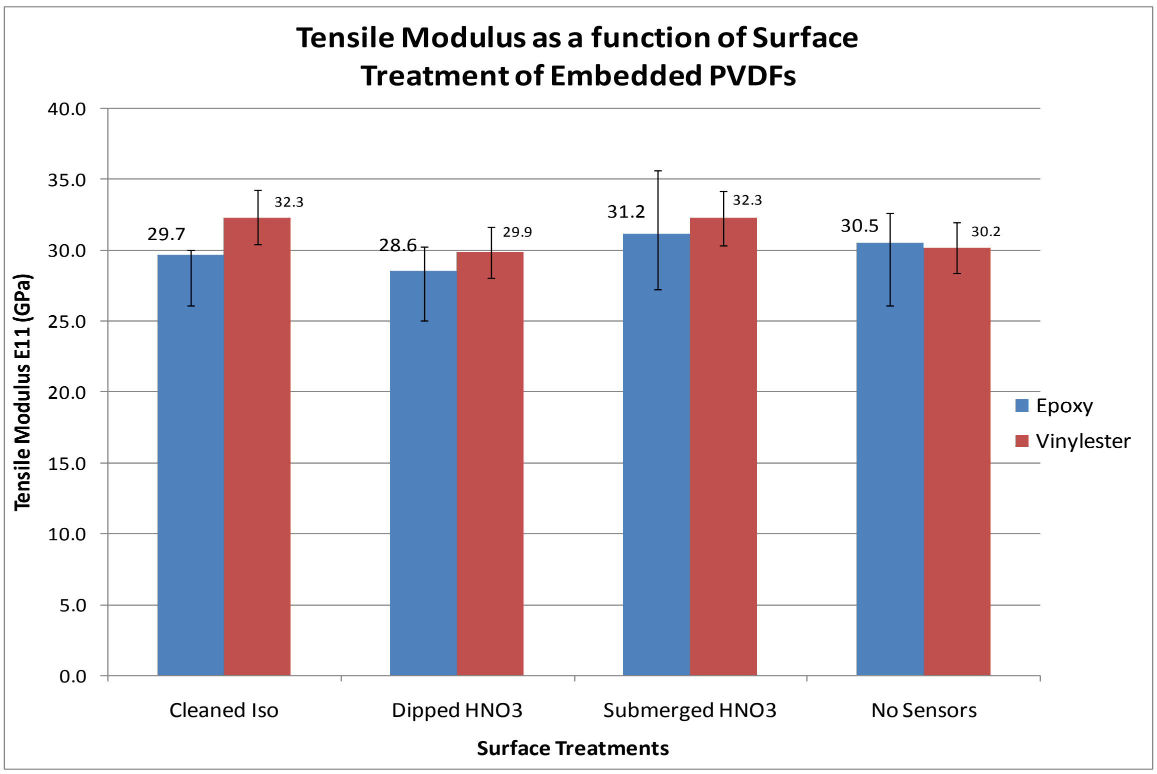

Figure 28, Coupon Modulus for samples with embedded PVDF films which were strain to 1 percent. (All values are normalized to 40% fiber volume fraction)

Thus, in spite of the lack of significance it was concluded that surface treatment was potentially beneficial to increasing the range over which the PVDF could be relied upon.

Addressing the effects on material properties, the tensile modulus was considered in Figure 28.

There was no appreciable degradation in stiffness associated with the sensor integration. The stiffness of those coupons with sensors, surface treated, by submersion in nitric acid for ten seconds are higher than those without any sensors. However, this was not considered a decisive effect, promoting the use of surface treatments, but rather was found to be a product of data scatter. Strength data complemented the results of the sensors embedded in epoxy laminates.

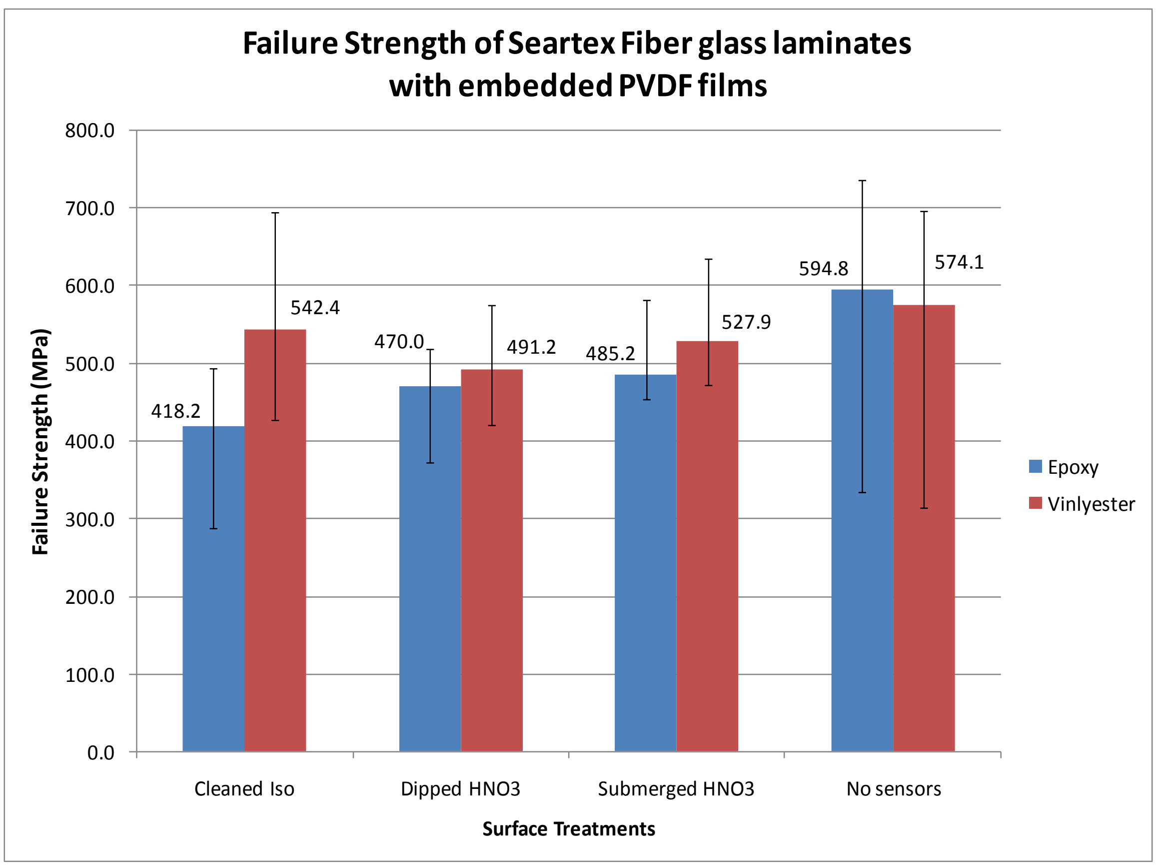

Figure 29, Tensile Strength of samples with embedded PVDF films (All values normalized to 40% fiber volume fraction and to coupon thickness unaffected by sensor integration)

It was found that there was a significant reduction in epoxy sample strength associated with sensor integration. However, surface treatment was able to recover some of the lost material strength. While currently not statistically significant, any increase in material strength was considered beneficial. The vinyl ester samples did not share the same result. The data presented in Figure 29 indicated a reduction in strength for those sensors dipped in nitric acid. Student T testing revealed that no vinyl ester value was found to be statistically different from that of those without embedded sensors. This meant, embedding PVDF films within vinyl ester laminates with any surface treatment would not produce a significant reduction in strength. As suspected the load carrying capacity, found in Table 10, configuration followed the same trends of the strength data. There was an increase in sample load carrying capacity associated with further surface treatment for epoxy samples. Also, vinyl ester samples showed a reduction in load carrying capacity for those sensors dipped in nitric acid. It was thus determined that the trends presented by the strength results were confirmed.

Table 10. Load Carrying Capability of test samples with embedded PVDF films.

PVDF films

	Load Carrying Capability (kN)	
Surface Treatment	**Vinylester**	**Epoxy**
No sensor controls	52.54	52.71
Cleaned with Isopropyl Alcohol	50.55	37.45
Dipped in 20% by weight Nitric Acid & cleaned with Isopropyl Alcohol	45.41	42.95
Submerged for 10 seconds in 20% by weight Nitric Acid & cleaned with Isopropyl Alcohol	49.18	44.46

Apparent linear strain at failure gave further evidence of the necessity for surface treatment of embedded PVDF films in epoxy laminates. The increase in strain at failure, seen in Table 11, due to surface treatment was a little more than one standard deviation. This indicated a significant increase in strain at failure due to surface treatment of the embedded PVDF films. The vinyl ester laminates did not share the same reinforcement. There was a slight reduction in failure strain due to surface treatment but all values were within one standard deviation, thus no significant trends were noted.

Table 11. Apparent linear strain at failure calculated via material modulus and failure strength.

PVDF films

	Apparent % Strain at Failure	
Surface Treatment	**Vinylester**	**Epoxy**
No sensor controls	1.90	1.95
Cleaned with Isopropyl Alcohol	1.72	1.45
Dipped in 20% by weight Nitric Acid & cleaned with Isopropyl Alcohol	1.64	1.55
Submerged for 10 seconds in 20% by weight Nitric Acid & cleaned with Isopropyl Alcohol	1.64	1.55

Based on the evidence thus far, it was recommended that the surface treatments developed and studied are an effective means of improving sensor response. Also, surface treatment improved, material properties, that would otherwise be degraded by the integration of PVDF films into the construction of fiberglass reinforced composites.

Acrylate Coated Fiber Optics

The acrylate coated fiber optics used was very similar to the SMF-28 fiber optic produced by Corning [42]. It was a single mode fiber optic with a core diameter of about

9-10 μm, a cladding diameter of 125 μm, and an acrylate coating diameter of roughly 400 μm [42]. These fibers were pulled from duplex telecommunication cables 4.572 m long. All other coating and material was stripped from the fibers prior to use in the study. It was decided that all fiber optics would have a gage length of about .1016m. Leaving some room for egress before arriving at the region of the sample reserved for the test grips. Due to the limited equipment and type of fiber optics used, there was no means of monitoring the fibers sensitivity to strain. Additionally, the logistic of successfully monitoring the fibers failure point, during strength testing, left many uncontrolled variables. These variables would affect the accuracy of the result, and thus the signal response was not monitored. However, a specific concern, voiced by the sponsors of this study, was the effect of the laminate cure cycle on the fiber optics signal strength.

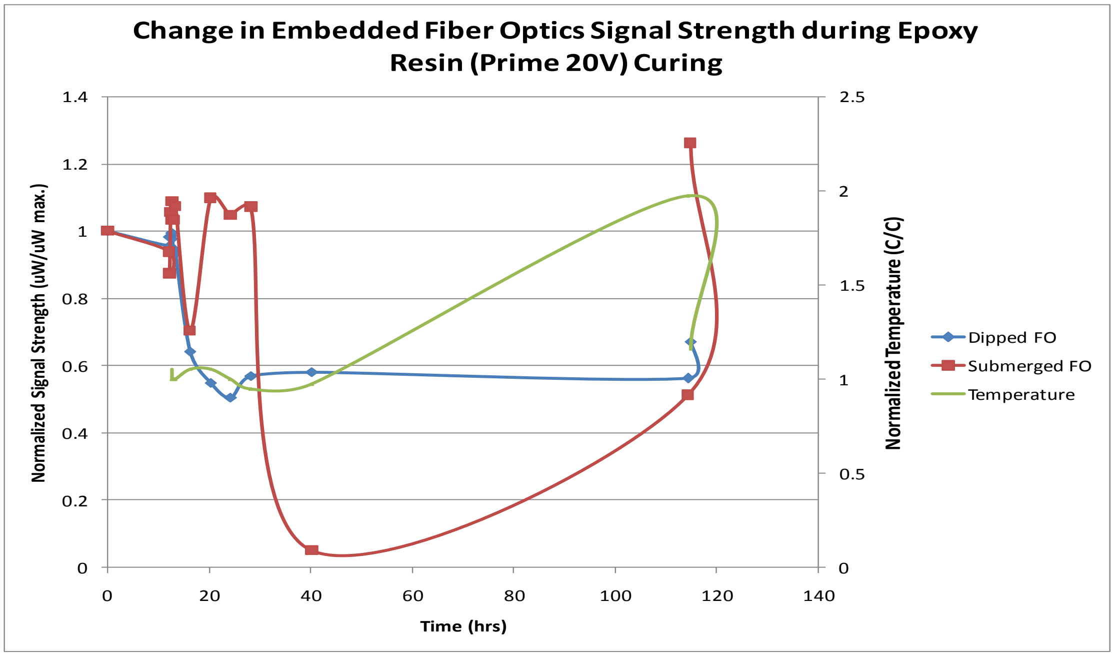

Figure 30. Signal Strength of the two acrylate coated fiber optics with different surface treatments over the course of the cure cycle (values normalized to initial signal strength [dipped 84.35 μW, submerged 58.6 μW] and room temperature)

Therefore, it was decided to monitor the signal strength of the fiber optics during the manufacturing process. Monitoring was accomplished through the use of an Optical Wavelengths Laboratory (OWL) ZOOM II power meter, capable of detecting several different single mode wavelengths, and an OWL LED laser light source; which produced a beam of light with a wavelength of 1550 nm [43][44]. The first attempts at signal strength found large fluctuations over the course of the curing cycle, as seen in Figure 30. The testing of two different fiber optics, with only one set of test equipment, was accomplished by moving the power meter and light source from one fiber to the other. It was hypothesized that this constant handling was the cause of the large fluctuations. Therefore, it was decided to only monitor one fiber optic during the course of injection, cure, and post cure. The fiber optics tested after this point where all subjected to submersion in nitric acid for 10 seconds, thus increasing the chances of surface treatment effect on signal strength. Testing found that the constant handling was the cause of the large signal fluctuations, and increased fiber failure. Figure 31, is an example of this improved signal response, which more accurately shows that curing has limited effect on signal strength. This result was the same for those acrylate coated fiber optics embedded in vinyl ester laminates, as seen in Figure 32. However, there are still some rather large differences in signal strengths between tests. The lack of repeatability between tests was due to the sensitive nature of the fiber optic technology. Any adjustment of the connectors, light source, and power meter produced a change the alignment of the components, and thus the signal strength transferred through the fiber optic.

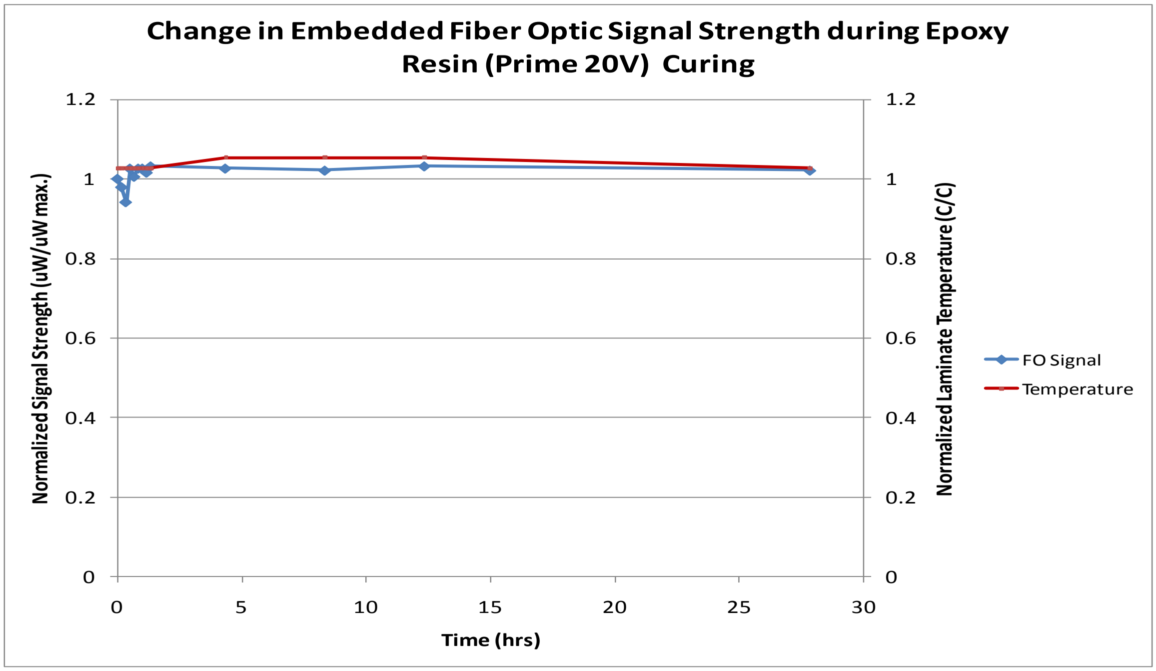

Figure 31, Signal strength a for one fiber optic surface treated by submersion in nitric acid for 10 seconds (normalized to initial signal strength [24.9 μW] and room temperature)

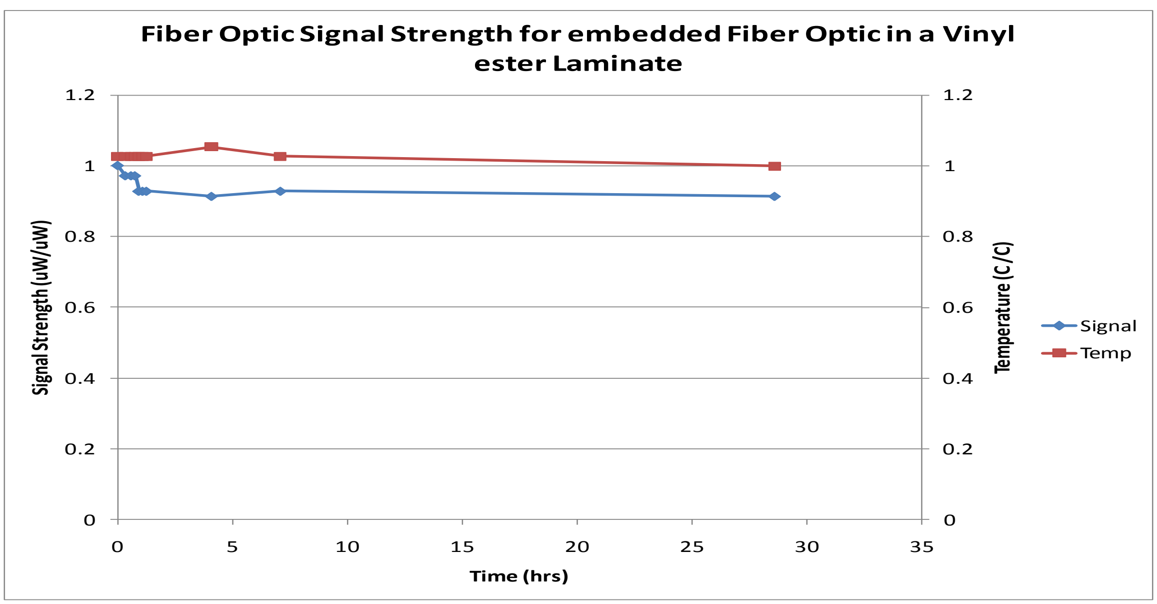

Figure 32. Signal strength of a fiber optics surface treated by submersion in nitric acid for 10 seconds (normalized to initial signal strength [9.09 μW] and room temperature)

The other part of the signal loss was the unavoidable handling of the fiber optics needed to correctly layup the laminate prior to injection. The reason for monitoring temperature during signal monitoring was the potential for temperature to cause a reduction in signal strength. However, the molds used were designed to avoid excessive thermal changes, during curing, which was evident from the figures above. It was concluded from the signal strength testing of the acrylate coated fiber optics that there was no noticeable effect due to surface treatment or integration within a fiberglass reinforce composite.

Addressing the effects on fiber optic embedment on material properties, the first property analyzed was tensile modulus. It was found that there was a slight increase in

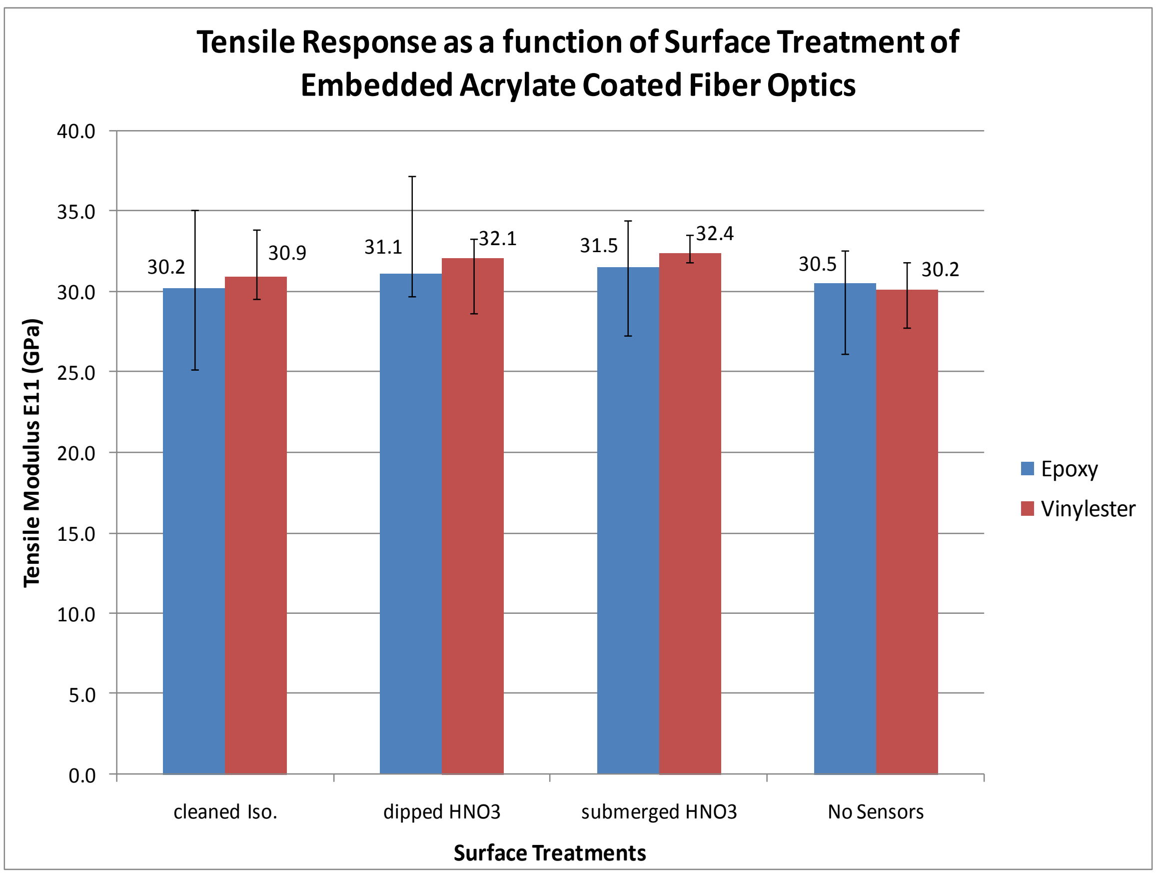

Figure 33. Tensile Modulus of parallel embedded acrylate coated fiber optics tested to one percent strain (All values normalized to 40% fiber volume fraction)

modulus associated with increased surface treatment, as seen in Figure 33. All values fell within the range produced for samples without sensors. Therefore, it was concluded that there was no noticeable effect on modulus due to fiber optic integration. Material strength revealed some interesting results. Figure 34, indicates a decay in material strength due to sensor embedment. However, the change in strength due to surface treatment was not as clear.

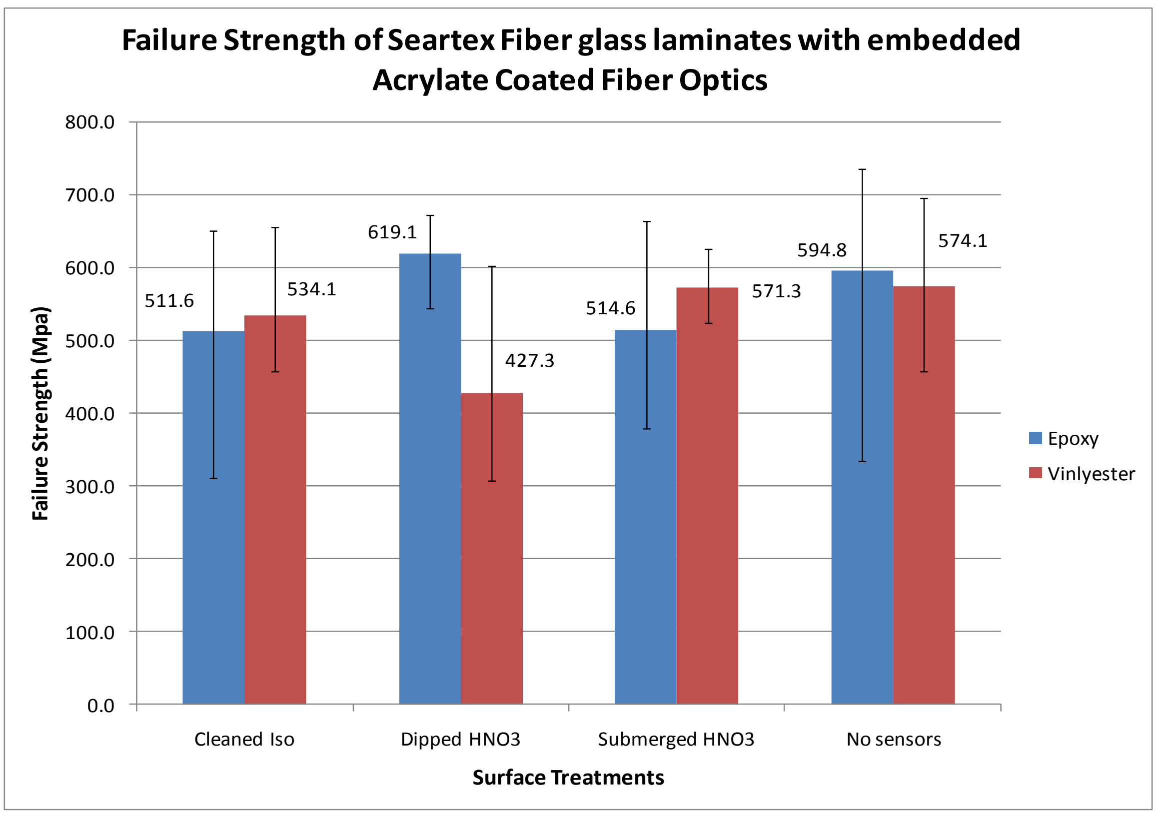

Figure 34. Tensile Strength of parallel embedded acrylate coated fiber optics parallel to the dominate fiber direction (All values normalized to 40% fiber volume fraction and to coupon thickness unaffected by sensor integration)

Samples created using vinyl ester resin had a reduction in strength for those fibers dipped in nitric acid, but those submerged in nitric acid for 10 seconds showed improvement.

Also, coupons with epoxy resin had a large increase in recovered strength, for those fibers dipped in nitric acid. The increase in strength exceeded that of the pristine samples, raising skepticism. Using student t testing it was determined that there was in fact no statistically significant difference in value between any embedded fiber optic configuration and those samples without fiber optics. With no significant reduction in strength due to fiber optic embedment no surface treatment was found to dominate. Thus overall it was concluded that while the results for tensile strength were not compelling, there was reason to conclude that the surface treatments were not necessarily needed. As with the strain gages and PVDF films, load carrying capacity of the samples with embedded acrylate coated fiber optics was analyzed as a check of the strength data.

Table 12. Tensile load carrying capacity at failure of samples with embedded fiber optics.

Acrylate Fiber Optic

	Load Carrying Capability (kN)	
Surface Treatment	**Vinylester**	**Epoxy**
No sensor controls	52.54	52.71
Cleaned with Isopropyl Alcohol	46.96	46.52
Dipped in 20% by weight Nitric Acid & cleaned with Isopropyl Alcohol	40.22	55.57
Submerged for 10 seconds in 20% by weight Nitric Acid & cleaned with Isopropyl Alcohol	49.95	46.62

Based on the data presented, in Table 12, the trends found in the strength data were not an artifact of local dimensional changes. There was no evidence to contradict the conclusions based on previous data; those results of apparent linear strain at failure were considered.

Table 13. Apparent strain at sample failure. (Based on sample modulus and failure strength).

Acrylate Fiber Optic

	Apparent % Strain at Failure	
Surface Treatment	**Vinylester**	**Epoxy**
No sensor controls	1.90	1.95
Cleaned with Isopropyl Alcohol	1.73	1.61
Dipped in 20% by weight Nitric Acid & cleaned with Isopropyl Alcohol	1.33	1.99
Submerged for 10 seconds in 20% by weight Nitric Acid & cleaned with Isopropyl Alcohol	1.76	1.62

The results, in Table 13, also follow that same trends found in tensile strength and load carrying capability. With no new trends it was concluded that the surface treatments were not necessary to minimize the effect of material degradation. However, due to the fluctuations further testing is warranted using the surface treatments used, as well as, potential alternatives.

Polyimide Coated Fiber Optics

The polyimide coated fiber optics used was supplied by the sponsors, Sandia National Laboratories Wind Energy Department. These fiber optics were the OFS CL POLY 1310 21 series [45]. The fiber optics were integrated into the laminates, in an identical manner to that of the acrylate coated fiber optics. Unlike the acrylate coated fiber optics, no signal was taken from the fiber optic during curing. The reason for this was the polyimide coating was too thin to strip off with mechanical strippers. The alternative was the use of a razor and a lighter, suggested by Jason Kiddy and his supervisor [46]. The coating should be carburized with the lighter and delicately removed with a razor. Given the amount of time necessary to accomplish such a task and the large probability of damaging the fiber optic past the point of any use, it was decided to forgo such a process. Polyimide, being a rather tough material chemically was not likely to excessively degrade due to surface treatment or embedment [39]. Therefore, without excessive degradation of the coating the fiber optic should produce similar signal result to that of the acrylate coated fiber optic during curing. While no signal data was collected from the polyimide coated fiber optics, it was still worth exploring the effects of such a composite configuration on the material.

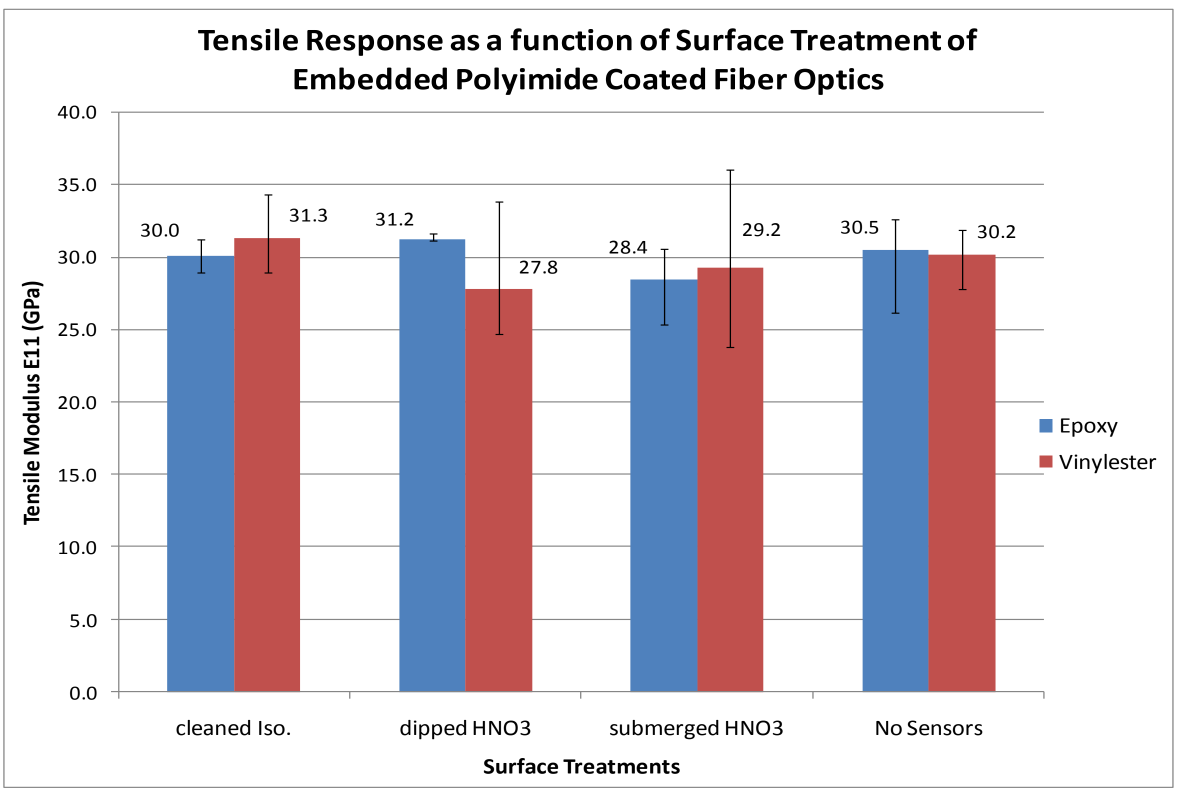

Figure 35. Tensile Modulus of parallel embedded polyimide coated fiber optic samples loaded to 1% strain (All values are normalized to 40% fiber volume fraction).

The effects on the material were the sole basis for gauging the necessity of surface treatment on embedded polyimide coated fiber optics. Based on the results presented in, Figure 35, it was determined that there was no noticeable effect on tensile modulus, due to fiber integration. The rationale behind this conclusion was that both resin samples, with embedded fiber optics, showed no statistically significant reduction in stiffness. There was however, a large reduction in strength, for both resins, associated with sensor integration as can be seen in Figure 36.

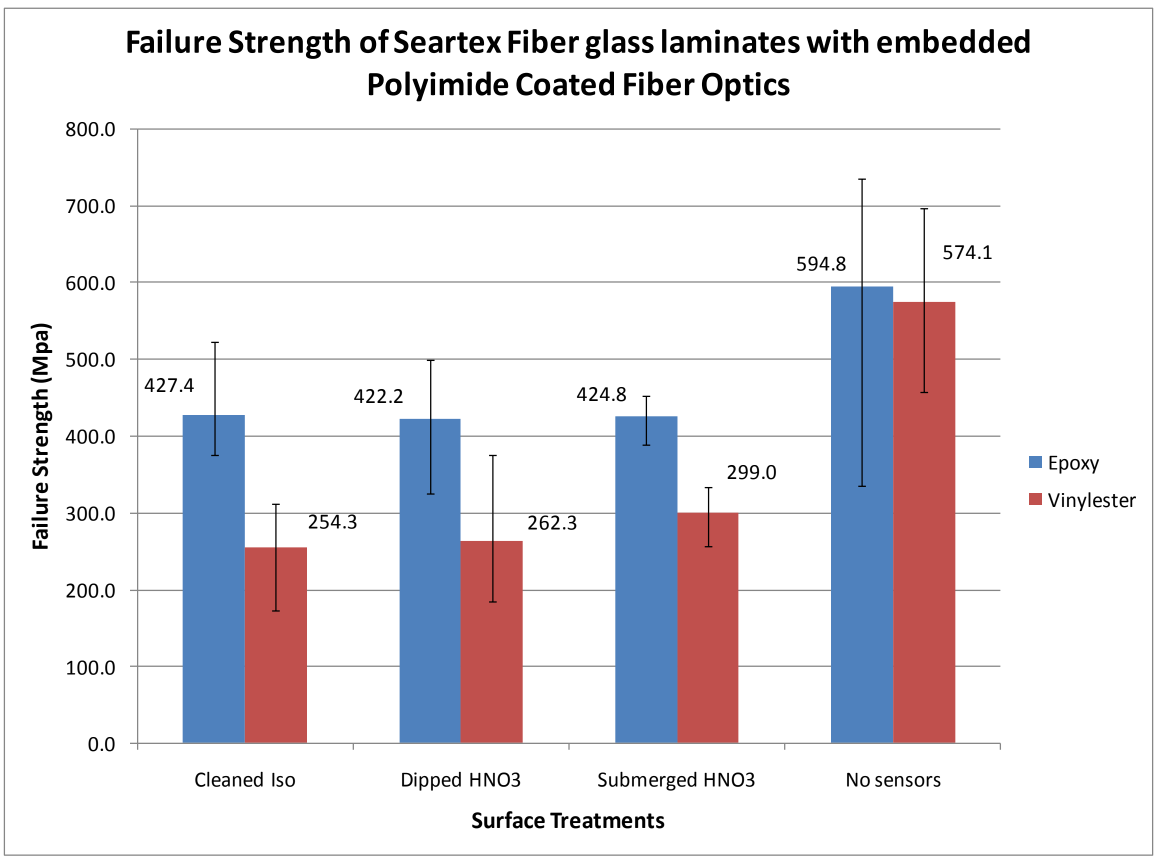

Figure 36, Tensile Strength of parallel embedded polyimide coated Fiber Optics (All values normalized to 40% fiber volume fraction and to sample thickness not affected by sensor)

Due to the very significant reduction in strength for those samples the modes of failure were studied with more scrutiny. While the gauge lengths of the polyimide coated fiber optics were identical to that of the acrylate coated fiber optics, it was found that the grip area was reduced. The reason for this was, the polyimide fiber optics where given more space than the acrylate fiber optics due to their larger minimum bend radius. This small change in area from the acrylate coated fiber optics to the polyimide coated fiber optics was enough to cause failure to initiate at the grips in the samples. While this was cause for re-evaluation and further testing, the failures were found to propagate into the fiber optic region prior to complete failure. This failure progression was why some insight could be gained from the results. An increase in strength due to surface treatment was noticed for those fiber optics in vinyl ester and no improvement was found for those embedded in epoxy. T testing of these results revealed that there was no significant difference between treatment techniques. Thus, further testing is necessary however to resolve this issue. The issue with grip area persisted in the load carrying capacity of the samples, as seen in Table 14. There was still the same trend for the vinyl ester samples found in the strength results. Additionally, the epoxy samples show a slight increase in load at failure due to surface treatment. This confirmed the finds stated previously, by the results of the strength evaluation. Apparent linear strain at failure was the last property explored by tensile testing of the samples with embedded fiber optic, coated in polyimide.

Table 14. Tensile load carrying capacity of composites with embedded polyimide fiber optics.

Polyimide Fiber Optic

	Load Carrying Capability (kN)	
Surface Treatment	**Vinylester**	**Epoxy**
No sensor controls	52.54	52.71
Cleaned with Isopropyl Alcohol	37.41	47.13
Dipped in 20% by weight Nitric Acid & cleaned with Isopropyl Alcohol	37.69	47.50
Submerged for 10 seconds in 20% by weight Nitric Acid & cleaned with Isopropyl Alcohol	40.05	48.53

Table 15. Apparent tensile strain at failure of samples with embedded polyimide coated fiber optics (Based on tensile modulus and failure strength).

Polyimide Fiber Optic

	Apparent % Strain at Failure	
Surface Treatment	**Vinylester**	**Epoxy**
No sensor controls	1.90	1.95
Cleaned with Isopropyl Alcohol	1.14	1.84
Dipped in 20% by weight Nitric Acid & cleaned with Isopropyl Alcohol	1.32	1.89
Submerged for 10 seconds in 20% by weight Nitric Acid & cleaned with Isopropyl Alcohol	1.43	2.01

It was found, in Table 15, that both resins showed a significant improvement in strain at failure related with increased surface treatment. However, both trends need further data to correct for the grip failures.

It was concluded, from the data presented from tensile testing, that surface treatment of those polyimide coated fiber optics embedded in both resins showed potential. However, further assessment is necessary because of the issue of required grip area.

FEA Study of Inclusions

To try and understand the strain field in the region around the inclusion due to changes in inclusion modulus, a finite element analysis case study was performed using ANSYS 11.0 student edition. A model was developed based on the tensile coupon geometry of an embedded PVDF film. The reason for choosing an embedded PVDF film was because of its relatively large geometry. The symmetry of the coupon about all three axes meant that only one eight of the coupon needed to be modeled in order to correctly reflex that of the actual sample. A list of the model's specifications are listed below.

- All values are given in pascals, meters, and newtons
- Sensor inclusion geometry 6.405E-3 m x 1.261E-2 m x 1.05E-4 m
- Composite thickness 8.5E-4 m
- Sample height and width respectively, 0.1016 m x 0.0254 m
- Applied load 44.48kN; applied to the top plane of the sample
- Boundary conditions
    - Y displacement on the bottom plane restricted to zero
    - X displacement on the left plane restricted to zero
    - Z displacement on the front plane restricted to zero
- Element type for both composite and sensor; SOLID 92
- 10499 elements in the model.

An image of the FEM model has been presented as Figure 37. The interest in the strain field surrounding the inclusion was the motivation for the increased mesh density around the inclusion.

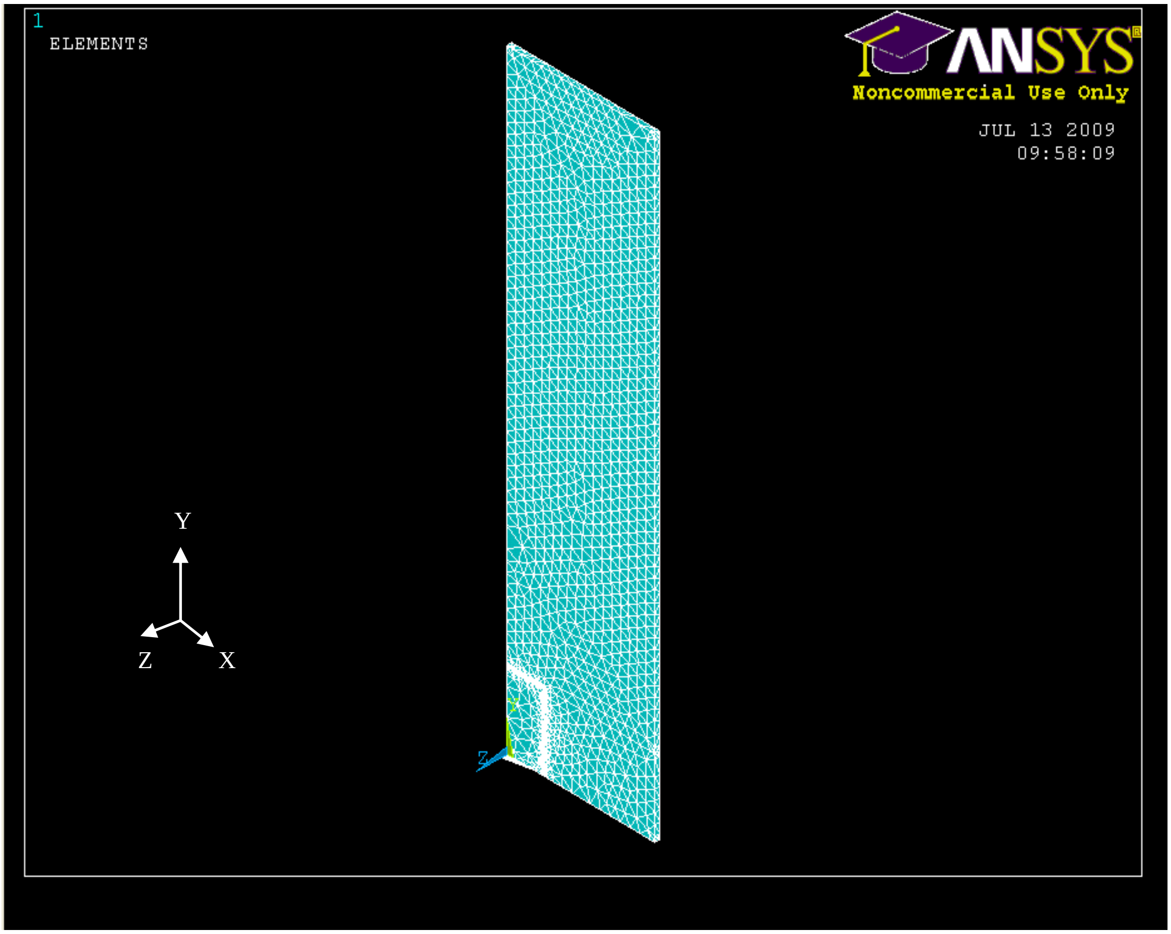

Figure 37, Completely meshed model of an embedded PVDF film in an epoxy laminate coupon

Seven different values, found in Table 16, were chosen to represent the modulus of the embedded sensor. These moduli ranged from 7 Pa, representative of a void, to 3.05E10 Pa, equivalent to the host composite material. The intended purpose of the FEM model was to change the modulus of the modeled inclusion and evaluate the change in strain field surrounding the sensors.

Table 16. List of Sensor region moduli tested in FEM case study.

Host Material Modulus

30.5 GPa

Array of Sensor Material Modulus

Test	Modulus
	(Pa)
1	7
2	3.50E+07
3	7.00E+07
4	1.05E+08
5	1.40E+08
6	1.28E+10
7	3.05E+10

Prior to exploring the effects of sensor modulus on the surrounding strain field, the model was validated by applying the load as detailed, and evaluating the longitudinal strain of the coupon with the sensor modulus equivalent to that of a void. Analytical predictions of the longitudinal strain for this configuration were calculated to be 1.6%. Represented in Figure 38, the fiberglass far field strain was estimated between 1.3% and 1.7%, thus validating the models accuracy.

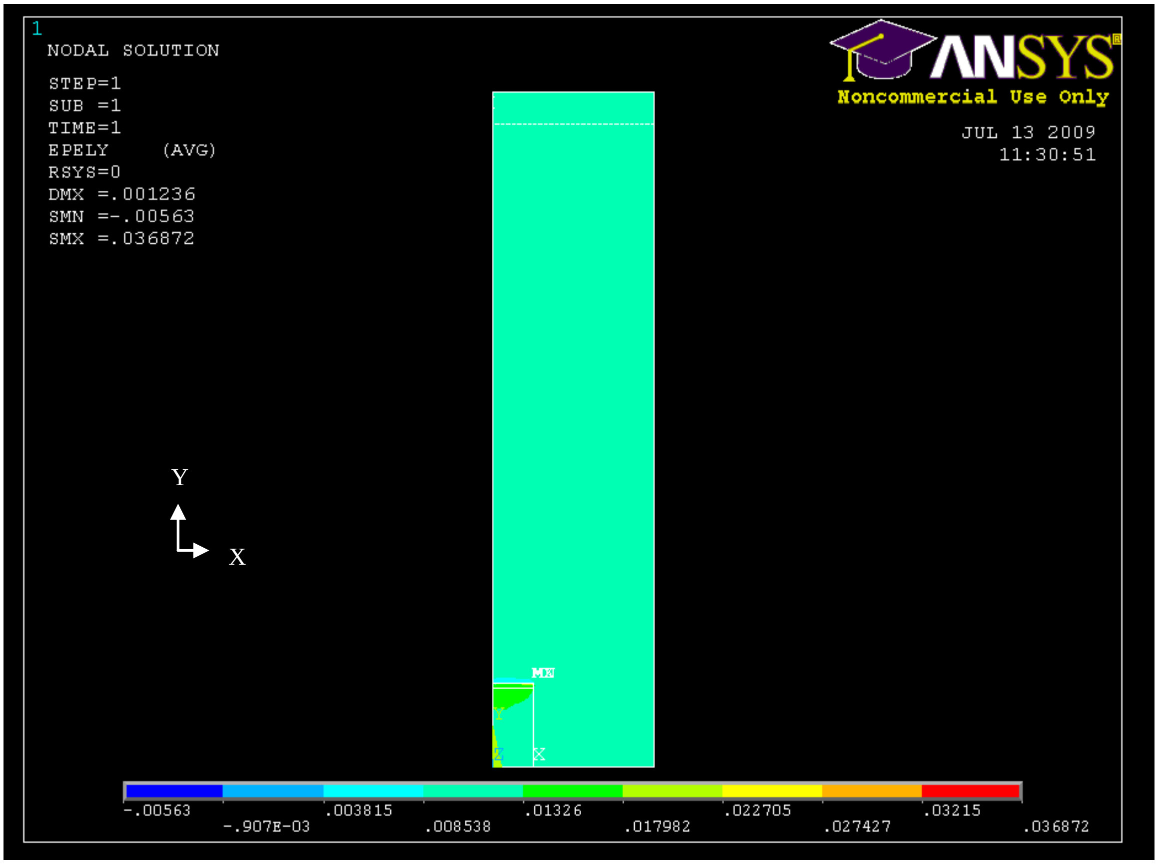

Figure 38. Validation test of FEA model prior to strain field evaluation.

Progressing on to the case study, based on Figure 39, it became clear that unless the modulus of the inclusion became close to the modulus of the fiberglass composite, there was limited effect on the strain of the fiberglass, except near the edges of the sensor in the Y direction. The result of this case study was beneficial to the overall study of embedded sensors in a qualitative sense. Illustrated in Figure 39, equivalent strain in the transverse direction showed little effect until the sensor modulus reached values of the same order of magnitude as the host material. It was determined that the far field strain was present less than 1.2mm (10% of the sensors width) away from the sensor edge for any embedded sensor with modulus less than that of aluminum.

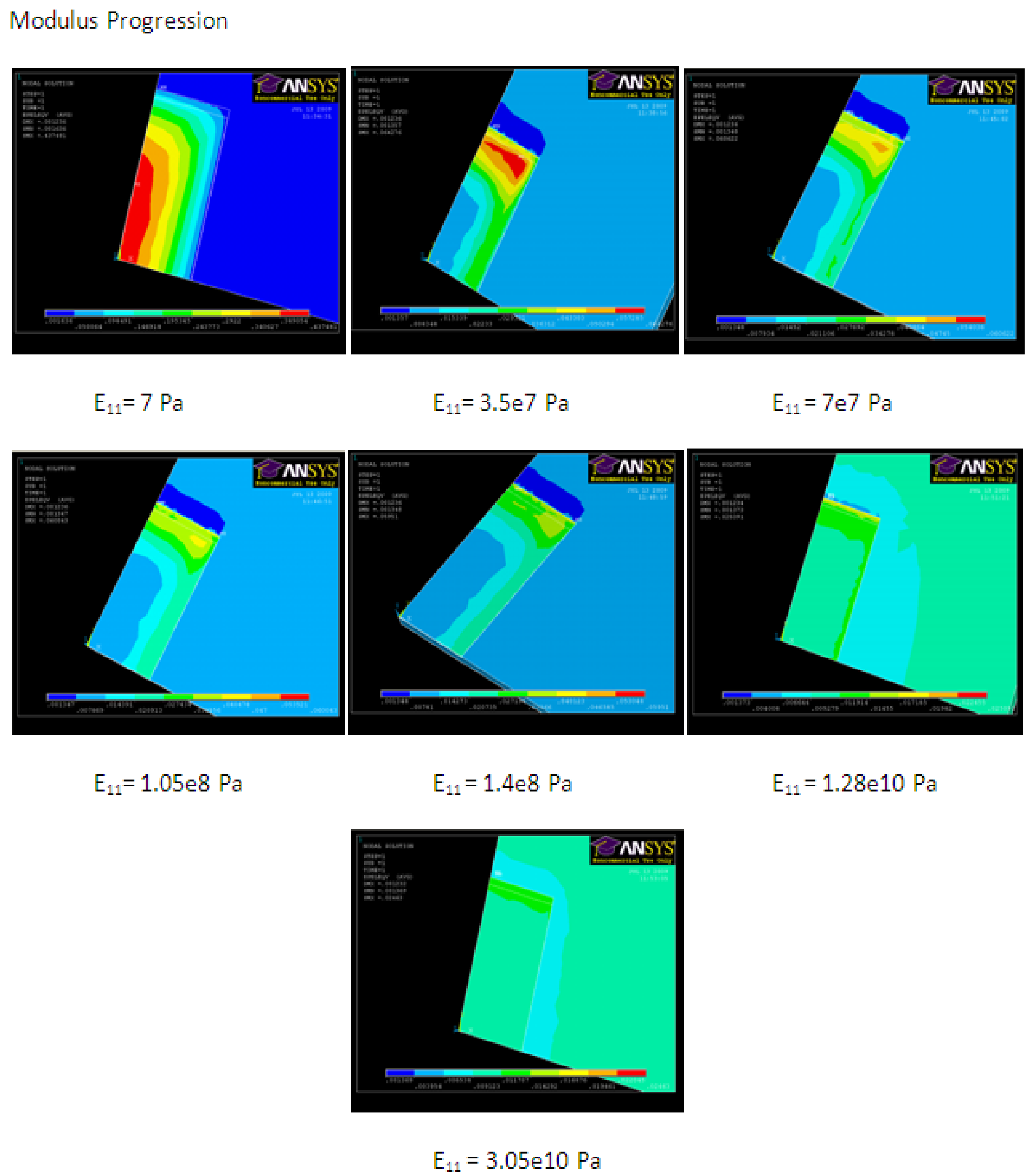

Figure 39. Case study of equivalent strain as inclusion modulus increases in stiffness.

With limited effect on the materials local strain in the transverse direction; actual sample strain, measured by an extensometer can be confidently relied upon. A second benefit to this study was that the samples width could be reduced with limited effect on the uniform stress distribution around the sensor. This is beneficial because of the ease of testing smaller samples. Strain in the longitudinal direction of the sample showed similar results. Far field strain was found at less than 20% of the sensors length for sensor moduli values equivalent or less than that of aluminum. Sensors exhibiting moduli equivalent to that of barium, which is unrealistic, achieved far field strain at less than 25% of the samples length. The results of this case study indicate that sensor integration does not show as significant affect on material integrity, as previously thought.

G_{1c} Testing of Embedded Sensors

All fracture toughness testing was performed on the Instron 8206 in EPS 138. The machine was able to be adapted for lower load testing. This adaptation was accomplished by disconnecting the standard 100kN load cell in the cross member and connecting a 2224.11N load cell, suspended from the upper grips. All samples were affixed with aluminum taps in a fashion compliant with ASTM standards, as seen in Figure 40. The initial crack length for all samples was recorded by measuring the distance between the far side of two dowel pins inserted into both tabs and the crack on either side of the sample. After which the samples were loaded until it was decided that the load was descending, which indicated propagation of the crack.

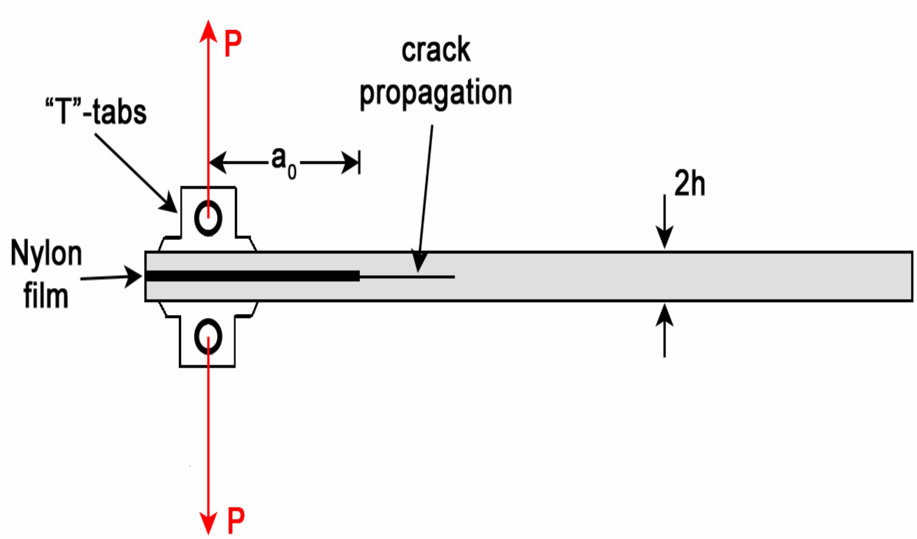

Figure 40. Fracture Toughness Double cantilever beam test configuration [16]

At that point the sample was unloaded, and the crack length was measured in the same manner as before. This process was performed during all tests until testing was completed. As mentioned earlier the samples were configured such that the sensor and the nylon film were not within 5mm of each other. This configuration meant that every sample had to be tested three times. The first to achieve the ASTM G_{1c} value, the second to progress the crack into the sensor, and the third to accurately evaluate the success or failure of the surface treatments developed. Due to this form of crack propagation, fiber bridging became a factor, seen in Figure 41. Fiber bridging is a phenomenon which occurs as the crack length increases. As the crack continues to propagate fibers within the plies on either side of the mid-plane remain attached to the resin on the opposing side of the crack surface. This bridging of the opening during the application of load increases the energy level necessary to continue propagation of the crack.

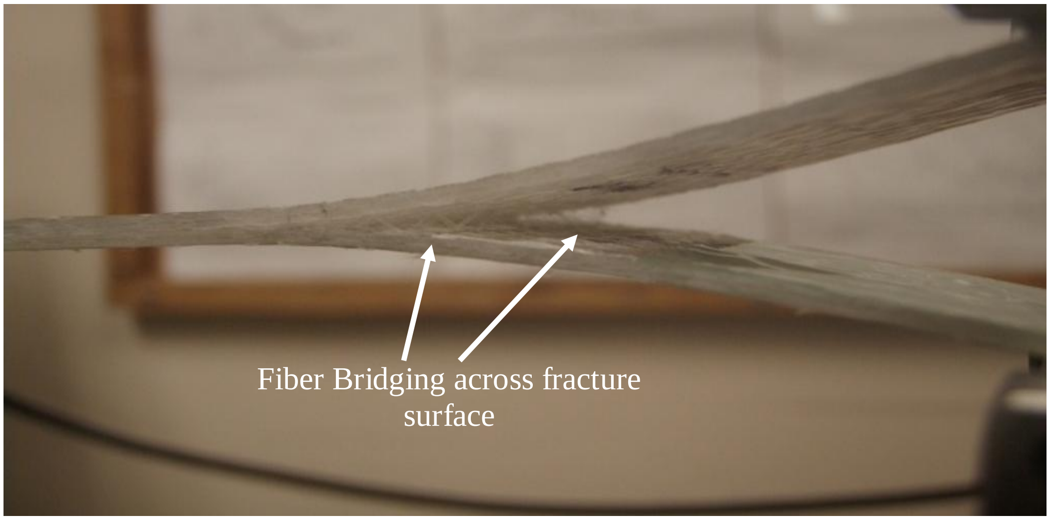

Figure 41. Fiber bridging of an epoxy G_{1c} sample during progressive crack growth.

Fiber bridging progressively increased the fracture toughness of the sample and thus the values used for evaluation of surface treatment success are considerably higher than those found through standard ASTM test evaluation. Due to fiber bridging's dominate role in fracture toughness for progressive crack growth, any increase seen by a surface treatment option cannot be directly correlated with increased bonding. However, because a successful bond between sensor and resin would result in an increase in the critical energy level necessary to propagate the fracture front, an increase in fracture toughness found to be statistically significant is an indicator of successful surface treatment. Lastly, no sample values were calculated using the ASTM standard, which is based upon modified beam theory. The sample values were calculated by numerically integrating the area between the load/displacement curves, shown in Figure 42. The reason for numerical integration was the non-linear region, near critical load, which frequently occurred during testing. This non-linear region has been hypothesized to be a result of construction with the 90s at the mid-plane, rather than the 0s.

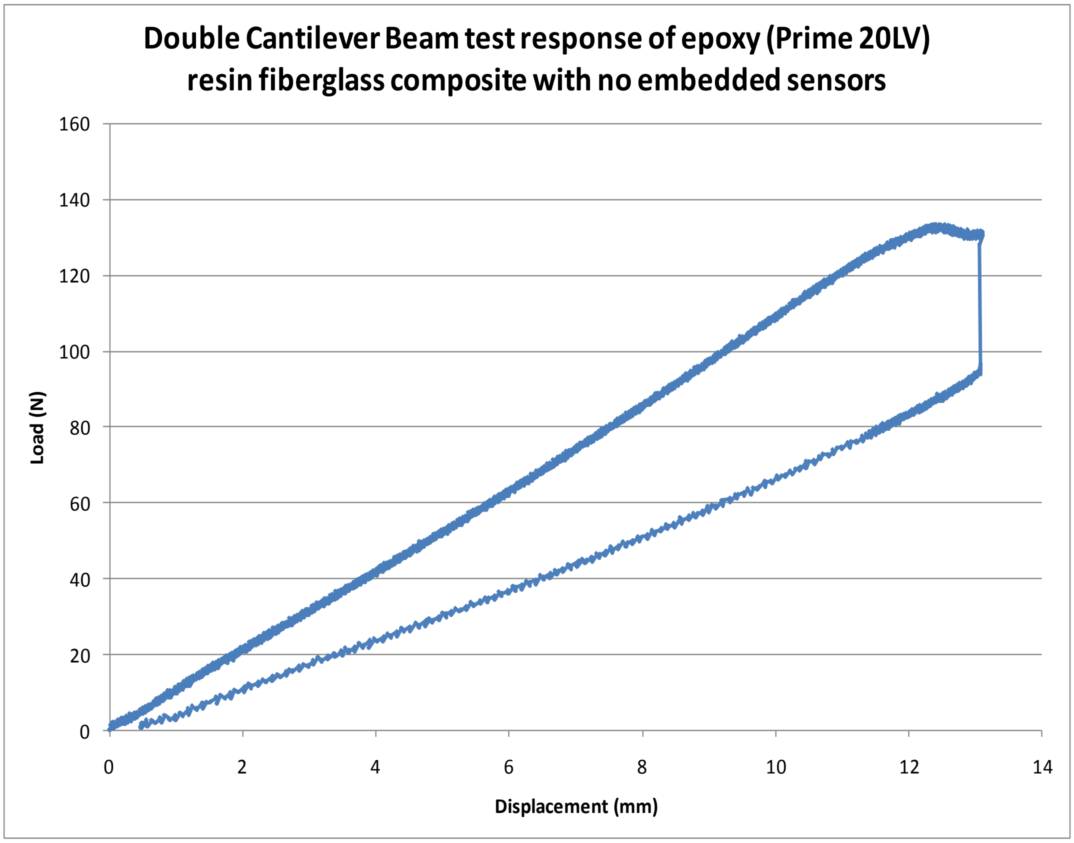

Figure 42. Example of the load displacement chart used in the determined of G_{1c} values.

Fractures in blades could also potentially occur by mode II. Therefore, while the results presented here are used as a means of evaluation they should not be used as the sole means of evaluation. Mode II fracture mechanics would likely interact with embedded sensors in ways not included in mode I testing. Table 17 below outlines all the test configurations used to evaluate the success of the two nitric acid surface treatments developed for this study.

Table 17, Test matrix of all the mode I fracture test configurations developed to evaluate the success of the surface treatments.

Mode I Fracture Toughness Test Matrix

Sensor	Surface Treatment	Minimum Number of samples	Location within in Laminate	Resins
Single Axis Strain Gage	cleaned with Isopropyl Alcohol	3	mid-plane	Prime 20 or Fibreglast 1110
Single Axis Strain Gage	Dipped in 20% by weight Nitric Acid and cleaned with Isopropyl Alcohol	3	mid-plane	Prime 20 or Fibreglast 1110
Single Axis Strain Gage	Submerged in 20% by weight Nitric Acid and cleaned with Isopropyl alcohol	3	mid-plane	Prime 20 or Fibreglast 1110
PVDF film	cleaned with Isopropyl Alcohol	3	mid-plane	Prime 20 or Fibreglast 1110
PVDF film	Dipped in 20% by weight Nitric Acid and cleaned with Isopropyl Alcohol	3	mid-plane	Prime 20 or Fibreglast 1110
PVDF film	Submerged in 20% by weight Nitric Acid and cleaned with Isopropyl alcohol	3	mid-plane	Prime 20 or Fibreglast 1110
Acrylate coated Fiber Optic	cleaned with Isopropyl Alcohol	3	mid-plane	Prime 20 or Fibreglast 1110
Acrylate coated Fiber Optic	Dipped in 20% by weight Nitric Acid and cleaned with Isopropyl Alcohol	3	mid-plane	Prime 20 or Fibreglast 1110
Acrylate coated Fiber Optic	Submerged in 20% by weight Nitric Acid and cleaned with Isopropyl alcohol	3	mid-plane	Prime 20 or Fibreglast 1110
Polyimide coated Fiber Optic	cleaned with Isopropyl Alcohol	3	mid-plane	Prime 20 or Fibreglast 1110
Polyimide coated Fiber Optic	Dipped in 20% by weight Nitric Acid and cleaned with Isopropyl Alcohol	3	mid-plane	Prime 20 or Fibreglast 1110
Polyimide coated Fiber Optic	Submerged in 20% by weight Nitric Acid and cleaned with Isopropyl alcohol	3	mid-plane	Prime 20 or Fibreglast 1110
Controls	N/A	3	N/A	Prime 20 or Fibreglast 1110

Number of vinyl ester laminates created	2
Number of epoxy laminates created	3

A note for all initial fracture toughness values reported below. Initial fracture toughness values are highly dependent on the geometry of the resin rich region at the end of the nylon crack initiator. This dependence led to large variations in fracture toughness.

Metal Foil Strain Gages

The same OMEGA single axis strain gage used during the tensile testing was used for G_{1c} evaluation testing [22]. All sensors were placed approximately equidistance between sample edges. It was found that both laminate resins showed improvement in fracture toughness. The values supporting this determination are show in Table 18 and Table 19.

Table 18. Fracture toughness values for epoxy laminates with embedded strain gages.

Sensor MFSG

Laminate	Surface Treatment	Initial G1c	Second G1c	Third G1c	Number of Data
26	cleaned	169.36	473.98	486.30	3
26	dipped	389.16	509.78	914.18	3
26	submerged	176.22	505.17	871.62	3
17,26	no sensors	367.82	609.11	753.69	8

The fracture toughness of samples with strains gages cleaned with isopropyl alcohol prior to embedding, were half that found for those sensors dipped in nitric acid. However, this increase was not shared for those sensors submerged in nitric acid for 10 seconds prior to cleaning and integration. The difference in increase would suggest that much further surface treatment would not be worth the cost of surface treating. Those vinyl ester laminates with embedded strain gages, surface treated prior to embedding saw a different trend in fracture toughness. There was an increase in fracture toughness associated with those sensors dipped in nitric acid.

Table 19. Fracture toughness values for vinyl ester composites with embedded strain gages.

Sensor MFSG

Laminate	Surface Treatment	Initial G1c	Second G1c	Third G1c	Number of Data
25	cleaned	190.67	423.40	522.58	3
25	dipped	253.25	515.32	584.25	3
25	submerged	205.60	494.05	530.11	3
16,25	no sensors	262.98	390.64	493.67	8

Submersion did not show this same increase, in fact it did not show any significant improvement. T testing indicated that this response was in fact scatter of the data rather than a significant trend. The benefit of this result was that there was no significant reduction in fracture toughness, for vinyl ester laminates, due to strain gage embedment.

These results combined with those found during tensile evaluation indicate that strain gage integration within epoxy laminates is successful given sensor surface treatment prior to integration. Based on the lack of positive fracture toughness results found for vinyl ester composites with embedded strain gages, it was determined that other surface treatment alternatives should be explored.

PVDF Films

The fracture toughness testing via the double cantilever beam technique for PVDF films was not as informative a process as for strain gages. Both laminate resins showed large reductions in fracture toughness due to sensor integration, as seen in Table 20, and Table 21.

Table 20. Fracture toughness values of epoxy laminates with embedded PVDF films.

Sensor PVDF

Laminate	Surface Treatment	Initial G1c	Second G1c	Third G1c	Number of Data Points
17,26	cleaned	382.32	324.85	442.18	3
17,26	dipped	331.86	345.28	314.79	3
17,26	submerged	156.98	371.83	533.65	3
17,26	no sensors	367.82	609.11	753.69	8

Additionally, large fluctuations in fracture toughness were noted and found to be insignificant artifacts of data scatter. The reason for the large amount of scatter was explored in more detail. All manufacturing records were checked against the samples. No errors in data collection and analysis were found.

Table 21. Fracture toughness values of vinyl ester laminates with embedded PVDF films.

Sensor PVDF

Laminate	Surface Treatment	Initial G1c	Second G1c	Third G1c	Number of Data Points
16,25	cleaned	206.80	275.52	268.34	3
16,25	dipped	169.04	294.47	242.04	3
16,25	submerged	236.08	329.62	274.75	3
16,25	no sensors	262.98	390.64	493.67	8

The progress of the crack through the sample during testing was checked. Being the largest sensor considered for embedment it was noticed that the crack propagated further than other sensors, and with a non-linear front, as seen in Figure 43. It is suspected that the size of the sensor led to increased scatter in data.

While the only information pertaining to embedment gathered was a significant decrease in fracture toughness due to integration.

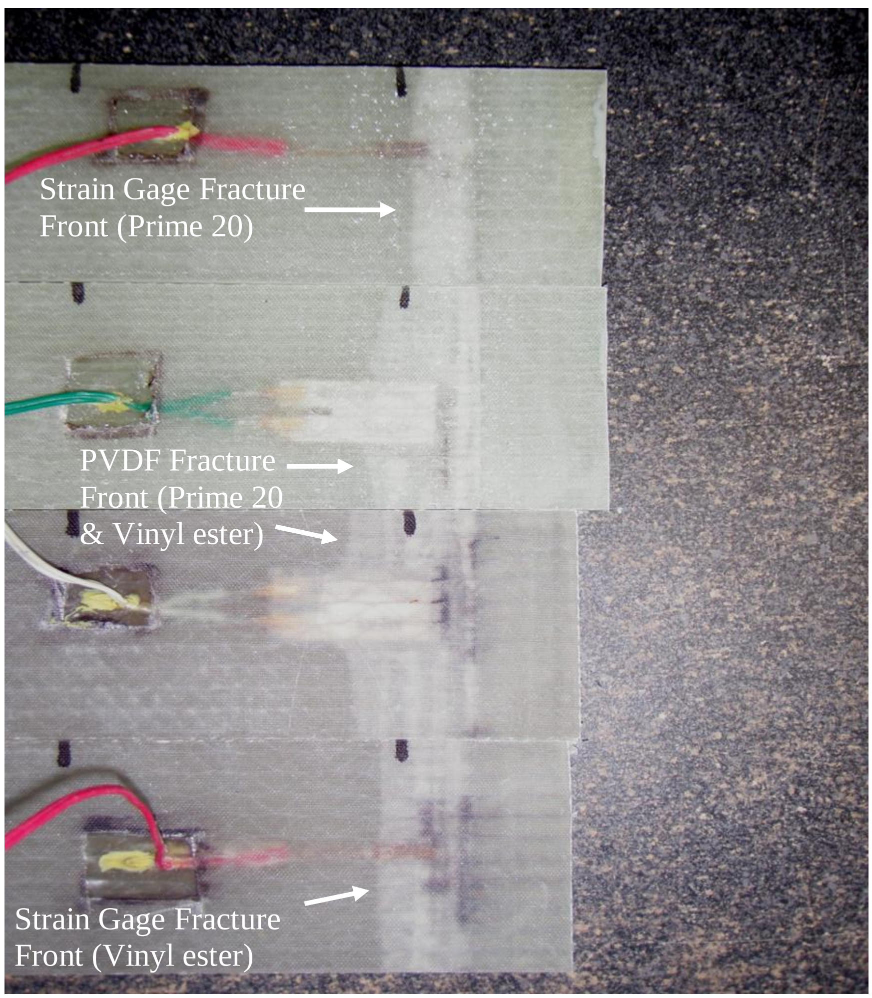

Figure 43, Fracture Front of Embedded PVDF films during mode I fracture.

Combined with the results of tensile testing it was concluded that if PVDF film integration was needed. The surface treatment techniques developed over the course of this study would be of benefit to structural health and sensor accuracy.

Acrylate Coated Fiber Optics

It was decided, due to the abundance of acrylate coated fiber optic available for this study, that two different fiber optic orientations would be considered. The first was orientation of the fiber optic in the dominant fiber direction. The second, was perpendicular to the dominant fiber direction. The reason for this additional configuration was because it was thought to be potentially the most detrimental configuration to material toughness. Based on the results gathered and presented in Table 22, Table 23, Table 24, and Table 25 this was the case.

Table 22. Fracture toughness of epoxy laminates with embedded acrylate coated fiber optics parallel to the dominate fiber glass direction.

Sensor A FO par

Laminate	Surface Treatment	Initial G1c	Second G1c	Third G1c	Number of Data Points
17,26	cleaned	356.41	707.17	951.46	3
17,26	dipped	282.27	677.05	690.76	3
17,26	submerged	289.76	550.43	518.40	3
17,26	no sensors	367.82	609.11	753.69	8

For those acrylate coated fiber optics embedded in epoxy there was a statistically significant decrease in toughness with increased surface treatment. An unexpected result with no hypothesis as of yet, indicating that further consideration was necessary. The trend was not shared by the vinyl ester laminates, which indicated an increase in toughness which was found to not be significant.

Table 23. Fracture toughness of vinyl ester laminates with embedded acrylate coated fiber optics parallel to the dominate fiber glass direction.

Sensor A FO par

Laminate	Surface Treatment	Initial G1c	Second G1c	Third G1c	Number of Data Points
16,25	cleaned	141.58	337.91	356.51	3
16,25	dipped	203.22	328.28	447.12	3
16,25	submerged	259.61	533.77	563.45	3
16,25	no sensors	262.98	390.64	493.67	8

However, with no significant reduction in toughness associated with fiber optic integration, an increase due to treatment is not necessary. The fracture toughness values gathered from those fiber optics perpendicular to the dominate fiber direction showed improvement with surface treatment for epoxy resin.

Table 24. Fracture toughness of epoxy laminates with embedded acrylate coated fiber optics perpendicular to the dominate fiber glass direction.

Sensor A FO perp

Laminate	Surface Treatment	Initial G1c	Second G1c	Third G1c	Number of Data Points
17,26	cleaned	369.96	441.57	357.64	3
17,26	dipped	394.73	363.16	446.68	3
17,26	submerged	506.93	585.96	714.12	3
17,26	no sensors	367.82	609.11	753.69	8

As hypothesized fiber optics oriented perpendicular to the dominate fiber direction was indeed more detrimental to fracture toughness. Cleaned fiber optics exhibited half the toughness of samples without fiber optics.

Table 25. Fracture toughness of vinyl ester laminates with embedded acrylate coated fiber optics perpendicular to the dominate fiber glass direction.

Sensor A FO perp

Laminate	Surface Treatment	Initial G1c	Second G1c	Third G1c	Number of Data Points
16,25	cleaned	169.68	334.94	431.17	3
16,25	dipped	181.08	580.53	422.89	3
16,25	submerged	198.84	413.89	427.63	3
16,25	no sensors	262.98	390.64	493.67	8

This significant decay in toughness was mitigated by the increase in fracture toughness recorded for fiber optics surface treated prior to embedding. The surface treatments did not appear to have an effect on fracture toughness for those samples created with vinyl ester. Additionally it was noticed that in fact there was no reduction in toughness noticed due to sensor integration. Visual monitoring of the fracture surface insured that the lack of effect on toughness was genuine. It was then determined that, with exception for those fiber optics parallel to the fiberglass embedded in epoxy, the surface treatments were successful and again necessary.

Polyimide Coated Fiber Optics

Fewer polyimide coated fiber optics were available compared to the acrylate coated fiber optic and therefore, the fiber optics were only oriented in the dominant fiber glass direction. The data presented in Table 26, indicate a slight increase in fracture toughness due to surface treatment for those fiber optics embedded in epoxy resin composite laminates.

Table 26. Fracture toughness of epoxy laminates with embedded polyimide coated fiber optics parallel to the dominate fiber glass direction.

Sensor P FO par

Laminate	Surface Treatment	Initial G1c	Second G1c	Third G1c	Number of Data Points
26	cleaned	523.41	767.10	995.85	3
26	dipped	420.44	966.57	1320.26	3
26	submerged	346.23	901.56	1010.63	3
17,26	no sensors	367.82	609.11	753.69	8

This increase was not statistically significant; however with no reduction in toughness due to fiber optic integration no improvement was necessary. There was a large reduction in fracture toughness due to surface treatment, found in Table 27. The decrease found in Table 27, indicated that surface treatment of fiber optics coated in polyimide, intended for embedment into vinyl ester laminates was not beneficial. However, it was found that these reductions were not statistically significant and that the only significant value was the third fracture toughness value for those fiber optics cleaned prior to embedding. The value of which was found to be almost twice as large as those found for samples without fiber optics. While an interesting result, all surface treatments are higher than that of the controls (no sensors). This would indicate that integration of the fiber optic was beneficial regardless of treatment, but due to the large amount of data scatter present in G_{1c} evaluation, further testing should be considered.

Table 27. Fracture toughness of vinyl ester laminates with embedded polyimide coated fiber optics parallel to the dominate fiber glass direction.

Sensor P FO par

Laminate	Surface Treatment	Initial G1c	Second G1c	Third G1c	Number of Data Points
25	cleaned	315.29	462.12	812.18	3
25	dipped	135.52	471.46	731.54	3
25	submerged	196.31	482.52	571.19	3
16,25	no sensors	262.98	390.64	493.67	8

Adding these finding to those of the tensile testing, the conclusion for vinyl ester laminates were amended. It was determined that surface treatment was potentially beneficial for those fiber embedded in vinyl ester but based on the data collected was not necessary. As for those fibers embedded in epoxy laminates, the results presented for fracture toughness indicated that surface treatment was necessary.

FESEM Images of Embedded Sensors

As a last means of evaluating surface treatment success, the sensors were imaged after testing using a Field Emission Scanning Electron Microscopy (FESEM). Images were taken across the thickness of untested samples, and of sensor surfaces post fracture. These images provided a means of qualitatively determining the success of sensor resin bonding. The justification behind the cross thickness imaging of undamaged tensile coupons was the visual exploration of bond success between sensor and resin, while limiting the damage of surface preparation on the sensor resin interface. Fracture surfaces were imaged for both cleaned and submerged sensors as a means of comparison.

Upon completion of the fracture toughness evaluation additional images were taken based on the values obtained. The rationale for these choices can be found in Tables 28 and 29.

Table 28, Rationale of the FEM images of the post fracture surface of the embedded sensors in composites constructed with vinyl ester.

Resin Fibreglast 1110 (Vinyl ester)

Sensor	Surface Treatment	Impetus
Single Axis Strain Gage	Dipped in 20% by weight Nitric Acid and cleaned with Isopropyl Alcohol	Largest fracture toughness of the three options as well as larger than no embedded sensor samples.
PVDF film	Cleaned in Isopropyl Alcohol	Large reduction in fracture toughness and control for treatment success.
PVDF film	Submerged in 20% by weight Nitric Acid and cleaned with Isopropyl Alcohol	Largest reduction of the three options of embedded sensor.
Acrylate coated Fiber Optic (Parallel)	Cleaned in Isopropyl Alcohol	Lowest fracture toughness value of the three treatment options and control for treatment success.
Acrylate coated Fiber Optic (Parallel)	Submerged in 20% by weight Nitric Acid and cleaned with Isopropyl Alcohol	Largest fracture toughness values of the options and larger than no embedded sensor samples
Acrylate coated Fiber Optic (Perpendicular)	Cleaned in Isopropyl Alcohol	Lowest fracture toughness value of the three treatment options and control for treatment success.
Acrylate coated Fiber Optic (Perpendicular)	Submerged in 20% by weight Nitric Acid and cleaned with Isopropyl Alcohol	Greatest toughness values of the three treatment options.
Polyimide coated Fiber optic (Parallel)	Cleaned in Isopropyl Alcohol	Greater than no embedded sensor sample toughness and control for treatment success.
Polyimide coated Fiber optic (Parallel)	Submerged in 20% by weight Nitric Acid and cleaned with Isopropyl Alcohol	Lowest fracture toughness value of the three treatment options.
No embedded Sensors	N/A	Comparison against embedded sensor samples

Table 29, Rationale for the FEM images of the post fracture surface of embedded sensors in composites constructed with epoxy.

Resin Prime 20 (Epoxy)

Sensor	Surface Treatment	Impetus
Single Axis Strain Gage	Cleaned in Isopropyl Alcohol	Reduction in fracture toughness and control for treatment success.
Single Axis Strain Gage	Submerged in 20% by weight Nitric Acid and cleaned with Isopropyl Alcohol	Greater than no embedded sensor samples and evaluation of treatment success.
PVDf film	Dipped in 20% by weight Nitric Acid and cleaned with Isopropyl Alcohol	Reduction in fracture toughness and evaluation of treatment.
PVDf film	Submerged in 20% by weight Nitric Acid and cleaned with Isopropyl Alcohol	Large increase in fracture toughness over dipped.
Acrylate coated Fiber Optic (Parallel)	Cleaned in Isopropyl Alcohol	Greater than no embedded sensor samples and control for treatment success.
Acrylate coated Fiber Optic (Parallel)	Submerged in 20% by weight Nitric Acid and cleaned with Isopropyl Alcohol	Greatest reduction in toughness of the three options as well as treatment evaluation.
Acrylate coated Fiber Optic (Perpendicular)	Cleaned in Isopropyl Alcohol	Large reduction in fracture toughness and control for treatment success.
Acrylate coated Fiber Optic (Perpendicular)	Submerged in 20% by weight Nitric Acid and cleaned with Isopropyl Alcohol	Large recovery of fracture toughness over cleaned and treatment evaluation.
Polyimide coated Fiber optic (Parallel)	Cleaned in Isopropyl Alcohol	Larger than no embedded sensor fracture toughness and control for treatment success.
Polyimide coated Fiber optic (Parallel)	Dipped in 20% by weight Nitric Acid and cleaned with Isopropyl Alcohol	Larger than no embedded sensor fracture toughness.
No embedded Sensors	N/A	Comparison against embedded sensor samples

All images were taken from the FESEM machine in the ICAL laboratory run by the Physics Department, at Montana State University.

Metal Foil Strain Gages

FESEM images of metal foil strain gages taken across the thickness of the samples showed limited bonding for those sensors embedded with no surface treatment, as seen in Figure 44.

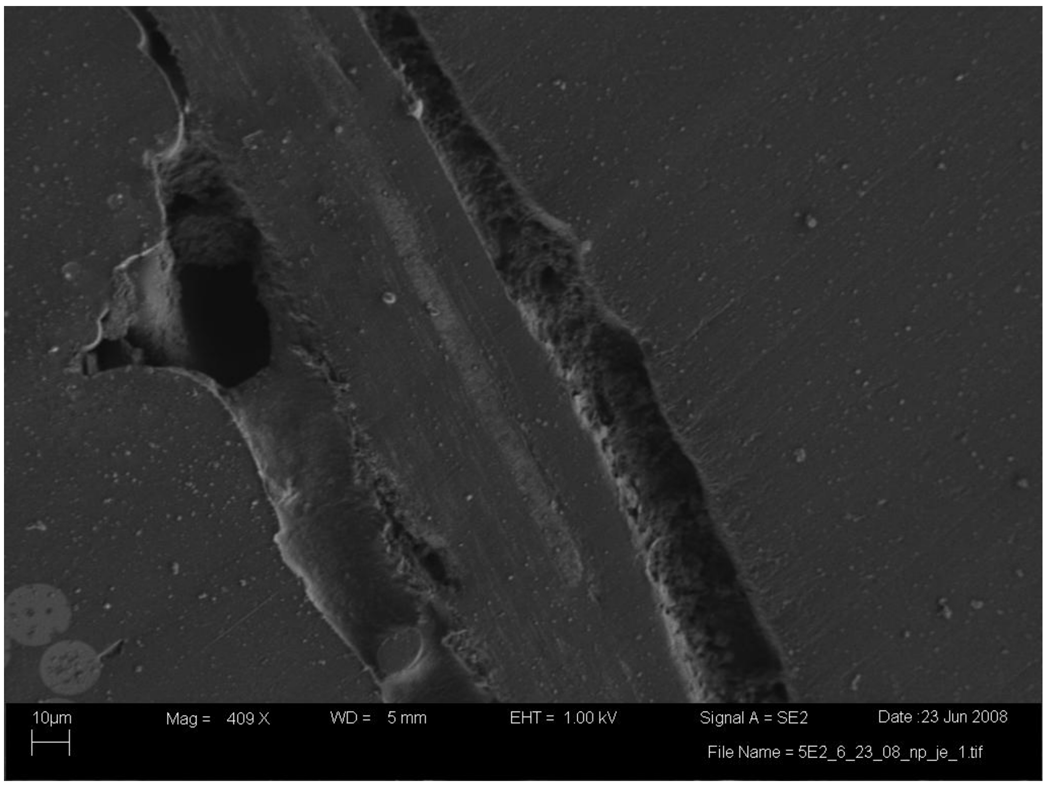

Figure 44. FESEM image of embedded strain gages with no surface treatments. Cross thickness view of the sensor, illustrating un-successful bonding between resin and sensor coating.

Images of unsuccessful bonding were frequent and were the reason surface treatment options for embedded sensors were developed. Once the surface treatments were developed it was determined that rather than continue with the sample imaging techniques, shown in Figure 44, imaging of the sensor surface was a better alternative. The reason being that continuing to image, as done previously, was informative, however, the chances of either polishing the surface past the sensor or to a local void was high, and could affect the conclusions drawn from this information. By imaging the surface of the embedded strain gages it became clear that the surface treatments developed had a significant effect on sensor\resin bonding. Figure 45, is an example of the images taken of cleaned strain gages embedment in epoxy laminates. There was no significant evidence of resin bonding on this sample other than this small particle of resin.

Figure 45. The surface of an embedded strain gage with no surface treatment, after failure. This was the largest resin particle found on the sensor surface.

This is in contrast with the successful bonding found between the epoxy resin and the strain gage surface treated with nitric acid for 10 seconds, in Figure 46. There were very noticeable patches of epoxy resin still attached to the sensor surface.

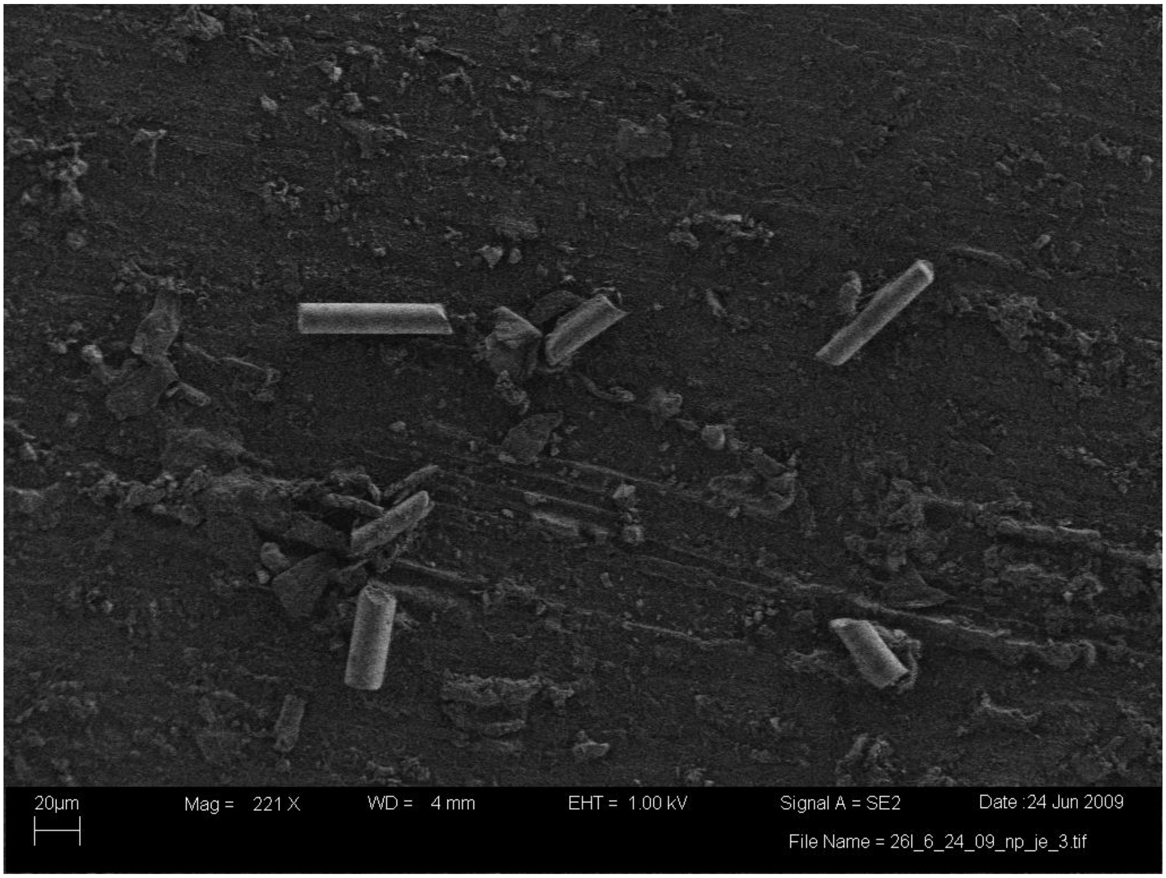

Figure 46. Epoxy resin bonding to embedded strain gage surface treated for 10 seconds in nitric acid. The amount of resin still present on the sensor coating surface suggests successful bonding.

This was also the case for those sensors embedded in vinyl ester laminates. The resin bonding found, in Figure 47, is clearly more successful than found, in Figure 48. Figure 47 is an example of the bonding between the vinyl ester resin and a strain gage dipped in nitric acid prior to integration within a laminate. Even this mid-level surface treatment was clearly advantageous over the surface bonding of the cleaned strain gage, of Figure 48.

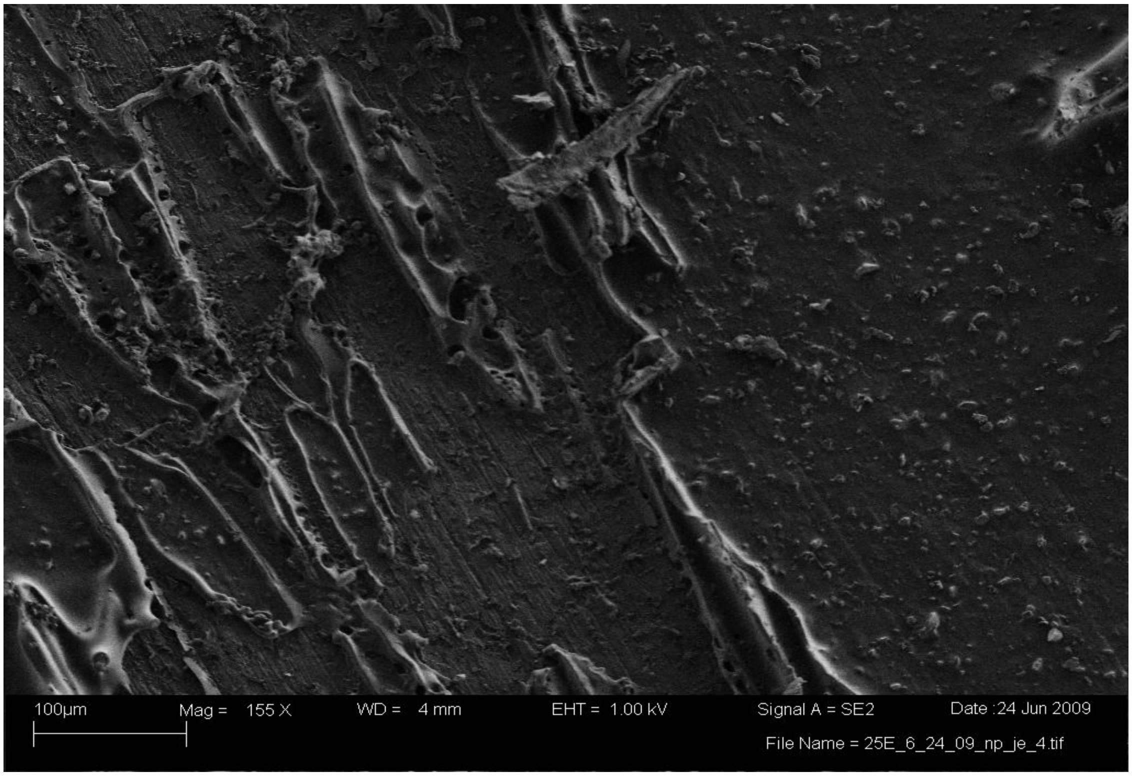

Figure 47. Sensor/resin bonding between vinyl ester resin and a strain gage dipped in nitric acid prior to embedment. There is a considerable amount of resin still adhered to the sensor surface.

Combining these finding with those already considered from both testing techniques it was determined that surface treatment showed few benefits for fiber reinforces composited using vinyl ester as the matrix. Given the reduction in strength, the stress level at sensor failure, and the slight drawbacks in sensitivity and load carrying capacity it was concluded that the benefits do not outweigh the costs. Alternative means of surface treatment for strain gages embedded in vinyl ester resin should be considered.

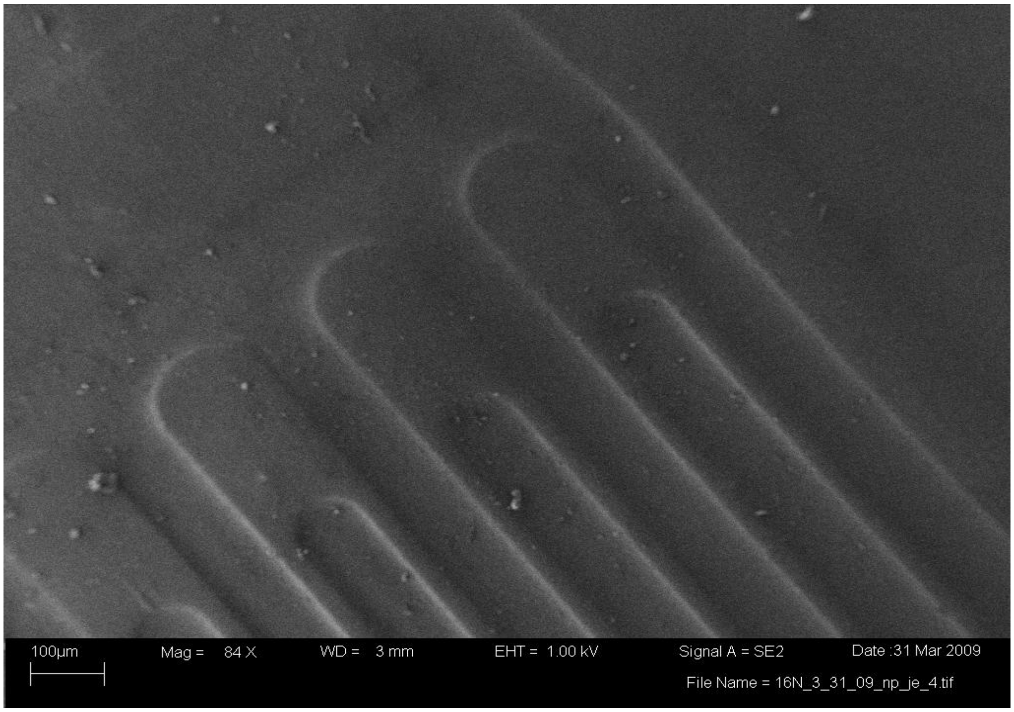

Figure 48. No significant resin bonding found for an embedded strain gage cleaned prior to embedment in vinyl ester laminates.

As for those strain gages embedded in composites employing epoxy as the fiber binder, the benefits outweighed the slight reduction in signal sensitivity. Thus it was recommended that surface treatment by submersion in 20% by mass nitric acid solution for 10 second is beneficial to sensor/material integration.

PVDF Films

Initial cross thickness images of PVDF films showed an interesting effect between the vinyl ester resin and the coatings of the PVDF. Several images taken in this manner show clear signs of chemical interaction between the liquid vinyl ester resin the acrylic and Mylar coatings of the PVDF films. An example of this chemical reaction during injection can be seen, in Figure 49. The chemical reaction is thought to have degraded the sensitivity and effectiveness of the PVDF films. The capacitive plates, used to collect the charge developed during induced strain on the PVDF film, was clearly degraded. By introducing voids and regions of altered silver ink (the capacitive plates) the collection of charge was un-doubtably retarded. This finding being noted, it was decided to continue testing as developed prior, in an attempt to quantify the effect of this chemical reaction.

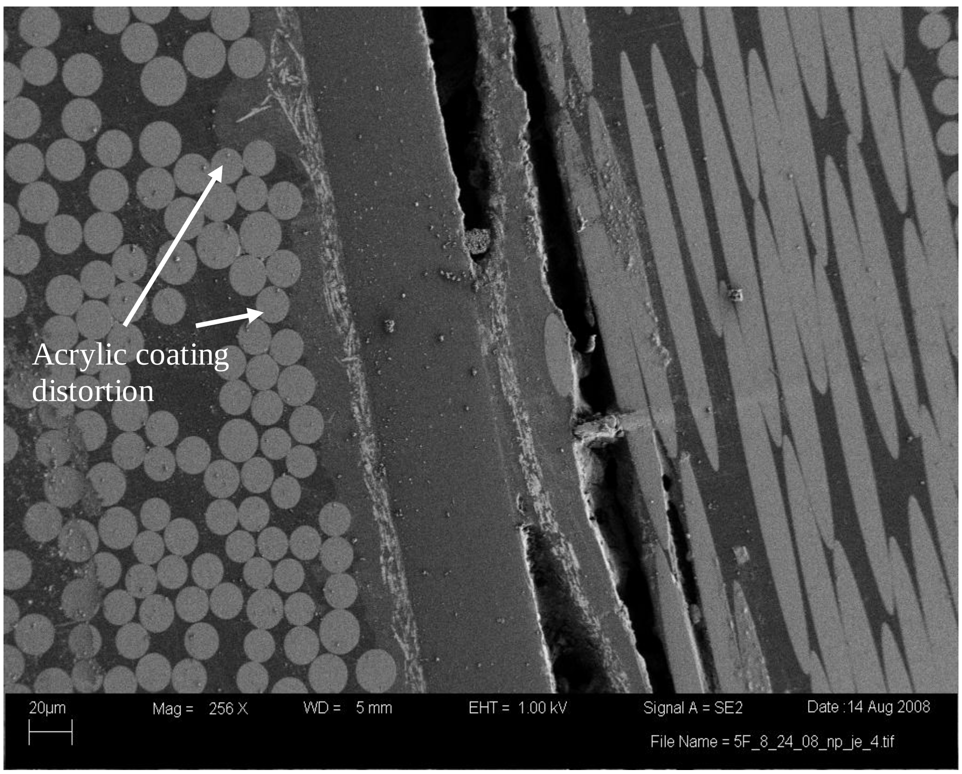

Figure 49. Chemical reaction between vinyl ester resin and PVDF film coatings. This reaction led to distortion of the top acrylic coating of the PVDF as well as the silver ink capacitive layer.

As with the strain gages, imaging of the cross thickness was halted, in favor of imaging the sensor surface for resin bonding. As suspected by the chemical reactivity of the vinyl ester resin and the PVDF coating, successful bonding between the two would be easily accomplished. Figure 50, is a comparison between a PVDF film submerged for 10 seconds in nitric acid and a PVDF cleaned prior to embedment in laminate. Given the reactivity between the acrylic top coating and ketone, solvent in the vinyl ester resin, the images, in Figure 50, are most likely of the Mylar bottom coating.

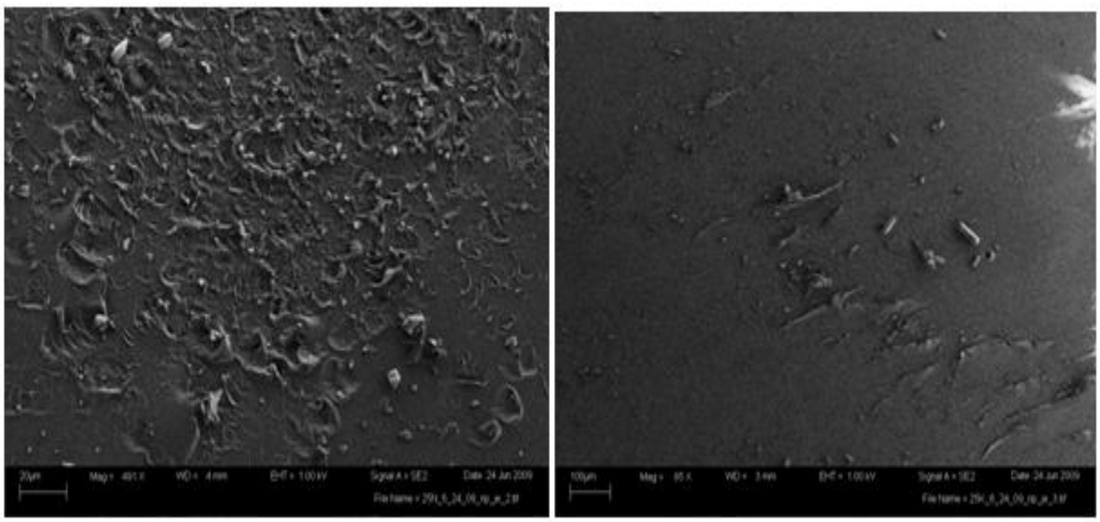

Figure 50. Comparison of surface\ resin bonding between PVDF films and vinyl ester resin (left is of a PVDF submerged for 10 second in nitric acid; right PVDF cleaned with isopropyl alcohol)

Without this chemical reaction between the resin and the coating, the surface bonding between the epoxy resin and the PVDF film was not as extensive. Figure 51, is the progression of surface bonding with increased surface treatment. The cleaned PVDF shows some signs of resin adhesion. The PVDF dipped in nitric acid showed more resin bonding than those cleaned, but the difference was not large. Finally, those PVDFs submerged for 10 seconds in nitric acid showed the most resin bonding, still not extensive but the presences of large resin coated regions was telling.

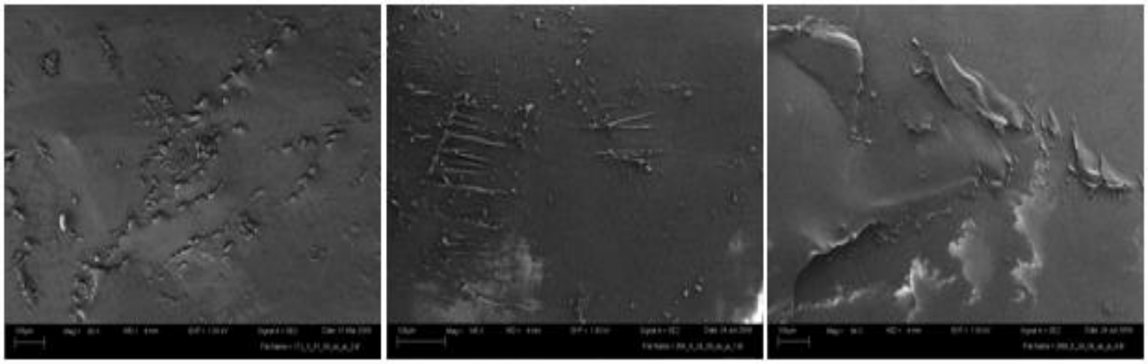

Figure 51. Progression of epoxy resin bonding to PVDF films due to surface treatment. (left to right; cleaned, dipped in nitric acid, submerged in nitric acid for 10 seconds)

After examining all the results for all forms of evaluation it was concluded that surface treatment for PVDF films worked well with both resins. The effect of the chemical reaction between the coating on the PVDF film and vinyl ester resin was not significant enough to render the sensor unusable even for the most extensive form of surface treatment. Thus, it was decided that submersion for 10 seconds in a 20% by weight solution of nitric acid prior to embedding was a successful form of sensor integration with composites constructed using vinyl ester resin. Similarly, it was decided that submersion of the PVDF, in nitric acid, was a viable means of increasing the bonding between epoxy resin and sensor.

Acrylate Coated Fiber Optics

Cross thickness imaging of acrylate coated fiber optics was ineffective at determining surface\resin bonding. FESEM images similar to that, of Figure 52, were common and could not be conclusively attributed to poor bonding. It was determined that the only means of qualitatively evaluating the effectiveness of surface treatment on sensor bonding was through the imaging the fracture surface of tested G_{1c} samples. Through the imaging of the fracture surfaces it was found that surface treatment was effective in increasing the amount of resin which bonded to the sensor.

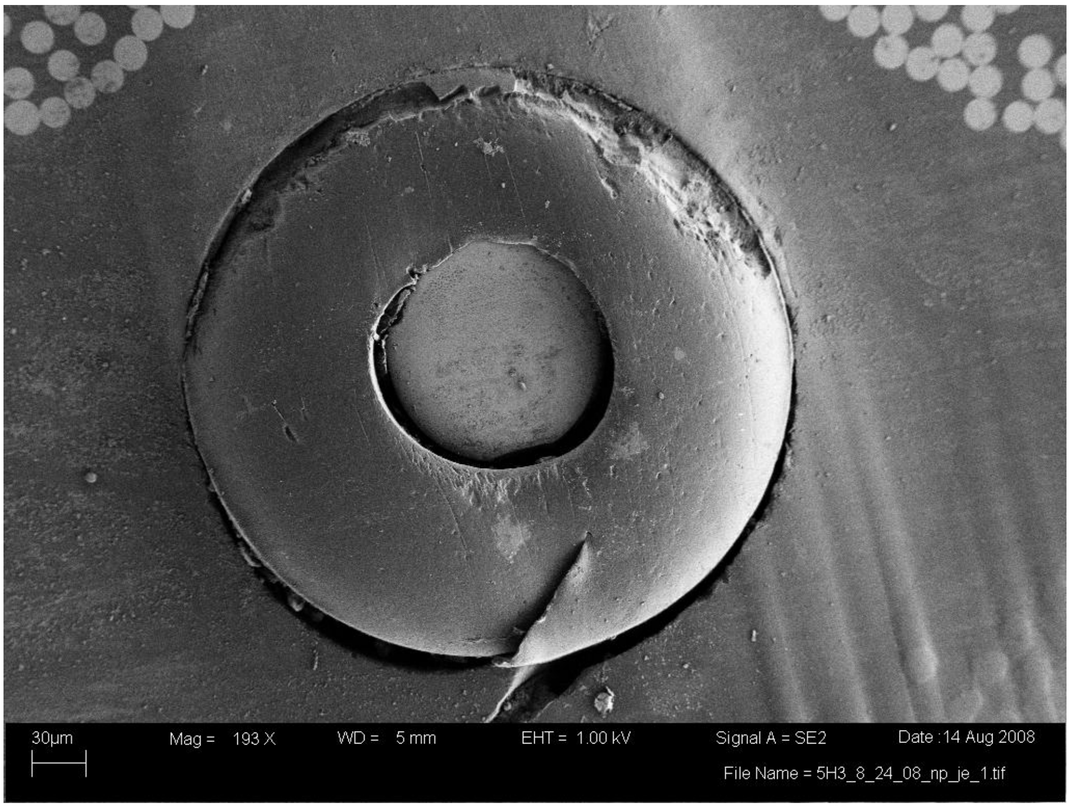

Figure 52. Cross thickness image of acrylate coated fiber optic embedded in vinyl ester laminate

Figure 53, is an example of the bonding between vinyl ester resin and the acrylate buffer coating of the embedded fiber optic. The upper left hand side of the fiber optic, in Figure 53, has clear signs of unsuccessful bonding, which are not present for those fiber optics with acrylate coating treated prior to embedment. In fact, the bonding between the coating and the vinyl ester resin is so successful that it appears that in some locations the fiber optic was not the weakest part of the laminate, as seen by Figure 54.

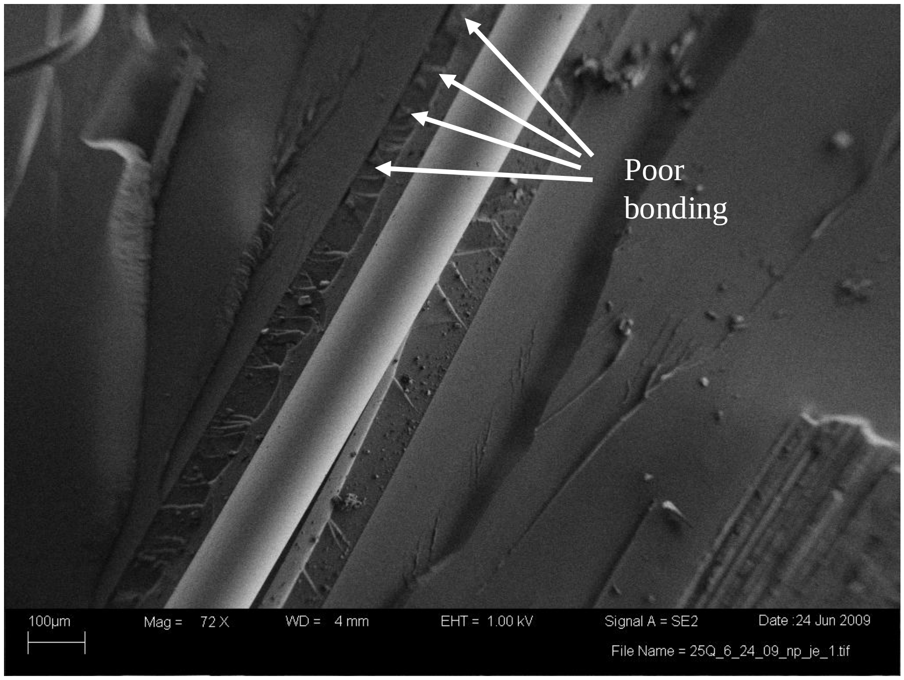

Figure 53. Acrylate coated fiber optic with no surface treatment embedded in vinyl ester laminate.

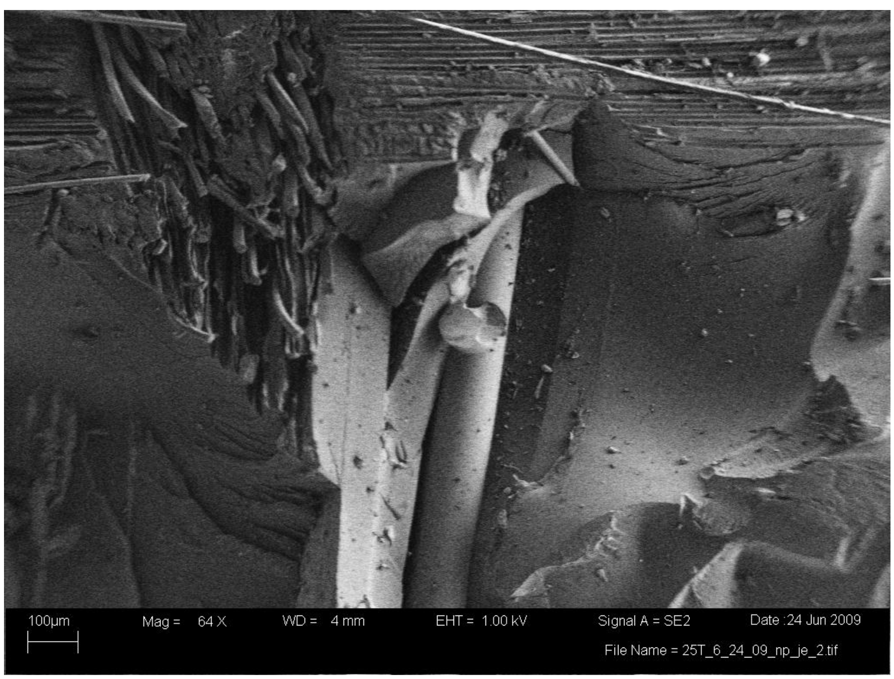

Figure 54. Fracture surface of vinyl ester sample with embedded acrylate coated fiber optic surface treated by submersion in nitric acid for 10 seconds.

The presence of fiberglass tows above the mid plane, in Figure 54, indicates that the path of least resistance was not through the fiber optic. The qualitative findings of the epoxy matrix interaction with the acrylate coated fiber optics was the same. There was a clear increase in sensor\resin bonding between the acrylate coating and the epoxy resin.

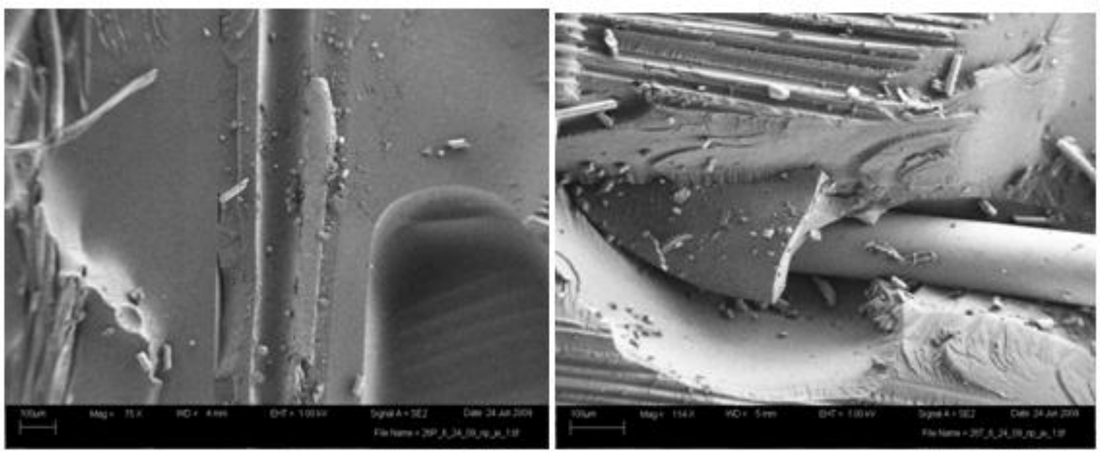

Figure 55. Effect of surface treatment of fiber optic coated in acrylate and embedded in epoxy laminates (left, fiber optic cleaned only, right, fiber optic submerged in nitric acid for 10 seconds.)

The presence of unsuccessful bonding can be found in the left hand image, of Figure 55. Also in the image on the right there is evidence that the fracture surface was not always on the same plane, as the embedded fiber optic, indicating strong bonds between sensor and resin.

It was concluded that submersion in a 20% by weight nitric acid solution for 10 seconds would increase the effectiveness of combined system. Some of the results found for those samples generated from vinyl ester laminates did not have a clear increase in bonding related to a raise in surface treatment. However, with no significant drawbacks and a majority of tests suggesting the necessity of surface treatment, submersion in nitric acid was the choice of surface treatment for fiber optics coated in acrylate, embedded in vinyl ester composites. The samples employing epoxy as the composite matrix were not as definitively conclusive but with only one significant drawback, submersion for 10 seconds in nitric acid, was found to be successful.

Polyimide Coated Fiber Optics

Unlike all the other potential sensors studied, due to limited supplies, fiber optics coated in polyimide were not imaged cross thickness. Solely examining the images of the fracture surface of the G_{1c} samples it was determined that the surface treatment had an effect on the amount of vinyl ester resin bonding to the polyimide coating of the fiber optics. As before, it was noticed that the fiber optic shown on the left, of Figure 56, which was cleaned with isopropyl alcohol, was not as securely adhered to the remaining composite.

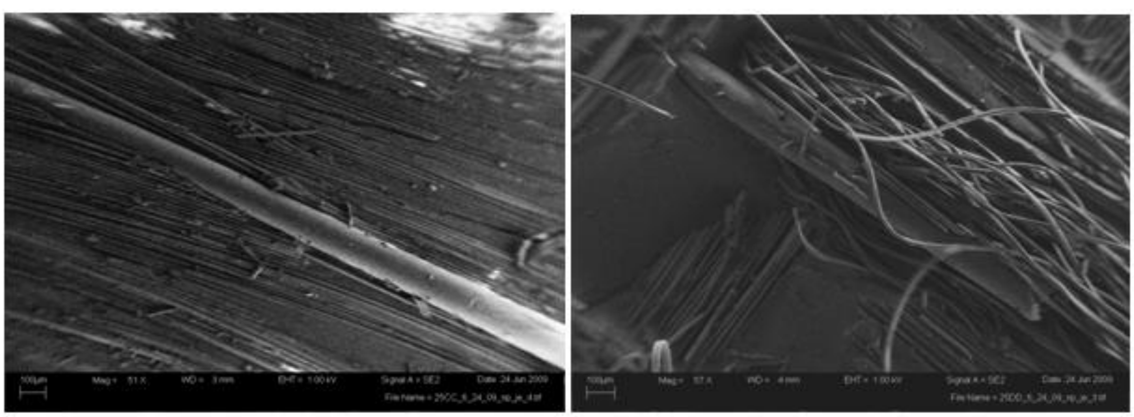

Figure 56. Comparison of surface treatment options for polyimide coated fiber optics in vinyl ester fiberglass composites (left; fiber optic cleaned only, right; fiber optic submerged in nitric acid for 10 seconds)

The fiber optic on the right in Figure 56, which was submerged in nitric acid for 10 seconds, was more securely adhered. Unsuccessful bonding was found along the surface of the polyimide coated fiber optics only cleaned prior to integration with epoxy laminates, as seen on the left of Figure 57.

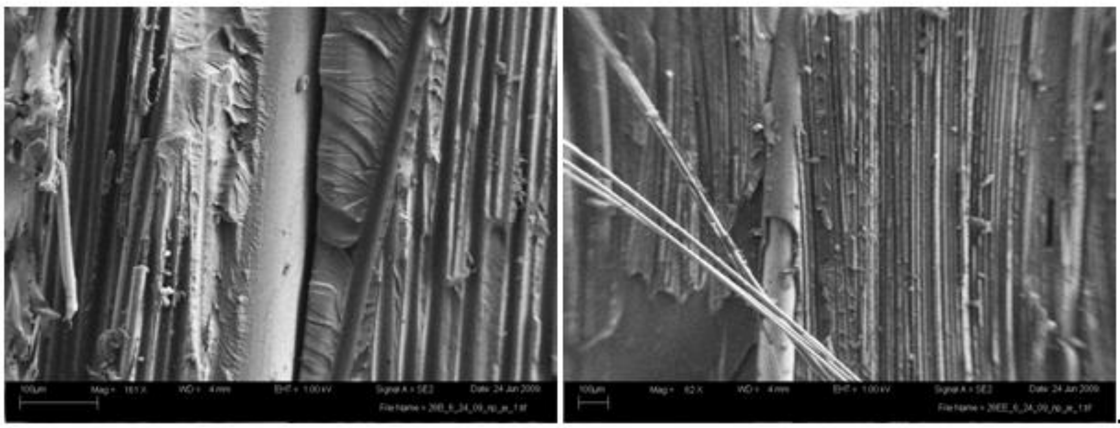

Figure 57, Comparison of surface treatment options for polyimide coated fiber optics embedded in epoxy fiberglass composites (left; fiber optic cleaned only, right; fiber optic submerged in nitric acid for 10 seconds)

However, successful bonding was examined, in Figure 57, for those fiber optics submerged in nitric acid for 10 seconds, confirming the need and success of surface treatment.

Compiling all the information from previous tests it was determined that for those fiber optics coated in polyimide and embedded in vinyl ester fiberglass composites, surface treatment was not necessary. The reason for this conclusion was the significant reduction in fracture toughness related to surface treatment compounded by the strength results which must be studied further to conclusively determine if the slight increase in strength can truly be attributed to surface treatment. It was also determined that submersion in a 20% by weight solution of nitric acid for 10 seconds was the most effective method of surface treatment explored for the successful integration of polyimide coated fiber optics and epoxy reinforced composites. This was a conclusion based on no noticeable drawbacks prohibiting use of the surface treatment. However, because of the questionable strength results found in this study further work should be done before any conclusive recommendations are made about surface treatment techniques for embedded fiber optics coated in polyimide.

CONCLUSIONS & FUTURE WORK

The conclusions, recommendations, and future work, based on the results presented here are considered to address the concept of embedded sensors as it pertains to the composite structures used in wind turbine blades. Additionally, it is considered that the manufacturing techniques and hierarchical evaluation procedure, which are results of this study, have not been seen by the author in others work in the field.

Conclusions

The first objective of this study were to evaluate and quantify the success of the manufacturing techniques developed to embed strain gages, PVDF films, and fiber optics coated in polyimide or acrylate, within composites of similar architecture to that found in the wind industry. Based on analysis of the data collected manufacturing recommendations were developed. The final objective of this study was to develop a hierarchical evaluation procedure which could be used to evaluate future sensor-composite combinations.

Compatibility Assessment Procedure

A challenge presented in this investigation was the development of a process through which the sensors could be successfully evaluated for laminate compatibility. The procedure illustrated below, in Figure 58, was developed based on the exploration into the four sensors included in this study. Assessment of compatibility between a specified sensor and laminate would considerably simplify the procedure shown below.

The reason for this is the absence of reconsideration of sensor choice during the evaluation process.

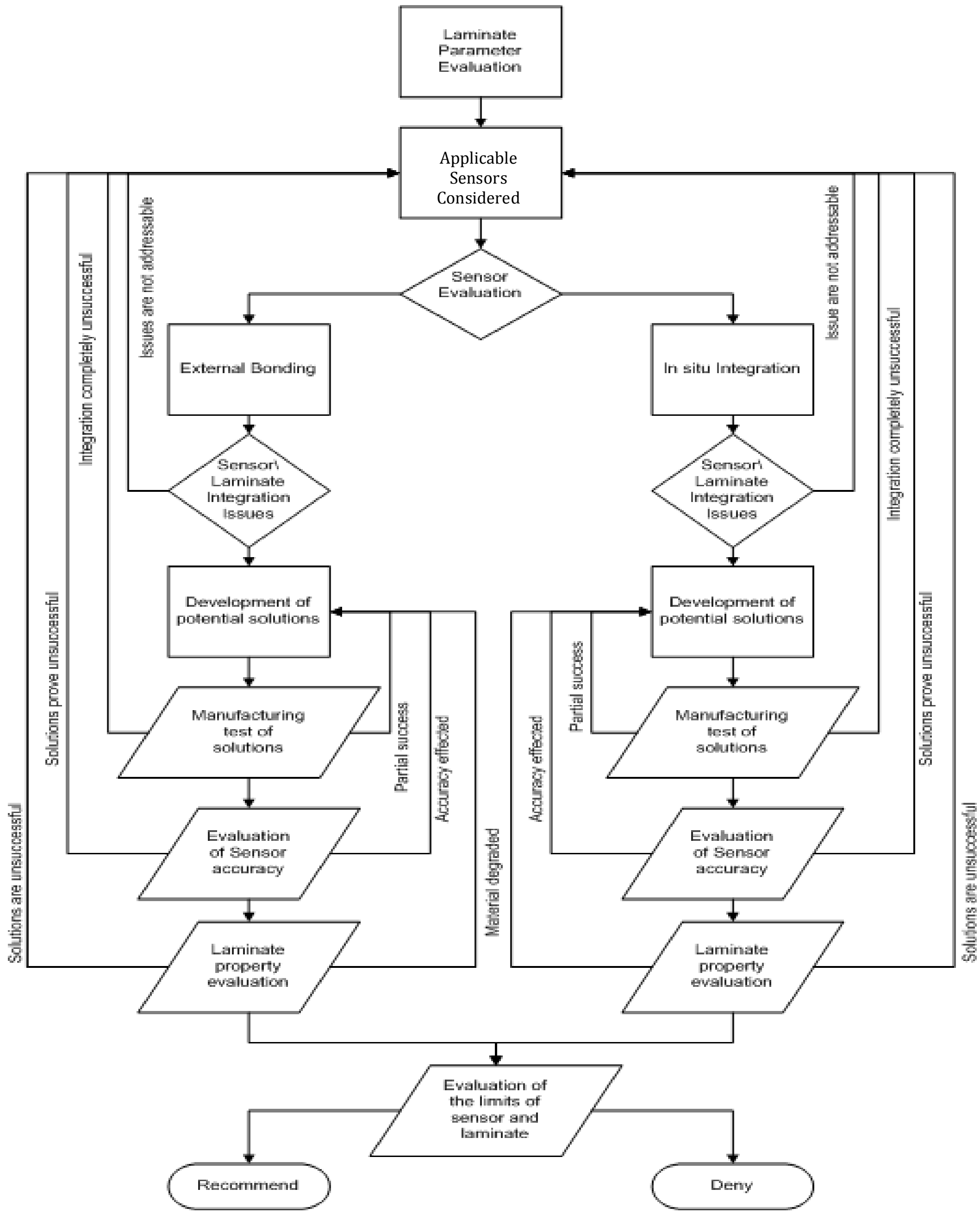

Figure 58. Flow chart of the procedure through which the compatibility of a sensor and laminate is evaluated.

The procedure for evaluation of compatibility should follow this sequence:

- Laminate Parameter Evaluation – what within the laminate is of interest to necessitate the need for monitoring of this sort.
- Applicable Sensors Considered - what sensors are available that meet the needs of the project.
- Sensor Evaluation – given the sensors geometry, monitoring technique, and durability, a decision as to what area of integration best suits the sensor.
- External Bonding – integrating the sensor by externally adhering the sensor to the laminate surface.
- In situ Integration - Inclusion of the sensor during manufacturing of the laminate.
- Sensor\Laminate Integration Issues – Prediction and assessment of potential issues associated with integration of each sensor.
- Development of Potential Solutions – Research and determination of techniques to alleviate or mitigate the issues of integration for each sensor.
- Manufacturing test of solutions – Appraisal of solution success through test manufacturing of the proposed permutation of laminate and sensor.
- Evaluation of Sensor Accuracy – Sensor accuracy determined through circuit continuity, and testing. (testing in the form of tensile response and the like)
- Laminate Property Evaluation – Laminate, material response quantified through testing (partial assessment can be determined concurrently with Evaluation of Sensor Accuracy).

- Evaluation of the limits of the sensor and laminate - determine the points at which the system would begin to fail as a result of the combination.

Manufacturing Recommendations

Analysis of the configurations considered in this paper concluded with a group of manufacturing recommendations for each of the four sensors considered, as it pertained to the fiber reinforcement architecture used. These recommendations were solely based upon the findings collected, which have been outlined in detail previously. For ease of reference these conclusions and recommendations have been compiled into Tables 30, 31, 32, and 33, below.

Table 30. Conclusions and Recommendations for Embedded Strain gages.

Fabric material Seartex Uni-directional (U14EU920-00940-T1300-100000)

Sensor Omega 1 axis strain gage (KFG-5-120-C1-11L1M2R)

Matrix resin	Recommended surface treatment	Additional Manufacturing notes	Rational
Vinyl ester	other forms of surface treatment be explored	Aresol adhesive should be applied to the sensor before placing at the mid-plane to resist the chance of lead wire movement.	Results indicating reduction in tensile strength and sensor accuracy outwiegh the increase in fracture toughness
Prime 20 (epoxy)	Submersion in a 20 percent by weight solution of Nitric Acid for 10 seconds, proceeded with rinsing of the sensor in distilled water and cleaned with Isopropyl Aclohol prior to embedding	Aresol adhesive should be applied to the sensor before placing at the mid-plane to resist the chance of lead wire movement.	Limitted reduction in sensor sensitivity was only drawback amist increase in failure strain, and fracture toughness

Table 31. Conclusions and Recommendation for embedded PVDF films.

Fabric material Seartex Uni-directional (U14EU920-00940-T1300-100000)

Sensor Measurement Specialities PVDF film (LDT0-028K/L w/crimps)

Matrix resin	Recommended surface treatment	Additional Manufacturing notes	Rational
Vinyl ester	Submersion in a 20 percent by weight solution of Nitric Acid for 10 seconds, proceeded with rinsing of the sensor in distilled water and cleaned with Isopropyl Aclohol prior to embedding	Aresol adhesive applied to sensor to prevent movement during injection. Avoid contact with solvents reactive with acyrlic polymer	Increase in sensitivity and stress at sensor failure, combined with strong qualatative finding.
Prime 20 (epoxy)	Submersion in a 20 percent by weight solution of Nitric Acid for 10 seconds, proceeded with rinsing of the sensor in distilled water and cleaned with Isopropyl Aclohol prior to embedding	Aresol adhesive applied to sensor to prevent movement during injection.	Increase in sensor response as well as material response at failure under tensile loading.

Table 32. Conclusions and Recommendations for embedded Fiber Optics coated in acrylate.

Fabric material Seartex Uni-directional (U14EU920-00940-T1300-100000)

Sensor Single Mode Fiber Optic coated in Acrylate (SMF-28)

Matrix resin	Recommended surface treatment	Additional Manufacturing notes	Rational
Vinyl ester	Submersion in a 20 percent by weight solution of Nitric Acid for 10 seconds, proceeded with rinsing of the sensor in distilled water and cleaned with Isopropyl Aclohol prior to embedding	fiber optics should be layed out on fabric at the desired locations and restrained by small patchs of scotch tape. Tape should also restain PVC jacketing used as fiber optic reinforcment during egress. Tape should to extend into the designated gage region.	Increase in fracture toughness for both fiber optic orientations combined with mixed improvements in tensile strength.
Prime 20 (epoxy)	Submersion in a 20 percent by weight solution of Nitric Acid for 10 seconds, proceeded with rinsing of the sensor in distilled water and cleaned with Isopropyl Aclohol prior to embedding	fiber optics should be layed out on fabric at the desired locations and restrained by small patchs of scotch tape. Tape should also restain PVC jacketing used as fiber optic reinforcment during egress. Tape should extend into the designated gage region.	Increase in fracture toughness for fiber optic orientation perpendicular to dominate fiberglass direction as well as mixed improvements in tensile strength

Table 33. Conclusions and Recommendations for embedded Fiber Optics coated with polyimide.

Fabric material Seartex Uni-directional (U14EU920-00940-T1300-100000)

Sensor Single Mode Fiber Optic coated in Polyimide (CL POLY 1310 21)

Matrix resin	Recommended surface treatment	Additional Manufacturing notes	Rational
Vinyl ester	no surface treatment necessary	fiber optics should be layed out on fabric at the desired locations and restrained by small patchs of scotch tape. Tape should also restain PVC jacketing used as fiber optic reinforcment during egress. Tape should to extend into the designated gage region. Extreme care should be taken to the fiber optic given the delicate nature of this form.	Qualative FESEM images are not sufficient information to indicate surface treatment at this time. However, inidicators suggest potential which should be examined further.
Prime 20 (epoxy)	Submersion in a 20 percent by weight solution of Nitric Acid for 10 seconds, proceeded with rinsing of the sensor in distilled water and cleaned with Isopropyl Aclohol prior to embedding	fiber optics should be layed out on fabric at the desired locations and restrained by small patchs of scotch tape. Tape should also restain PVC jacketing used as fiber optic reinforcment during egress. Tape should to extend into the designated gage region. Extreme care should be taken to the fiber optic given the delicate nature of this form.	Fracture toughness values in combination with FESEM images indicate successful bonding

Based on the data collected it has been concluded that the manufacturing techniques developed for the given composite architectures considered showed relative success for the majority of sensor-composite combinations. However, further testing is needed to confirm some of the findings presented here.

Future Work

The conclusions and recommendation made here are based on finding collected from only a small segment of configurations routinely experienced by the wind industry. Therefore, while these conclusions represent progress which can be helpful, further work is necessary before complete certainty can be applied to the embedding of sensors within wind turbine blades.

A list of suggestions of future work by the author can be found below.

- Detailed assessment of the causes of mixed results found for fiber optics coated in acrylate.
- Re-evaluation of tensile strength for those polyimide coated fiber optics embedded in vinyl ester, and epoxy reinforced composites.
- Testing of Fiber optics with Fiber Optic Bragg Grating under curing conditions, as well as tensile, flexure, and fatigue loading.
- Exploration into alternative surface treatments tailors to each individual sensor
- Mode II fracture testing
- Tensile fatigue testing of all configurations presented within this document.
- Flexure testing of samples with embedded sensors
- Re-evaluation of all configurations with carbon fiber reinforcement
- Thick laminate sample testing.
- Partial blade integration as verification prior to full scale blade testing
- Full scale blade testing of embedded sensors and retrieval system

The majority of suggestions are at the coupon level. However, partial and full scale blade testing are not trivial methods of evaluation. The easiest avenue through which to complete partial blade integration would be to further modify the prototype developed by James Blockey and Jonathan Ehersman [4] [12]. With any existing blade cross section modified with active control surfaces, sensor integration would not be difficult. Sensors could be externally bonded to the blade. Internally bonded sensors could be simulated by covering the sensors with more fiber glass.   In order to test the integration of strain sensors it is recommended that the root 25% of a smaller scale blade be used. Full scale blade testing is recommended to take two forms. Externally bonded sensors to existing blades, is already underway. It is recommended that common locations of sensors be determined. The reason being, direct comparison between externally bonded sensors and embedded sensors could be achieved, given identical blade configurations. Embedding sensors would start by encasing sensors in the resin at the surface of the fabric. Further embedding would follow given acceptable results. It is recommended that sensor embedding follow the manufacturing techniques developed over the course of this study with one exception. Rather than weave sensor wiring through fabric layers it is recommended that wiring be retrieved through fabric layer ends. Lastly, it is recommended for full scale blade trails that all support systems be externally adhered to the blade surface, with the data acquisition system housed in the rotor hub.

REFERENCES

1. Merriam-Webster Online. [Online] 2008. [Cited: Dec 31, 2008.] http://www.merriam-webster.com/dictionary/energy.

2. *Annual Energy Outlook 2008 with Projections to 2030.* s.l. : Energy Information Administration, 2008.

3. *Advanced Wind Technology: New Challenges for a New Century.* Laxson, R. Thresher and A. Athens, Greece : National Renewable Energy Laboratory, 2006. European Wind Energy Conference.

4. Blockey, James Craig**.** *FEASIBILITY IN DEVELOPING SMART STRUCTURES FOR USE IN WIND TURBINE BLADES.* Mechanical and Industrial Engineering Dept., Montana State University. Bozeman : s.n., 2008. MS Thesis.

5. Lowitz, Melissa. The Encyclopedia of Earth . *Altamont Pass, California.* [Online] 2008. [Cited: Dec 31, 2008.] http://www.eoearth.org/article/Altamont_Pass,_California.

6. *Improving Wind Turbine Gearbox Reliability.* W. Musial, S. Butterfield, B. McNiff. Milan, Italy : National Renewable Energy Laboratories, 2007. 2007 European Wind Energy Conference.

7. United States - Wind Resource Map. s.l. : National Renewable Energy Laboratories, 2008.

8. Rumsey, Mark. Blade Sensors. [PowerPoint Presentation]. s.l. : Sandia National Laboratories; Wind Energy Technology Department, 2007.

9. Hau, Erich. *Wind Turbines, Fundmentals, Technologies, Application, Economics.* 2nd Edition. s.l. : Springer, 2006.

10. *Sandia National Laboratories Wind Reliability Workshop* . Allbuquerque, NM : s.n., 2009.

11. Johnson, Scott J, van Dam, C.P and Berg, Dale E**.** *Active Load Control Techniques for Wind Turbines.* s.l. : Sandia National Laboratories, 2009.

12. Ehersman, Jonathan, *INTEGRATION OF ACTUATORS AND SENSORS IN TO COMPOSITE STRUCTURES,* Mechanical & Industrial Engineering Dept., Montana State University. Bozeman: s.n., 2009, Master's Thesis

13. Sridhar Kota, Robert Gavin, Richard Vander Veen. Smart Blade for Utility Scale Wind Turbines. *FlexSys Wind Energy LLC.* Ann Arbor Michigan : s.n., 2009.

14. Barbero, Ever J. *Introduction to Composite Materials Design.* s.l. : Taylor & Francis Inc., 1998.

15. Schmitt, James T**.** *Damage Initiation and Post-Damage Response of Composite Laminates by Multiaxial Testing and Nonlinear Optimization.* Mechanical & Industrial Engineering Dept., Montana State University. Bozeman : s.n., 2008. MS Thesis.

16. Agastra, Pancasatya. *MIXED MODE DELAMINATION OF GLASS FIBER/POLYMER MATRIX COMPOSITE MATERIALS.* Chemical Engineering , Montana State University. Bozeman : s.n., 2006. MS Thesis.

17. *Composite Materials Fatigue issues in Wind Turbine Blade Construction.* Mandell, John, Samborsky, Daniel and Agastra, Pancasatya. Bozeman : s.n., 2008.

18. Wheeler, Anthony J. and Ahmand, Ganji R. *Introduction to Engineering Experimentation.* Second Edition. Upper Saddle River : Pearson Education Inc., 2004.

19. Holman, J.P**.** *Experimental Methods for Engineers.* 4th Edition. s.l. : McGraw-Hill Inc., 1984.

20. Reardon, Brain, et al. *Wind Turbine Blades Sensors.* Industrial & Mechanical Engineering, Montana State University. Bozeman : s.n., 2007. B.S. Project Report.

21. *Low Cost Inspection for Improved Blade Reliability.* Cairns, Douglas, Palmer, Nathan and Ehresman, Jon**.** Bozeman : American Institute of Aeronautics & Astronautics, Montana.

22. Omega Engineering. [Online] [Cited: 04 14, 2009.] http://www.omega.com/literature/transactions/volume3/strain.html.

23. Griffin, Dayton A. *WindPACT Turbine Design Scaling Studies Technical Area 1-Composite Blades for 80-to 120 Meter Rotor.* Golden, Colorado 80401 : National Renewable Energy Laboratory, 2001.

24. *Fundmental Understanding of Piezoelectric Strain Sensors.* Sirohi, Jayant and Chopra, Inderjit. s.l. : Journal of Intelligent Material Systems and Structures, 2000, Vol. 11 .

25. DeCusatis, Casimer and Sher DeCusatis, Carolyn. *Fiber Optic Essentials.* San Diego : Elsevier, 2006. 978-0-12-208431-7.

26. Fuhr, Peter. Measuring with Light Part 2: Fiber-Optic Sensing—From Theory to Practice. *Sensors Weekly.* 2001.

27. TPI Composites, Inc**.** *Parametric Study for Large Wind Turbine Blades.* s.l. : Sandia National Laboratories, 2002.

28. *The Effect of Embedded Sensors on the Strength of Composite Laminates.* Kim, Ki-Soo, Breslauer, Menachem and Springer, George**.** Stanford : Journal of Reinforced Plastics and Composites , 1992, Vol. Vol. II. 0731-6844/92/08 0949-10.

29. *Monitoring of Impacted Aramid-Reinforced Composites by Embedded PVDF Acoustic Emission Sensors.* Caneva, C., De Rosa, I.M. and Sarasini, F**.** 44, Rome : Blackwell Publising Ltd, 2008, Vol. Strain.

30. *Electromechanical fatigue behavior of graphite/epoxy laminate embedded with piezoelectric actuator.* Mall, S and Hsu, T L. 1, Wright-Patterson AFB : Smart Material Structures , 1999, Vol. 9. 0964-1726/00/010078+07.

31. *Polyimide-coated small-diameter optical fiber sensors for embedding in composite laminate structures.* Satori, Kouji, et al. Tokyo : Smart Structures and Materials, 2001. 0277-786X/01.

32. Frazao, O, Oliveira, R. and Dias, I. A Simple Smart Composite using Fiber Bragg Grating Sensors for strain and temperature discrimination. *Microwave and Optical Technology Letters.* 2009, Vol. Vol. 51, No. 1.

33. *Strain monitoring in glass fiber reinforced composites embedded with carbon nanopaper sheet using Fiber Bragg Grating (FBG) sensors.* Zhao, Xuefeng, et al. s.l. : Elsevier, Composites Part B. , 2008, Vol. 40. 134–140.

34. Rumsey, Mark, Images of TPI blade construction with embedded fiber optics, Sandia National Laboratories, 5-2008

35. *Standard Test Method for Mode I Interlaminar Fracture Toughness of Unidirectional Fiber-Reinforced Polymer Matrix Composites (D 5528-01).* West Conshohocken : ASTM International. 19428-2959.

36. Prime 20, Epoxy Infusion System. s.l. : SP systems, 2002.

37. Glast, Fibre**.** Product Data Sheet; 1110 General Purpose Vinyl ester Resin. 2008.

38. *Chemical Resistance of Plastics and Elastomers.* 3rd Edition. s.l. : William Andrew Publishing/Plastics Design Library, 2001.

39. Labview is a trademark of National Instruments. [Online] http://www.ni.com/labview/.

40. Piezo Film Product Guide and Price List. Hampton, VA : Measurement Specialities , 2008.

41. Corning SMF-28 ULL Optical Fiber with Corning Ultra-Low Loss Technology Production Information. Corning,NY : Corning Incorporated, 2008.

42. ZOOM 2 VFL, Optical Power Meter w/integrated VFL. Whitewater, WI : Optical Wavelength Laboratories, 2009.

43. Laser OWL 1550, Singlemode Laser Source. Whitewater,WI : Optical Wavelength Laboratories, 2009.

44. ClearLite Specialty Coated Photonic Fibers . *Specification Sheet.* s.l. : OFS, 2005.

45. *Electronic discussion of polyimide coating removal*, Jason Kiddy, electronic mail, 2009, Bozeman

APPENDICES

APPENDIX A:

TECHNICAL BACKGROUND OF WIND TURBINES

Current industrial wind turbines are built using a multitude of different design criteria. These criteria differ from location to location, but in general the overall design concepts have been narrowed down to a few, which have been proven to work. Design aspects covered here do not constitute the complete design picture needed for implementation of industrial wind turbines. Only the design concepts which were most intimately related to the implementation of sensors into the blade construction are addressed. Subjects such as electrical systems, control systems, energy yield, installation, operation, and economics would, undoubtedly, be affected by the integration of sensors into blade construction.

The basic techniques of harvesting winds' kinetic energy are an acceptable jumping off point for discussion. Neglecting the long history associated with wind energy there are basically two types of wind turbines. Vertical axis wind turbines commonly called Darrieus-rotor type. The other being the horizontal axis wind turbine; which is the dominate style of wind collection used in industrial application to date. Vertical axis wind turbines have not been equal to their horizontal counterparts due to issues of manufacturing complexity, low tip speed ratio, inability to self start and the lack of power output control via pitching of the rotor blades [9]. Horizontal axis wind turbines have developed as the dominate form because of several aspects; the first is the ability to control the power output of the turbine via blade pitch control. Additionally, the blade shape can be aerodynamically tailored to achieve the highest possible efficiency, and such designs have a significant technical developmental advantage over its counterparts. Blade pitch control provides a decisive advantage, and has lead to industrial wind turbines, which are primarily constructed in the form shown below, in Figure 59.These turbines have three blades, variable gearbox, pitch and yaw control, and a generator housed in the nacelle of the structure.

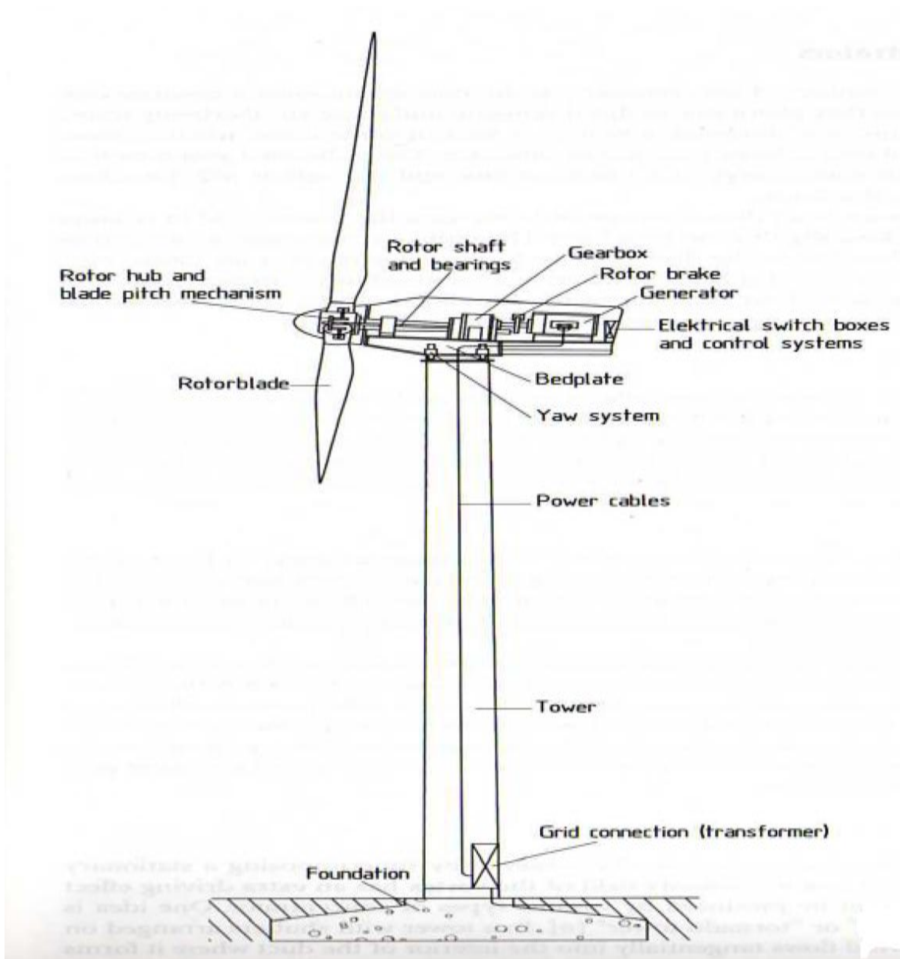

Figure 59. General Configuration of Current Industrial Wind Turbines [9]

A brief mention of the physical principles utilized in wind energy is necessary. The basic principle used for determining the amount of energy which can be extracted from free-stream airflow is owed, to Albert Betz. Betz formulated the theoretical maximum amount of power which can be converted using a disc energy converter, positioned perpendicular to the direction of flow through elementary momentum (A.1.1). The amount of power contained in a free-stream air flow can be evaluated by the amount of kinetic energy in a stream of air (A.1.2) given a mass flow rate (A.1.3).

$$\boldsymbol{P = \tfrac{1}{2}\rho\, v^3 A} \qquad (\boldsymbol{W}) \qquad \text{A.1.1}$$

P = power (W)
ρ = density (kg/m^3)
v = velocity (m/s)
A = cross-sectional area (m^2)

$$\boldsymbol{E = \frac{1}{2} m v^2} \qquad (\boldsymbol{Nm}) \qquad \text{A.1.2}$$

E = energy (Nm)
m = mass (kg)
v = velocity (m/s)

$$\boldsymbol{\dot{m} = \rho v A} \qquad (\boldsymbol{kg/s}) \qquad \text{A.1.3}$$

$\dot{m}$ = mass flow rate (kg/s)
ρ = density (kg/m^3)
v = velocity (m/s)
A = cross-sectional area (m^2)

It then becomes a question of how much power can be extracted from the air. If continuity is assumed for an incompressible fluid, the mass flow rates before and after the converter must be identical. In order to achieve this while still harvesting the energy, in the free stream of air, the area over which the free stream flows must increase. The increase is shown by the equation of continuity below (A.1.4).

$$\boldsymbol{\rho v_1 A_1 = \rho v_2 A_2} \qquad (\boldsymbol{kg/s}) \qquad \text{A.1.4}$$

ρ = density (kg/m^3)
v = velocity (m/s)
A = cross-sectional area (m^2)

The difference in velocity is the amount of power in the air converted into mechanical power. As seen in formulation (A.1.5), one location of maximum power conversion occurs if the air velocity after the converter was zero. This is trivial in fact, because if such a scenario were to occur, continuity could only be satisfied if the upstream velocity was also zero.

$$\boldsymbol{P = \tfrac{1}{2}\dot{m}(v_1{}^2 - v_2{}^2)} \qquad (\boldsymbol{W}) \qquad \text{A.1.5}$$

P = power (W)
$\dot{m}$ = mass flow rate (kg/s)
v = velocity (m/s)

It is because continuity must be satisfied that an alternative relationship between the upstream velocity and downstream velocity must exist. The alternative relationship can be determined by evaluating the force exerted on the wind turbine.

$$\boldsymbol{F = \dot{m}(v_1 - v_2)} \qquad (\boldsymbol{N}) \qquad \text{A.1.6}$$

F = force (N)
$\dot{m}$ = mass flow rate (kg/s)
v_1 = velocity before converter (m/s)
v_2 = velocity after converter (m/s)

The equation of force exerted on the wind turbine is developed through conservation of momentum (A.1.6). Newton's third law allows for development of a second form of the power collected by the wind energy converter, were *v'* is the air velocity in the plane of the converter (A.1.7).

$$P = Fv' = \dot{m}(v_1 - v_2)v' \quad (W) \qquad \text{A.1.7}$$

P = power (W)
F = force (N)
$\dot{m}$ = mass flow rate (kg/s)
v' = velocity at the energy converter (m/s)
v_1 = velocity before converter (m/s)
v_2 = velocity after converter (m/s)

By equating the two expressions for power it can be shown that the flow velocity at the disc is equal to the arithmetic mean of the upstream and downstream velocity. Once the velocity in the plane of the energy converter is known the equation for mass flow rate (A.1.3) is satisfied and thus can be substituted giving the final form of power collected (A.1.8).

$$P = \frac{1}{4}\rho A({v_1}^2 - {v_2}^2)(v_1 + v_2) \qquad (W) \qquad \text{A.1.8}$$

P = power (W)
ρ = density (kg/m^3)
A = cross-sectional area (m^2)
v_1 = velocity before converter (m/s)
v_2 = velocity after converter (m/s)

The ratio between the power converted and the wind without the converter is defined as the "power coefficient" c_p. The coefficient is dependent on the ratio of downstream to upstream velocity can be seen in Figure 60. The maximum value is known as the "Betz factor" which has a nominal value of .593.

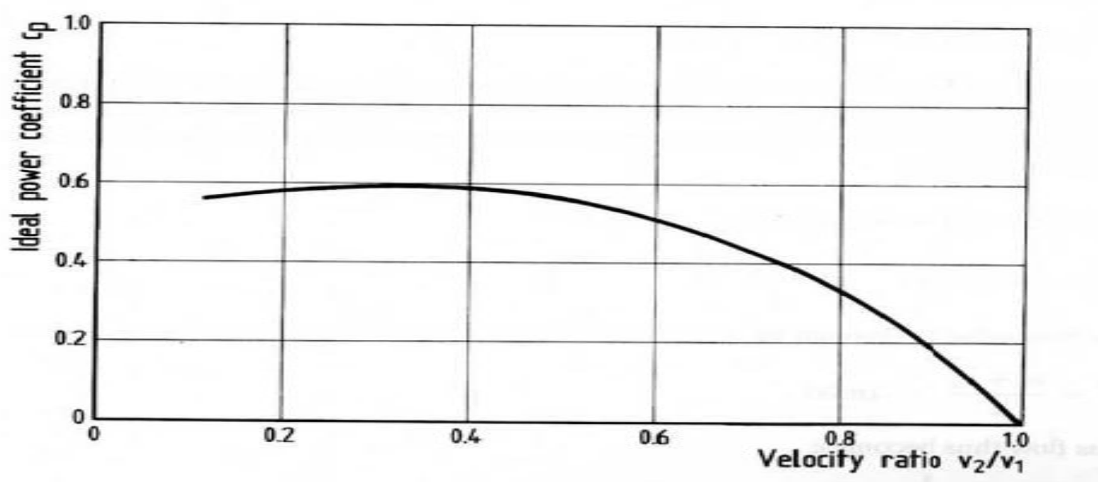

Figure 60. Curve of Convertible Wind Power over Contained Power as related to wind velocity downstream of the turbine over upstream wind velocity [9]

The Betz factor is the theoretical maximum amount of power which can be extracted from any free-stream airflow. However, this limit does not take into consideration the design of the energy converter. It is in the design of the converter where the phenomena of drag and lift affect the actual value of the power coefficient. Pure drag type wind converters can only harvest about 20% of the wind energy. The lack of efficiency in drag-wind converters is the reason current industrial wind turbines implement aerodynamic lift blade designs, into their construction. A more detailed description of Betz's work can be found in, *Wind Turbines,* by Erich Hau [9].

The designs of current industrial wind turbines employ this aerodynamic design for increased power conversion and results in loading which is unique to this design. Both drag based designs and lift based designs have load components, in the direction of air flow, and in the plane of the turbine blades. These loads are due to momentum transfer between the air and the blades. However, aerodynamic blades have additional load components due to the lift generated from the change in air velocity around the blades. The load profiles can be seen in Figure 61 [9]. These loads are highly dependent on the angle of attack of the leading edge of the blade into the incoming air flow, thus are dependent on the pitch of the blade.

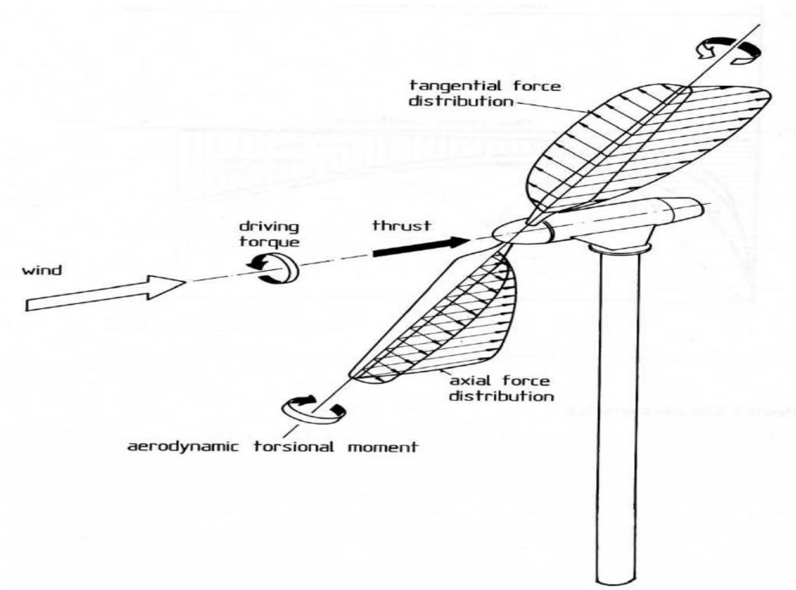

Figure 61. Characteristic load distribution on wind turbine blades [9]

Because of the dependence on pitch two different dominate methods of power control have been developed, active pitch control or passive or stall control. Passive control, refers to wind turbines that are designed with a fixed angle of attack into the wind. This eliminates extra weight and is fundamentally easier to transfer loads from the blades to the hub. Passive controls are designed such that at a desired wind velocity the air flowing over the blade becomes turbulent, effectively reducing lift and load on the wind turbine blade. The difficulty of this design is that it can only be designed for one optimal wind velocity. The second method is Active controls. Active pitch control systems can mechanically adjust the angle of attack of the wind turbine blades, which provides for the optimal performance of the wind turbine over an operational range of wind velocities not a single velocity. The disadvantage of active pitch control is the additional weight and load complexity. However, unlike passive pitch control the blades of an active control method can be feathered out of the wind during extreme conditions. Feathering further reduces the loads on the blades which would have to be endured in a passive control system. The adjustability of active control translates into an increased power coefficient and power which can be seen in Figure 62 [9].

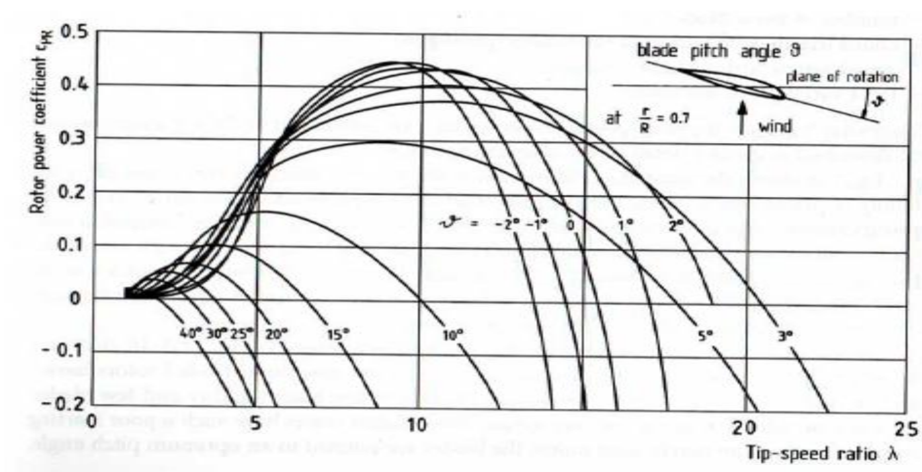

Figure 62. Array of Power Coefficient Curves as related to the ratio of blade tip speed over wind velocity. [9]

The two design philosophies have proven themselves in small wind turbine design. To date active control systems have taken the lead in large scale models due to the disadvantages of passive control. Economically, it becomes harder to justify the increase in material needed to maintain the structural integrity of passive control designs. The aerodynamic designs begin to become unpredictable at the megawatt level and in operation the load fluctuation becomes intolerable. Therefore, large industrial wind turbines are generally constructed with active control systems [9].

The next aspect of harvesting wind is blade design. The first is how many blades? Current land based industrial wind turbines are constructed primarily with three blades. The primary reason is that three blades are proven to achieve the highest power coefficient without adding excessive parasitic weight to the system while still being able to self start. These facts can be clearly seen below in Figure 63 and 64 [9].

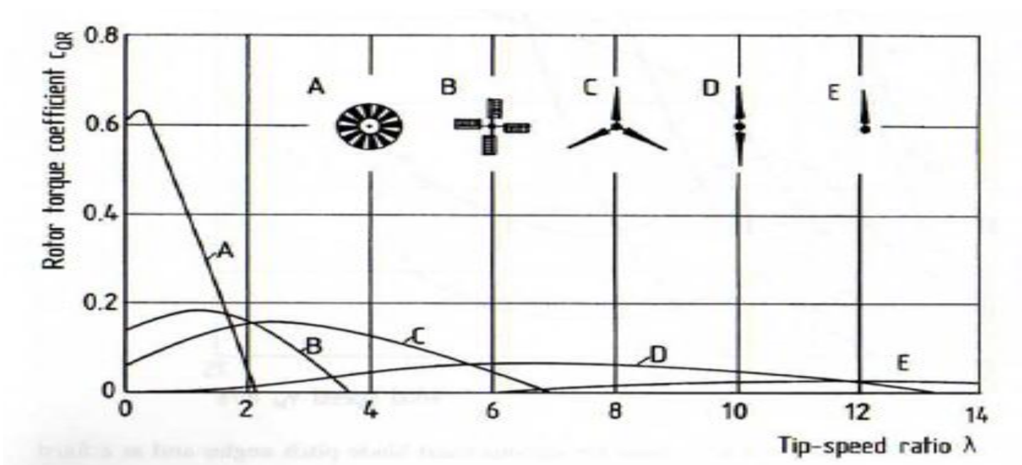

Figure 63. Characteristic Torque curves as related to blade tip speed over wind velocity [9]

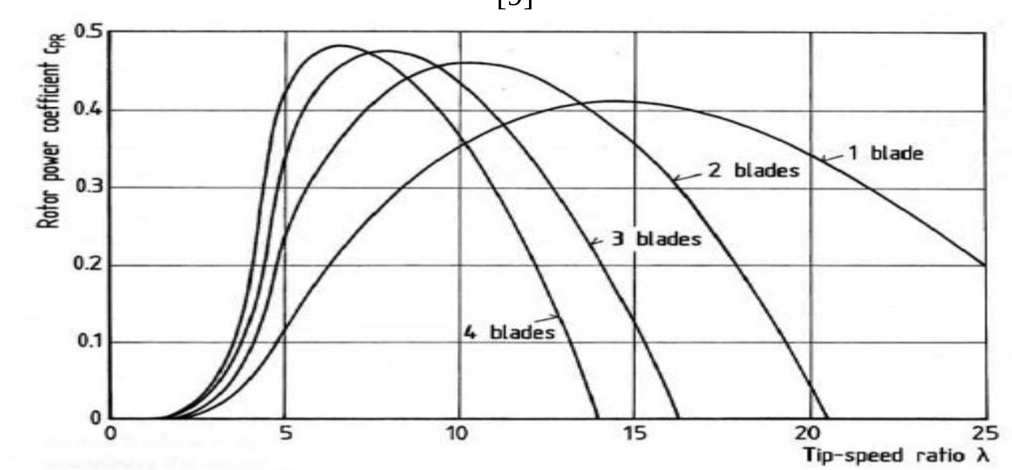

Figure 64. Effect of blade number on Power conversion as compared to tip speed ratio [9]

Generally fewer blades the faster the wind turbine will rotation, primarily because of the reduced weight of the blades. Increasing the speed is beneficial as Figure 64 illustrates there is a significant increase in the power coefficient of the wind turbine blade between one blade and two blade designs. However this trend is not linear and quickly becomes unproductive as there is not enough of an improvement to justify the weight. From a power prospective two or three blades seem optimal. Starting torque seen in Figure 63 differentiates the two designs among other aspects. The two blade design has a poor starting torque; it cannot self start unless the blades are pitched to the optimal angle of attack. Since three blade designs can self start they are currently dominate the industry.

Most industrial wind turbine blades employ an aerodynamic design to increase the power coefficient. Design of an aerodynamic blade is not a trivial task. Still there are some basic rules to aid in the design process. First is the optimal aerodynamic shape of the blade itself. Without diving into the mathematics, Figure 65 shows the optimum rotor blade shape based on the blades tip speed ratio and the number of blades used. The optimal chord length follows a hyperbolic trend with respect to the wind turbine radius. Chord length references to the length between the leading edge and trailing edge of the blade. This shape produces some difficulties in manufacturing. First, such contours are difficult to reliably manufacture, and second, as Figure 65 would indicate, at high tip speed ratios the blade shape is too thin to successfully construct with adequate stiffness (3).

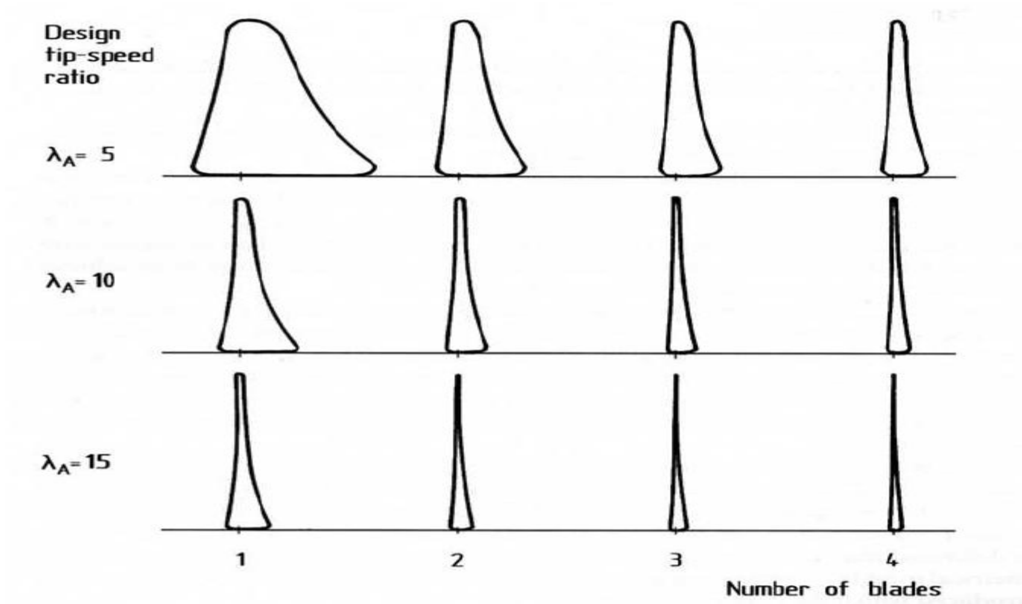

Figure 65.Array of Aerodynamically optimal blade contours [9]

It has been found that a trapezoidal shape is a good approximation of the optimal blade shape. There are only minimal differences between this design which is very feasible and the optimum. While a blade with its entire length conforming closely to this optimum shape has its advantages the most critical portion of the blade for power generation is the outer half.

In addition to this optimum blade shape is the airfoil shape of the blades cross section. The airfoil cross sections of wind turbine blades were developed from those used in the aviation industry. This approach is justified because of the similarities between the wind and aviation industry. The requirements placed on wind turbine blades are not identical to those for aircraft and there for need special considerations. With this goal in mind the LS and SERI series airfoil shapes have been developed. These designs minimize losses associated with surface roughness which is a significant problem for airfoil shapes. These design improvements for wind turbines can be seen in Figure 66, where the LS-1 blade design is considerably more resilient, with regard to surface roughness, for airfoil designs developed for aviation [9].

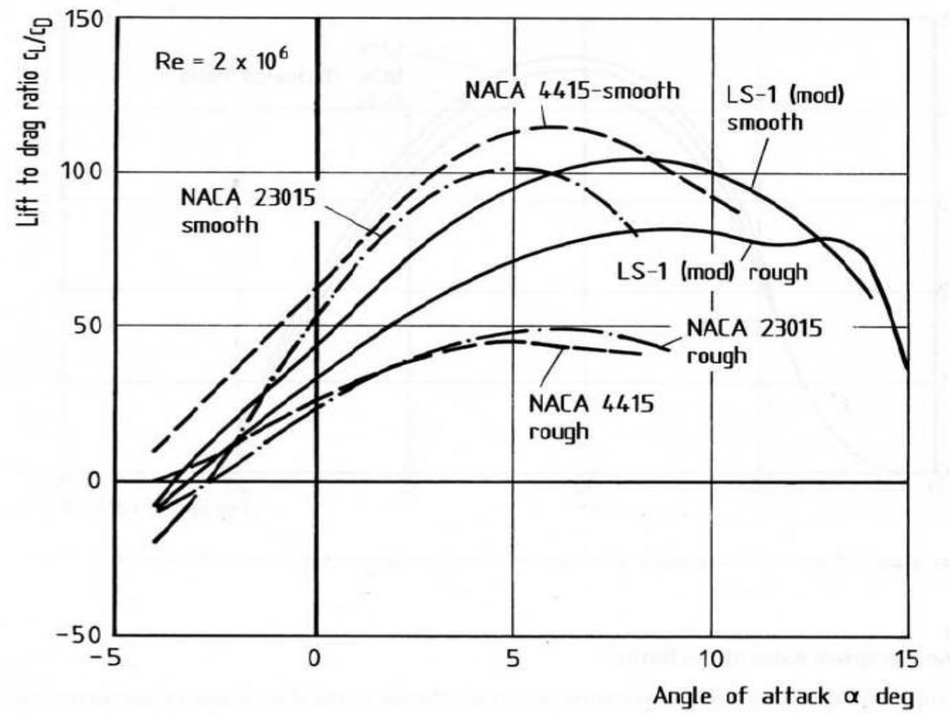

Figure 66.Effects of Surface roughness on lift to drag [9]

The amount of wind energy that can be converted into electrical energy, and the design of the components to achieve this, all play a major role in the loads and stresses experienced by the assembled wind turbine. During operation there are numerous sources of loads, but all can be grouped into three distinct categories. Steady state loads which do not change in value greatly with the rotation of the rotor. Cyclic loads, which alternate depending on the orientation of the rotor. Stochastic loads, which are truly random, are the last of the three categories.

All loads associated with these three categories, which can be seen below in Figure 67, can occur independently and simultaneously depending on the situation [9].

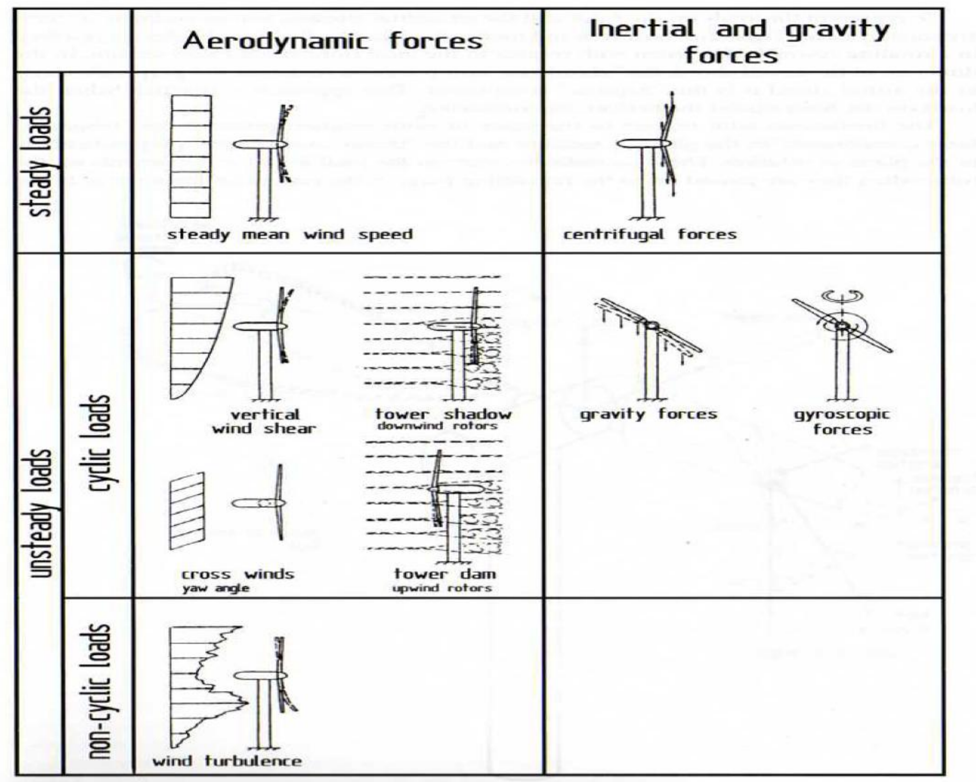

Figure 67.General Categories of loading components on wind turbines [9]

To design for these loads and stresses wind turbines are divided into classes, depending on what wind conditions they were designed for. Classes are generally based on average wind velocity, the maximum wind speed expected for a given duration, and the level of turbulence expected. Additionally, wind turbines are designed based on what are normal wind conditions and extreme wind conditions, the data from which has generally been collected from meteorological studies in the area of interest. Extreme wind conditions for obvious reason exclude natural disasters. Besides these load conditions wind turbines must also be developed to survive other influences, such as lightning strikes, ice accretion, solar radiation, and changes in air density. All these load conditions must consequently take into consideration the operating state of the wind turbine, for example start up, and shut down. By including these states of operation, the wind conditions can further be divided, into load case over each state. Lastly, wind turbines are designed to withstand additional loads associated with failure of a subsystem, which could add stresses to the subsequent systems which are not covered by the load cases [9].

Industrial wind turbine components are designed on an ultimate or limit load design basis, and on a fatigue design basis. In fact, many of the main components of a turbine are fatigue design driven, such as the blades which capture the wind energy, the gearbox bearing which stabilize the rotor axles, even the tower and nacelle in some designs. It's seen in Figure 67 the number of load conditions which are cyclic or stochastic greatly outweigh those few steady state conditions. The two main sources of failure in industrial wind turbine are blades and gearboxes. Both of which are primarily designed on a fatigue basis [9].

The blades are the vehicle through which the wind's energy is captured and are subject to the full array of load cycles. The two primary sources of cyclic loading on wind turbine blades are wind velocity variations, which cause changes in load in the flapwise, and chordwise directions of the wind turbine blade, and gravitational loads associated with the weight of the blades themselves as the rotor rotates about its axis. Figure 68 below is an example of these two fatigue load components at work on the WKA-60 [9]. The chordwise bending moment is nearly constant throughout the load cycles with the flapwise bending moment decreasing as things progress. The reason for the decrease is that while the aerodynamic loads on the flapwise direction alternate with wind velocity, pitch, and yaw, the chordwise bending moments will always fluctuate with the same intensity as the wind turbine rotates.

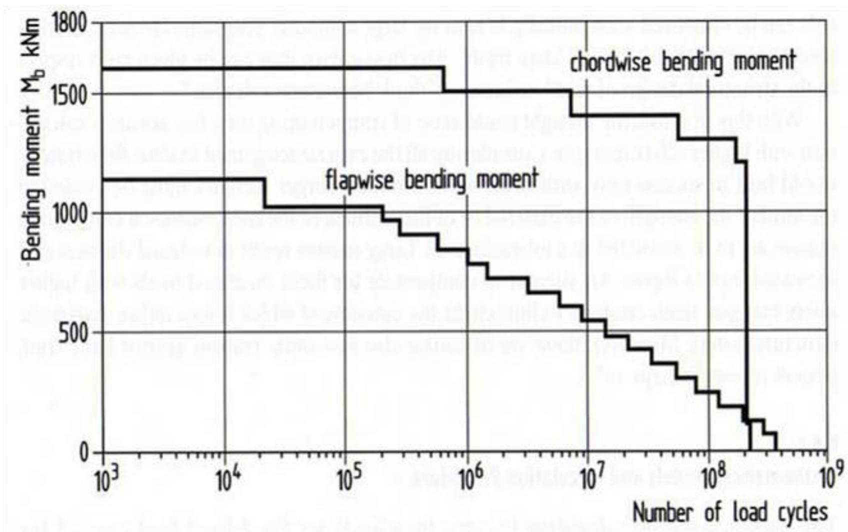

Figure 68.Stress magnitude of the two major directions on a blade as related to load cycles [9]

Leading to the notion that while fluctuations in wind velocity can produce ultimate loads with enough magnitude to damage the structure, the level of damaged developed through fatigue of the blade in the chordwise direction may very well produce failure of the structure before such an extreme event could ever happen [9].

By understanding the load conditions likely to be experienced by the rotor blades the design of the blade structure was developed. These designs stem from those developed in the field of aeronautics. Current wind turbine blade cross sections are comprised of the outer aerofoil geometry with a bonded spar box and spar webs used to stiffen the blade in the longitudinal direction as can be seen in Figure 69 [9].

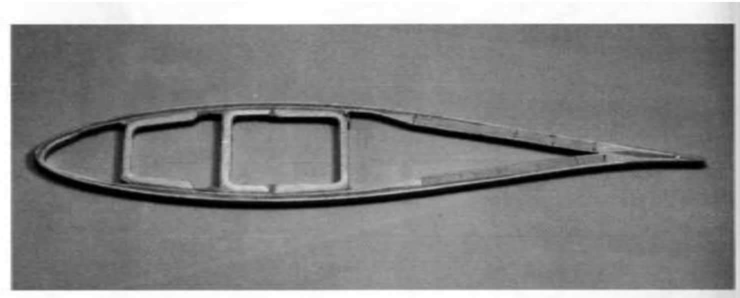

Figure 69. Typical Cross Section of Composite Wind Turbine blade [9]

This design has the center of mass forward as far as possible. The reason for this is to reduce the risk of blade flutter. These designs are currently constructed of fiber reinforced composites, because this material can not only be tailored to the load conditions but is a strong and stiff material compared to its weight. Additionally, fiber reinforced composites are capable of being produced with superior surface finishes than that of riveted and welded counterparts. However, composite materials possess their own unique challenges with regards to connection with other components which are constructed of metallic materials. Two current techniques used to achieve connection between components is the cross bolt connection, shown in Figure 70, and the bonded-in sleeve, shown in Figure 71. These designs marry the ability to reliably fasten the blades to the rotor hub while not adding undue weight to an already massive structure [9]. Blade design has evolved to address the issues of stiffness, ultimate loading, and fatigue but this is not the complete picture. Fatigue related degradation of the blades can be greatly enhanced by vibration of the wind turbine. Blade vibration can occur in multiple modes, one being aero elastic instability such as flutter. Another, oscillatory wind loading at resonant frequencies of the blade in the longitudinal direction, as well as chordwise vibration associated with the alternating gravitational loads on the blades

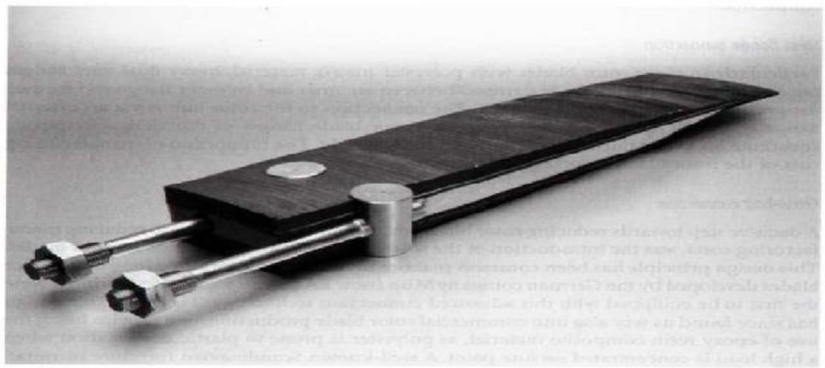

Figure 70. Cut away of cross bolt connection method used on turbine blades [9]

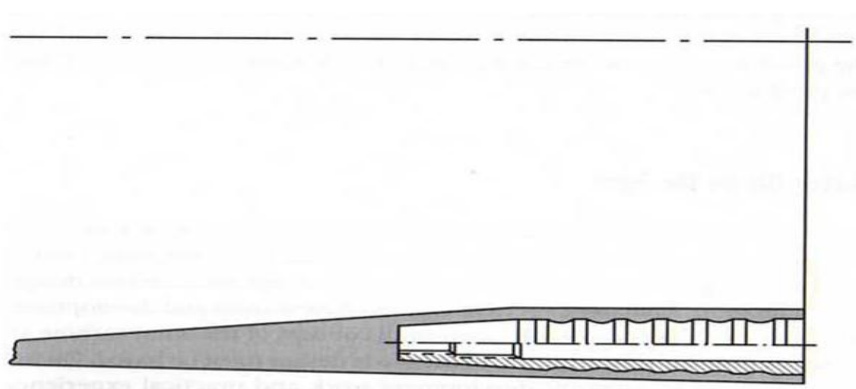

Figure 71. Connection sleeves bonded in blade root pioneered by Vestas [9]

These vibrations not only potentially increase the rate of fatigue on the blades themselves but the vibration in the chordwise and longitudinal directions are transferred to subsequent turbine components. The transfer of loading increases fatigue on these components, and increases the likely hood of fatigue related failures [9].

Current industrial wind turbines employ active pitch controls to address these load conditions. The ability to control the magnitude of these loads can increase structural survivability [9].

While the load conditions seen by the blades of a wind turbine are primarily determined by the aerodynamics of wind flow over the blades, this is not the case for the turbines mechanical drive train. The conversion of the kinetic energy to mechanical energy is the sole purpose of the blades and is governed by aerodynamics. The drive train of the wind turbine is designed to convert that mechanical energy into electrical energy. These components are conventional for power plant technology, but it is the unique use which poses problems for an otherwise mature form of technology.

Drive train refers to the rotor hub, low speed axle, gear box, high speed axle, brake, and generator; other components are included but these are the primary components needed for successful mechanical electrical conversion. There are several different possibilities of arrangement of these components, but there are only two that are current standard system designs. The first of which is the series connection from the hub to the gearbox, via the low speed axle, and then to the generator through the high speed axle, which has the brake mounted to it. The other is the direct rotor driven generator design were the rotor hub is directly connected to the generator. The latter design has the advantage of reliability and servicing. However, it must incorporate a frequency converter to smooth out the electric fluctuations due to the constant changes in rotor speed, and is generally heavier that the series design due to the specialty generator which must be used.   Both designs can be seen in Figures 72 and 73 below, but the series design is the dominate design in industry [9].

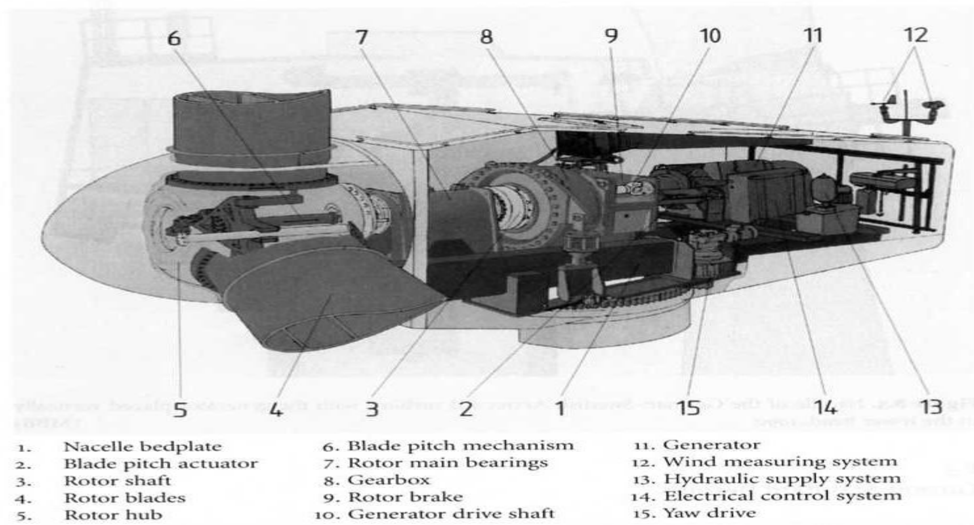

Figure 72. Traditional Series Configuration of Wind Turbine Drive train [9]

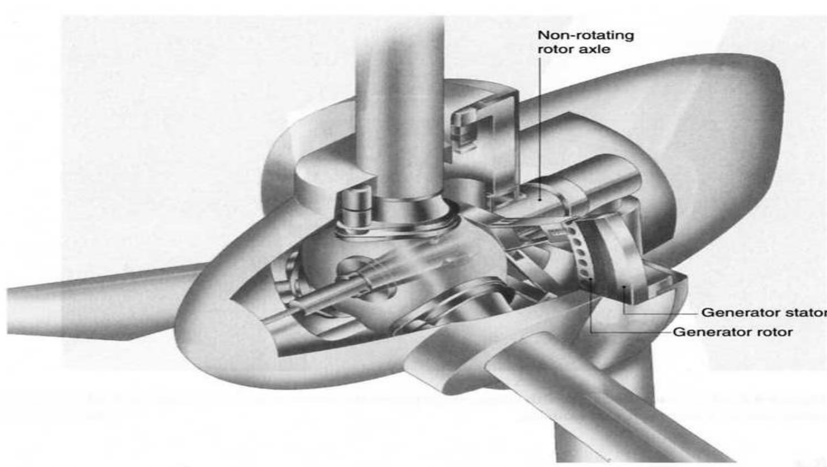

Figure 73. Configuration of Direct Rotor-Generator Drive train [9]

Of the primary components used in the construction of the turbine one stands, in current history, as the component most susceptible to premature failure despite no fundamental deficiency in design approach. That component is the gearbox used in the series connection design. Originally, these problems were most likely due to inaccurate assessment of the loads on the gearbox however this does not appear to be the source of the problem [9]. Current statistics have indicated that gearbox failure does not initiate in the gears, but in the bearings, used within the gearbox [6]. Due to that lack of gearbox, the direct rotor driven generator does not suffer this same downfall.

The integration of the gearbox into the wind turbine has primarily fallen into one design, for the series configuration. Generally, it involves one, roller bearing, on the low speed axle close to the rotor hub and two Trunnion mounts, which attach the gearbox to the bedplate of the nacelle, as seen in Figure 74 below.

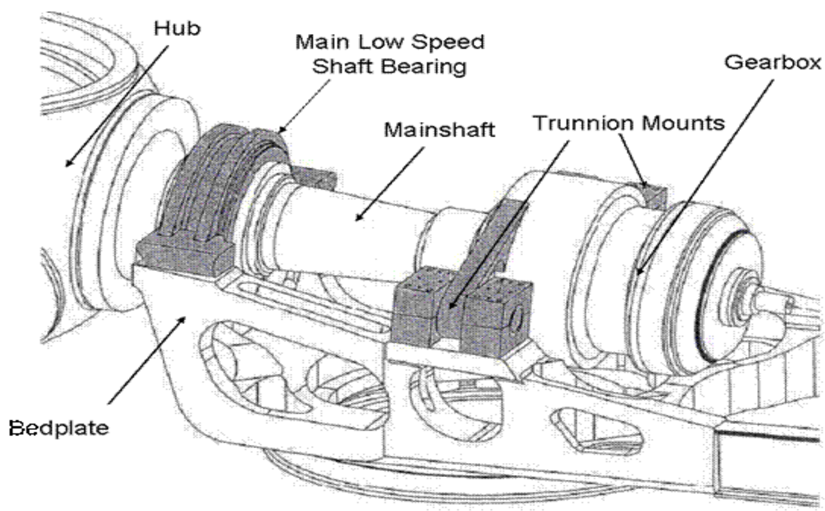

Figure 74. Traditional Three Point Slow Speed Axle and Gearbox Mounting [6]

These Trunnion mounts, generally, are connected to the bedplate via elastomeric materials to reduce noise emissions [6][9]. The Trunnion configuration is preferable over other designs, such as two separate bearing supporting the low speed axle, because of the reduced size and weight placed on the tower. However, the three point mounting does place additional loads on the gearbox, which can be avoided in a two bearing design.

Due to the great difference in rotational speed of the low speed axle and the high speed axle, turbine gearboxes are, primarily, a modified planetary gear configuration. The reason for this is the increase gear ratio per stage of the planetary gear configuration as well as the significant reduction in gearbox size and weight over the parallel shaft system. The gearbox is modified from traditional planetary gearbox design because it marries the parallel gearbox approach with the planetary gearbox. The justification for this approach is that by including the parallel gear design the low speed and high speed axles are no longer coaxial. This allows for easy supply of power through the low speed axle to the pitch control components in the hub. The modified planetary configuration of gearbox has three bearing locations which are susceptible to failure, the planetary gear bearing, intermediate shaft-locating bearing and the high speed shaft-locating bearing [6]. Figure 75 is a clear view of the three bearing locations which have shown consistent failures despite sound bearing design considerations. While these failures are not completely understood further field testing is underway to try and evaluate these sources.

Gearbox and blade failures are the most prevalent in current industrial wind turbines, but there are other components subject to unfavorable conditions during operation. First, is the generator; power production from wind energy is highly dynamic in nature, which is not compatible with the public electrical grid.

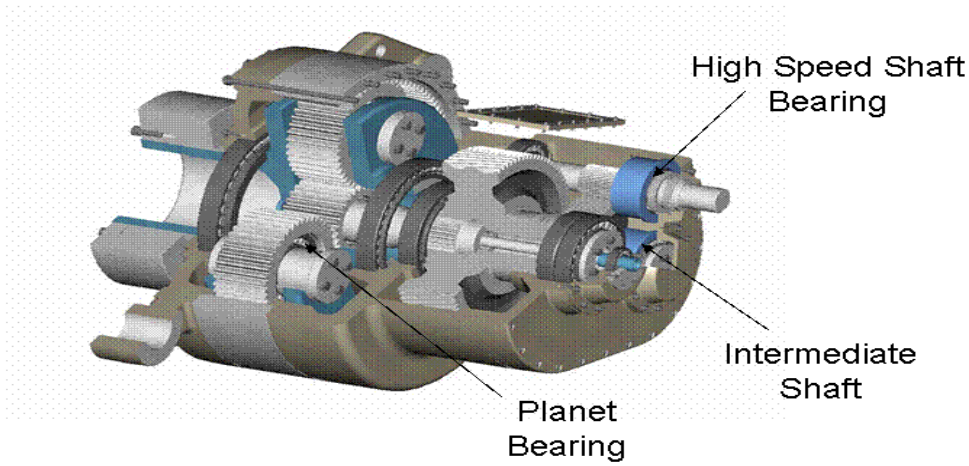

Figure 75. General Modified Gearbox Configuration used in Wind Turbines [6]

There are several approaches used to address this problem however pitch control of the blades is preferred. By adjusting the pitch of the blade the loads on the blade and subsequent components is reduced, thus reducing the power generated and smoothing out any unwanted fluctuations, in electrical power. The effect of this approach can be seen, in Figure 76 below.

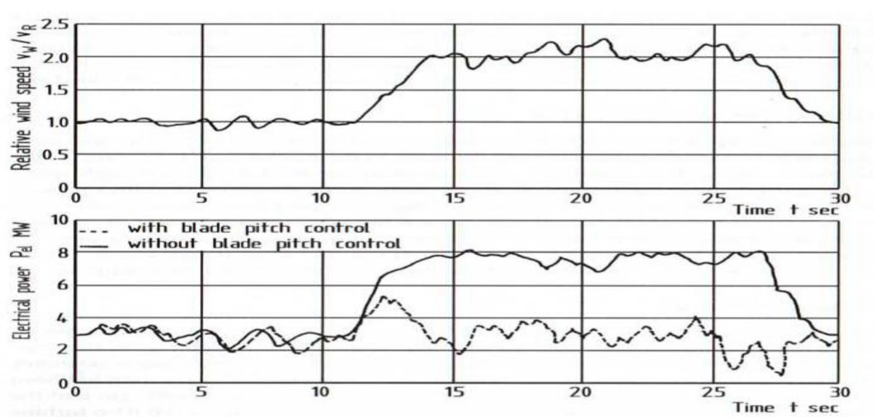

Figure 76. Generator power smoothing using blade pitch control [9]

The second component which is subject to unfavorable loading especially cyclic loading is the yaw system of the turbine. Horizontal differences in wind velocity across the swept area of the wind turbine stress the active yaw controls on industrial wind turbines. This stochastic loading can increase wear on the electric yaw drive, as well as, the bull and pinion gear used to control the turbines position. To address these problems the azimuth bearing is designed to resist small loads. Large loads are contour acted with a yaw brake, but excessive use leads to premature failure. Yaw brake failure is not present in three blade wind turbines because of the symmetric loading present in this design. However, as turbine design progresses, two and one blade designs may become preferred and that will lead to a reevaluation of the yaw system because of the increased yaw moments associated with these types of turbines, as seen in Figure 77 [9].

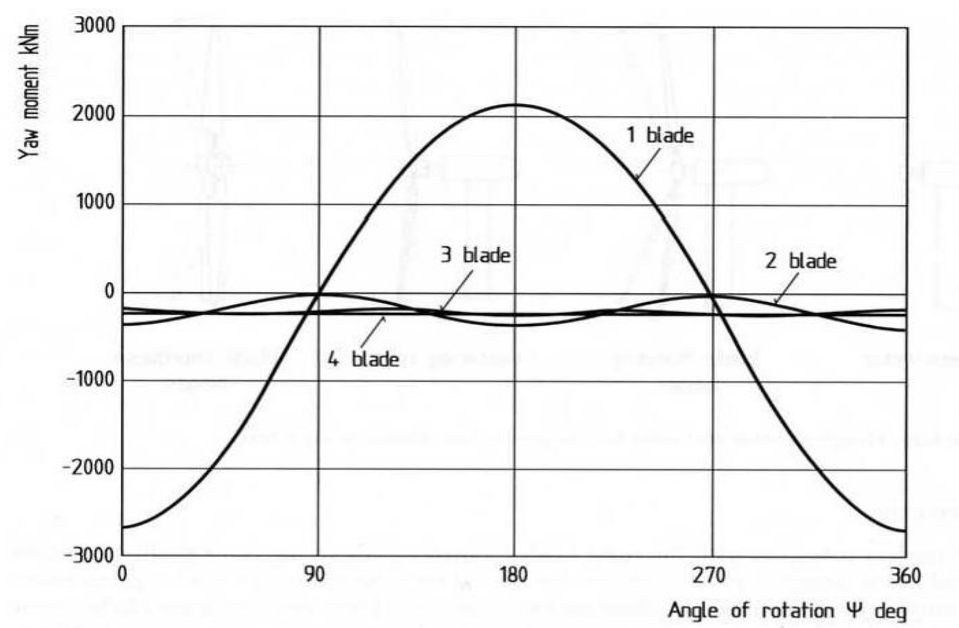

Figure 77. Yaw moment as a function of blade number [9]

These issues only briefly touch on what is a very dynamic and complex system, which has been in use of centuries. By systematically addressing these issues wind turbines can become more efficient and economically attractive form of energy capture, than is currently possible.

APPENDIX B:

LAMINATES CREATED FOR THIS STUDY

Table 34, The first laminates created to study embedded sensors,

Test Plate Created to Date

Laminate	Date	Matrix	Sensor embedded	Surface treatment	Purpose
1	3/25/2008	Epoxy (Prime 20L)	Acrylate Fiber Optics w/ and w/o polymer jacket	none	become familiar with the steps needed to embed sensors
2	4/1/2008	Epoxy (Prime 20L)	none	none	epoxy control samples
3	4/3/2008	Vinylester (Fibre glast 1110 series)	none	none	vinylester control samples
4	4/14/2008	Epoxy (Prime 20L)	3 axis Strain gages, PVDF, Thermister,Thermocouple , acrylate Fiber optic	none	explore signal retreival from sensors embedded in epoxy laminate
5	4/23/2008	Vinylester (Fibre glast 1110 series)	3 axis strain gages, PVDF,Thermocouple,Fiber optic	none	explore signal retreival from sensors embedded in vinylester laminate

Table 35, Further test plates created to explore surface treatment options

Test Plate Created to Date

Laminate	Date	Matrix	Sensor embedded	Surface treatment	Purpose
6	6/30/2008	Epoxy (Prime 20L)	3 Axis Strain Gage, PVDF, Acrylate Fiber Optics	Surface treated w/ emry cloth & cleaned with Acetone	Concentrate on three sensors. Start to explore surface treatment options in epoxy laminates
7	7/28/2008	Vinylester (Fibre glast 1110 series)	3 Axis Strain Gage, PVDF, Acrylate Fiber Optics	Surface treated w/ emry cloth & cleaned with Acetone	Concentrate on three sensors. Start to explore surface treatment options in vinylester laminates
8	8/4/2008	Epoxy (Prime 20L)	3 Axis Strain Gage, PVDF, Acrylate Fiber Optics	Surface treated w/ Nitric Acid and cleaned w/ Isopropyl Alcohol	Create Test plate to evaluate surface treatment options in epoxy laminate
9	8/28/2008	Vinylester (Fibre glast 1110 series)	3 Axis Strain Gage, PVDF, Acrylate Fiber Optics	Surface treated w/ Nitric Acid and cleaned w/ Isopropyl Alcohol	Create Test plate to evaluate surface treatment options in vinylester laminate, start to retrieve signal from fiber
10	9/12/2008	Vinylester (Fibre glast 1110 series)	3 Axis Strain Gage, PVDF, Acrylate Fiber Optics	Surface treated w/ Nitric Acid and cleaned w/ Isopropyl Alcohol	Replace laminate 9 because of manufacturing defects , initial try at fiber optic reinforcement (AL capillary tubes), collection of signal

Table 36, Continuation of test laminate manufacturing. Testing of fiber optic signal strength.

Test Plate Created to Date

Laminate	Date	Matrix	Sensor embedded	Surface treatment	Purpose
11	9/26/2008	Epoxy (Prime 20L)	Acrylate Fiber Optic	Surface treated w/ Nitric Acid and cleaned w/ Isopropyl Alcohol	Second laminate used to evaluate fiber optic reinforcement techniques (Al capillary tubes) collection of
12	10/3/2008	Epoxy (Prime 20L)	Acrylate Fiber Optic	Surface treated w/ Nitric Acid and cleaned w/ Isopropyl Alcohol	Laminate to test second fiber optic reinforcement technique (wire jacketing), collection of signal strength over time
13	10/10/2008	Epoxy (Prime 20L)	Acrylate Fiber Optic	Surface treated w/ Nitric Acid and cleaned w/ Isopropyl Alcohol	Laminate to test fiber optic reinforcment technique with new technique of jacket collection, collection of signal strength over time
14	10/16/2008	Epoxy (Prime 20L)	Acrylate Fiber Optic	Surface treated w/ Nitric Acid and cleaned w/ Isopropyl Alcohol	Laminate to further test fiber optic reinforcment technique with new technique of jacket collection, collection of signal
15	11/11/2008	Epoxy (Prime 20L)	3 Axis Strain Gage, PVDF, Acrylate Fiber Optics	Surface treated w/ Nitric Acid and cleaned w/ Isopropyl Alcohol	Fiber Optic Signal strength test with optic reinforcement as well as initial attempts at creating G1c test coupons

Table 37, Start of mode I fracture toughness laminate creation.

Test Plate Created to Date

Laminate	Date	Matrix	Sensor embedded	Surface treatment	Purpose
16	11/26/2008	Vinylester (Fibre glast 1110 series)	3 Axis Strain Gage, PVDF, Acrylate Fiber Optics	Surface treated w/ Nitric Acid and cleaned w/ Isopropyl Alcohol	Mode 1 crack propagation testing (G1c testing)
17	11/25/2008	Epoxy (Prime 20L)	3 Axis Strain Gage, PVDF, Acrylate Fiber Optics	Surface treated w/ Nitric Acid and cleaned w/ Isopropyl Alcohol	Mode 1 crack propagation testing (G1c testing)
18	1/22/2009	Epoxy (Prime 20L)	Acrylate Fiber Optic	Surface treated w/ Nitric Acid and cleaned w/ Isopropyl Alcohol	Fiber Optic signal strength test with optic reinforcment
19	1/27/2009	Epoxy (Prime 20L)	Acrylate Fiber Optic	Surface treated w/ Nitric Acid and cleaned w/ Isopropyl Alcohol	Fiber Optic signal strength test with optic reinforcment
20	2/3/2009	Vinylester (Fibre glast 1110 series)	Acrylate Fiber Optic	Surface treated w/ Nitric Acid and cleaned w/ Isopropyl Alcohol	Fiber Optic signal strength test with optic reinforcment

Table 38, Continuation of test laminate creation of all forms.

Test Plate Created to Date

Laminate	Date	Matrix	Sensor embedded	Surface treatment	Purpose
21	2/6/2009	Vinylester (Fibre glast 1110 series)	Acrylate Fiber Optic	Surface treated w/ Nitric Acid and cleaned w/ Isopropyl Alcohol	Fiber Optic signal strength test with optic reinforcment
22	2/12/2009	Vinylester (Fibre glast 1110 series)	Acrylate Fiber Optic	Surface treated w/ Nitric Acid and cleaned w/ Isopropyl Alcohol	Fiber Optic signal strength test with optic reinforcment
23	2/12/2009	Epoxy (Prime 20L)	1axis Strain Gages ,PVDF, Polyimide Fiber Optics	Surface treated w/ Nitric Acid and cleaned w/ Isopropyl Alcohol	Manufacturing of additional tensile testing coupons with embedded sensors.
24	2/20/2009	Vinylester (Fibre glast 1110 series)	1 axis Strain Gages, PVDF, Acrylate Fiber Optics	Surface treated w/ Nitric Acid and cleaned w/ Isopropyl Alcohol	Manufacturing of additional tensile testing coupons with embedded sensors.
25	2/24/2009	Vinylester (Fibre glast 1110 series)	1 axis Strain Gages, PVDF, Acrylate Fiber Optics, Polyimide Fiber Optics	Surface treated w/ Nitric Acid and cleaned w/ Isopropyl Alcohol	Manufactured for additional G1c test coupons

Table 39, Completion of test laminate creation for embedded sensors.

Test Plate Created to Date

Laminate	Date	Matrix	Sensor embedded	Surface treatment	Purpose
26	2/26/009	Epoxy (Prime 20LV)	1 axis Strain gages, PVDF, Acrylat Fiber Optics, Polyimide Fiber Optics	Surface treated w/ Nitric Acid and cleaned w/ Isopropyl Alcohol	Manufactured for additional G1c test coupons
27	5/11/2009	Epoxy (Prime 20LV)	no sensors	no surface treatments	compare fracture toughness of new resin batch with older batch
28	5/13/2009	Epoxy (Prime 20LV)	1 axis Strain gages, PVDF, Acrylat Fiber Optics, Polyimide Fiber Optics	Surface treated w/ Nitric Acid and cleaned w/ Isopropyl Alcohol	Manufacturing of additional tensile testing coupons with embedded sensors.
29	6/12/2009	Vinylester (Fibre glast 1110 series)	1 axis Strain gages, PVDF, Acrylat Fiber Optics, Polyimide Fiber Optics	Surface treated w/ Nitric Acid and cleaned w/ Isopropyl Alcohol	Manufacturing of additional tensile testing coupons with embedded sensors.

APPENDIX C:

TEST SAMPLES & EQUIPMENT GEOMETRY

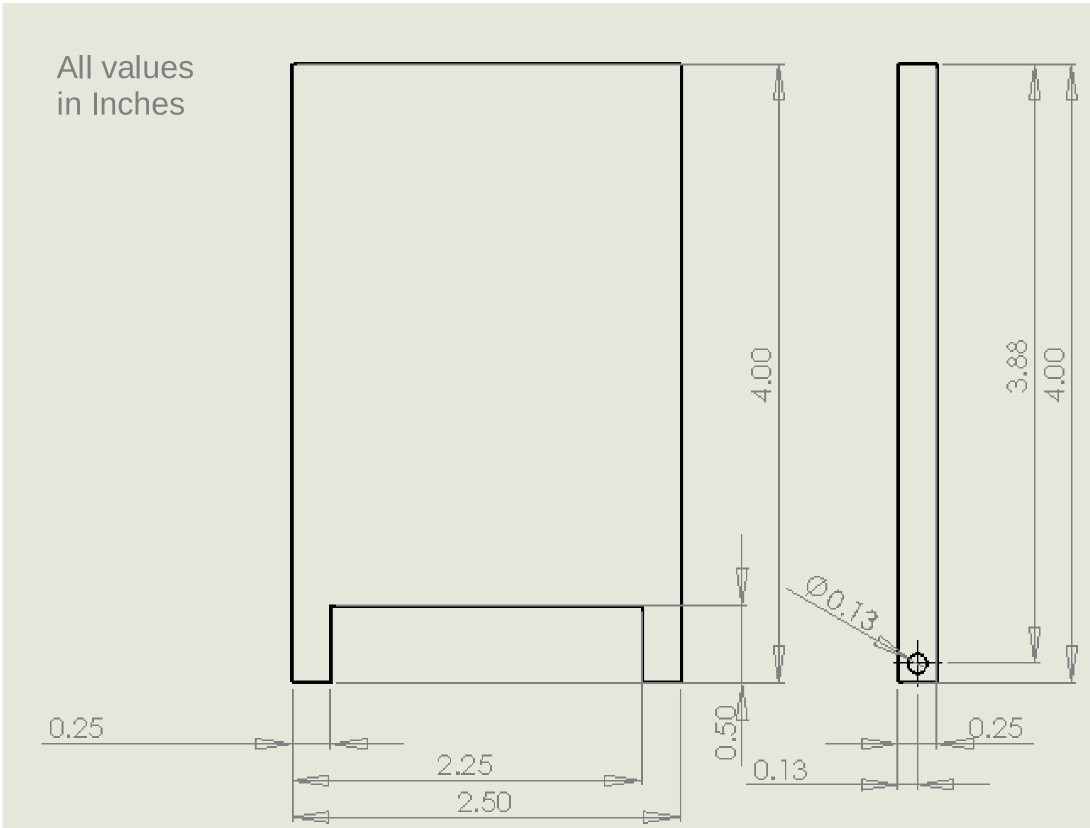

Figure 78, Mode I Fracture Toughness Loading Clevis Geometry.

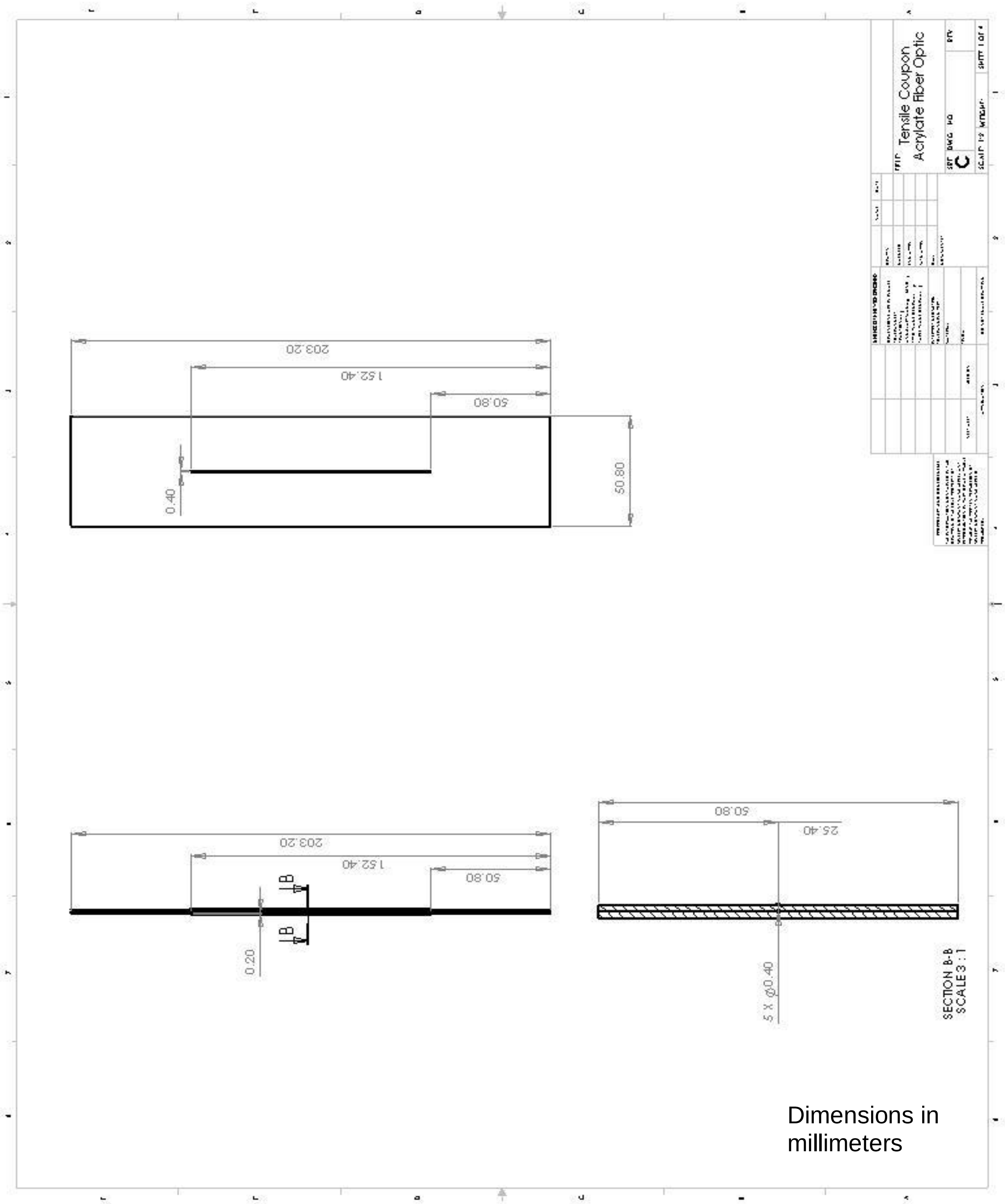

Figure 79. Dimensions for the tensile coupons with embedded acrylate coated fiber optics.

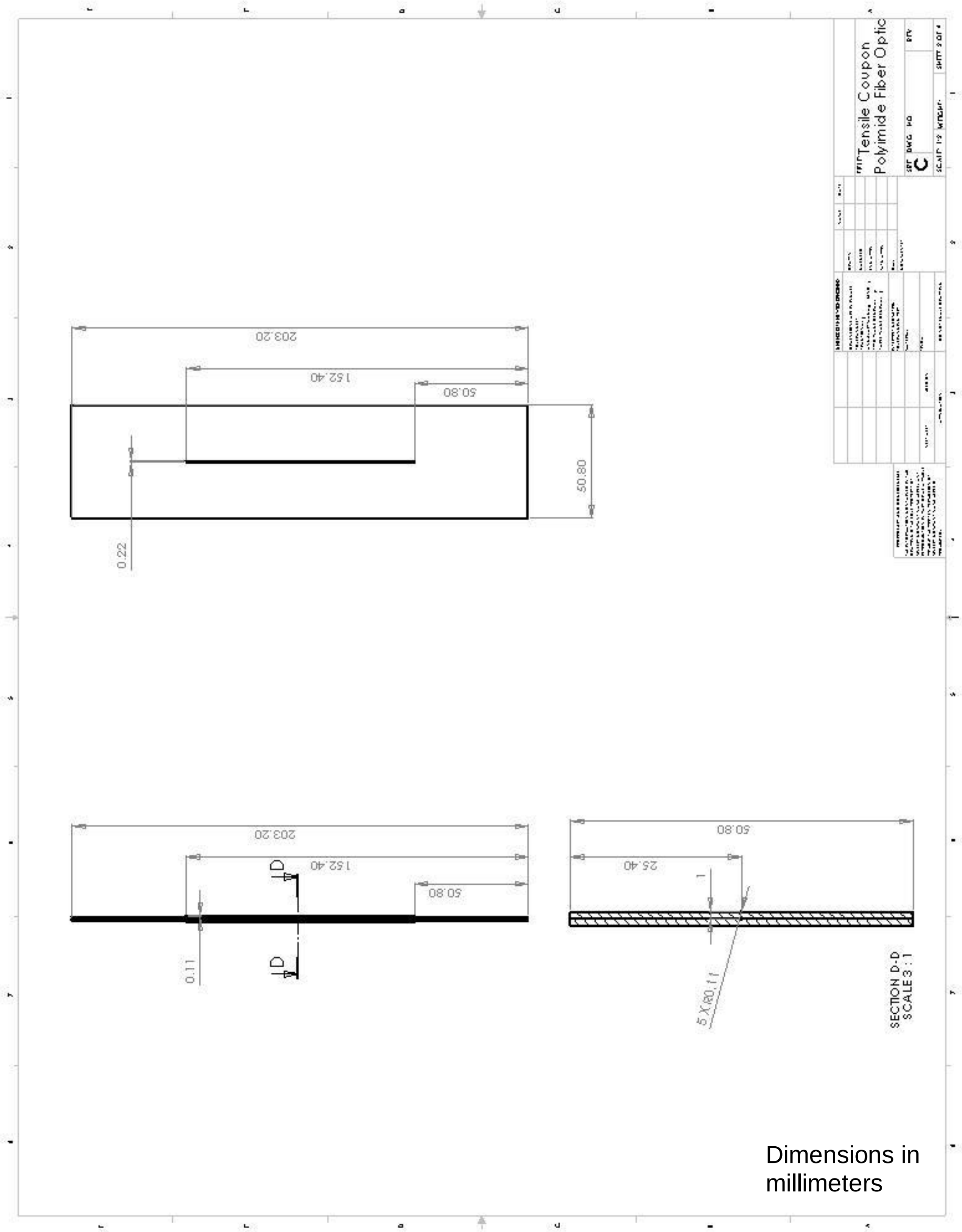

Figure 80, Dimensions for the tensile coupons with embedded polyimide coated fiber optics

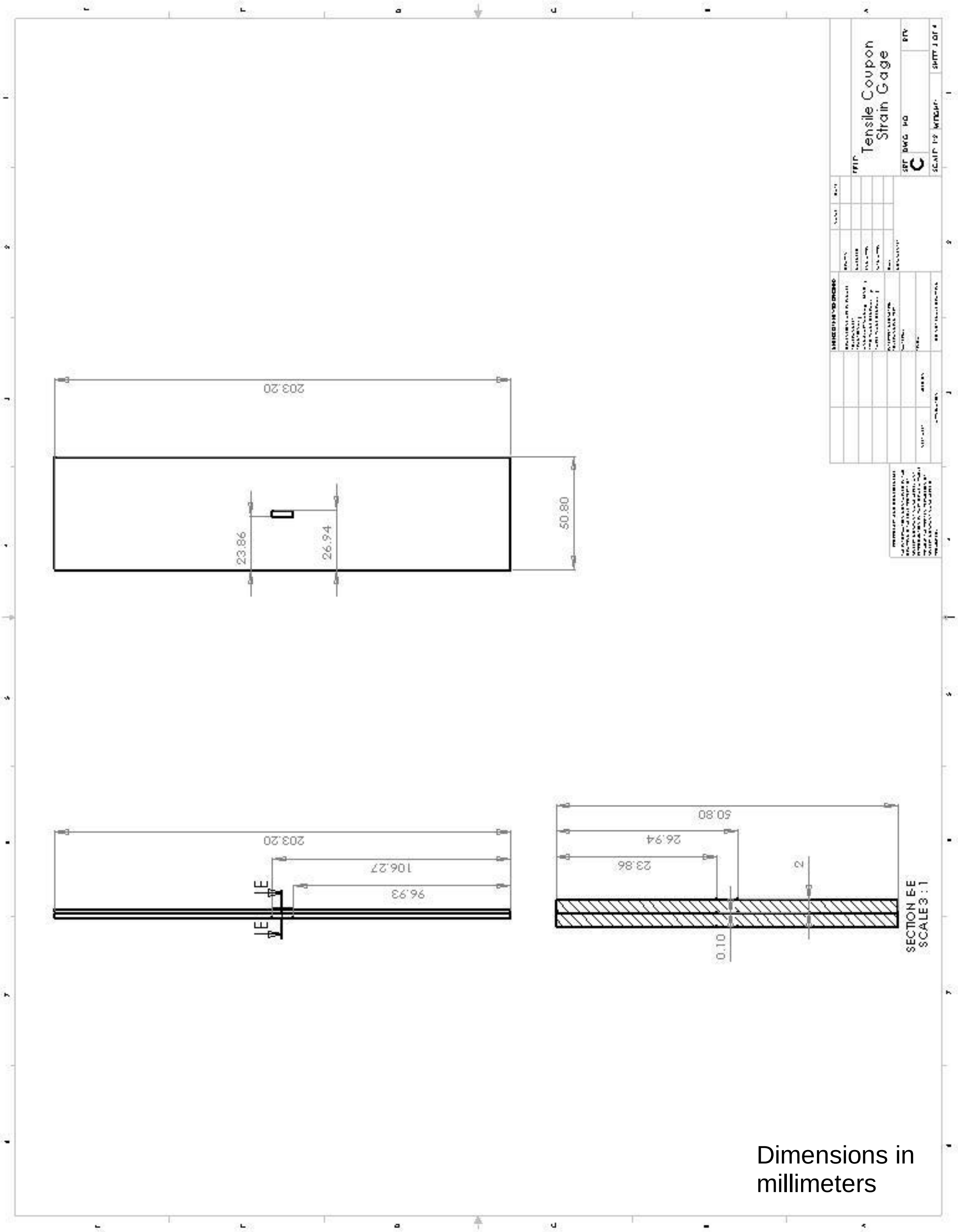

Figure 81, Dimensions for the tensile coupons with embedded strain gages.

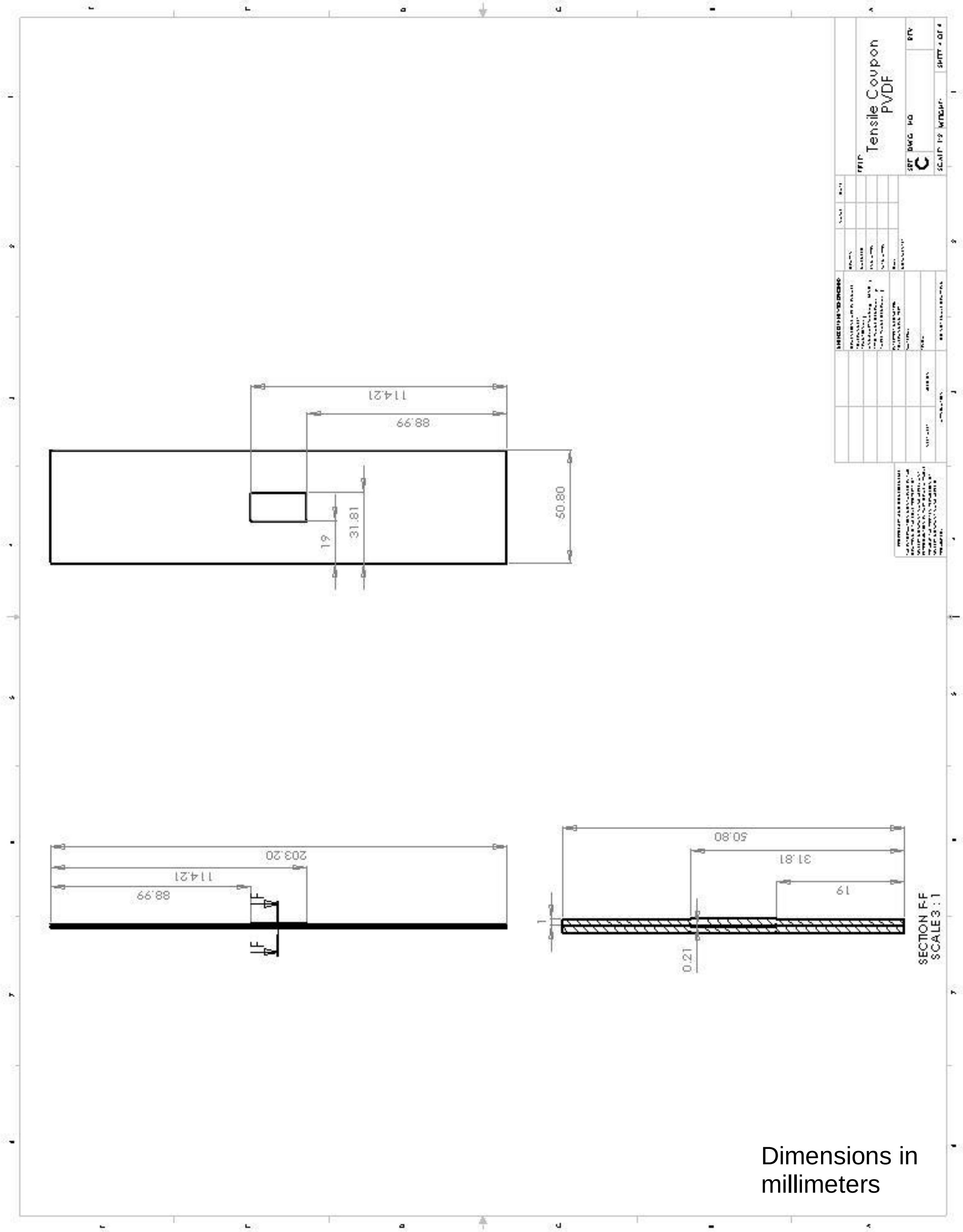

Figure 82, Dimensions for the tensile coupons with embedded PVDFs.

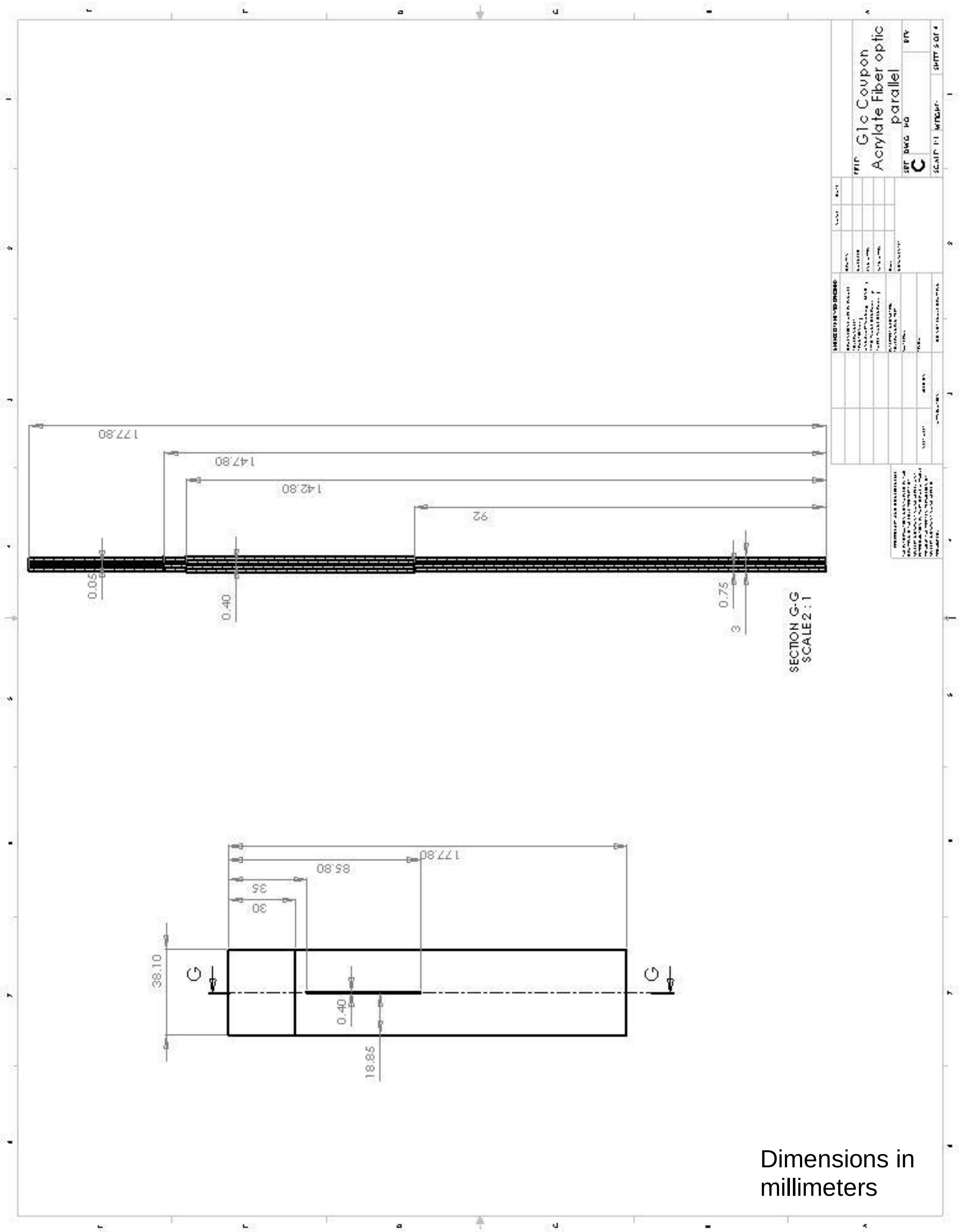

Figure 83, Dimensions for the G1c coupons with embedded acrylate coated fiber optics parallel to the dominant fiber direction

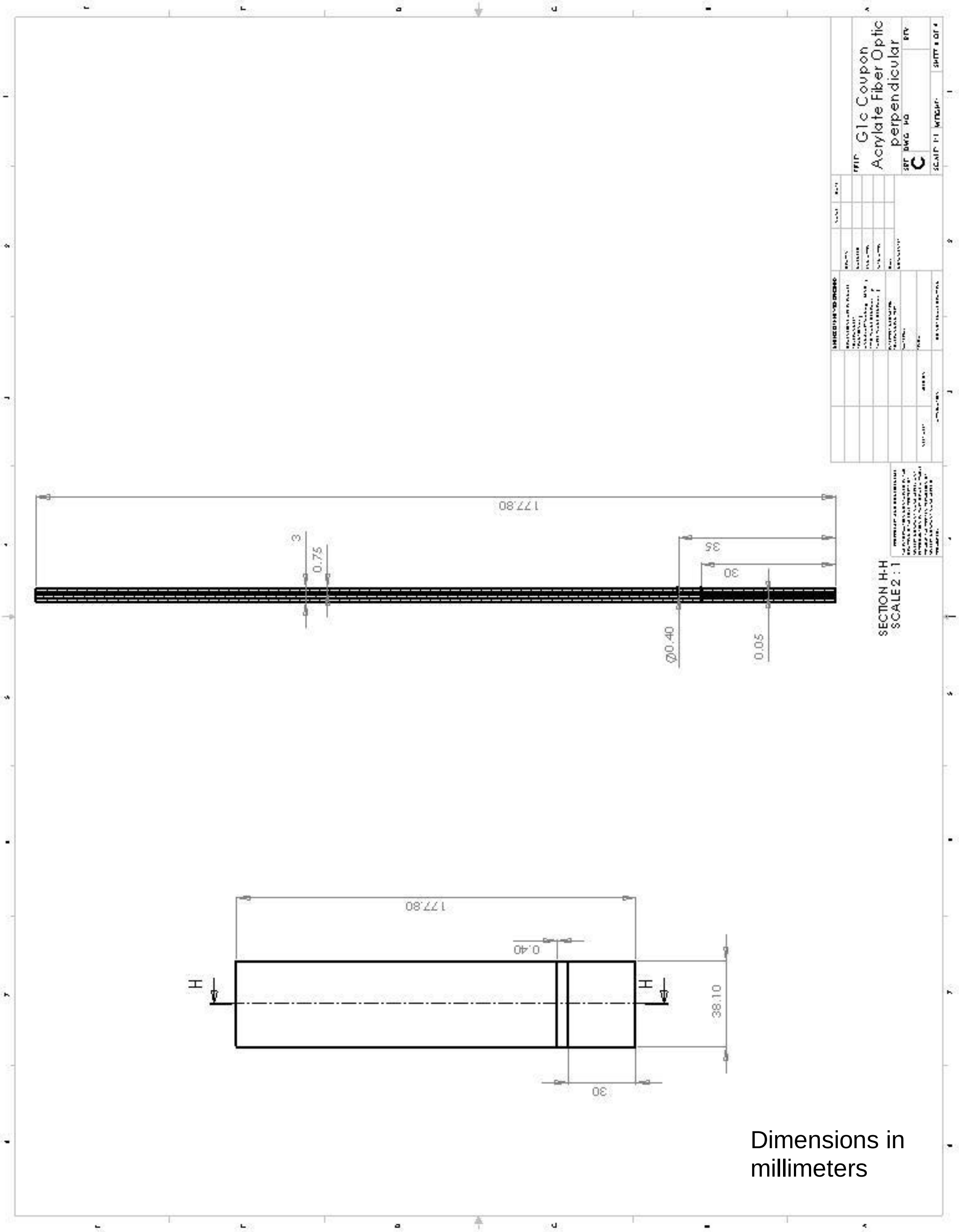

Figure 84, Dimensions of the G1c coupons with embedded acyrlate coated fiber optics perpendicular to the dominant fiber direction.

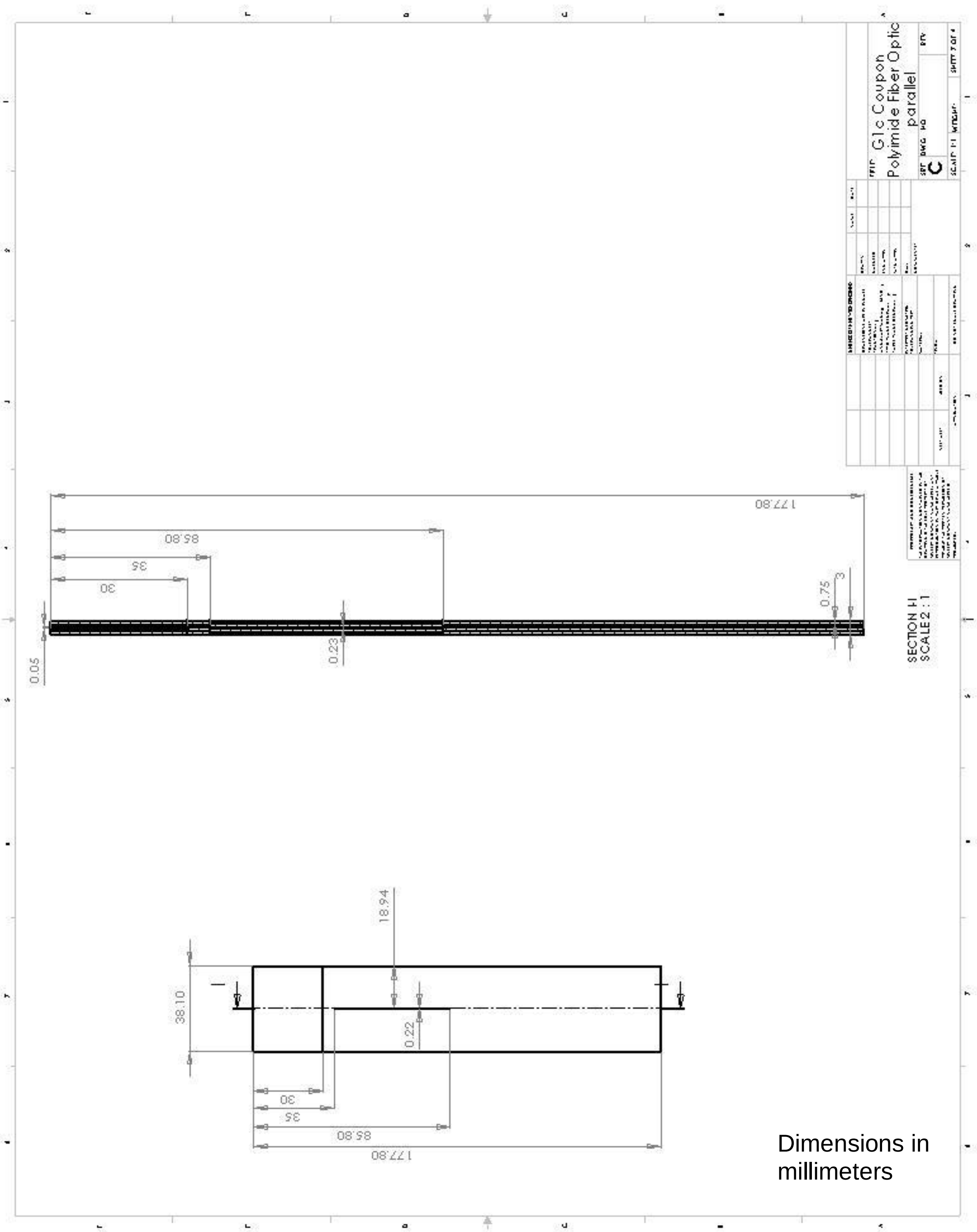

Figure 85, Dimensions of the G1c coupons with embedded polyimide coated fiber optics parallel to the dominant fiber direction.

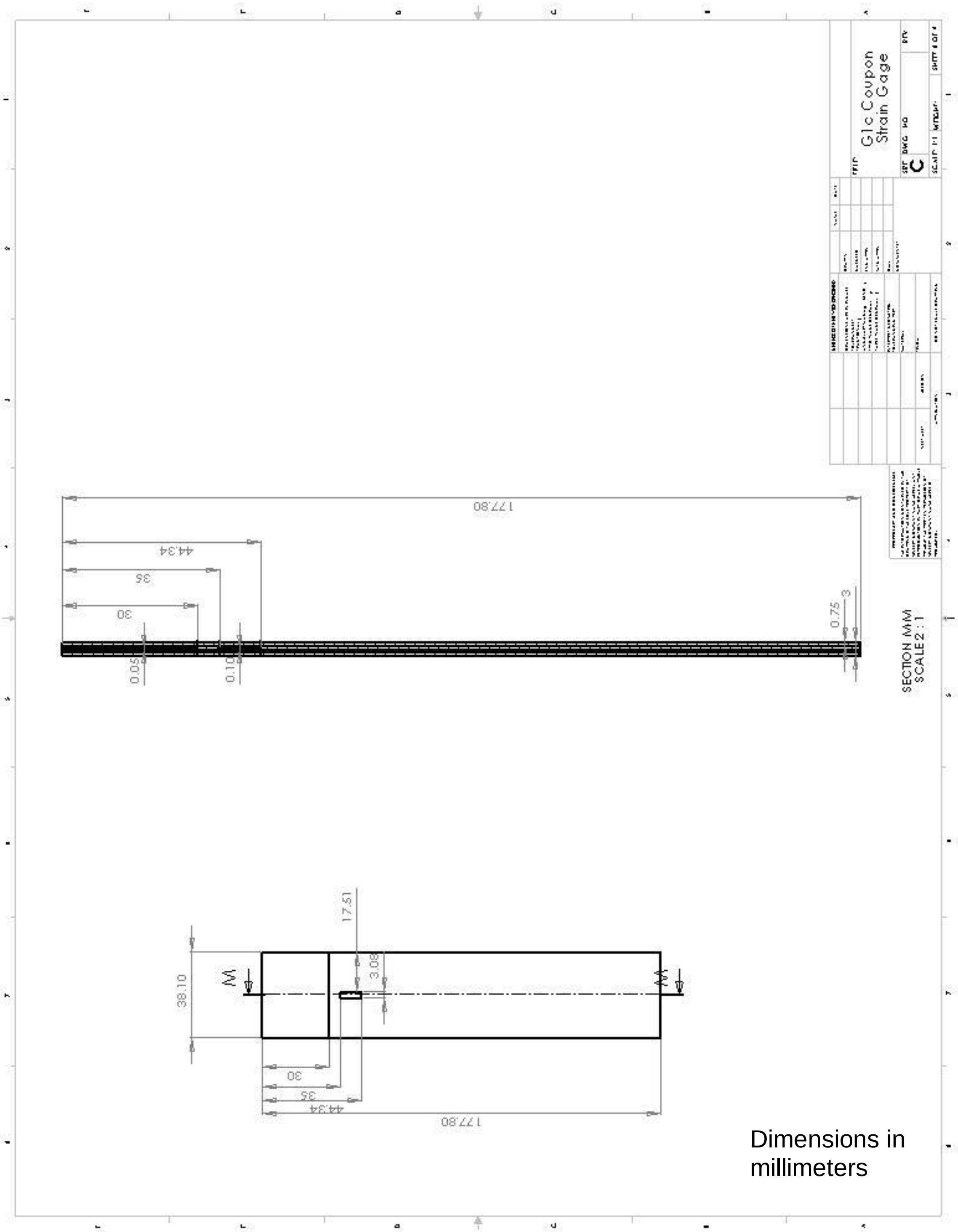

Figure 86, Dimensions of the G1c coupons with embedded strain gages.

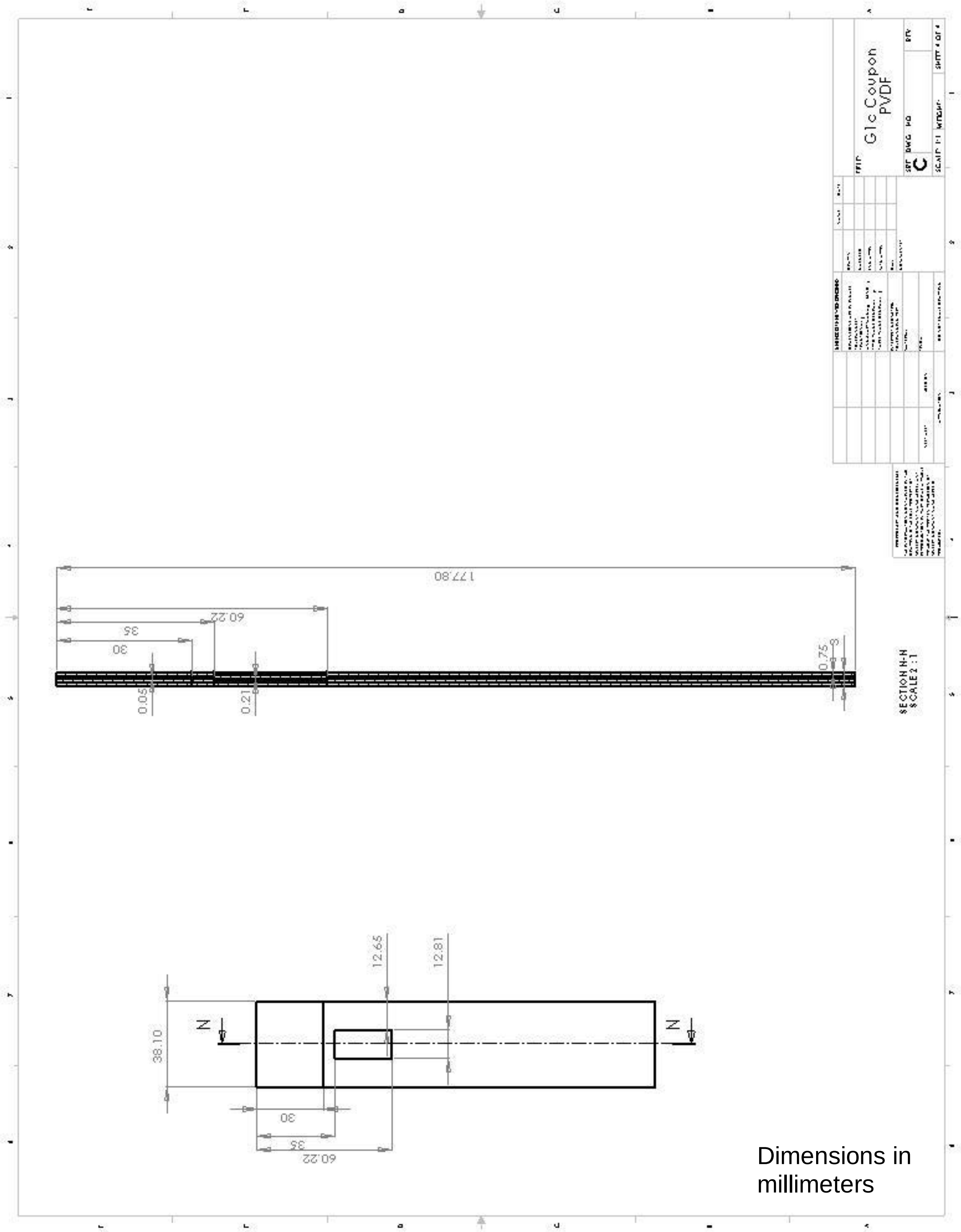

Figure 87, Dimensions of the G1c coupons with embedded PVDF films.

APPENDIX D:

TEST LOAD CONDITIONS

Table 40, Test Conditions for Tensile Modulus testing.

Sensor	Objectives	Extension Rate	Limiting Factor	Rationale	Griping Area (m^2)
Strain Gage	Mat'l Modulus and sensor response	1.016 mm/min	1 % strain	adequate feed rate	0.00129
PVDF films	Mat'l Modulus and sensor response	2.032 mm/min	1 % strain	minimize charge decay	0.00129
Acrylate Fiber Optic	Mat'l Modulus and sensor response	1.016 mm/min	1 % strain	adequate feed rate	0.00129
Polyimide Fiber Optic	Mat'l Modulus and sensor response	1.016 mm/min	1 % strain	adequate feed rate	0.000968

Table 41, Testing Conditions for Tensile Strength evaluation.

Sensor	Objectives	Extension Rate	Limiting Factor	Rationale	Griping Area (m^2)
Strain Gage	Mat'l Strength and sensor failure	2.032 mm/min	Sample Failure	Large failure loads necessitated a faster exten. Rate	0.00129
PVDF	Mat'l Strength and sensor failure	2.032 mm/min	Sample Failure	Large failure loads necessitated a faster exten. Rate	0.00129
Acrylate Fiber Optic	Mat'l Strength and sensor failure	2.032 mm/min	Sample Failure	Large failure loads necessitated a faster exten. Rate	0.00129
Polyimide Fiber Optic	Mat'l Strength and sensor failure	2.032 mm/min	Sample Failure	Large failure loads necessitated a faster exten. Rate	0.000968

Table 42, Test conditions for mode I fracture toughness determination.

Sensor	Objectives	Extension Rate	Limiting Factor	Rationale
Strain Gage	Critical Fracture Toughness values	5mm /min	Large Stable Crack growth region or significant reduction in load	Accordance with ASTM test standards
PVDF films	Critical Fracture Toughness values	5mm /min	Large Stable Crack growth region or significant reduction in load	Accordance with ASTM test standards
Acrylate Fiber Optic	Critical Fracture Toughness values	5mm /min	Large Stable Crack growth region or significant reduction in load	Accordance with ASTM test standards
Polyimide Fiber Optic	Critical Fracture Toughness values	5mm /min	Large Stable Crack growth region or significant reduction in load	Accordance with ASTM test standards

APPENDIX E:

EXPERIMENTAL TEST PROCEDURES

Tensile Test Procedures
Machine: Instron 8206

1. Turn the power switch to the on position. Located on the left hand side of the machine.
2. Allow the machine to perform initial setup programs.
3. Insure that the cross member is securely clapped to the support beams. Adjust if necessary.
4. Insure emergency stop is not engaged.
5. Turn the actuators on. Green button on the left of the front panel.
6. Disconnect the two co-axial cables connected to channels 201 and 202 of the Agilent Data Acquisition system, and connect to channels 1 and 2 of the National Instruments Data Acquisition system.
7. Turn on the computer supporting the National Instruments Data Acquisition system.
8. Once, the computer is running open the Either tensile test program. *Strain Gage Program* or *PVDF Program*.
9. Create new data file folders.
10. Calibrate the Extensometer, and load cell prior to testing.
11. Move the lower grip to correctly except the tensile test samples.
12. Check machine grips and replace with correct jaws if necessary to correctly grip samples.
13. Configure breadboard and power supply depending on embedded sensor tested.
    a. Strain Gages
        i. Connect positive and negative terminates of channel 1 of the power supply to the terminals on the breadboard.
        ii. Disconnect charge amplifier from terminal strips of the breadboard.
        iii. Connect Wheatstone bridge to the positive and negative terminal bands on the board.
        iv. Check alligator clip wire connections to Wheatstone bridge.
        v. Use Data Acquisition system or multimeter to produce a 5V difference between terminals on power supply.
    b. PVDF
        i. Connect positive terminal of channel 1 of the power supply to the positive terminal of the breadboard. Connect the negative to ground.
        ii. Connect negative terminal of channel 2 of the power supply to the negative terminal of the breadboard. Connect the positive to ground.
        iii. Use the Data Acquisition system or multimeter to produce a 6V difference for both channels.

iv. Disconnect all Wheatstone bridges from power strips on the breadboard.
v. Connect the Op Amp to the power strips on the breadboard.
vi. Check connection to Op Amp of the alligator clip wiring.

14. Create appropriate data file paths for Data Acquisition program.
15. Sampling rate of 50 hertz, and averaging every 5 samples.
16. Load test sample into the machine and apply 3000 psi to each grip.
17. Connect alligator clips to sensor connections.
18. Test for circuit continuity.
19. Start data recording program.
20. Initial loading.
21. Once complete stop machine, then data recorder.
22. Check first few tests to insure appropriate response.
23. Remove and continue as needed.

Machine: Instron 5882

1. Turn on the Gateway computer and monitor supporting the machine.
2. Turn on the control module, switch located in the back of the module located under the computer monitor.
3. Turn on the machine, switch located on the right hand side of machine.
4. Allow to warm up.
5. Connect co-axial cables from output channels X and Y to channels 1 and 2 of National Instruments Data Acquisition system.
6. Configure outputs in the Tensile Test program as desired.
7. Load 2 inch grips into the machine.
8. Turn on the computer supporting the National Instruments Data Acquisition system.
9. Once, the computer is running open the either tensile test program. *Strain Gage Program* or *PVDF Program*.
10. Create new data file folders.
11. Start control program, Merlin.
12. Start test program Tensile Test. Frame Ready light will turn green when ready.
13. Create appropriate data file paths for Data Acquisition program.
14. Sampling rate of 50 hertz, and averaging every 5 samples.
15. Test calibration of the load cell. Check both computer programs.
16. Test calibration of extensometer. Check both computer programs.
24. Move the lower grip to correctly except the tensile test samples.
25. Check machine grips and replace with correct jaws if necessary to correctly grip samples.
26. Configure breadboard and power supply depending on embedded sensor tested.
    a. Strain Gages
        i. Connect positive and negative terminates of channel 1 of the power supply to the terminals on the breadboard.

ii. Disconnect charge amplifier from terminal strips of the breadboard.
iii. Connect Wheatstone bridge to the positive and negative terminal bands on the board.
iv. Check alligator clip wire connections to Wheatstone bridge.
v. Use Data Acquisition system or multimeter to produce a 5V difference between terminals on power supply.

b. PVDF
   i. Connect positive terminal of channel 1 of the power supply to the positive terminal of the breadboard. Connect the negative to ground.
   ii. Connect negative terminal of channel 2 of the power supply to the negative terminal of the breadboard. Connect the positive to ground.
   iii. Use the Data Acquisition system or multimeter to produce a 6V difference for both channels.
   iv. Disconnect all Wheatstone bridges from power strips on the breadboard.
   v. Connect the Op Amp to the power strips on the breadboard.
   vi. Check connection to Op Amp of the alligator clip wiring.

27. Load sample into grips with desired gripping force.
28. Connect alligator clips to sensor connections.
29. Test for circuit continuity.
30. Start data recording program.
31. Initial loading.
32. Once complete stop machine, then data recorder.
33. Check first few tests to insure appropriate response.
34. Remove and continue as needed.

Mode I Fracture Toughness Test Procedure
Machine: Instron 8206

1. Disconnect the 100kN load cell from the frame.
2. Raise the cross member to allow the 2.224kN load cell to hang from the upper grip.
3. Remove the jaws from the upper grip and place the 2.224kN load cell in the grips. Support load cell wiring.
4. Turn the power switch to the on position. Located on the left hand side of the machine.
5. Allow the machine to perform initial setup programs.
6. Load the Clevises into the 2.224kN load cell and lower grips. Take care that the pin locations are aligned.
7. Turn on machine actuators.
8. Adjust the lower grip so the displacement reads 0mm.
9. Adjust the cross member height to accept the test samples.

10. Secure the cross member by tightening the clamp screws.
11. Disconnect the coaxial cables from channels 201 and 202 from the Agilent Data Acquisition system and connect to channels 1 and 2 of the National Instruments Data Acquisition system.
12. Turn on supporting computer. And initiate Labview Program titled *G1c Program.*
13. Supply appropriate information to *G1c Program.* Sampling rate 50hertz and averaged every 5 samples.
14. Calibrate Load cell.
15. Test load cell, and position sensor response.
16. Load sample into the clevises with 1/8 " dowel pins.
17. Define appropriate loading rates on machine control module.
18. Start data recorder in *G1c Program.*
19. Start machine loading.
20. Once the fracture has propagated unload the sample and stop machine.
21. Stop data recorder.
22. Check test response for the first few tests.
23. Remove sample and continue as needed.

APPENDIX F:

DATA ACQUISITION SYSTEM & PROGRAMS

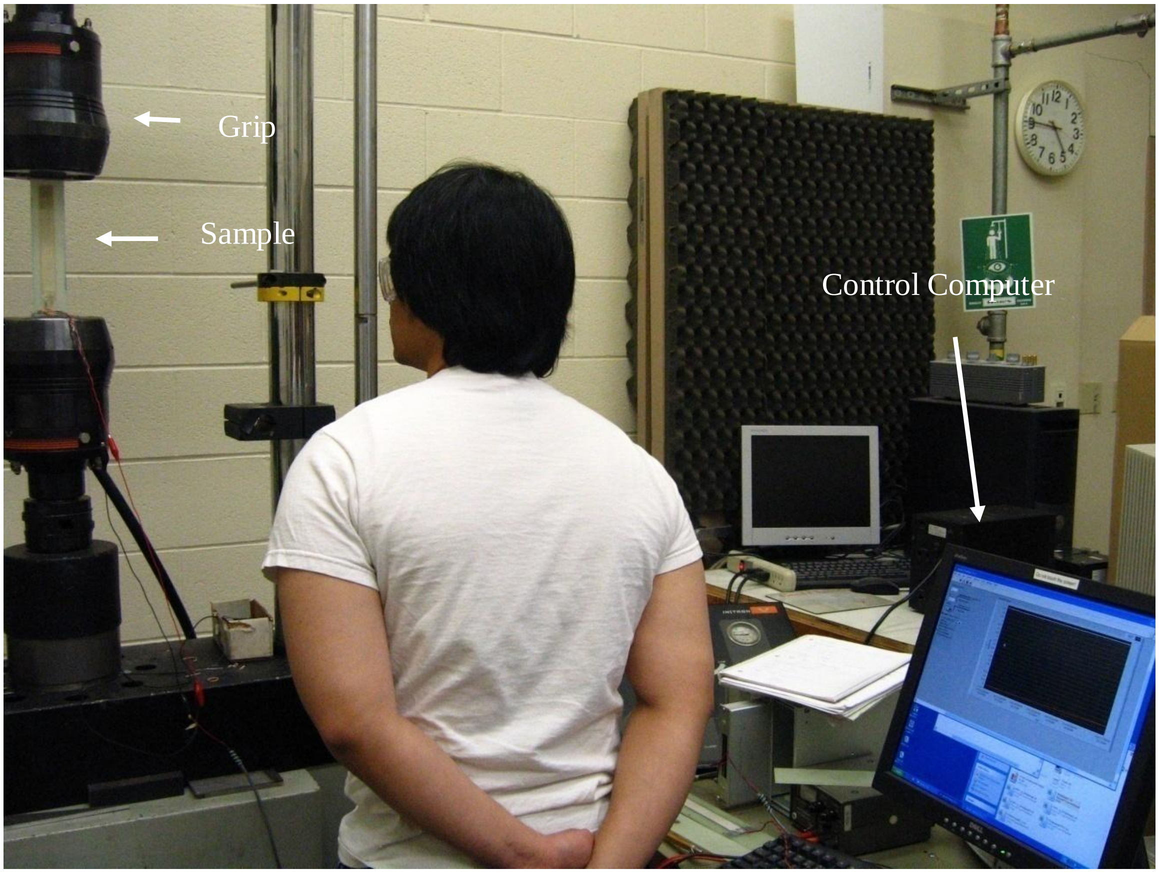

Figure 88, Test system configuration on the Instron 8206.

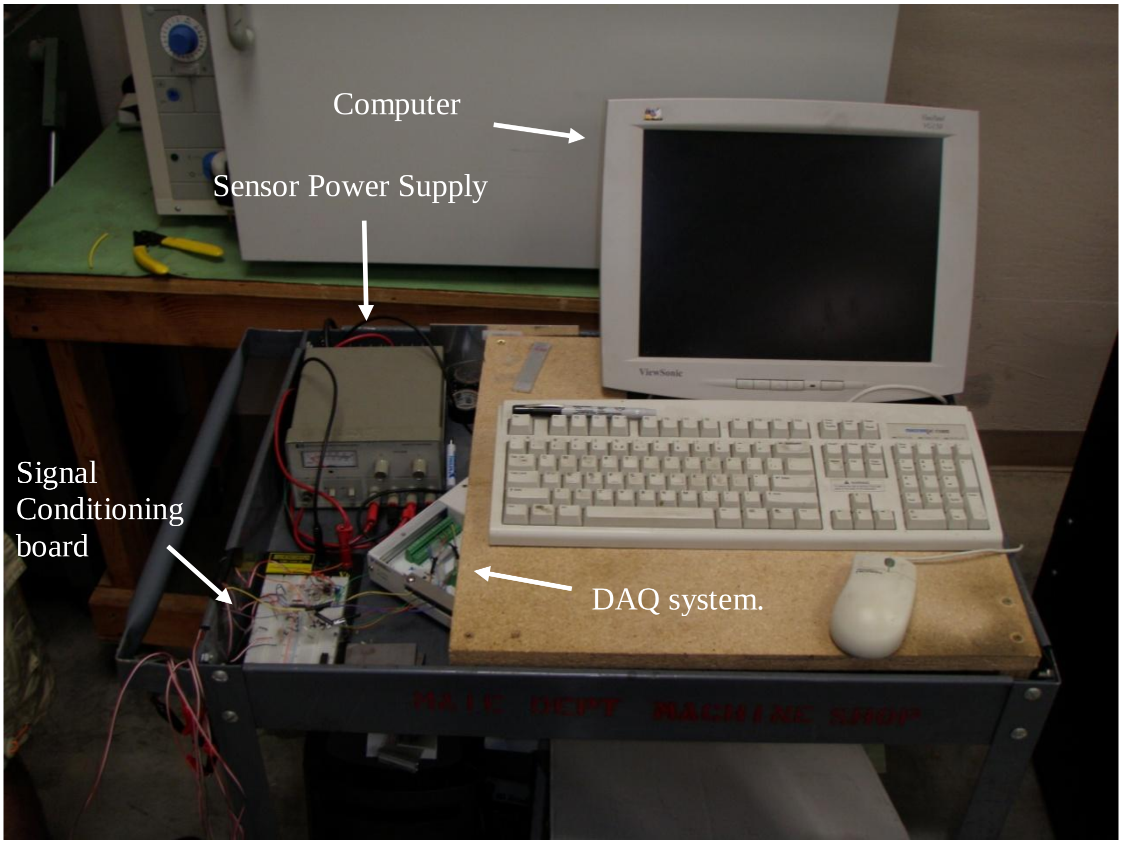

Figure 89, Data Acquisition system used in the study.

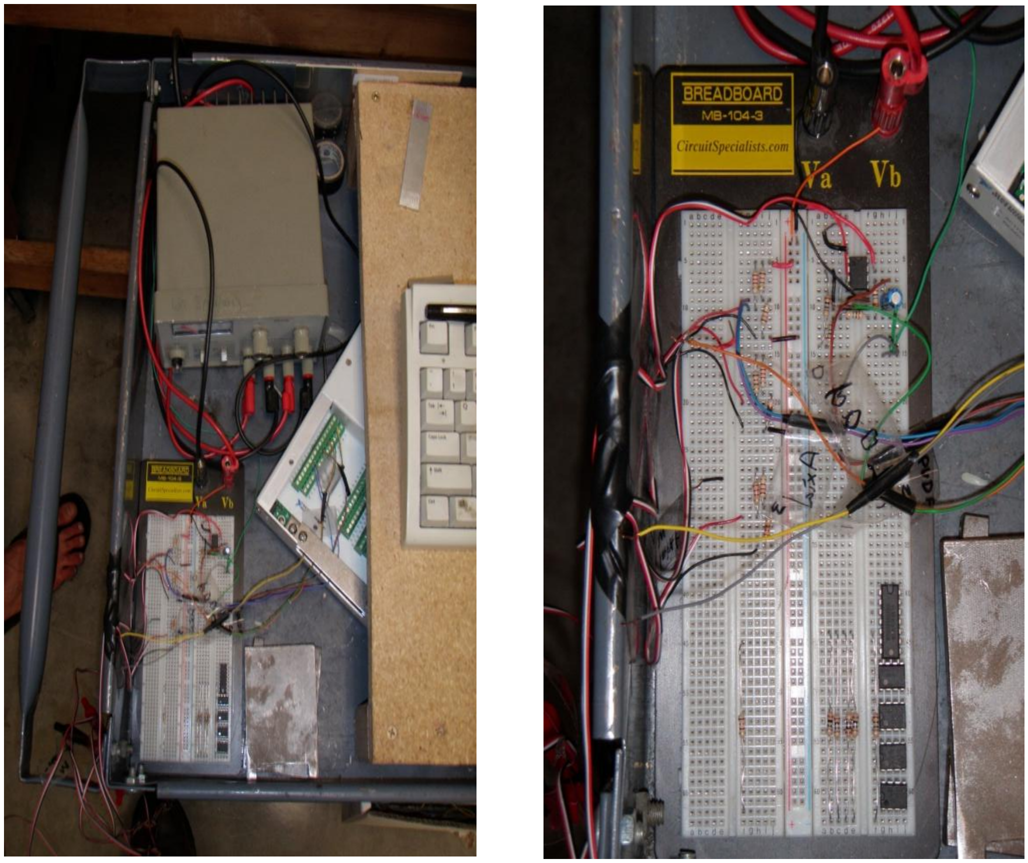

Figure 90, Data acquisition unit, breadboard, and power supply.

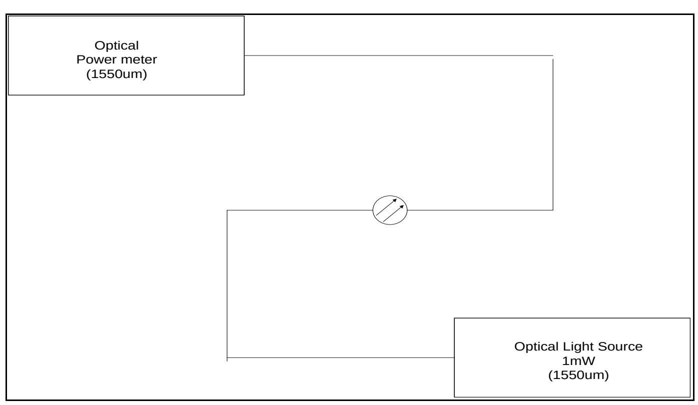

Figure 91, Signal Conditioning for Fiber optics.

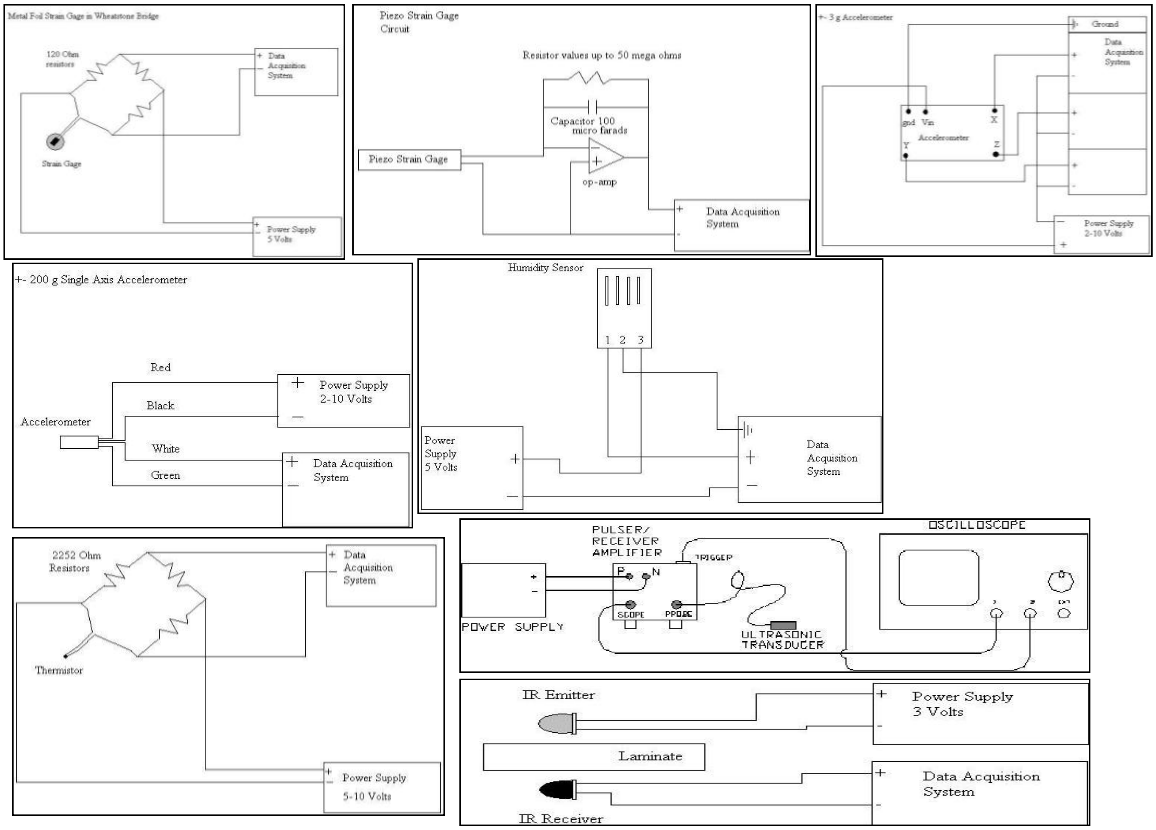

Figure 92, Signal conditioning for all sensors used in the study [4].

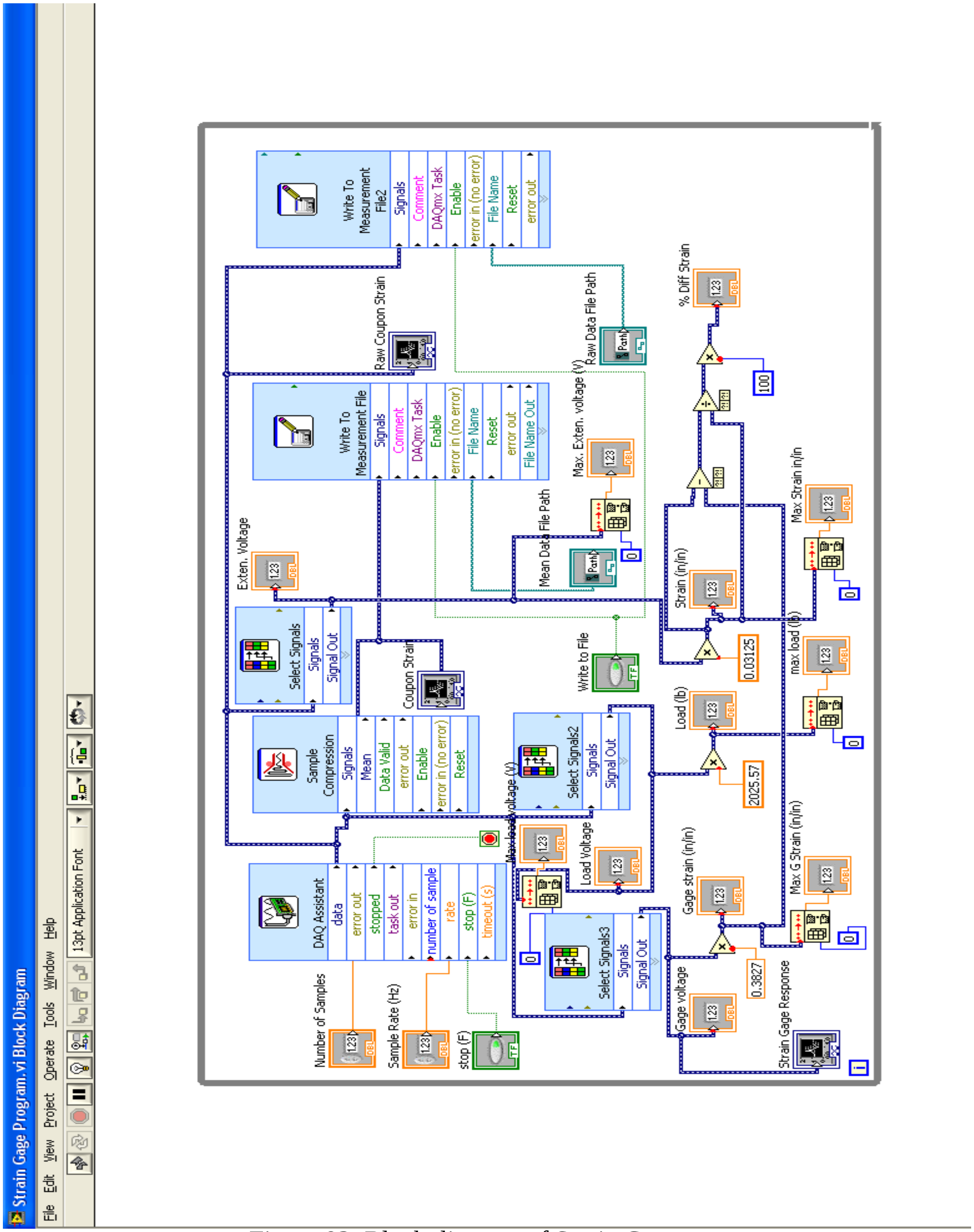

Figure 93, Block diagram of Strain Gage program.

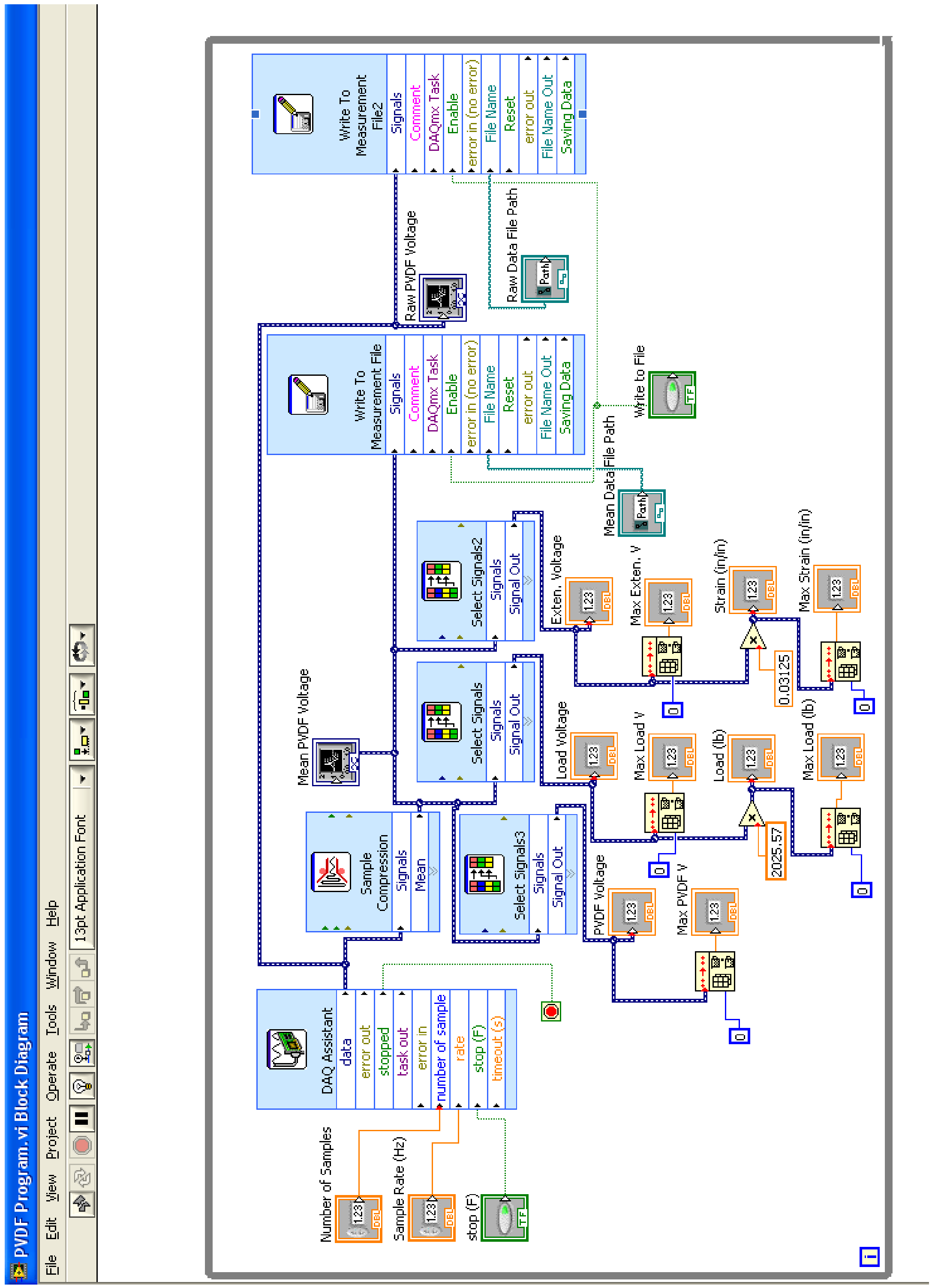

Figure 94. Front Panel of PVDF Program.

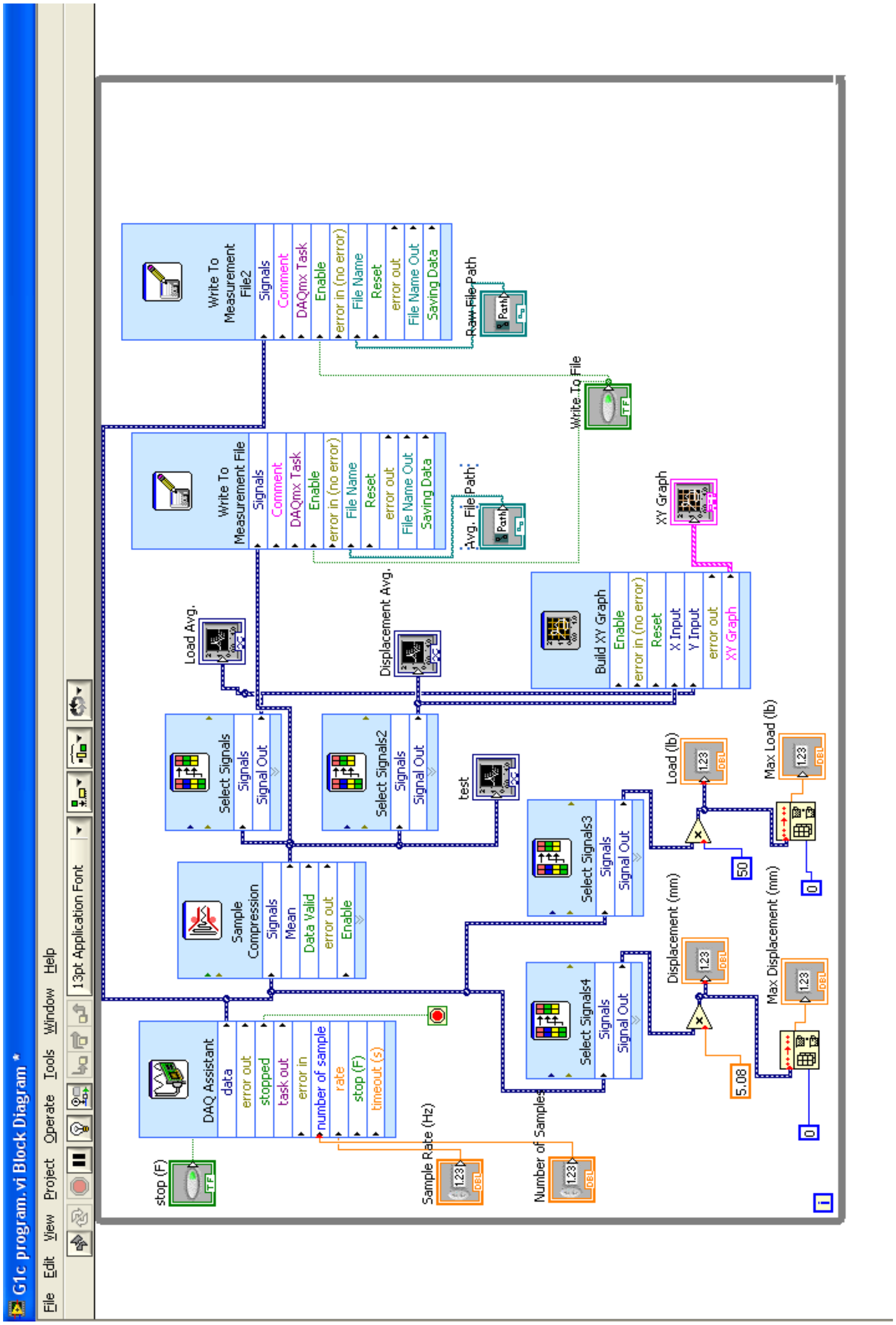

Figure 95, Block Diagram of G1c Program.

APPENDIX G:

EXAMPLES OF TEST DATA ANALYSIS

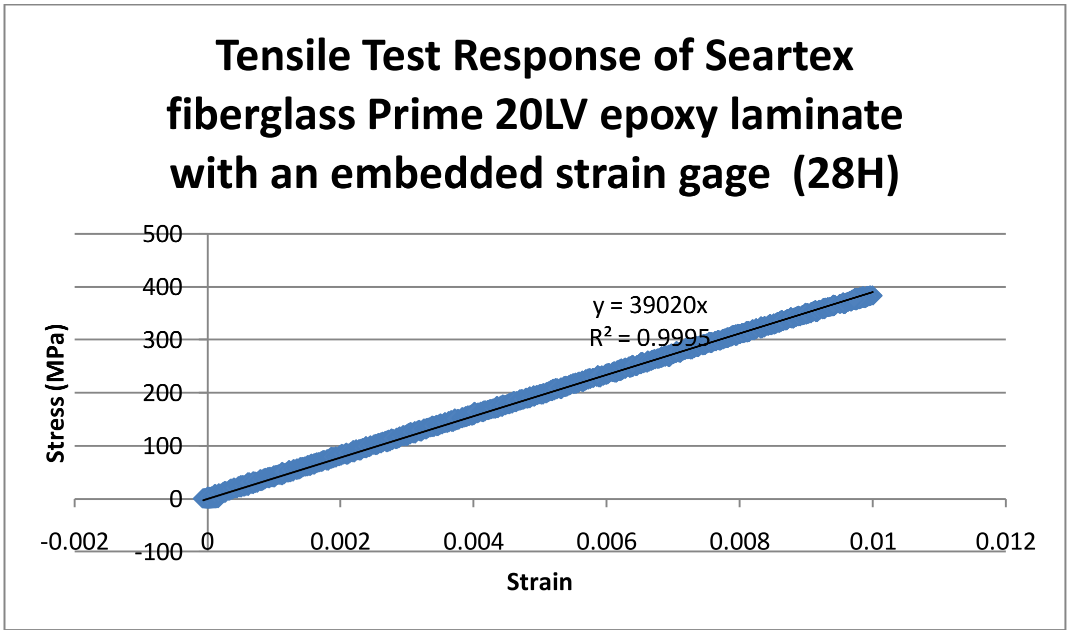

Figure 96, Representative stress strain response for samples constructed with embedded single axis strain gages.

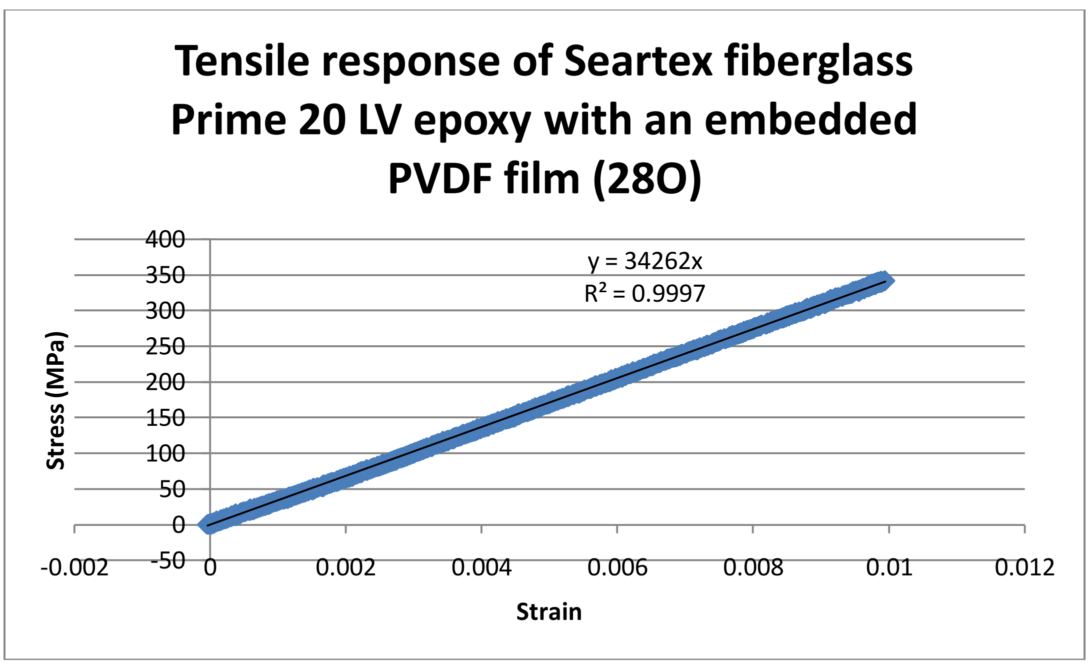

Figure 97, Representative stress strain response for samples constructed with embedded single axis strain gages.

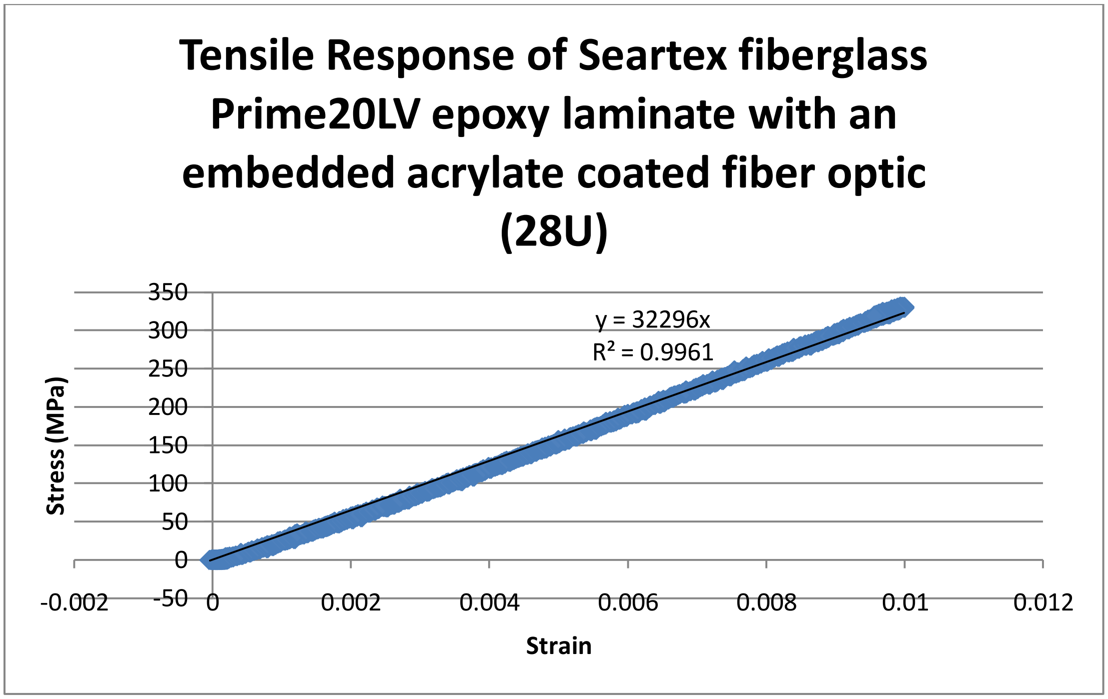

Figure 98, Representative stress strain curve for samples with embedded acrylate coated fiber optics

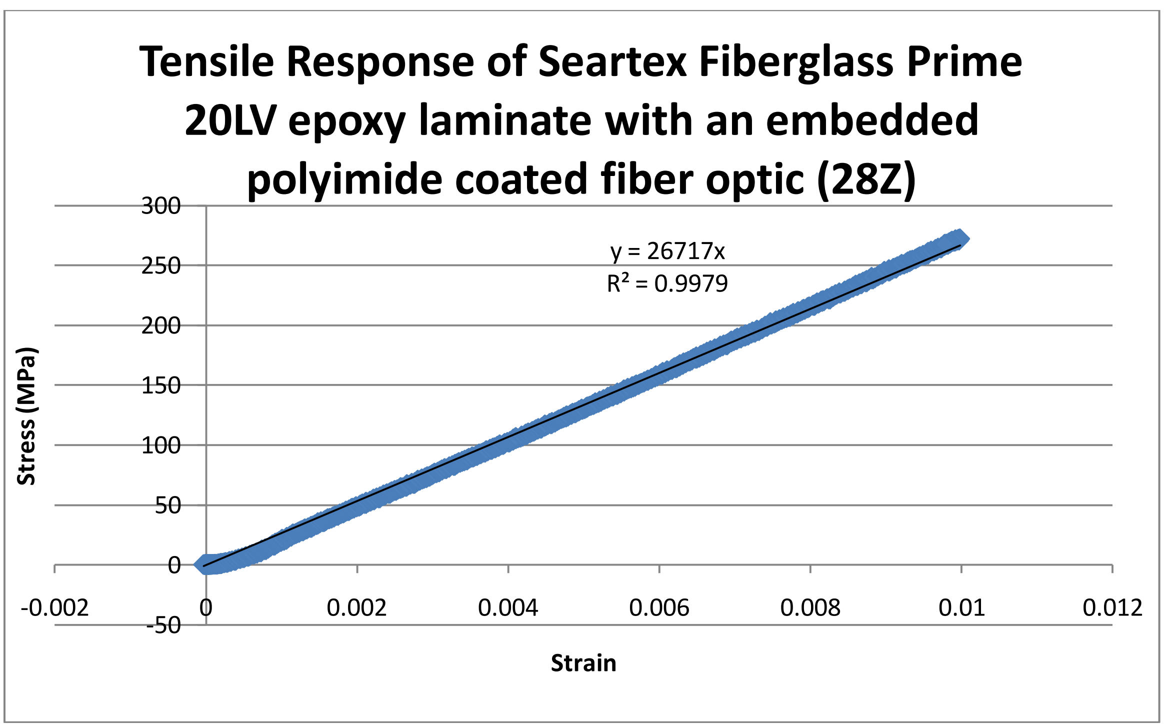

Figure 99, Representative stress strain curve for samples with embedded polyimide coated fiber optics

Example calculations given from an embedded strain gage within an epoxy laminate.

Tensile Modulus Example

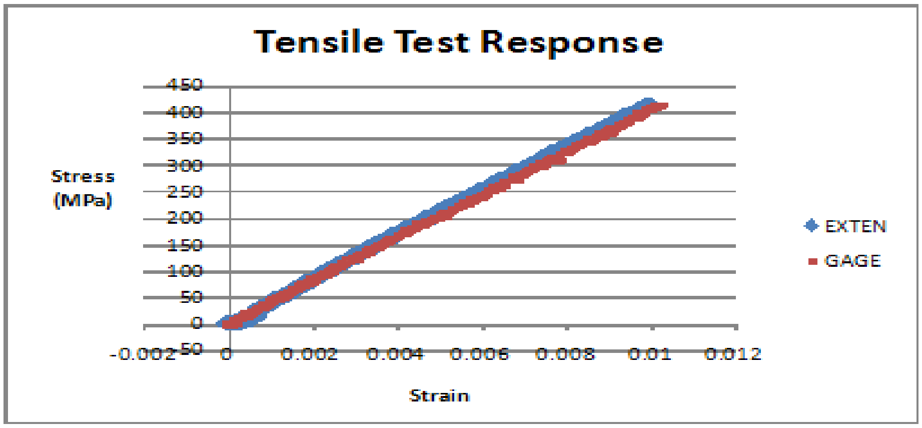

Modulus based on Extensometer

$$E_e := 41.65\text{GPa}$$

(slope of stress strain curve)

Sensor Sensitivity Example

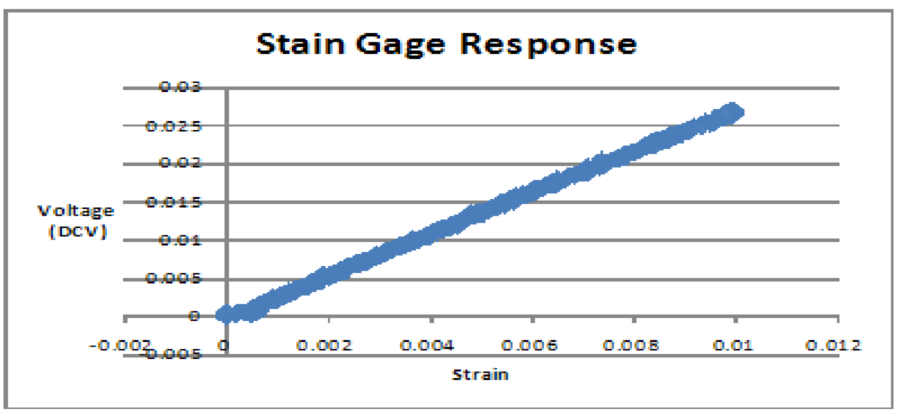

Sensor Sensitivity

$$m_s = 2.67 \frac{V}{\%\text{strain}}$$

(slope of signal voltage strain curve)

Sensor Failure Pt

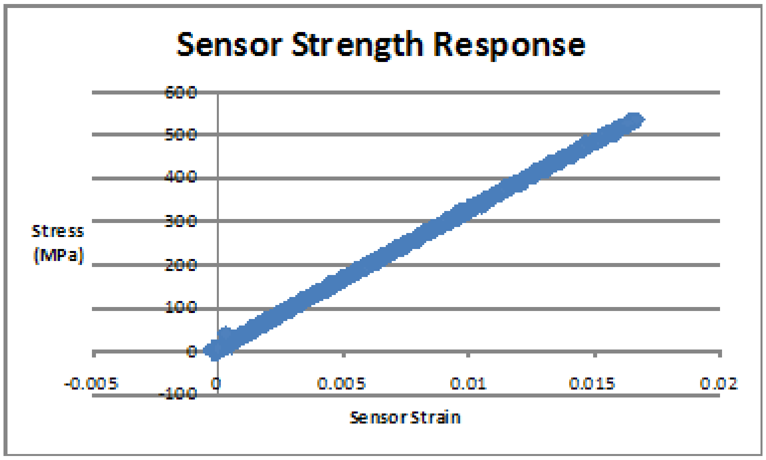

Sensor Failure Pt.

$max_s := 533.69 MPa$

Stress at the maximum value of reliable sensor strain

Material Strength

Maximum Load during test

$max_L := 45587.41 N$

Sample X Area

$A_s := 8.54 \cdot 10^{-5} m^2$

width and thickness are averaged from three locations not effected by sensor embedding.

Material Strength

$$S_m := \frac{max_L}{A_s}$$

$S_m = 533.81 \, MPa$

Maximum Load

Maximum load during test

$max_L = 45.587 \, kN$

Apparent Linear Strain at Failure

$$\varepsilon_a := \frac{S_m}{E_e}$$

$\varepsilon_a = 0.013$

Mode I Fracture Toughness (G1c)

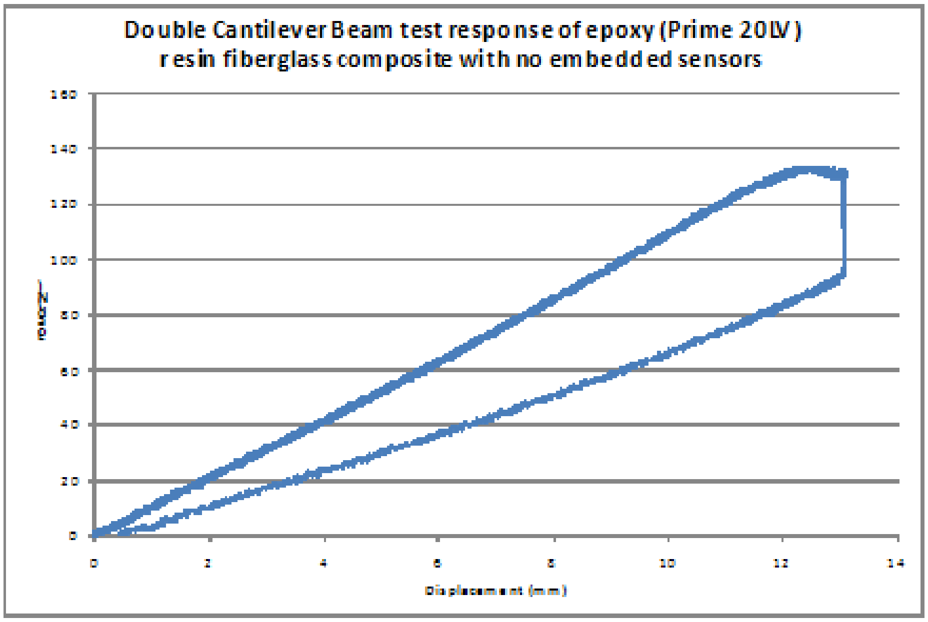

Maximum Load

$P_{max} := 135N$

Maximum Displacment

$\delta_{max} := 13.0mm$

Energy Into the Sample

$$E_{in} = \sum_{i=1}^{\delta_{max}} \left[\frac{(P_i + P_{im1})}{2} \cdot (\delta_i - \delta_{im1}) \right]$$

$E_{in} := 1.923J$

P_i = load at current displacement step
P_{im1} = load at previous displacement step
δ_i = displacement value at current step
δ_{im1} = displacement value at previous step

Energy Recovered from the Sample

$$E_{rec} = \sum_{i=\delta_{max}}^{P_o} \left[\frac{(P_i + P_{im1})}{2} \cdot (\delta_i - \delta_{im1}) \right]$$

$E_{rec} := 1.235J$

P_i = load at current displacement step
P_{im1} = load at previous displacement step
δ_i = displacement value at current step
δ_{im1} = displacement value at previous step
P_o= load equal to zero on return.

Energy Dissipated

$E_{dis} := E_{in} - E_{rec}$ $\qquad E_{dis} = 0.688\,J$

Change in Crack Length

$\Delta a = a_r - a_o$

a_r = average crack length after loading

a_o = average crack length before loading

(Lengths are averaged from crack length on either edge of the sample.)

$a_o := .0349m$

$a_r := .0522m$

$\Delta a := a_r - a_o$ $\qquad \Delta a = 0.017\,m$

Fracture Toughness

$$G_{1c} = \frac{E_{dis.}}{2 \cdot \Delta a \cdot w}$$

w = width of the sample

$w := .0381m$

$$G_{1c} := \frac{E_{dis}}{2 \cdot \Delta a \cdot w} \qquad G_{1c} = 521.9\,\frac{J}{m^2}$$

APPENDIX H:

ANSYS FEM INCLUSION BATCH FILE

```
!!!!!clears previous work!!!
finish
/clear,nostart

!!!!!!Dimensions!!!!!!!
!Newtons!
!meters!
!Pascals!


!!!!!!!!!!!!!!!!!!!Moving to the Preprocesser!!!!!!!!!!!!
/prep7

!!!!keypoints!!!!
k,1,0,0,-.000955
k,2,0,0,-.000105
k,3,0,0,0
k,4,.006405,0,0
k,5,.0254,0,0
k,6,.0254,0,-.00085
k,7,.006505,0,-.00085
k,8,.006405,0,-.000955
k,9,0,.01261,-.000955
k,10,0,.01261,-.000105
k,11,0,.01261,0
k,12,.006405,.01261,0
k,13,.006405,.01261,-.000105
k,14,.006405,.01261,-.000955
k,15,0,.01271,-.00085
k,16,.006505,.01271,-.00085
k,17,0,.1016,-.00085
k,18,0,.1016,0
k,19,.0254,.1016,0
k,20,.0254,.1016,-.00085
k,21,.006405,0,-.000105
k,22,.0254,.01271,0
k,23,.0254,.01271,-.00085
k,24,.006405,.01271,-.00085
k,25,.006505,.01261,-.00085
k,26,.006505,.01271,0
k,27,.006505,0,0
k,28,0,.01271,0
```

```
kplot

!!!!!!!Generate volumes!!!!!
v,2,3,4,21,10,11,12,13   !!!!sensor!!!!
v,1,2,21,8,9,10,13,14           !2!      !behind sensor!!!
v,9,10,15,14,13,24              !3!      !top prism!
v,7,8,21,25,14,13               !4!      !side prism!
v,14,13,24,16                   !5!      !top pyramid!
v,25,14,13,16                   !6!      !side pyramid!
V,7,21,4,27,16,13,12,26                  !7!      !side trapezoidal prism!
v,10,11,28,15,13,12,26,16       !8!      !top trapezoidal prism!
v,6,7,27,5,23,16,26,22                   !9!      !right of sensor!
v,15,28,22,23,17,18,19,20       !10!      !top of sensor!

vplot

!!!!!Add volume together to make glass!!!!
vadd,2,3,4,5,6,7,8,9,10                  !11!

!!!!!glue sensor to glass!!!!
vglue,1,11

vplot
!!!!!!!!!!!!!Define elements to be Used!!!!!!!!!!!!!
et,1,solid92
et,2,solid92

!!!!!!!!!!!!!Define material properties!!!!!!!!!!!!!!
!!!!!!!Fiberglass!!!!!!!
mp,ex,1,9e9                     !Pascals!
mp,ey,1,3.05e10                          !Pascals!
mp,ez,1,4e9                     !Pascals!
mp,prxy,1,.27
mp,gxy,1,4.1e9                           !Pascals!
mp,gxz,1,4.1e9                           !Pascals!
mp,gyz,1,4.1e9                           !Pascals!

!!!!!!Sensor!!!!!!!!
mp,ex,2,3.05e10   !Pascals!
mp,prxy,2,.3

!!modulus to study!!!
!!7 Pa!!
```

```
!!3.5e7 Pa!!
!!7e7 Pa  (aluminum)!!
!!1.05e8 Pa!!
!!1.4e8 Pa!!
!!1.28e10  Pa (barium)!!
!!30.5e9   Pa (fiberglass)!!



!!!!!Mesh Glass region!!!!
Type,1
mat,1
vsel,,,,11
smrtsize,10
vmesh,11

!!!!Mesh Sensor!!!
Type,2
mat,2
vsel,,,,1
smrtsize,10
vmesh,1

vsel,all

!!!!!!!define y symmetry!!!!!!
nsel,s,loc,y,0,0
dsym,symm,y,0
nsel,all

!!!!!!!define x symmetry!!!!
nsel,s,loc,x,0,0
dsym,symm,x,0
nsel, all

!!!!!!define z symmetry!!!
nsel,s,loc,z,0,0
dsym,symm,z,0
nsel,all

!!!!!!define constrain in the x direction!!!!
nsel,s,loc,x,.0254,.0254
d,all,ux,0,0
nsel,all
```

```
!!!!!!define constrain in the z direction!!!
nsel,s,loc,z,0,0
d,all,uz,0,0
nsel,all

!!!!!Apply surface load !!!!
!!!!!!define pressure of top nodes!!!!
sfa,44,,pres,-4.925e8  !pascals!

!!!!move to solution module!!!
finish
/solu
solve

!!!move to post processor!!!!
/post1
plnsol,epel,eqv,2
```